

Metal-Catalyzed Generation of Main-Group Electrophiles: Mechanisms and Applications

vorgelegt von

Master of Science
Toni Tapio Metsänen
aus Viljakkala, Finnland

Von der Fakultät II - Mathematik und Naturwissenschaften
der Technischen Universität Berlin
zur Erlangung des akademischen Grades

Doktor der Naturwissenschaften
Dr. rer. nat.

genehmigte Dissertation

Promotionsausschuss:

Vorsitzender: Prof. Dr. Andreas Grohmann

Gutachter: Prof. Dr. Martin Oestreich

Gutachter: Prof. Dr. Warren E. Piers

Tag der wissenschaftlichen Aussprache: 28. April 2016

Berlin 2016

This thesis was prepared at the Institut für Chemie, Technische Universität Berlin between September 2012 and April 2016 under the supervision of Professor Dr. MARTIN OESTREICH.

I thank Professor Dr. MARTIN OESTREICH for giving me an opportunity to work on challenging and interesting projects. His endless support allowed me to stay focused on my chemical puzzles.

I would like to thank Professor Dr. WARREN. E. PIERS for accepting the invitation to be the external evaluator for this thesis.

I am grateful to Professor Dr. ANDREAS GROHMANN for acting as the chairman of the doctoral committee.

The analytic centers of the Institut für Chemie, Technische Universität Berlin are acknowledged for their expert advice and help. I would like to especially thank Dr. ELISABETH IRRAN and PAULA NIXDORF from the X-ray crystallography service, as well as Dr. MARIA SCHLANGEN-AHL and MARC GRIFFEL from the laboratory of mass-spectrometry for outstanding service and advice. From the Bunker Team, I would like to thank ERIK NEUMANN for friendly and efficient service.

I thank the past and present members of OESTREICH group, especially my Big Lab mates, and the fellow members of C.R.A.P., O.W.L., and A.S.T.H.M.A. Dr. TIMO STAHL is gratefully acknowledged for the patient introduction into SCHLENK techniques, diligent syntheses of the ruthenium thiolate complexes, and advanced NMR spectroscopy. My correction team XICHANG DONG, FRANCIS FORSTER, and MANISH PAREEK made writing of this thesis easy. I would like to thank Dr. THOMAS FALLON, CAROLIN FOPP, Dr. CHINMOY K. HAZRA, SEBASTIAN KEESS, soon-to-be Dr. JENS MOHR, and Dr. ANTOINE SIMONNEAU for extracurricular activities. STEPHANIE KROMBACH is thanked for helping me through all the bureaucracy and paper work during the last three and a half years.

I am grateful to my collaborators who expanded my chemical world beyond synthetic organic chemistry. I am indebted to Professor Dr. MARTIN KAUPP and Dr. PETER HROBÁRIK for the fruitful collaboration that led to my first publication. I would like to express my thanks to Professor Dr. MATTHIAS DRIESS, Dr. DANIEL GALLEGÓ, and Dr. TIBOR SZILVÁSI for the painstaking joint effort into the strange world of iron SiNSi pincer complexes.

I was fortunate to work with two talented and motivated students: FRANCIS “FRANZ” FORSTER and JULIEN “JONNY” FUCHS.

I would like to thank all my former colleagues who have helped me in the past. I would have never made it without you. I thank Professor Dr. P. ANDREW EVANS for the interesting year and a half I got to spend in Liverpool. Especially, I thank my fellow G20 survivors Dr. TOMASS BAIKSTIS, Dr. REBECCA GRANGE, Dr. SERGIO MARATO, Dr. SHANE MCKENNA, THOMAS NATION, Dr. RYAN O'CONNOR, Dr. STEPHEN "MIGHTY" OJO, Dr. SAMUEL OLIVER, BARBARA VARDA, and Dr. STEPHANIE YIP. I also thank Professor Dr. PETRI PIHKO for his continued support. Special thanks to the members of the PIHKO group who, among many other things, showed me how to correctly assemble a short-plug distillation apparatus. I need to thank ANNUKKA ENERVI, MIRA HAVUKAINEN, and LAURA PITKÄJÄRVI who helped me get through Physical Chemistry 1.

I thank all my friends and family who have kept supporting me through the years. Special thanks to ANTTI N. T. SALMINEN for designing the covers of this thesis and MIKKO P. PUULA for the design of the *Organometallics* cover.

Most of all, I thank LAURA and ELIEL. Without you, I would be completely lost.

*Ei unelma valoa vaadi
vaan rohkeutta*

”Viestintuoja”
Viimeinen Atlantis, 2010
Stam1na

*Schönke dan
kiitokset humpasta*

“Kiitokset Humpasta”
Pahviche, 2002
Eläkeläiset

PUBLICATIONS

Parts of this work have been published:

- [1] *“Insight into the Mechanism of Carbonyl Hydrosilylation Catalyzed by Brookhart’s Cationic Iridium(III) Pincer Complex”*,
T. T. Metsänen, P. Hrobárik, H. F. T. Klare, M. Kaupp, M. Oestreich,
J. Am. Chem. Soc. **2014**, 136, 6912–6915.

- [2] *“Temperature-Dependent Chemoselective Hydrosilylation of Carbon Dioxide to Formaldehyde or Methanol Oxidation State”*,
T. T. Metsänen and M. Oestreich,
Organometallics **2015**, 34, 543–546.

- [3] *“Peripheral mechanism of a carbonyl hydrosilylation catalysed by an SiNSi iron pincer complex”*,
T. T. Metsänen, D. Gallego, T. Szilvási, M. Driess, M. Oestreich,
Chem. Sci. **2015**, 6, 7143–7149.

ORAL PRESENTATIONS

- [1] T. T. Metsänen, *“Insight into the Mechanism of Carbonyl Hydrosilylation Catalyzed by Brookhart’s Cationic Iridium(III) Pincer Complex”*,
17th International Symposium on Silicon Chemistry (ISOS), Berlin, 3–8 August **2014**.

- [2] T. T. Metsänen, *“Cooperative Si–H bond activation: generation of electrophilic silicon for carbon dioxide reduction”*,
UniCat meeting, Berlin, December 12th **2013**.

POSTER PRESENTATIONS

- [1] T. T. Metsänen, D. Gallego, T. Szilvási, M. Driess, and M. Oestreich,
“Peripheral Mechanism of a Carbonyl Hydrosilylation Catalyzed by an SiNSi Iron Pincer Complex”,
ICIQ-UniCat Summer School in Berlin (Germany), July 6–9 **2015**.

ZUSAMMENFASSUNG

Der erste Teil dieser Dissertation beschäftigt sich mit den Mechanismen metallkatalysierter Aktivierungen von Hauptgruppenhydriden. Der von BROOKHART entwickelte Iridium(III)-POCOP-Pincerkomplex kann als LEWIS-Säure Hydrosilane aktivieren. Die Silylgruppe wird durch einen S_N2 -Si-Mechanismus übertragen, wie bereits für Bor-LEWIS-Säuren gezeigt. Der anschließende Hydridtransfer weicht allerdings vom vorgeschlagenen Mechanismus ab. Kontrollexperimente zeigten, dass das Iridiumdihydrid, welches als Hydriddonor vermutet wurde, kein Hydrid auf das Kohlenstoffatom des Silylcarboxoniumions überträgt. Im Gegensatz dazu wurde in Anwesenheit eines Überschusses an Hydrosilan das Silylcarboxoniumion leicht zum gewünschten Silylether reduziert. Durch Kombination spektroskopischer Untersuchungen und quantenchemischer Berechnungen wurden neue Iridium-trihydridkomplexe als *de facto* Hydriddonoren identifiziert, die durch die Koordination überschüssigen Hydrosilans an das Dihydrid entstehen.

Die Untersuchung der durch den Eisen(0)-SiNSi-Pincerkomplex katalysierten Hydrosilylierung zeigte einen unbekannten Mechanismus. Der Eisen(0)-Komplex wurde als Präkatalysator identifiziert, welcher den aktiven Eisen(II)-Komplex nach oxidativer Addition des Hydrosilans bildet. Kinetische und stöchiometrische Experimente sowie Deuteriummarkierungsexperimente und der stereochemische Verlauf an einem silicium-stereogenen Hydrosilan schließen alle bekannten Mechanismen aus. Somit wurde ein neuer, durch DFT-Berechnungen gestützter peripherer Mechanismus vorgeschlagen, in dem die Reaktion außerhalb der äußeren Sphere stattfindet, in der Peripherie des Metallzentrums. Das Siliciumatom der am Eisen(II)-Zentrum gebundenen Silylgruppe agiert als LEWIS-Säure in der Carbonylaktivierung.

Der zweite Teil dieser Arbeit beschreibt Anwendungen von Rutheniumthiolatkomplexen in der katalytischen kooperativen Aktivierung von Hauptgruppenhydriden. Hierbei wurde die Reduktion von CO_2 mit Hydrosilanen, -boranen und -alanen ermöglicht. Die Hydrosilylierung liefert abhängig von der Reaktionstemperatur selektiv Bis(silyl)acetale bzw. silyliertes Methanol. Die Hydroborierung reduziert selektiv in die Methanol-oxidationsstufe. Die rutheniumthiolatkatalysierte Hydroaluminierung reduziert CO_2 bei Raumtemperatur mit Bevorzugung der Formaldehydoxidationsstufe.

Die Al-H-Bindungsaktivierung durch den Rutheniumthiolatkomplex fand in der defluorierenden FRIEDEL-CRAFTS-Alkylierung elektronenreicher Aromaten Anwendung. Die Reaktion verläuft bei Raumtemperatur unter Bildung der gewünschten Diarylmethane in guter Regioselektivität.

ABSTRACT

The first part of this thesis focuses on the mechanisms of metal-catalyzed main-group hydride activation reactions. The iridium(III) POCOP pincer complex introduced by BROOKHART was found to activate hydrosilanes as a LEWIS acid. The silyl group is transferred by S_N2 -Si mechanism as proposed and previously shown for boron LEWIS acids. However, the following hydride transfer was found to differ from the originally proposed mechanism. Control experiments unequivocally showed that the iridium dihydride assigned as the hydride donor was in fact reluctant to transfer a hydride to the carbon atom of the silylcarboxonium ion. Conversely, in the presence of excess hydrosilane the silylcarboxonium ion was readily reduced to the desired silyl ether. Combined spectroscopic and computational analysis identified new iridium trihydride complexes resulting from the coordination of excess hydrosilane to the iridium dihydride as the *de facto* hydride donors.

Investigation of the iron(0) SiNSi pincer complex-catalyzed hydrosilylation was revealed to proceed *via* an unprecedented mechanism. The iron(0) complex was found to act as a precatalyst forming the active iron(II) complex by oxidative addition of hydrosilane. A series of kinetic, stoichiometric, and deuterium-labelling experiments as well as the stereochemical course at a silicon-stereogenic hydrosilane excluded all traditional mechanisms. Supported by DFT calculations, a new peripheral mechanism is proposed where the reaction occurs beyond the outer-sphere at the periphery of the metal center. The silicon atom of the silyl group attached to the iron(II) center is found to act as a LEWIS acid, activating the carbonyl group.

The second part of this thesis describes applications of ruthenium thiolate complexes in the catalytic cooperative activation of main-group hydrides. The reduction of carbon dioxide is realized with hydrosilanes, hydroboranes, and hydroalanes. The hydrosilylation affords selectively bis(silyl)acetals or silylated methanol, depending on the reaction temperature. The hydroboration is selective for the reduction to the methanol oxidation state. Ruthenium thiolate-catalyzed hydroalumination reduces carbon dioxide at room temperature, favoring the formaldehyde oxidation state.

The Al-H bond activation by the ruthenium thiolate complex is used in the defluorinative FRIEDEL-CRAFTS alkylation of electron-rich arenes. The reaction proceeds readily at room temperature giving the desired diarylmethanes in good regioselectivity.

TABLE OF CONTENTS

TABLE OF CONTENTS

THEORETICAL PART I

1	INTRODUCTION	1
1.1	Mechanisms of Metal-Catalyzed Generation of Group 13 Electrophiles	3
1.1.1	Inner-Sphere Mechanisms	3
1.1.2	Outer-Sphere Mechanisms	13
1.2	Mechanisms of Metal-Catalyzed Generation of Group 14 Electrophiles	18
1.2.1	Inner-Sphere Mechanisms	18
1.2.2	Outer-Sphere Mechanisms	29
1.2.2.1	Cooperative Activation Mechanisms	29
1.2.2.2	LEWIS-Acid Activation Mechanisms	33
1.3	Objective	41
2	MECHANISTIC INVESTIGATION INTO BROOKHART'S IRIIDIUM(III) POCOP PINCER COMPLEX-CATALYZED CARBONYL HYDROSILYLATION	43
2.1	Introduction	43
2.2	Mechanistic Investigation into Iridium POCOP Pincer Complex- Catalyzed Carbonyl Carbonyl Hydrosilylation	47
2.2.1	Hydrosilylation Using Silicon-Stereogenic Hydrosilanes	47
2.2.2	Identification of the Hydride Source	50
3	MECHANISTIC INVESTIGATION INTO IRON(II) SiNSi PINCER COMPLEX- CATALYZED CARBONYL HYDROSILYLATION	65
3.1	Synthesis of Iron(0) SiNSi Pincer Complex and Application in the Carbonyl Hydrosilylation	65
3.2	Mechanistic Investigation into Iron SiNSi Pincer Complex-Catalyzed Carbonyl Hydrosilylation	66
4	SUMMARY	81

THEORETICAL PART II

5	CARBON DIOXIDE REDUCTION	85
5.1	Reduction of Carbon Dioxide into Formate Oxidation State	85
5.2	Reduction of Carbon Dioxide into Formaldehyde Oxidation State	87
5.3	Reduction of Carbon Dioxide into Methanol Oxidation State	90
5.4	Reduction of Carbon Dioxide into Methane	93
5.5	Summary	95
5.6	Ruthenium Thiolate-Catalyzed Hydrosilylation of Carbon Dioxide	95
6	FUNCTIONALIZATION OF C–F BONDS	101
6.1	Introduction	101
6.2	Catalytic Generation of Alumenium Ions by Cooperative Al–H Bond Activation in Defluorinative FRIEDEL–CRAFTS Alkylation	106
7	SUMMARY	115

EXPERIMENTAL PART

1	GENERAL INFORMATION	119
2	GENERAL PROCEDURES	129
2.1	General Procedure for the Hydrosilylation of Ketones Catalyzed by Brookhart's Iridium(III) Pincer Complex 73 ⁺ (GP1)	129
2.2	General Procedure for the Reductive Si–O Bond Cleavage of Silyl Ethers (GP 2)	129
2.3	General Procedure for the Stoichiometric Reaction of Iron(0) complex 124 with Hydrosilanes 23 (GP 3)	130
2.4	Carbon Dioxide Reduction (GP 4)	130
2.5	Ruthenium Thiolate-Catalyzed Hydrodefluorinative FRIEDEL–CRAFTS Alkylation (GP 5)	130

3	DESCRIPTION OF EXPERIMENTS	133
3.1	Mechanistic Investigations	133
3.1.1	Iridium(III) POCOP Pincer Complex-Catalyzed Carbonyl Hydrosilylation	133
3.1.2	Iron SiNSi Pincer Complex-Catalyzed Carbonyl Hydrosilylation	156
3.2	Applications of Catalytically Generated Main-Group Electrophiles	174
3.2.1	Hydrosilylation of Carbon Dioxide Catalyzed by Ruthenium Thiolate Complex	174
3.2.2	Catalytic Generation of Alumenium Ions by Cooperative Al–H Bond Activation in Defluorinative FRIEDEL–CRAFTS Alkylation	184

APPENDIX

A1	X-RAY CRYSTAL STRUCTURE DATA	193
A1.1	Molecular Structure of 107e	193
A1.2	Molecular Structure of 107a	194
A2	ABBREVIATIONS	195
A3	BIBLIOGRAPHY	199
A4	CURRICULUM VITAE	215

THEORETICAL PART I

MECHANISMS

1 INTRODUCTION

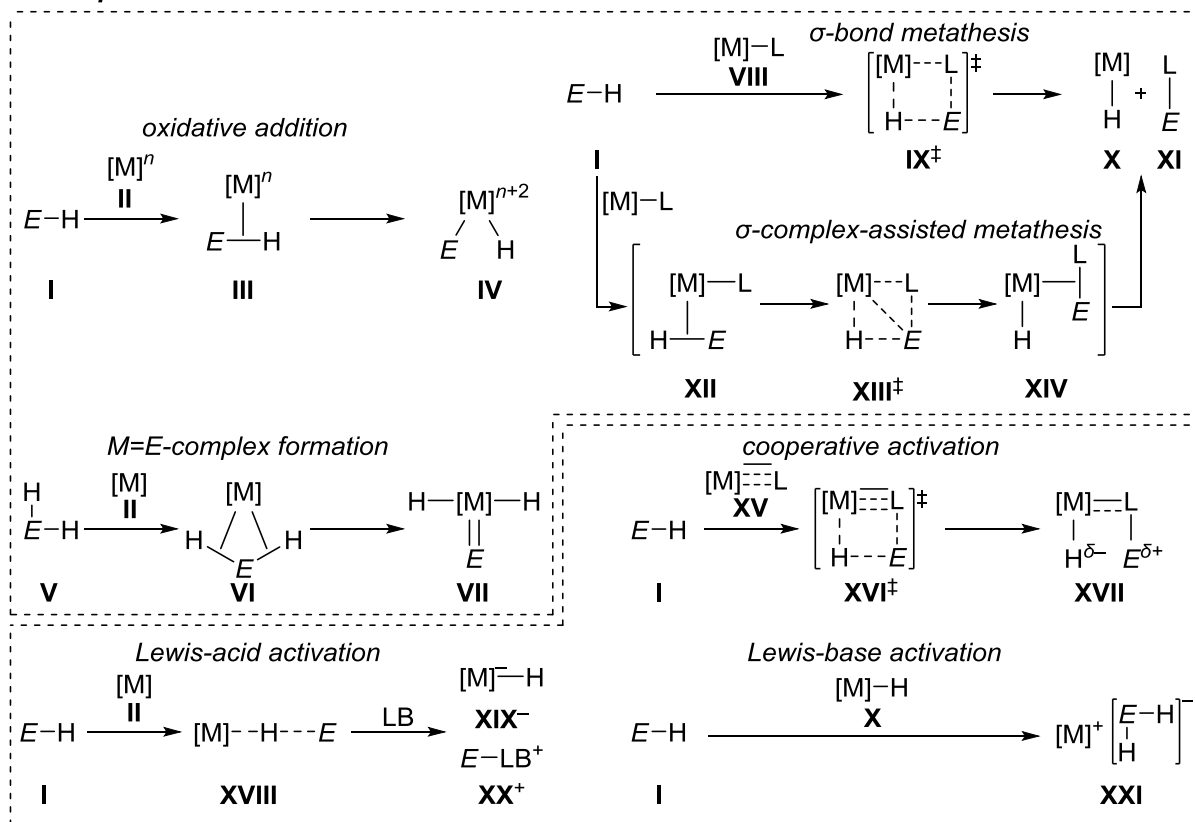
Metal-catalyzed generation of main-group electrophiles gives access to some of the most reactive intermediates at a synthetic chemists deposit.^[1,2] The ability to generate variety of highly electrophilic main-group LEWIS acids under mild catalytic conditions opens unique reactivity. The mechanisms of metal-catalyzed main-group hydride activation can be divided into two main categories according to the related dihydrogen activation mechanisms:^[3] inner- and outer-sphere (Scheme 1.1). In the inner-sphere mechanisms both the main-group element reagent and the substrate are in contact with the metal center whereas in the outer-sphere mechanisms only one of the two is directly in contact with the metal. A typical inner-sphere mechanism involves oxidative addition of the main-group hydride to the metal center ($I+II \rightarrow III \rightarrow IV$). Alternatively, dihydro compound **V** can undergo two consecutive oxidative additions to form an $M=E$ bond containing complex **VII**. σ -Bond metathesis mechanism involves the activation of $E-H$ bond *via* concerted four-centered transition state IX^\ddagger . Mechanisms including coordination of the substrates prior to the σ -bond metathesis ($XII \rightarrow XIII^\ddagger \rightarrow XIV$) are classified as σ -complex-assisted metathesis. The outer-sphere mechanisms typically involve ionic intermediates whereas the reactions occurring at the inner sphere of the metal are usually charge neutral.^[4] Cooperative activation of $E-H$ bonds *via* σ -bond metathesis-type transition state XVI^\ddagger gives metal hydride **XVII**. Coordination of main-group hydride **I** to a LEWIS-acidic metal complex **II** activates the main-group element for nucleophilic attack by a LEWIS-basic substrate (LB). Finally, the $E-H$ bond can be activated by LEWIS bases ($I+X \rightarrow XXI$).

[1] For the synthesis and reactivity of boron cations, see: a) K. Kölle, H. Nöth, *Chem. Rev.* **1985**, 85, 399–418; b) W. E. Piers, S. C. Bourke, K. D. Conroy, *Angew. Chem.* **2005**, 117, 5142–5163; *Angew. Chem. Int. Ed.* **2005**, 44, 5016–5036; for aluminum, gallium, and indium cations, see: c) D. A. Atwood, *Coord. Chem Rev.* **1998**, 176, 407–430.

[2] For the synthesis and reactivity of silylium ions, see: a) A. Schulz, A. Villinger, *Angew. Chem.* **2012**, 124, 4602–4604; *Angew. Chem. Int. Ed.* **2012**, 51, 4526–4528; b) H. F. T. Klare, M. Oestreich, *Dalton Trans.* **2010**, 39, 9176–9184; for germylum ions, see: c) A. Schäfer, M. Reißmann, S. Jung, A. Schäfer, W. Saak, E. Bredler, T. Müller, *Organometallics* **2013**, 32, 4713–4722; for stannylum ions, see: d) A. Schäfer, W. Saak, D. Haase, T. Müller, *J. Am. Chem. Soc.* **2011**, 133, 14562–14565; for selected reviews, see: e) V. Y. Lee, A. Sekiguchi, *Organometallic Compounds of Low-Coordinate Si, Ge, Sn and Pb*; Wiley, Chichester, **2010**; f) V. Y. Lee, A. Sekiguchi, *Acc. Chem. Res.* **2007**, 40, 410–419; g) T. Müller, *Adv. Organomet. Chem.* **2005**, 53, 155–215.

[3] a) O. Eisenstein, R. H. Crabtree, *New J. Chem.* **2013**, 37, 21–27; b) A. Comas-Vives, G. Ujaque, A. Lledós, *Adv. Inorg. Chem.* **2010**, 62, 231–260; c) R. M. Bullock, *Chem. Eur. J.* **2004**, 10, 2366–2374; d) R. Noyori, M. Yamakawa, S. Hashiguchi, *J. Org. Chem.* **2001**, 66, 7931–7944.

[4] M. Iglesias, F. J. Fernández-Alvarez, L. A. Oro, *ChemCatChem* **2014**, 6, 2486–2489.

inner-sphere mechanisms

Scheme 1.1: Classification of E–H bond activation mechanisms.

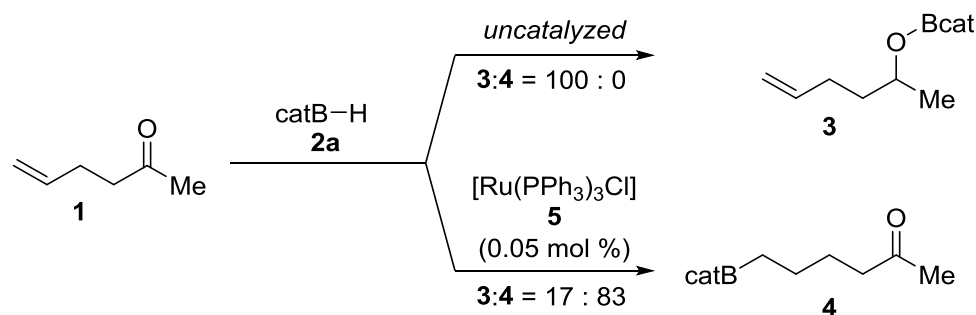
The following chapters give an overview of the various mechanisms of the E–H bond activation focusing on the catalytically relevant pathways. The majority of the detailed mechanistic investigations have been conducted regarding catalytic generation of silicon and boron electrophiles. Presumably due to scarce number of methodologies of the generation of other main-group electrophiles, the mechanisms for hydrogermane, -stannane, and -alane activation are not as well understood. Chapter 1.1 presents the established mechanisms of metal-catalyzed generation of group 13 electrophiles, focusing on hydroborane activation. The isolated examples of hydroalane activation will be mentioned together with analogous hydroborane mechanisms. In addition to hydroboranes, representative examples of mechanisms involving other sources of boron electrophiles are described. Chapter 1.2 centers around generation of silicon electrophiles and mainly on the activation of hydrosilanes. The hydrogermane and -stannane activation mechanisms are discussed together with their silicon counterparts.

1.1 Mechanisms of Metal-Catalyzed Generation of Group 13 Electrophiles

Organoboron reagents are widely used in organic chemistry.^[5] Metal-catalyzed activation of hydroboranes opens complementary reactivity to the stoichiometric and uncatalyzed reactions. The mechanisms of these transformations are often relatively well understood. In addition to boron, the availability and high reactivity made the use of aluminum reagents common in organic chemistry.^[6] However, most of the classic organoaluminum chemistry is stoichiometric and only a few metal-catalyzed reactions have been developed and the detailed mechanisms of these reactions are mostly unknown.

1.1.1 Inner-Sphere Mechanisms

In 1985 NÖTH investigated the hydroboration of alkenes in the presence of carbonyl groups.^[7] The hydroborane **2a** was shown to hydroborate the carbonyl group in an uncatalyzed reaction. Addition of 0.05 mol % WILKINSON's catalyst (**5**) gave **4** with good chemoselectivity, showing that the metal catalyst not only increases the reactivity of hydroboranes, but can also give access to complementary products (Scheme 1.2).



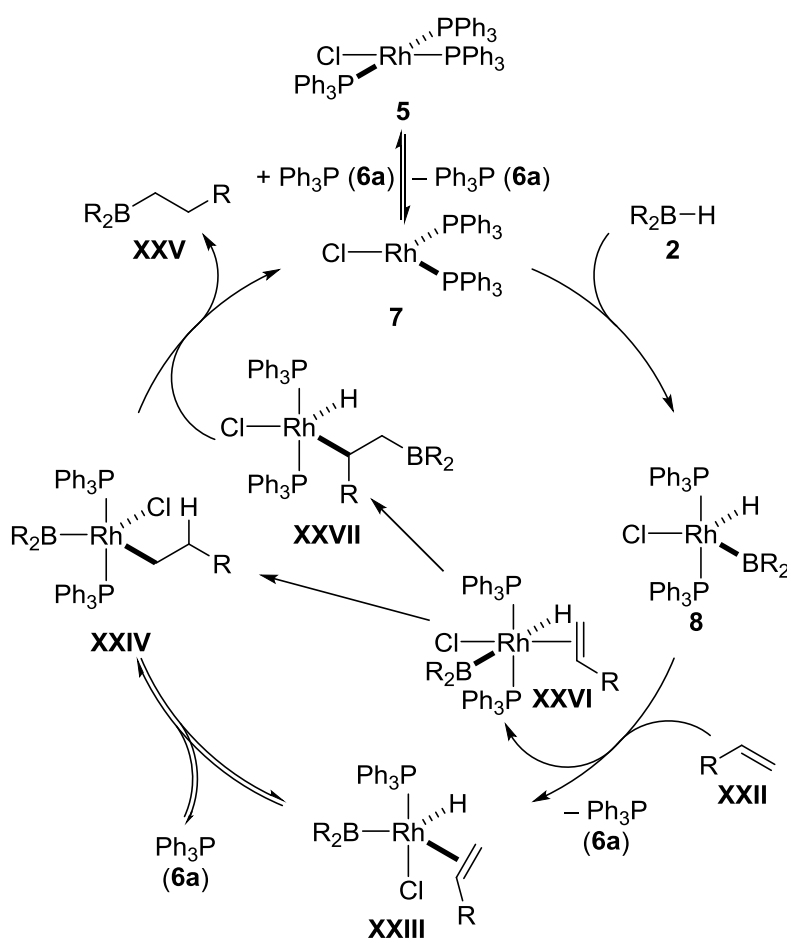
Scheme 1.2: Hydroboration of hex-5-en-2-one (**1**) with catecholborane (**2a**).

^[5] a) N. Miyaura, *Top. Curr. Chem.* **2002**, 219, 11–59; b) N. Miyaura, A. Suzuki, *Chem. Rev.* **1995**, 95, 2457–2483; c) A. Suzuki, *Acc. Chem. Rev.* **1982**, 15, 178–184; d) A. Pelter, *Chem. Soc. Rev.* **1982**, 11, 191–225

^[6] a) M. Dahlmann, M. Lautens in *Catalytic Heterofunctionalization* (Eds.: A. Togni, H. Grützmaier), Wiley-VCH, Chichester, **2001**; b) *Reduction by the Alumino- and Borohydrides in Organic Synthesis*, 2nd edition (Ed.: J. Seyden-Penne), Wiley-VCH, New York, **1997**.

^[7] D. Männing, H. Nöth, *Angew. Chem.* **1985**, 97, 854–855; *Angew. Chem. Int. Ed. Engl.* **1985**, 24, 878–879.

The mechanism of the reaction was proposed to initiate after dissociation of a phosphine ligand **6a** to afford complex **7** (Scheme 1.3). Oxidative addition of the hydroborane **2** to the rhodium(I) center gives the key intermediate **8**. Dissociation of a second phosphine ligand **6a** and coordination of the alkene followed by alkene insertion to the Rh–H bond and recoordination of the phosphine ligand leads to the alkyl complex (**8**→**XXIII**→**XXIV**). Reductive elimination releases the alkylborane **XXV** and the catalyst **7**. The mechanism was later supported by a careful mechanistic investigations by EVANS.^[8] Additionally, deuterium-labeling studies suggested that the insertion into the Rh–H bond is reversible (**XXIII** \rightleftharpoons **XXIV**).



Scheme 1.3: Proposed mechanisms of alkene hydroboration catalyzed by WILKINSON's catalyst.

^[8] a) D. A. Evans, G. C. Fu, *J. Org. Chem.* **1990**, 55, 2280–2282; b) D. A. Evans, G. C. Fu, B. A. Anderson, *J. Am. Chem. Soc.* **1992**, 114, 6679–6685.

The mechanistic studies by EVANS were later questioned by BURGESS, MARDER, and BAKER.^[9] The authors conducted a series of stoichiometric experiments, isolated several decomposition products, and repeated some of the deuterium-labeling experiments of EVANS. BURGESS, MARDER, and BAKER argued that the hydroboration catalyzed by WILKINSON's catalyst is significantly more complicated than proposed and that many of the decomposition products formed during the reaction might be catalytically active as well. The authors showed that the hydroborane **2a** used for the reaction was partially decomposed under the catalytic conditions forming highly reactive BH₃ (**2b**) that could also act as the reducing agent.^[10] Based on experiments with excess phosphine **6a**, a revised mechanism was proposed where the alkene insertion takes place without phosphine dissociation (**8**→**XXVI**→**XXIV**).

In addition to the experimental investigations, the reaction has also been studied computationally but no consensus has been reached by DFT calculations either.^[11] MOROKUMA carried out extensive calculations on all the proposed mechanisms and supported the associative mechanism in that the mechanism proceeding *via* **XXVI** was the lowest in energy. However, the insertion to the Rh–B bond (**XXVI**→**XXVII**) instead of Rh–H (**XXVI**→**XXIV**) was found to be the preferred mechanism.

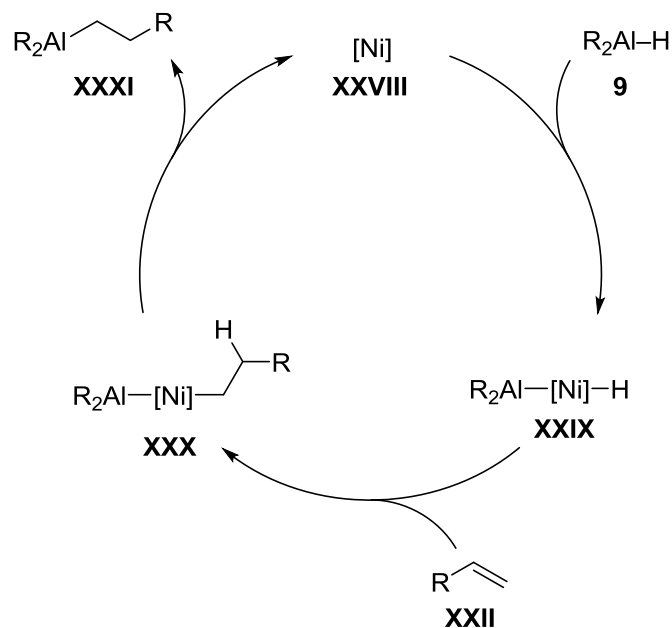
Nickel-catalyzed hydroalumination was proposed to proceed *via* an analogous mechanism (Scheme 1.4).^[12] The oxidative insertion of the hydroalane **9** to the nickel **XXVIII** gives the nickel(II) hydride **XXIX**. Alkene **XXII** insertion to the Ni–H bond followed by reductive elimination gives the hydroaluminated product **XXXI** and regenerates the nickel(0) **XXVIII**.

^[9] K. Burgess, W. A. van der Donk, S. A. Wescott, T. B. Marder, R. T. Baker, J. C. Calabrese, *J. Am. Chem. Soc.* **1992**, *114*, 9350–9359.

^[10] This so-called “Trojan-horse mechanism” was proposed for other hydroboration reactions: a) K. Burgess, M. Jaspars, *Tetrahedron Lett.* **1993**, *34*, 6813–6816; b) S. Harder, J. Spielmann, *J. Organomet. Chem.* **2012**, *698*, 7–14.

^[11] a) D. G. Musaev, A. M. Mebel, K. Morokuma, *J. Am. Chem. Soc.* **1994**, *116*, 10693–10702; b) A. E. Dorigo, P. von Ragué Schleyer, *Angew. Chem.* **1995**, *107*, 108–111; *Angew. Chem. Int. Ed. Engl.* **1995**, *34*, 115–118; c) C. Widauer, H. Grützmacher, T. Ziegler, *Organometallics* **2000**, *19*, 2097–2107.

^[12] a) J. J. Eisch, K. C. Fichter, *J. Am. Chem. Soc.* **1974**, *96*, 6815–6817; b) J. J. Eisch, S. R. Sexsmith, K. C. Fichter, *J. Organomet. Chem.* **1990**, *382*, 273–293; c) J. J. Eisch, X. Ma, M. Singh, G. Wilke, *J. Organomet. Chem.* **1997**, *527*, 301–304.



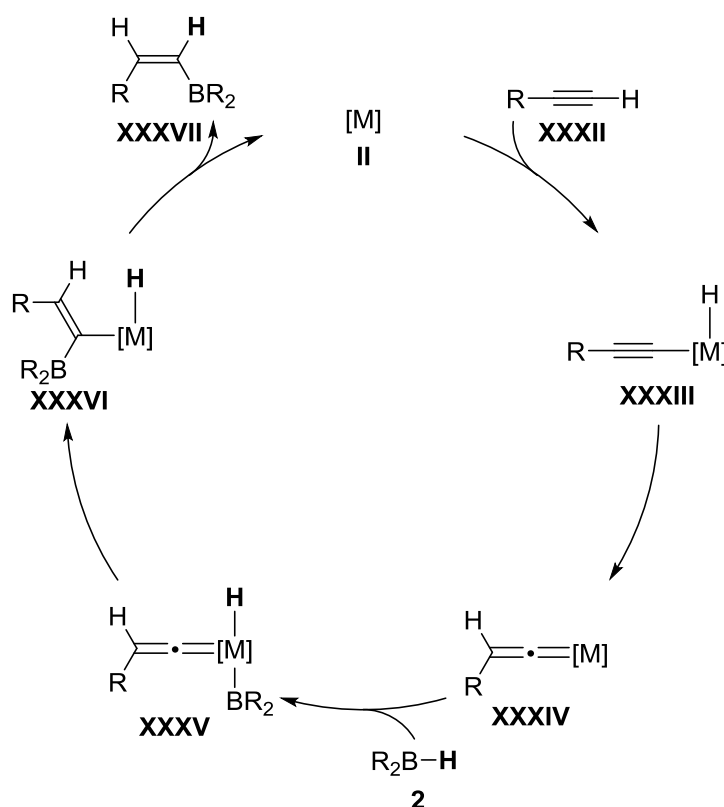
Scheme 1.4: Nickel-catalyzed hydroalumination of alkenes.

Hydroboration of alkynes typically occurs stereospecifically in *syn*-fashion through similar mechanisms as proposed for alkenes.^[13] In 2000 MIYAURA presented a rhodium-catalyzed method to selectively obtain (*E*)-vinyl boranes through a proposed vinylidene intermediate **XXXIV** (Scheme 1.5).^[14] The insertion of the metal center to the alkynyl $\text{C}_{\text{sp}}-\text{H}$ bond and isomerization gives the vinylidene complex **XXXIV**. Following oxidative addition of hydroborane, 1,2-boryl migration and reductive elimination furnish the (*E*)-vinyl borane (**XXXV**→**XXXVI**→**XXXVII**). The catalytic system reported by MIYAURA required stoichiometric base to inhibit the conventional *syn*-hydroboration. In 2012, LEITNER overcame this restriction by a PCNCP ruthenium pincer complex that allowed for the synthesis of the *E*-vinyl borane **XXXVII** without added base. The proposed mechanism was complementary to the MIYAURA mechanism.^[15]

^[13] I. Beletskaya, A. Pelter, *Tetrahedron* **1997**, 53, 4957–5026.

^[14] T. Ohmura, Y. Yamamoto, N. Miyaura, *J. Am. Chem. Soc.* **2000**, 122, 4990–4991.

^[15] C. Gunanathan, M. Hölscher, F. Pan, W. Leitner, *J. Am. Chem. Soc.* **2012**, 134, 14349–14352.

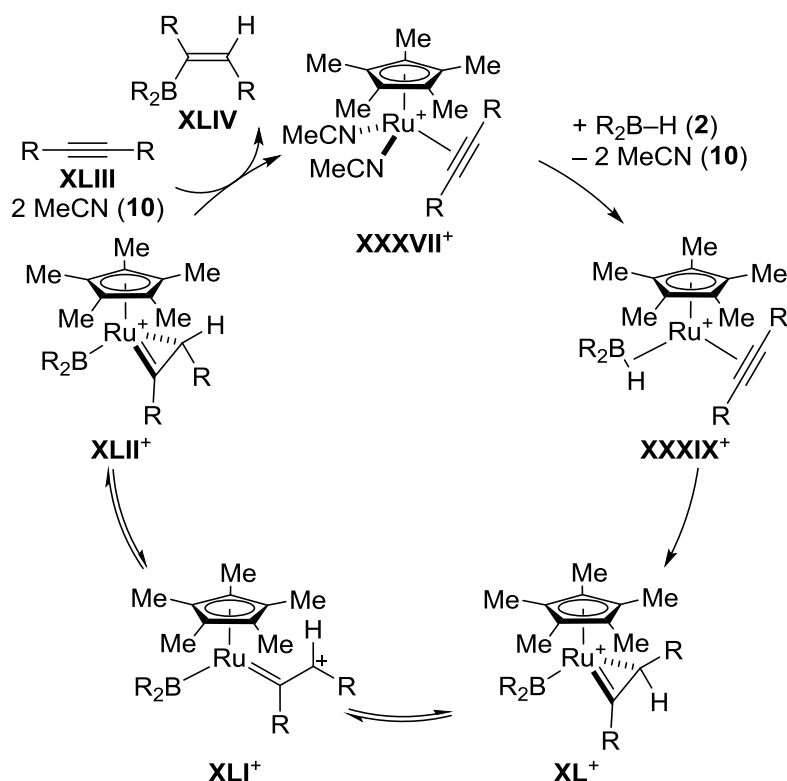


Scheme 1.5: Formal *trans*-hydroboration via a vinylidene intermediate ([M] = [RhCl(*i*Pr₃P)_{*n*}]).

As evident by the mechanism in Scheme 1.5, the methods reported by MIYAUURA and LEITNER are limited to terminal alkynes. The *trans*-hydroboration of internal alkynes reported by FÜRSTNER^[16,17] could not proceed *via* the vinylidene intermediate **XXXIV** and a new mechanism was proposed to explain the observed selectivity (Scheme 1.6). The alkyne was proposed to coordinate to the cationic ruthenium center replacing one of the acetonitrile (**10**) ligands. Dissociation of two more acetonitriles and coordination of hydroborane gives complex **XXXIX**⁺. Hydride transfer from boron to the alkyne carbon leads to the formation of ruthenacyclopropene **XL**⁺. To release the steric stress between the R group and the Cp* ligand isomerization through a carbene intermediate **XLI**⁺ is proposed. Reductive elimination from the sterically favored ruthenacyclopropene isomer **XLII**⁺ gives the *trans*-borylated alkene **XLIV**.

^[16] B. Sundararaju, A. Fürstner, *Angew. Chem.* **2013**, 125, 14300–14304; *Angew. Chem. Int. Ed.* **2013**, 52, 14050–14054.

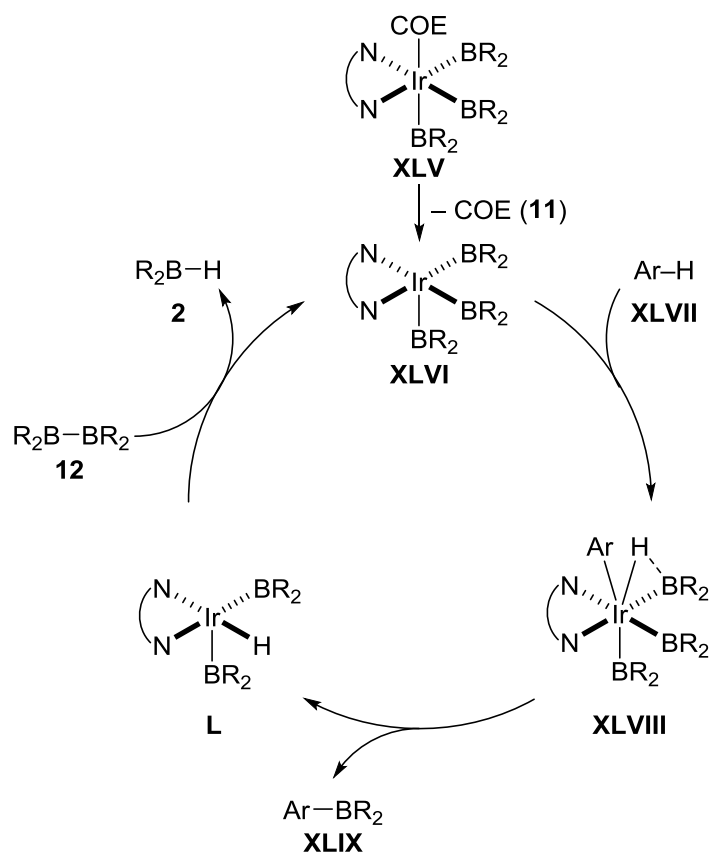
^[17] The proposed mechanism is similar to the TROST–WU mechanism of *trans*-hydrosilylation of alkynes (Scheme 1.19).



Scheme 1.6: Ruthenium-catalyzed *trans*hydroboration of internal alkynes (counteranion PF_6^- omitted for clarity).

The iridium-catalyzed borylation of C–H bonds developed by ISHIYAMA, MIYAURA, and HARTWIG has emerged as one of the most efficient ways to build C–B bonds.^[18] The reaction is proposed to start with the dissociation of the cyclooctene ligand (Scheme 1.7, **XLV**→**XLVI**). The revealed highly reactive iridium center will then undergo oxidative addition to the C–H bond (**XLVI**→**XLVIII**). The C–H bond cleavage has been proposed to be assisted by the boryl group at the metal center. Reductive elimination of the borylated product **XLIX** gives complex **L**. Finally, addition of diborane **12** and elimination of hydroborane **2** regenerate the active catalyst **XLVI**.

^[18] a) T. Ishiyama, J. Takagi, K. Ishida, Miyaura, N. R. Anastasi, J. F. Hartwig, *J. Am. Chem. Soc.* **2002**, *124*, 390–391; b) T. M. Boller, J. M. Murphy, M. Hapke, T. Ishiyama, N. Miyaura, J. F. Hartwig, *J. Am. Chem. Soc.* **2005**, *127*, 14263–14278; for reviews of C–H bond borylation, see: c) I. A. I. Mkhalid, J. H. Barnard, T. B. Marder, J. M. Murphy, J. F. Hartwig, *Chem. Rev.* **2010**, *110*, 890–931; d) J. F. Hartwig, *Chem. Soc. Rev.* **2011**, *40*, 1992–2002.

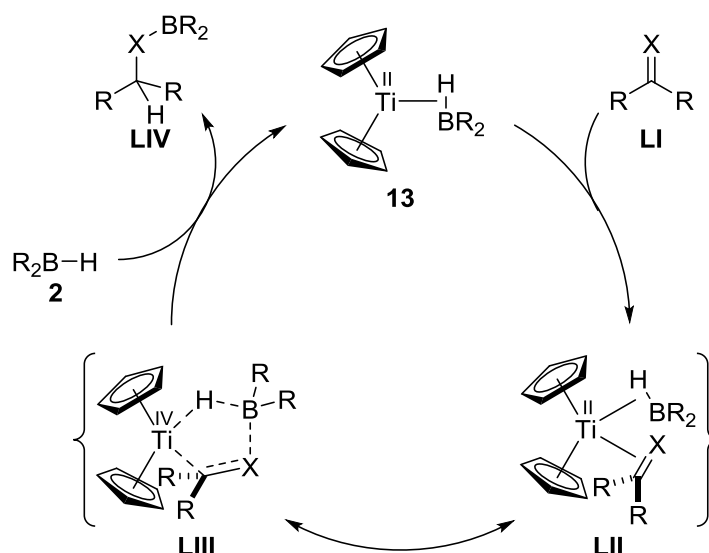


Scheme 1.7: Mechanism of C–H bond borylation proposed by ISHIYAMA, MIYAURA, and HARTWIG [COE (**11**) = cyclooctene].

Titanocene complexes **13** were shown to hydroborate alkenes and alkynes^[19] as well as ketones and imines (Scheme 1.8).^[20] The mechanism involves simultaneous activation of the hydroborane and the substrate *via* the intermediate {**LII**↔**LIII**}. The key reaction intermediate was proposed to be a resonance structure between the Ti(II) σ -complex **LII** and the Ti(IV) metallacycle **LIII**. Reductive elimination of the hydroborated substrate **LIV** is followed by the coordination of hydroborane **2** to give **13**.

^[19] a) C. N. Muhoro, X. He, J. F. Hartwig, *J. Am. Chem. Soc.* **1999**, 121, 5033–5046; b) J. F. Hartwig, C. N. Muhoro, *Organometallics* **2000**, 19, 30–38.

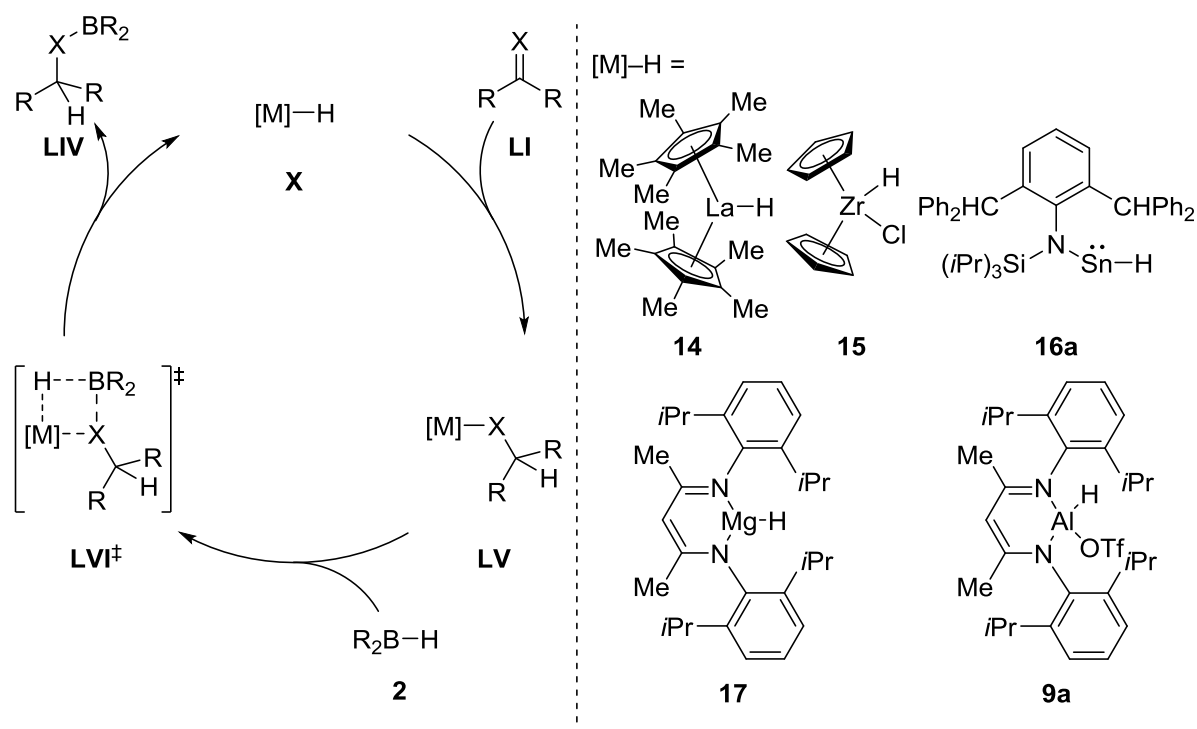
^[20] A. A. Oluyadu, S. Ma, C. N. Muhoro, *Organometallics* **2012**, 32, 70–78.



Scheme 1.8: Mechanism of titanocene(II)-catalyzed hydroboration ($X = \text{CH}_2, \text{O}, \text{NR}$).

Metal centers that are unable or reluctant to undergo oxidative addition/reductive elimination sequences often react *via* the σ -bond metathesis mechanism (Scheme 1.9).^[21] The fundamental step includes the insertion of the unsaturated substrate to the metal hydride **X** to give the intermediate **LV**. The following concerted σ -bond metathesis (**LVI**[‡]) between M–O and B–H bonds yields the hydroborated substrate **LIV** concomitantly with the metal hydride **X**.

^[21] For La–H, see: a) K. N. Harrison, T. J. Marks, *J. Am. Chem. Soc.* **1992**, *114*, 9220–9221; for Zr–H, see: b) S. Pereira, M. Srebnik, *Organometallics* **1995**, *14*, 3127–3128; for Ti, see c) X. He, J. F. Hartwig, *J. Am. Chem. Soc.* **1996**, *118*, 1696–1702; d) for Mg–H, see: M. Arrowsmith, T. J. Hadlington, M. S. Hill, G. Kociok-Köhn, *Chem. Commun.* **2012**, *48*, 4567–4569; for Sn–H and Ge–H, see: e) T. J. Hadlington, M. Hermann, G. Frenking, C. Jones, *J. Am. Chem. Soc.* **2014**, *136*, 3028–3031; for a review of σ -bond metathesis, see: f) R. Waterman, *Organometallics* **2013**, *32*, 7249–7263.

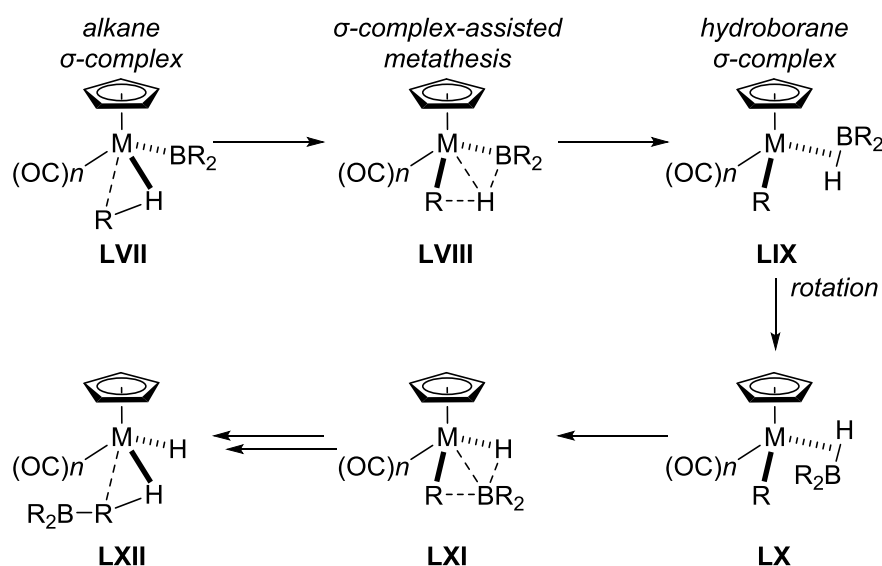


Scheme 1.9: σ -Bond metathesis mechanism ($X = O, CH_2$).

An interesting, related mechanism to the σ -bond metathesis is the so-called σ -complex-assisted metathesis (σ -CAM).^[22] This unusual mechanism is exemplified by the alkane borylation by HARTWIG (Scheme 1.10).^[23] The alkane was shown to coordinate to the metal center forming the σ -complex **LVII**. The following σ -bond metathesis transition state leads into the borane σ -complex **LIX**. Hydroborane rotation and a second σ -complex-assisted metathesis give the product (**LX**→**LXI**→**LXII**). The key distinction between a normal σ -bond metathesis and the σ -CAM is that σ -bond metathesis is preceded and followed by two separate molecules whereas in the σ -CAM all the reacting partners remain coordinated to the metal center throughout the reaction.

^[22] R. N. Perutz, S. Sabo-Etienne, *Angew. Chem.* **2007**, *119*, 2630–2645; *Angew. Chem. Int. Ed.* **2007**, *46*, 2578–2592.

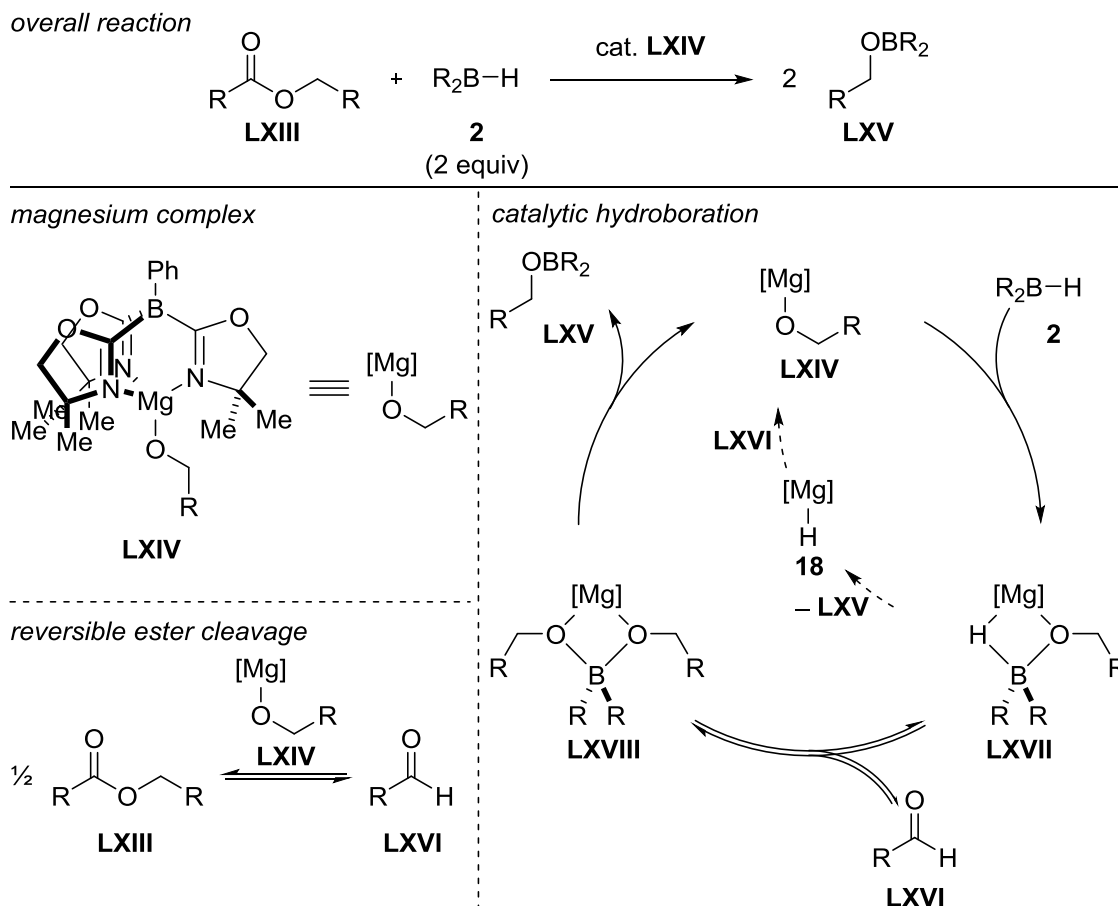
^[23] C. E. Webster, Y. Fan, M. B. Hall, D. Kunz, J. F. Hartwig, *J. Am. Chem. Soc.* **2003**, *125*, 858–859.



Scheme 1.10: σ -Complex-assisted metathesis mechanism (M = Fe, W).

Hydroboration of esters **LXIII** catalyzed by magnesium complex **LXIV** was investigated by the group of SADOW (Scheme 1.11).^[24] Detailed kinetic analysis revealed that the reaction was zero order in the hydroborane and half order in the ester excluding the expected σ -bond metathesis mechanism. Additionally, stoichiometric experiments indicated reversible TISHCHENKO-type cleavage of the ester **LXIII** into two equivalents of aldehyde **LXVI**. To explain the unexpected rate law, the authors proposed that the released aldehyde **LXVI** inserts to the Mg–H bond of **LXVII** to give the intermediate **LXVIII**. Product **LXV** dissociation regenerates the magnesium alkoxide. The alternative product formation directly from the intermediate **LXVII** via the magnesium hydride **18** would not agree with the zero order on $[\text{R}_2\text{B-H}]$.

^[24] D. Mukherjee, A. Ellern, A. D. Sadow, *Chem. Sci.* **2014**, 5, 959–964.

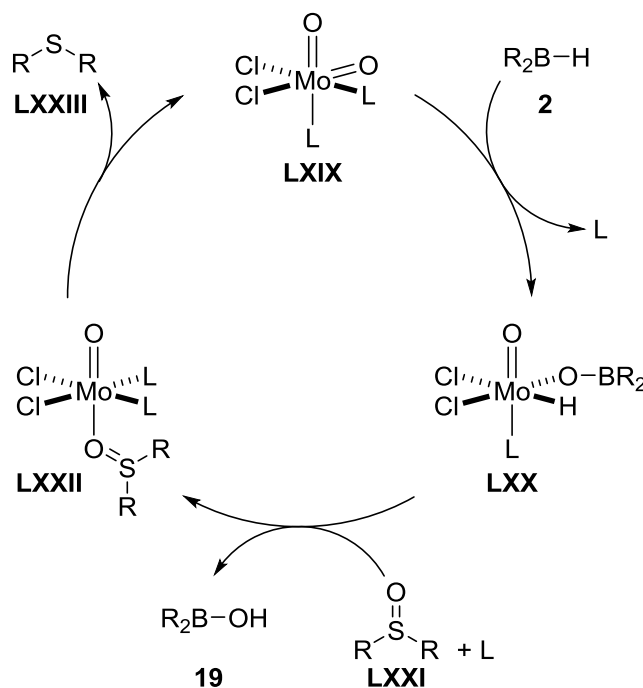


Scheme 1.11: Magnesium-catalyzed hydroboration of esters.

1.1.2 Outer-Sphere Mechanisms

High-valent metal oxo-complexes have been shown to be able to activate hydroboranes *via* an unusual $[2\sigma+2\pi]$ addition across the $[\text{M}]=\text{O}$ bonds (Scheme 1.12).^[25] Activation of hydroborane **2** by the molybdenum complex **LXIX** gives the intermediate **LXX**. The molybdenum hydride **LXX** reductively eliminates the borinic acid **19** and coordinates the sulfoxide **LXXI**. Deoxygenation of the sulfoxide produces the sulfide **LXXIII** and regenerates the molybdenum oxo-complex **LXIX**.

^[25] a) A. C. Fernandes, C. C. Romão, *Tetrahedron Lett.* **2007**, 48, 9176–9179; b) A. C. Fernandes, J. A. Fernandes, F. A. Almeida Paz, C. C. Romão, *Dalton Trans.* **2008**, 6686–6688; c) S. C. A. Sousa, I. C. Cabrita, A. C. Fernandes, *Chem. Soc. Rev.* **2012**, 41, 5641–5653.



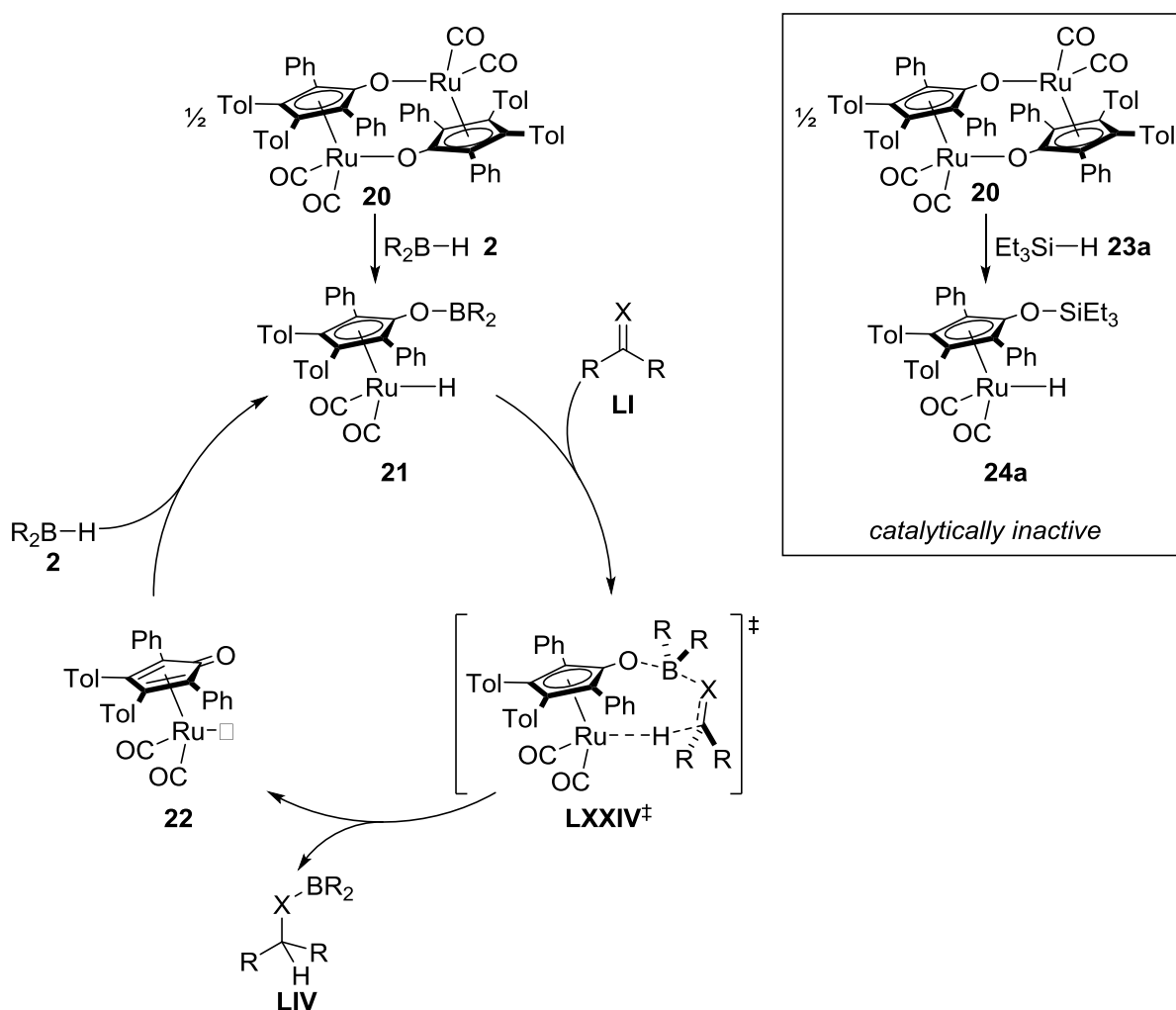
Scheme 1.12: Molybdenum oxo-complex-catalyzed deoxygenation of sulfoxides with hydroboranes.

Despite the success in dihydrogen activation, the cooperative activation of E–H bonds has not attracted attention until recently.^[26] SHVO's catalyst is one of the most successful catalysts in cooperative hydrogenation.^[27] This complex was not utilized in E–H bond activation until 2009 when CLARK and coworkers were able to show that the complex **20** was able to catalyze hydroboration of aldehydes, imines, and ketones (Scheme 1.13).^[28] The mechanism of the reaction was suggested to be analogous to the corresponding hydrogenation mechanism. The cooperative hydroborane activation gives the complex **21**. Concerted hydroboration (LXXIV^\ddagger) releases the product **LIV** and gives the unsaturated complex **22**. Activation of B–H bond regenerates the active catalyst **21**.

[26] For recent reviews, see: a) J. R. Knusnutdinova, D. Milstein, *Angew. Chem.* **2015**, 127, 12406–12445; *Angew. Chem. Int. Ed.* **2015**, 54, 12236–12273; b) M. Trincado, H. Grützmacher in *Cooperative Catalysis* (Ed.: R. Peters), Wiley-VCH, Weinheim, **2015**, p. 67–110.

[27] B. L. Conley, M. K. Pennington-Boggio, E. Boz, T. J. Williams, *Chem. Rev.* **2010**, 110, 2294–2312.

[28] L. Koren-Selfridge, H. N. Londino, J. K. Vellucci, B. J. Simmons, C. P. Casey, T. B. Clark, *Organometallics* **2009**, 28, 2085–2090.



Scheme 1.13: Cooperative hydroboration catalyzed by SHVO's catalyst analog **20** ($X = O, NR$).

Interestingly, the authors also tried to use the catalyst **20** for Si–H bond activation. Although the catalyst was found to activate triethylsilane **23a**, the silylated complex **24a** was found to be catalytically inactive in the hydrosilylation of aldehydes.^[29]

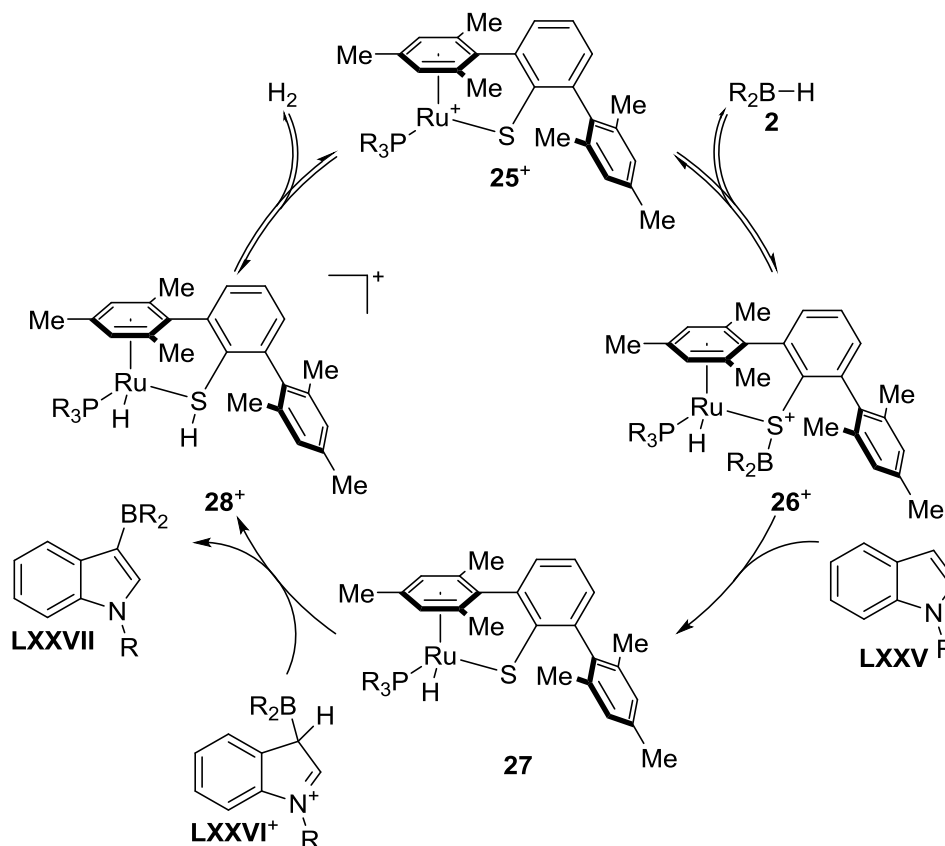
OHKI, TATSUMI, and OESTREICH have shown that the ruthenium thiolate complex **25**⁺ used originally for dihydrogen activation^[30] and later for hydrosilane activation (see Scheme 1.30) catalyzes also electrophilic dehydrogenative borylation of nitrogen heterocycles (Scheme 1.14).^[31] The cooperative hydroborane activation was supported by careful NMR analysis as

^[29] C. P. Casey, S. W. Singer, D. R. Powell, R. K. Hayashi, M. Kavana, *J. Am. Chem. Soc.* **2001**, *123*, 1090–1100.

^[30] Y. Ohki, Y. Takikawa, H. Sadohara, C. Kesenheimer, B. Engendahl, E. Kapatina, K. Tatsumi, *Chem. Asian. J.* **2008**, *3*, 1625–1635.

^[31] T. Stahl, K. Mütther, Y. Ohki, K. Tatsumi, M. Oestreich, *J. Am. Chem. Soc.* **2013**, *135*, 10978–10981.

well as X-ray crystal structure of **26⁺**. The activated boryl group of **26⁺** is attacked by the nucleophilic indole C-3 carbon. The resulting WHELAND intermediate **LXXVI⁺** is deprotonated by the ruthenium hydride **27** to furnish the borylated indole **LXXVII** and the dihydrogen adduct **28⁺**. Release of dihydrogen regenerates the active ruthenium catalyst **25⁺**.

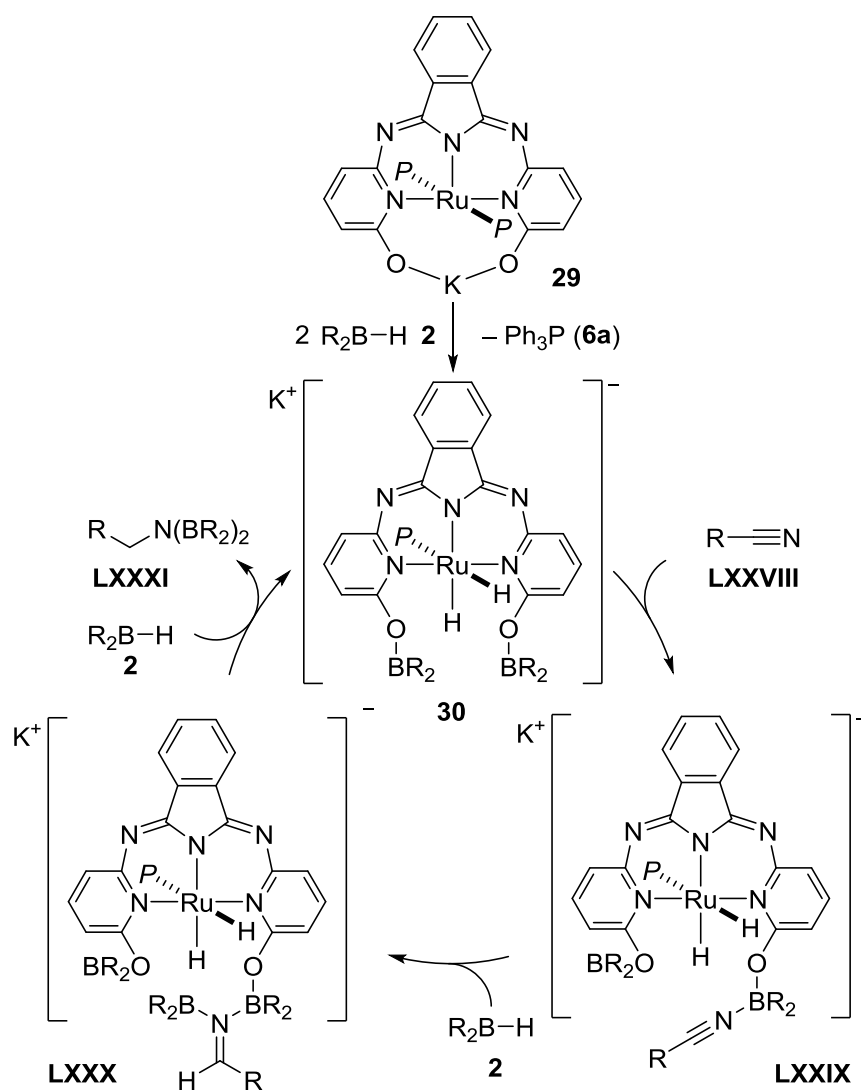


Scheme 1.14: Ruthenium thiolate **25⁺**-catalyzed borylation of indoles (counteranion $\text{BAR}_4^{\text{F}_4^-}$ omitted for clarity).

The anionic NNN ruthenium pincer complex **29** was utilized in nitrile hydroboration (Scheme 1.15).^[32] The mechanism proposed by SZYMCAK is initiated by borylation of the precatalyst **29** to the complex **30**. The borinic esters were proposed to form LEWIS pairs with the nitrile **LXXVIII**. Outer-sphere hydride and boryl transfer gives the intermediate **LXXX** with the imine still coordinated to the boron. A second hydroboration produces the bisborylated amine **LXXXI** and the active catalyst **30**. Interestingly, it is not clear if the ruthenium center is actively involved in the catalytic cycle after the initial hydroboration (**29**→**30**). Through the rest of the catalytic cycle the substrate is being activated by the LEWIS-acidic boron atom and

^[32] J. B. Geri, N. K. Szymczak, *J. Am. Chem. Soc.* **2015**, 137, 12808–12814.

the experimental evidence could not reveal whether the subsequent hydroborations occur stepwise, assisted by the ruthenium, or *via* concerted additions of hydroboranes.^[33]



Scheme 1.15: Cooperative hydroborane activation proposed by SZYMCAK ($P = Ph_3P$).

^[33] The mechanism where the ruthenium center remains a bystander during the active catalytic cycle, could be defined as a peripheral mechanism (*vide infra*).

1.2 Mechanisms of Metal-Catalyzed Generation of Group 14 Electrophiles

Hydrosilanes are usually relatively inert air- and moisture-stable liquids. Nevertheless, the Si–H bond is readily activated to give formally a hydride and a silicon cation.^[34] The ease of handling, relatively low toxicity, and high reactivity in metal-catalyzed reactions has made hydrosilanes attractive reagents, not just as hydrogen surrogates in reduction chemistry but also in the synthesis of various organosilicon compounds. The continuous demand for efficient hydrosilylation processes has spurred numerous mechanistic investigations of these transformations. The chemistry of hydrogermanes remains less developed but according to the known examples, their reactivities and mechanisms are often comparable to their silicon counterparts.^[35] Unlike with most hydrosilanes and hydrogermanes,^[36] the Sn–H bond of hydrostannanes are readily cleaved homolytically to form tin-centered radicals.^[37] The high toxicity of hydrostannanes and the tendency to react *via* radical pathways have abated the wide use of tin electrophiles.

1.2.1 Inner-Sphere Mechanisms

Early mechanistic investigations of metal-catalyzed hydrosilylation reactions focused on the industrially important hydrosilylation of alkenes. The first detailed mechanism involving Si–H bond activation was reported in 1965 by CHALK and HARROD (Scheme 1.16).^[38] The authors investigated platinum-catalyzed hydrosilylation of alkenes and proposed a mechanism where the hydrosilane **23** first oxidatively adds to the metal center **II** to give silyl hydride complex **LXXXII**. Migratory insertion of the alkene **LXXXIII** to the metal hydride gives silyl alkyl complex **LXXXV** which releases the desired product **LXXXVI** *via* reductive elimination.

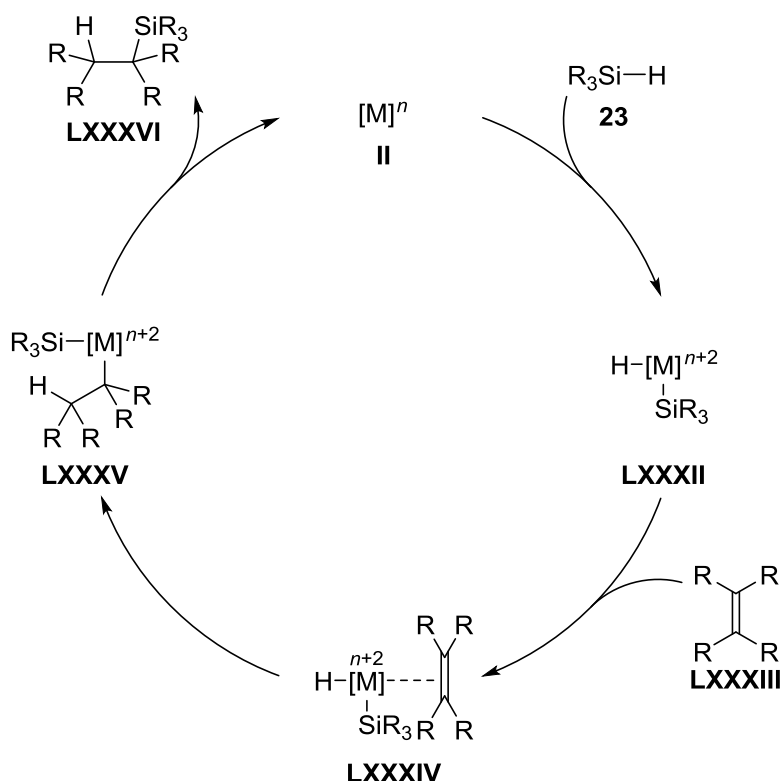
^[34] a) *The Chemistry of Organic Silicon Compounds*, Vol. 3 (Eds.: Z. Rappoport, Y. Apeloig), Wiley, Chichester, **2001**; b) *The Chemistry of Organic Silicon Compounds*, Vol. 2 (Eds.: Z. Rappoport, Y. Apeloig), Wiley, Chichester, **1998**; c) *The Chemistry of Organic Silicon Compounds* (Eds.: S. Patai, Z. Rappoport), Wiley, Chichester, **1989**.

^[35] *The chemistry of organic germanium, tin and lead compounds*, Vol. 1 (Ed.: S. Patai), Wiley, Chichester, **1995**.

^[36] C. Chatgililoglu, *Chem. Rev.* **1995**, 95, 1229–1251

^[37] N. D. Smith, J. Mancuso, M. Lautens, *Chem. Rev.* **2000**, 100, 3257–3282.

^[38] A. J. Chalk, J. F. Harrod, *J. Am. Chem. Soc.* **1965**, 87, 16–21.



Scheme 1.16: CHALK-HARROD mechanism of the hydrosilylation of alkenes.

CHALK-HARROD-type mechanisms have also been proposed in the palladium-catalyzed hydrogermylation of alkynes^[39] and copper-catalyzed hydrostannylation of alkynes.^[40]

Later, a so-called modified CHALK-HARROD mechanism was proposed where the order of events is changed such that the Si-C bond is formed first (Scheme 1.17, **LXXXVIII**→**LXXXIX**).^[41] The following reductive elimination of the alkyl hydride releases the product **XC**.^[42] The same initial intermediate **LXXXIX** can lead to two other distinct products as well.^[43,44] In the dehydrogenative mechanism, a β -hydride elimination takes place giving

^[39] H. Konoshita, T. Nakamura, H. Kakiya, H. Shinokubo, S. Matsubara, K. Oshima, *Org. Lett.* **2001**, 3, 2521–2524.

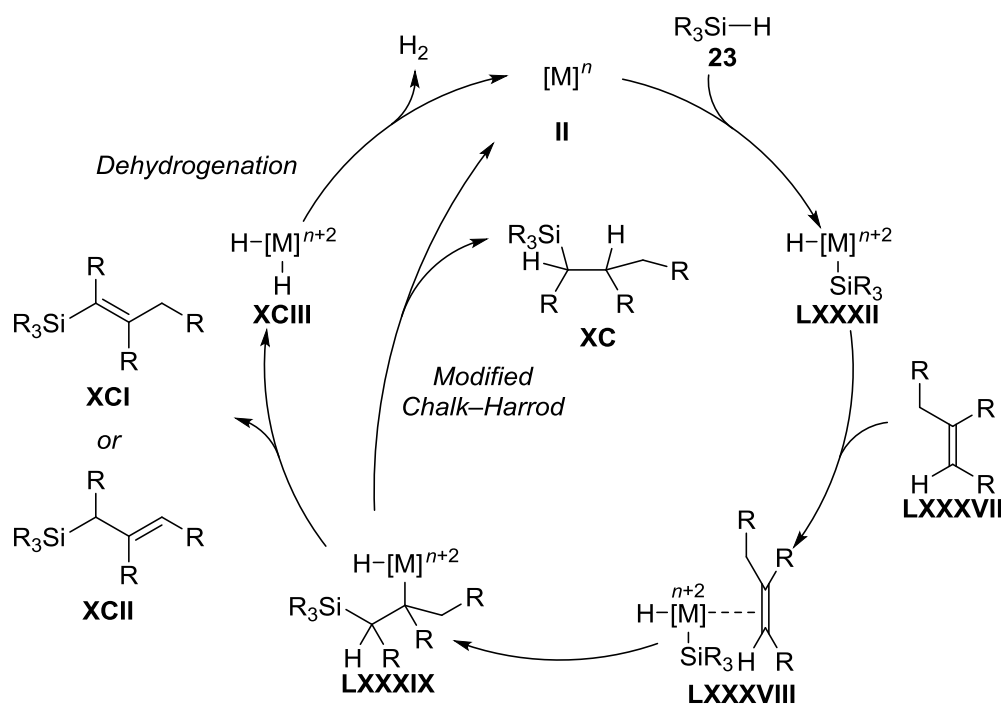
^[40] L. T. Leung, S. K. Leung, P. Chiu, *Org. Lett.* **2005**, 7, 5249–5252.

^[41] a) M. A. Schroeder, M. S. Wrighton, *J. Organomet. Chem.* **1977**, 128, 345–358; b) C. L. Reichel, M. S. Wrighton, *Inorg. Chem.* **1980**, 19, 3858–3860; c) C. L. Randolph, M. S. Wrighton, *J. Am. Chem. Soc.* **1986**, 108, 3366–3374.

^[42] For comparative computational analysis of CHALK-HARROD and the modified CHALK-HARROD mechanisms, see: a) S. Sakaki, N. Mizoe, M. Sugimoto, *Organometallics* **1998**, 17, 2510–2523; b) G. Giorgi, F. De Angelis, N. Re, A. Sgamellotti, *Fut. Gen. Comp. Syst.* **2004**, 20, 781–791.

^[43] For early examples of dehydrogenative silylation of alkenes, see: a) A. Millan, E. Towns, P. M. Maitlis, *J. Chem. Soc., Chem. Commun.* **1981**, 673–674; b) F. Seitz, M. S. Wrighton, *Angew.*

vinyllic or allylic silanes (**XCI** or **XCII**, respectively) and dihydrogen complex **XCIII**. Formal reductive elimination of dihydrogen closes the catalytic cycle.^[45] Often mixtures of **XC**, **XCI**, and **XCII** can be seen, indicating that several mechanistic pathways are operating at the same time.



Scheme 1.17: Modified CHALK-HARROD mechanism including the formation of vinyllic and allylic silanes *via* dehydrogenation.

The palladium-catalyzed hydrostannylation and hydrogermylation reactions investigated by OSHIMA were also proposed to proceed *via* the modified CHALK-HARROD-type mechanism.^[46] A related mechanism has been proposed by GEVORGYAN in the hydrosilylation, -germylation, -stannylation as well as distannylation and silastannylation of reactive cyclopropenes **XCIV**

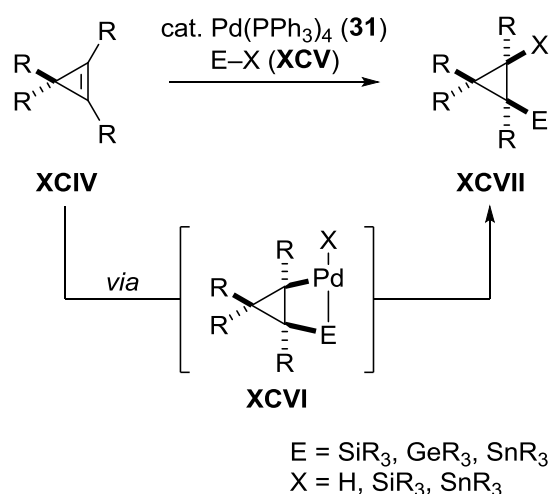
Chem. **1988**, 100, 281–283; *Angew. Chem. Int. Ed. Engl.* **1988**, 27, 289–291; c) M. R. Kesti, R. M. Waymouth, *Organometallics* **1992**, 11, 1095–1103, for recent examples of selective synthesis of vinyllic or allylic silanes, see: d) J. R. McAtee, S. E. S. Martin, D. T. Ahneman, K. A. Johnson, D. A. Watson, *Angew. Chem.* **2012**, 124, 3723–3727; *Angew. Chem. Int. Ed.* **2012**, 51, 3663–3667 (vinyllic silanes using R_3Si-I); e) J. R. McAtee, G. P. A. Yap, D. A. Watson, *J. Am. Chem. Soc.* **2014**, 136, 10166–10172 (allylic silanes using R_3Si-I); f) C. C. H. Atienza, T. Diao, K. J. Weller, S. A. Nye, K. M. Lewis, J. G. P. Delis, J. L. Boyer, A. K. Roy, P. J. Chirik, *J. Am. Chem. Soc.* **2014**, 136, 12108–12118 (allylic silanes using R_3Si-H).

[44] For dehydrogenative germylation, see: N. Furukawa, N. Kurogi, Y. Seki, *Organometallics* **1999**, 18, 3764–3767. Although no mechanism was provided, the reaction is likely to proceed *via* a similar mechanism as shown here for the dehydrogenative silylation.

[45] Often a sacrificial dihydrogen acceptor is required for efficient turnover.

[46] Y. Ichinose, H. Oda, K. Oshima, K. Utimoto, *Bull. Chem. Soc. Jpn.* **1987**, 60, 3468–3470.

(Scheme 1.18).^[47] Exclusive *syn*-addition was observed in all cases and the insertion takes place at the sterically less hindered face via intermediate **XCVI**.



Scheme 1.18: Palladium-catalyzed functionalization of cyclopropenes.

The hydrosilylation of alkynes typically proceeds *via* CHALK–HARROD or modified CHALK–HARROD-type mechanisms leading to exclusive *syn*-silylation (Scheme 1.19, **XCIX**→**C**).^[48] Unusual *trans*-hydrosilylation was first reported in 1981 by NILE.^[49] The rhodium-catalyzed formation of the (*E*)-vinylsilanes **CIV** was explained by isomerization *via* a carbene intermediate **CI** (Scheme 1.19). TANKE and CRABTREE reported a similar reactivity using iridium catalysts.^[50] The authors did not find the carbene **CI** as a feasible intermediate but proposed the reversible formation of the metallacyclopentene **CII** instead as the isomerization pathway.

TROST investigated the hydrosilylation of alkynes and found that ruthenium complexes **32**⁺ and **33**⁺ gave unusual MARKOVNIKOV products.^[51] In addition, control reactions with deuterium-labeled hydrosilanes showed that the hydrosilylation occurs in an *anti*-fashion. To explain the observed selectivity, TROST and WU also proposed carbene **CI** or

^[47] A. Trofimov, M. Rubina, M. Rubin, V. Gevorgyan, *J. Org. Chem.* **2007**, 72, 8910–8920.

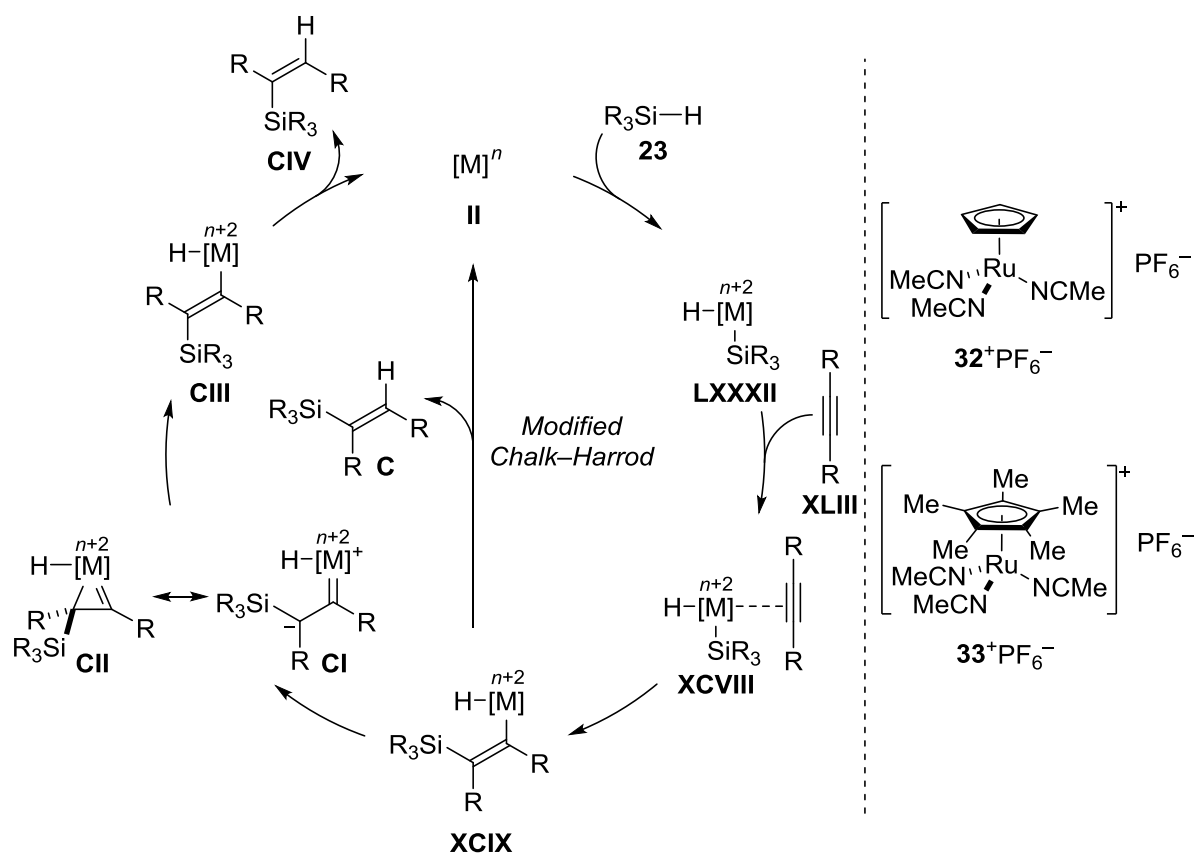
^[48] B. Marciniec in *Hydrosilylation. A Comprehensive Review on Recent Advances* (Ed. B. Marciniec), Springer, Netherlands, **2009**, p. 53–86.

^[49] K. A. Brady, T. A. Nile, *J. Organomet. Chem.* **1981**, 206, 299–304.

^[50] R. S. Tanke, R. H. Crabtree, *J. Am. Chem. Soc.* **1990**, 112, 7984–7989.

^[51] a) B. M. Trost, Z. T. Ball, *J. Am. Chem. Soc.* **2001**, 123, 12726–12727; b) B. M. Trost, Z. T. Ball, *J. Am. Chem. Soc.* **2002**, 125, 30–31.

ruthenacyclopropene **CII** as the intermediate leading to the isomerization of the alkene intermediate.^[52]

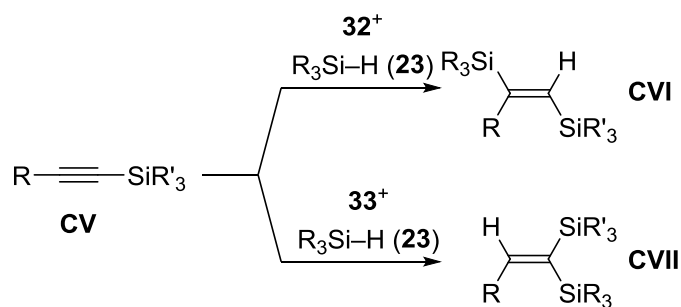


Scheme 1.19: Mechanism of *trans*-selective hydrosilylation of alkynes.

In 2013, WU demonstrated that silyl-substituted alkynes could be hydrosilylated through an *anti*-MARKOVNIKOV *syn*-addition with the complex 32^+ or through MARKOVNIKOV *anti*-addition with the complex 33^+ (Scheme 1.20).^[53] The switch in the selectivity was explained by the relative stability of the intermediates during the isomerization through the intermediate **CII**.

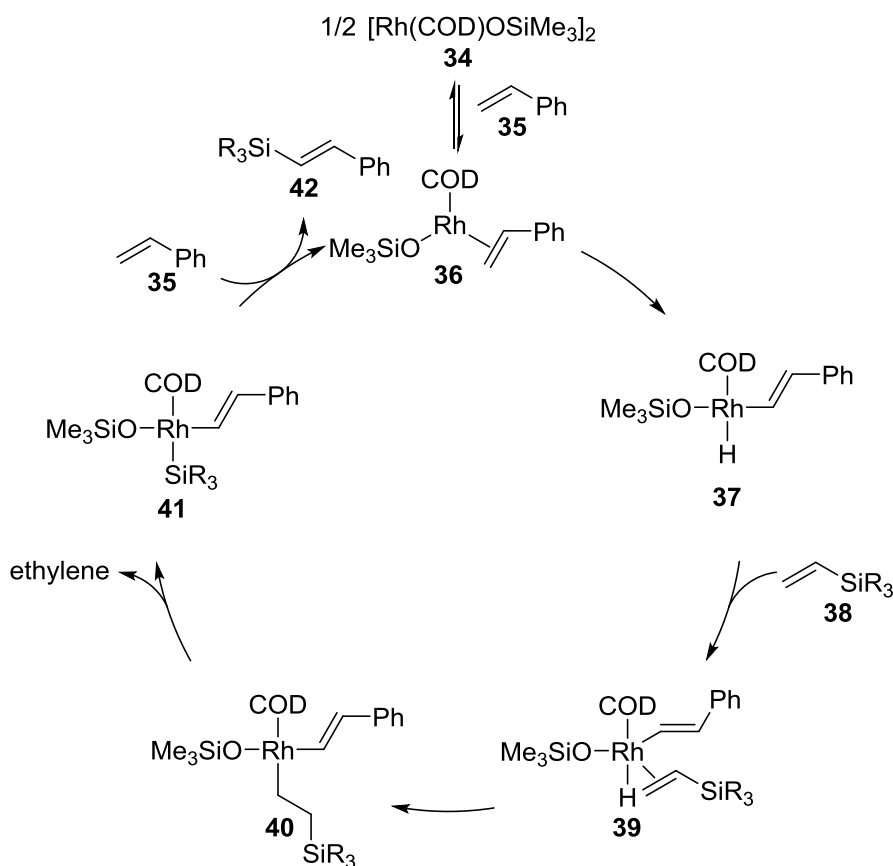
^[52] L. W. Chung, Y.-D. Wu, B. M. Trost, Z. T. Ball, *J. Am. Chem. Soc.* **2003**, *125*, 11578–11582.

^[53] S. Ding, L.-J. Song, L. W. Chung, X. Zhang, J. Sun, Y.-D. Wu, *J. Am. Chem. Soc.* **2013**, *135*, 13835–13842.



Scheme 1.20: Regio- and stereodivergent hydrosilylation of alkynes by Wu.

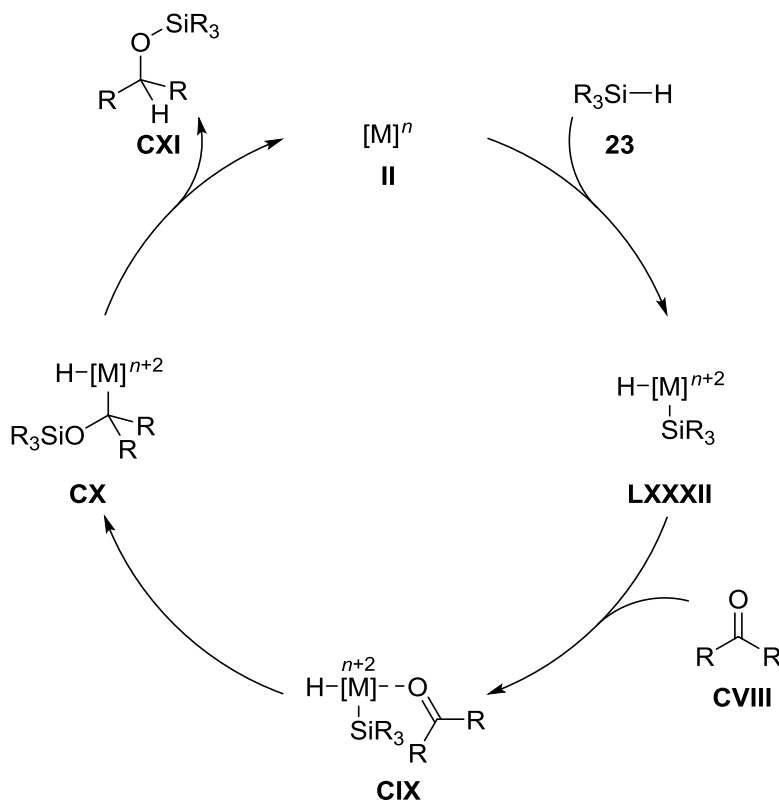
The C- sp^2 silylation of styrene **35** developed by MARCINIEC allows the functionalization with vinylsilanes **38** (Scheme 1.21).^[54] The proposed mechanism begins with oxidative addition of the alkene C–H bond to the metal center forming the intermediate **37**. Following vinylsilane coordination (**39**), and insertion to the metal hydride gives the complex **40**. The β -silyl elimination releases ethylene to form the silyl complex **41**. Finally, a reductive elimination releases the (*E*)- β -silyl styrene **42**.



Scheme 1.21: Rhodium-catalyzed silylation of alkenes (COD = 1,5-cyclooctadiene).

^[54] B. Marciniec, E. Walczuk-Guściora, C. Pietraszuk, *Organometallics* **2001**, 20, 3423–3428.

The hydrosilylation mechanism of carbonyl groups was first studied by OJIMA. The authors proposed that the mechanism would be similar to the modified CHALK–HARROD mechanism (Scheme 1.22, **II**→**LXXXII**). Coordination of the oxygen atom to the metal center (**CIX**) followed by silyl transfer gives intermediate **CX** which releases the silyl ether **CXI** via reductive elimination.^[55]



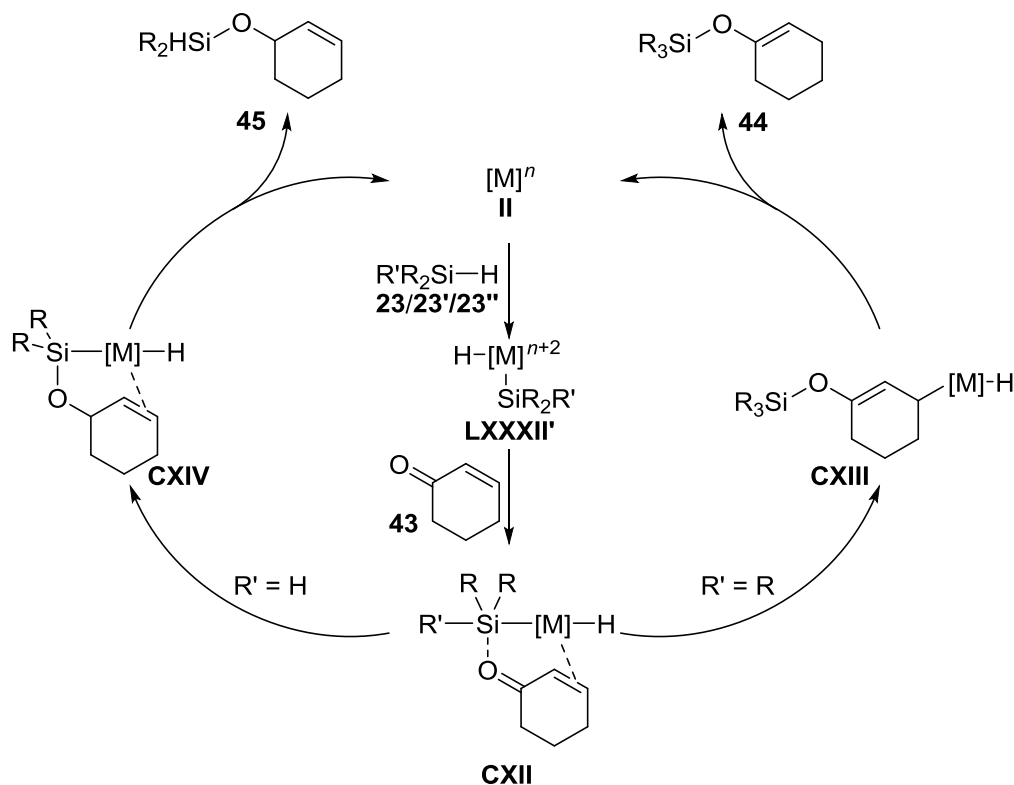
Scheme 1.22: Mechanism of carbonyl hydrosilylation proposed by OJIMA.

The rhodium-catalyzed hydrosilylation of α,β -unsaturated carbonyl compounds was investigated by CHAN (Scheme 1.23).^[56] Monohydrosilanes **23** were found to give selective 1,4-reduction while di- and trihydrosilanes **23'**/**23''** gave 1,2-reduction. The observed change in selectivity could not be explained with the OJIMA mechanisms, hence an alternative mechanism was proposed. After the initial oxidative addition of the hydrosilane (**II**→**LXXXII'**), the oxygen atom of the carbonyl group coordinates to the silicon atom and not to the rhodium center of the complex to give **CXII**. In the case of monohydrosilane the rhodium center then undergoes allylic transposition to give intermediate **CXIII**. Reductive elimination

^[55] a) I. Ojima, M. Nihonyanagi, T. Kogure, M. Kumagai, S. Horiuchi, K. Nakatsugawa, Y. Nagai, *J. Organomet. Chem.* **1975**, 94, 449–461; b) I. Ojima, T. Kogure, M. Kumagai, S. Horiuchi, T. Sato, *J. Organomet. Chem.* **1976**, 122, 83–97.

^[56] G. Z. Zheng, T. H. Chan, *Organometallics* **1995**, 14, 70–79.

releases the silyl enol ether **44** and regenerates the catalyst **II**. With di- or trihydrosilanes **23'**/**23''** the intermediate **CXII** can lead to hydride transfer from the silyl group to the carbon center of the carbonyl (**CXIV**). The reductive elimination of the hydrosilane releases the 1,2-reduced silyl ether **45** and the catalyst **II**.^[57]

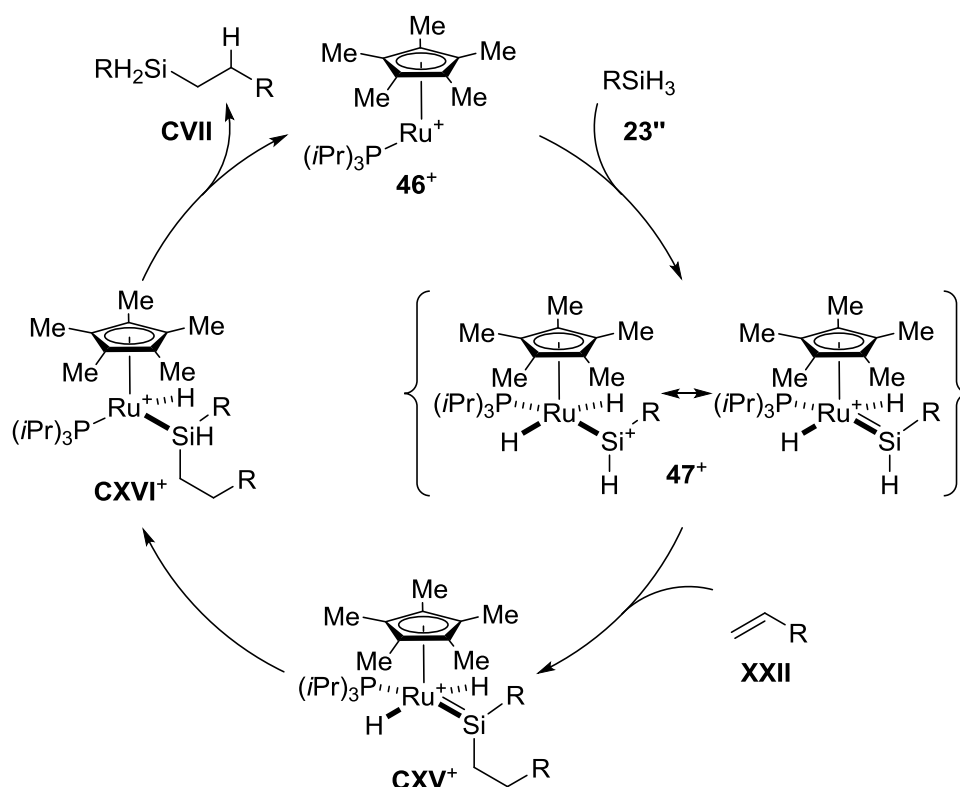


Scheme 1.23: Mechanism of 1,2- and 1,4-hydrosilylation of α,β -unsaturated carbonyl compounds.

The ability of di- and trihydrosilanes **23'**/**23''** to form silylene complexes with transition metal centers gives access to highly reactive complexes. In 2003, TILLEY and GLASER reported the ruthenium silylene complex-catalyzed hydrosilylation of alkenes (Scheme 1.24).^[58] Based on the exclusive *anti*-MARKOVNIKOV selectivity, a new mechanism was proposed. The silylene hydride group **47⁺** is proposed to directly add to the alkene **XXII** in a concerted $[2\sigma+2\pi]$ -cycloaddition to give **CXV⁺**. Hydride migration from the ruthenium to the silicon atom followed by reductive elimination releases the product **CVII** and the ruthenium catalyst **46⁺**.

^[57] The mechanism with di- and trihydrosilanes could in fact be considered as an outer-sphere mechanism.

^[58] a) P. B. Glaser, T. D. Tilley, *J. Am. Chem. Soc.* **2003**, *125*, 13640–13641; b) M. A. Rankin, D. F. MacLean, G. Schatte, R. McDonald, M. Stradiotto, *J. Am. Chem. Soc.* **2007**, *129*, 15855–15864.



Scheme 1.24: Hydrosilylation of alkenes *via* a silylene complex **47⁺** (counteranion $B(C_6F_5)_4^-$ omitted for clarity).

A similar silylene mechanism was adapted by HOFMANN, GADE, and co-workers in the rhodium-catalyzed hydrosilylation of ketones.^[59]

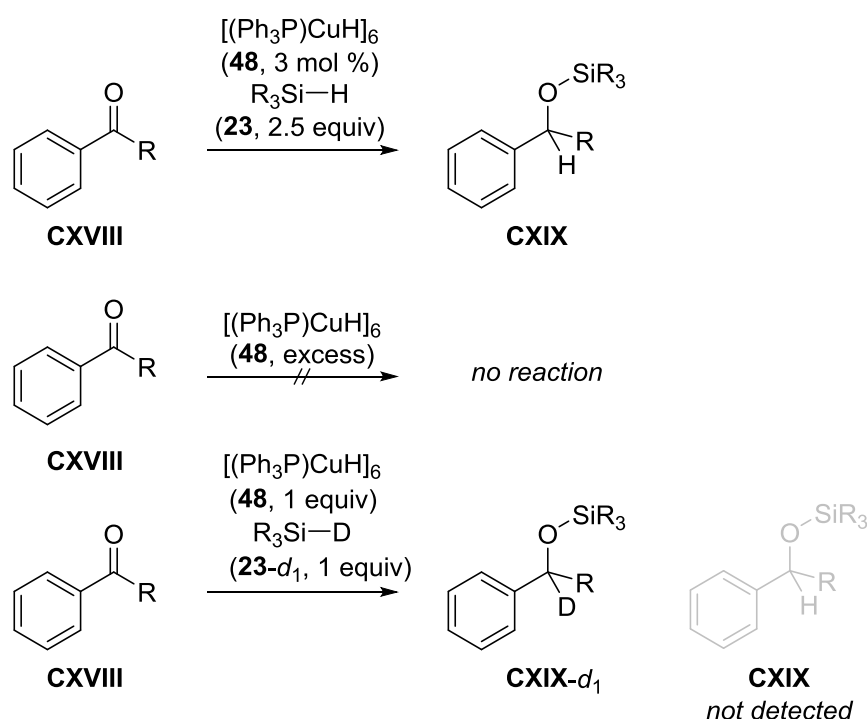
As with hydroborations the majority of the hydrosilylation reactions catalyzed by early transition metals operate by a σ -bond metathesis mechanism. Typically in these mechanisms a metal hydride reduces the carbonyl to form a metal alkoxide. Following σ -bond metathesis between the M–O and Si–H bonds releases the product and regenerates the metal hydride analogous to the σ -bond metathesis mechanism with hydroboranes (Scheme 1.9).^[60]

The σ -bond metathesis mechanism has been widely studied and generally accepted for many early transition metals. However, some of these reactions have been questioned. The copper hydride-catalyzed hydrosilylation of carbonyls was assumed to proceed *via* a σ -bond

^[59] N. Schneider, M. Finger, C. Haferkemper, S. Bellemin-Laponnaz, P. Hofmann, L. H. Gade, *Angew. Chem.* **2009**, 121, 1637–1641; *Angew. Chem. Int. Ed.* **2009**, 48, 1609–1613.

^[60] S. Rendler, M. Oestreich in *Modern Reduction Methods* (Eds.: P. G. Andersson, I. J. Munslow), Wiley-VCH, Weinheim, **2008**, p. 183–207.

metathesis mechanism.^[61] The stoichiometric control experiments by LIPSHUTZ^[62] and NIKONOV^[63] have shown that an alternative mechanism might be in effect (Scheme 1.25). When ketone **CXVIII** was treated with stoichiometric amounts of STRYKER's reagent **48** in the absence of hydrosilane **23**, no conversion was observed. Meanwhile, a stoichiometric experiment between copper hydride **48**, deuterium-labeled hydrosilane **23-d₁**, and carbonyl compound **CXVIII** led to exclusive deuterium incorporation at the methine position of the silyl ether **CXIX-d₁**. Despite these results against the σ -bond metathesis, no conclusive alternative mechanism has been proposed.^[64]



Scheme 1.25: Inconclusive mechanistic experiments questioning the σ -bond metathesis mechanism.

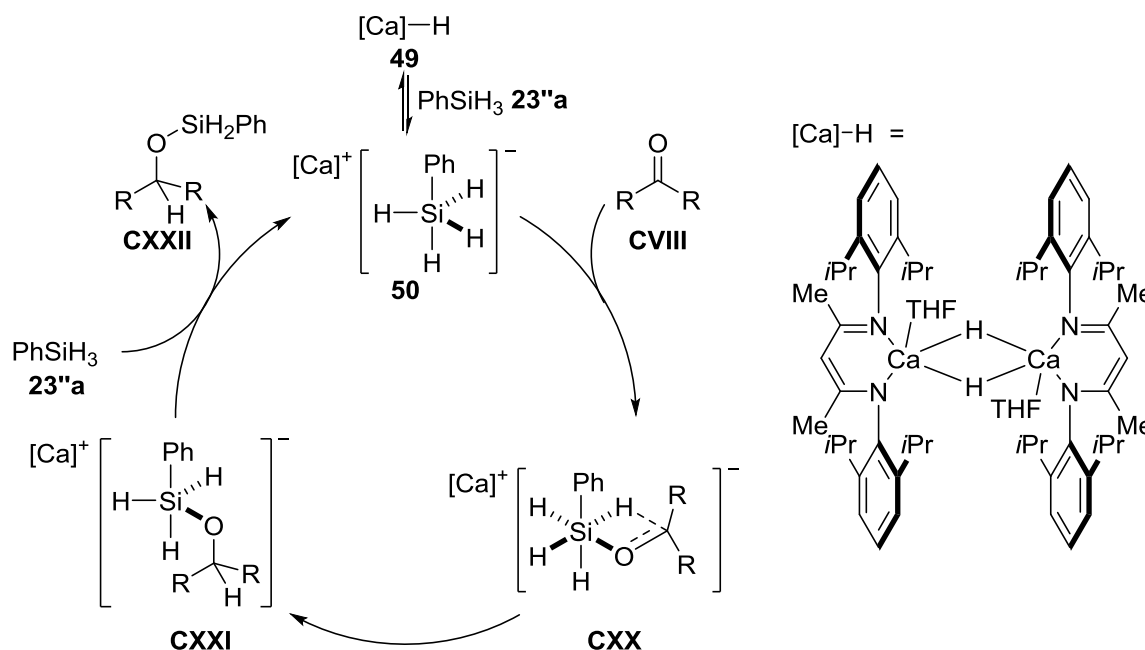
^[61] a) B. H. Lipshutz, W. Chrisman, K. Noson, *J. Organomet. Chem.* **2001**, 624, 367–371; the related dehydrogenative silylation of alcohols has been shown to proceed via a σ -bond metathesis mechanism, see: b) H. Ito, T. Ishizuka, T. Okumura, H. Yamanaka, J.-i. Tateiwa, M. Sonoda, A. Hosomi, *J. Organomet. Chem.* **1999**, 574, 102–106; c) S. Rendler, G. Auer, M. Oestreich, *Angew. Chem.* **2005**, 117, 7793–7797; *Angew. Chem. Int. Ed.* **2005**, 44, 7620–7624; d) S. Rendler, O. Plefka, B. Karatas, G. Auer, R. Fröhlich, C. Mück-Lichtenfeld, S. Grimme, M. Oestreich, *Chem. Eur. J.* **2008**, 14, 11512–11528.

^[62] B. H. Lipshutz, K. Noson, W. Chrisman, A. Lower, *J. Am. Chem. Soc.* **2003**, 125, 8779–8789.

^[63] O. G. Shirobokov, L. G. Kuzmina, G. I. Nikonov, *J. Am. Chem. Soc.* **2011**, 133, 6487–6489.

^[64] LIPSHUTZ proposed a silyl cuprate as the active catalyst, whereas NIKONOV proposed that the copper center would activate the carbonyl as a LEWIS acid. For more proposed mechanisms, see: a) Ref. [61b]; b) C. R. Waidmann, L. A. Silks, R. Wu, J. C. Gordon, *Catal. Sci. Technol.* **2013**, 3, 1240–1245.

The calcium hydride **49**-catalyzed hydrosilylation was proposed to proceed *via* the formation of a hypervalent silyl hydride **50** (Scheme 1.26).^[65] The addition of the extra hydride to the silicon center increases the LEWIS acidity of the silicon.^[66] The concerted hydride transfer *via* six-coordinated silicon intermediate **CXX** gives the silyl ether **CXXI**. The product **CXXII** is released after hydride transfer to a second trihydrosilane **23''a**.



Scheme 1.26: Proposed mechanism of calcium hydride-catalyzed hydrosilylation of ketones.

As with hydroboranes, σ -complex-assisted metathesis-type reaction have been proposed for hydrosilanes as well (see Scheme 1.10). Likewise, these processes have only been observed *in silico* and direct experimental evidence has not been obtained yet.^[22,67]

^[65] J. Spielmann, S. Harder, *Eur. J. Inorg. Chem.* **2008**, 1480–1486.

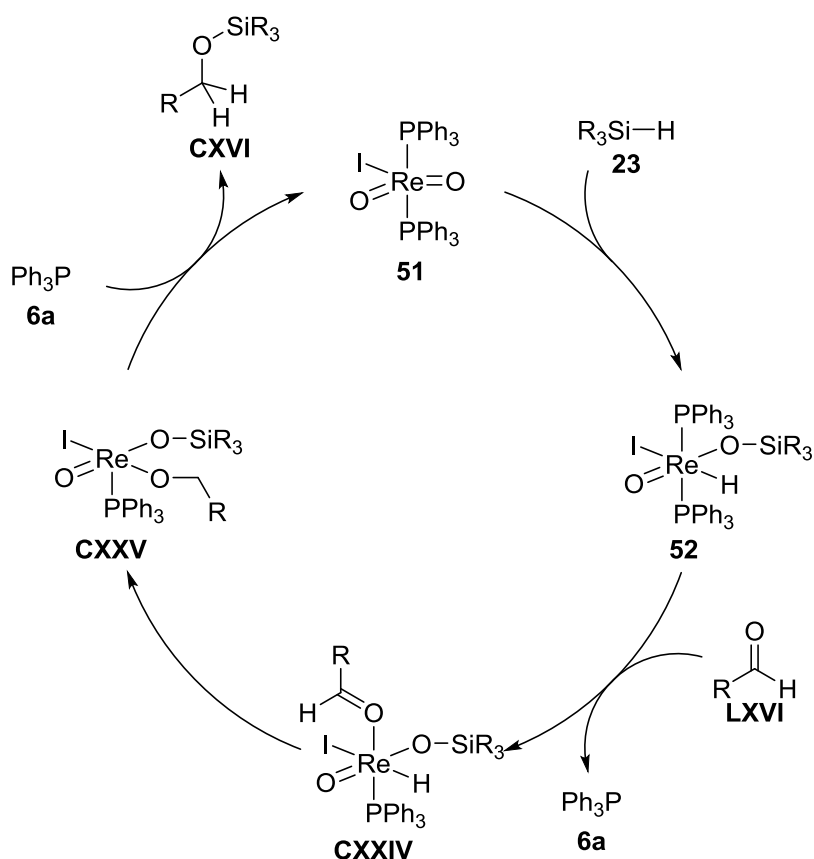
^[66] a) S. E. Denmark, G. L. Beutner, *Angew. Chem.* **2008**, 120, 1584–1663; *Angew. Chem. Int. Ed.* **2008**, 47, 1560–1638; b) S. Rendler, M. Oestreich, *Synthesis* **2005**, 1727–1747; c) M. Kira, L. C. Zhang in *Chemistry of Hypervalent Compounds* (Ed.: K.-y. Akiba), Wiley-VCH, New York, **1999**, p. 147–169; d) C. Chuit, R. J. P. Corriu, C. Reye, J. C. Young, *Chem. Rev.* **1993**, 93, 1371–1448.

^[67] For Ge–H bond activation involving proposed σ -CAM mechanism, see: M. Murai, K. Matsumoto, R. Okada, K. Takai, *Org. Lett.* **2014**, 16, 6492–6495.

1.2.2. Outer-Sphere Mechanisms

1.2.2.1 Cooperative Activation Mechanisms

The cooperative activation of hydrosilanes was first utilized in catalysis by TOSTE and co-workers in 2003 (Scheme 1.27).^[68] The rhenium(V) dioxo-complex **51** was proposed to activate hydrosilanes **23** by $[2\sigma+2\pi]$ -addition of the Si–H and Re=O bonds to give **52**. Following insertion of the carbonyl group into the metal hydride (**LXVI**→**CXXIV**) and subsequent silyl transfer produces the silyl ether **CXVI** and regenerates the catalyst **51**.

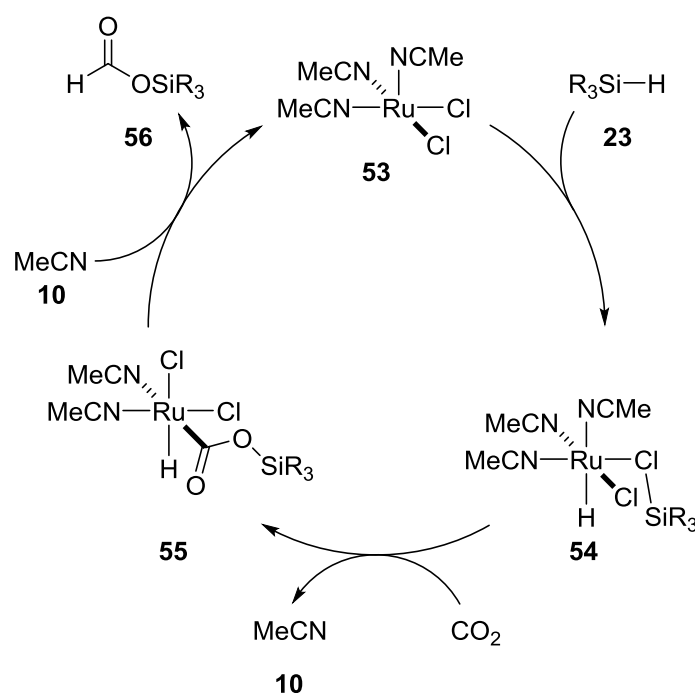


Scheme 1.27: Proposed mechanism of aldehyde hydrosilylation catalyzed by rhenium complex **51**.

The ruthenium-catalyzed hydrosilylation of carbon dioxide into silyl formate by DEGLMANN, HOFMANN, and PITTER was proposed to involve an interesting activation mode (Scheme

^[68] a) J. J. Kennedy-Smith, K. A. Nolin, H. P. Gunterman, F. D. Toste, *J. Am. Chem. Soc.* **2003**, 125, 4056–4057; b) K. A. Nolin, J. R. Krumper, M. D. Pluth, R. G. Bergman, F. D. Toste, *J. Am. Chem. Soc.* **2007**, 129, 14684–14696.

1.28).^[69] The hydrosilane **23** is activated by the Ru–Cl bond of **53** forming the ruthenium hydride **54** with an η^1 -coordinated silyl chloride. After carbon dioxide coordination to the ruthenium center, the silyl group is intramolecularly transferred to the oxygen atom giving the metal formate intermediate **55**. Following reductive elimination and recoordination of the acetonitrile ligand (**10**) releases the silyl formate **56** and the catalyst **53**.

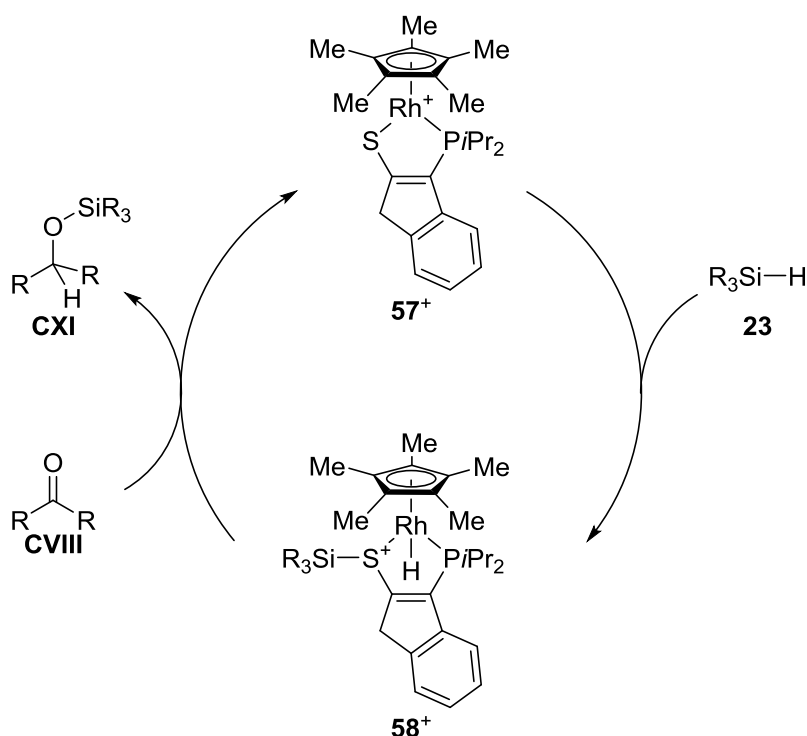


Scheme 1.28: Ruthenium-catalyzed hydrosilylation of carbon dioxide involving cooperative activation of hydrosilane.

In 2008, STRADIOTTO and co-workers studied cationic rhodium and iridium complexes **57**⁺ containing a polar M–S bond (Scheme 1.29).^[70] The complexes were shown to activate hydrosilanes **23** by heterolytic cleavage of the Si–H bond across the M–S bond to give complex **58**⁺ with a metal hydride and a silylated sulfur ligand. The complex **58**⁺ was proposed to be able to transfer the silyl group and a hydride to a carbonyl group giving silyl ether **CXI** and complex **57**⁺.

^[69] P. Deglmann, E. Ember, P. Hofmann, S. Pitter, O. Walter, *Chem. Eur. J.* **2007**, *13*, 2864–2879.

^[70] K. D. Hesp, R. McDonald, M. J. Ferguson, M. Stradiotto, *J. Am. Chem. Soc.* **2008**, *130*, 16394–16406.



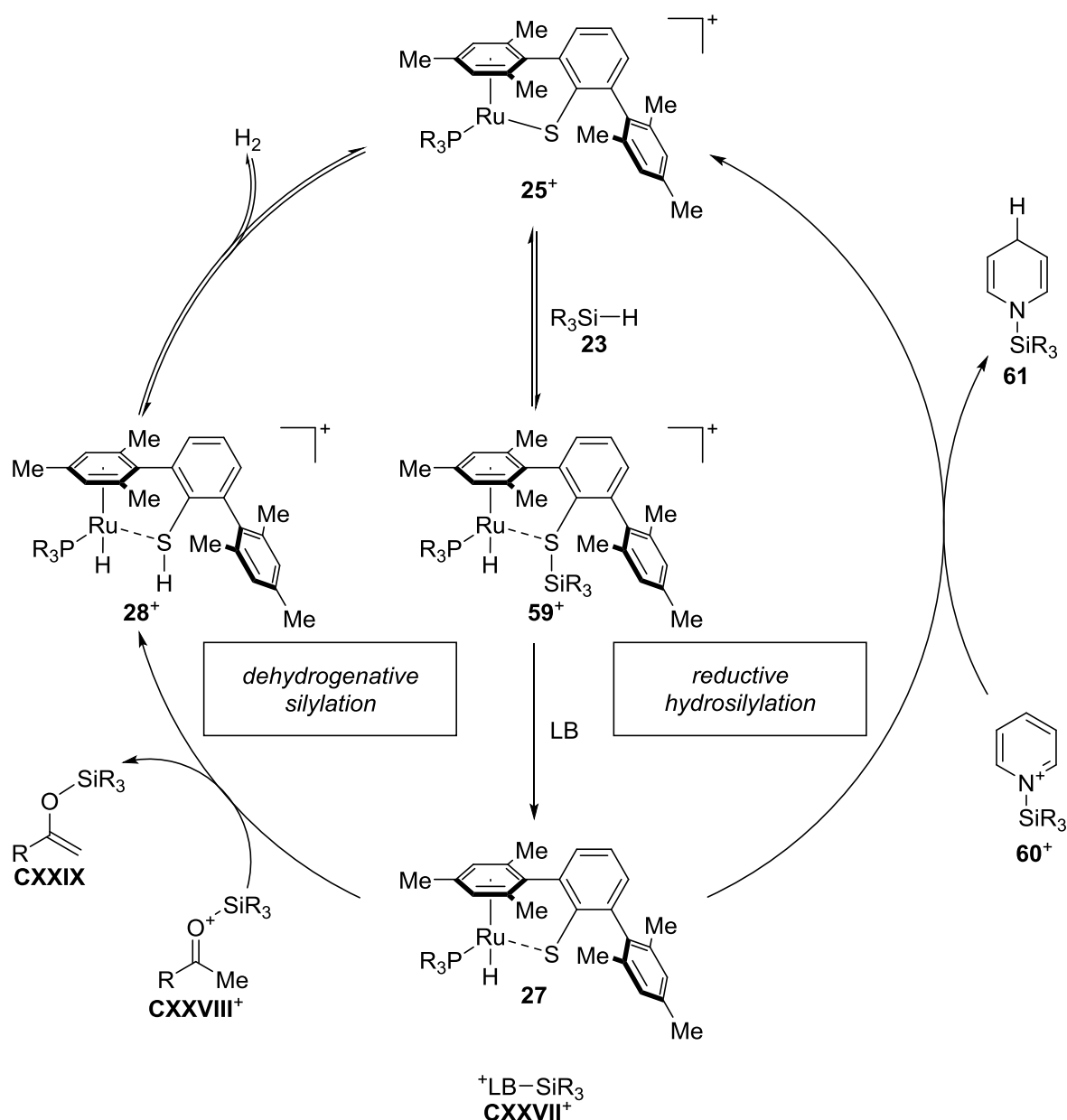
Scheme 1.29: Cooperative activation of Si–H bonds by rhodium thiolate complex **57⁺** in carbonyl hydrosilylation (counteranion $\text{B}(\text{C}_6\text{F}_5)_4^-$ omitted for clarity).

In addition to the dehydrogenative borylation of indoles (see Scheme 1.14), the ruthenium thiolate complex **25⁺** was utilized by OESTREICH in catalytic Si–H bond activation (Scheme 1.30). The activation mode of complex **59⁺** was investigated in detail by stoichiometric experiments, NMR spectroscopy, DFT calculations, and by X-ray crystallography. The combined results provided conclusive evidence for the cooperative activation mode.^[71] The activated silyl group **59⁺** is then attacked by the LEWIS-basic substrate to give the ruthenium hydride **27** and the corresponding silylated intermediate **CXXVII⁺**. Depending on the nature of the substrate, the ruthenium hydride complex **27** was shown to be able to act as a hydride source giving reductive hydrosilylation products (**60⁺**→**61**, shown for pyridine 1,4-reduction)^[72] or as a base leading to dehydrogenative silylation (**CXXVIII⁺**→**CXXIX**, shown for dehydrogenative ketone silylation).^[73]

^[71] T. Stahl, P. Hrobárik, C. D. F. Königs, Y. Ohki, K. Tatsumi, S. Kemper, M. Kaupp, H. F. T. Klare, M. Oestreich, *Chem. Sci.* **2015**, 6, 4324–4334.

^[72] a) T. Stahl, H. F. T. Klare, M. Oestreich, *J. Am. Chem. Soc.* **2013**, 135, 1248–1251; b) C. D. F. Königs, H. F. T. Klare, M. Oestreich, *Angew. Chem.* **2013**, 125, 10260–10263; *Angew. Chem. Int. Ed.* **2013**, 125, 10260–10263.

^[73] a) H. F. T. Klare, M. Oestreich, J.-i. Ito, H. Nishiyama, Y. Ohki, K. Tatsumi, *J. Am. Chem. Soc.* **2011**, 133, 3312–3315; b) C. D. F. Königs, H. F. T. Klare, Y. Ohki, K. Tatsumi, M. Oestreich, *Org. Lett.* **2012**, 14, 2842–2845; c) C. D. F. Königs, M. F. Müller, N. Aiguabella, H. F. T. Klare, M. Oestreich, *Chem. Commun.* **2013**, 49, 1506–1508; d) J. Hermeke, H. F. T. Klare, M. Oestreich, *Chem. Eur. J.* **2014**, 20, 9250–9254; e) L. Omann, M. Oestreich, *Angew. Chem.*



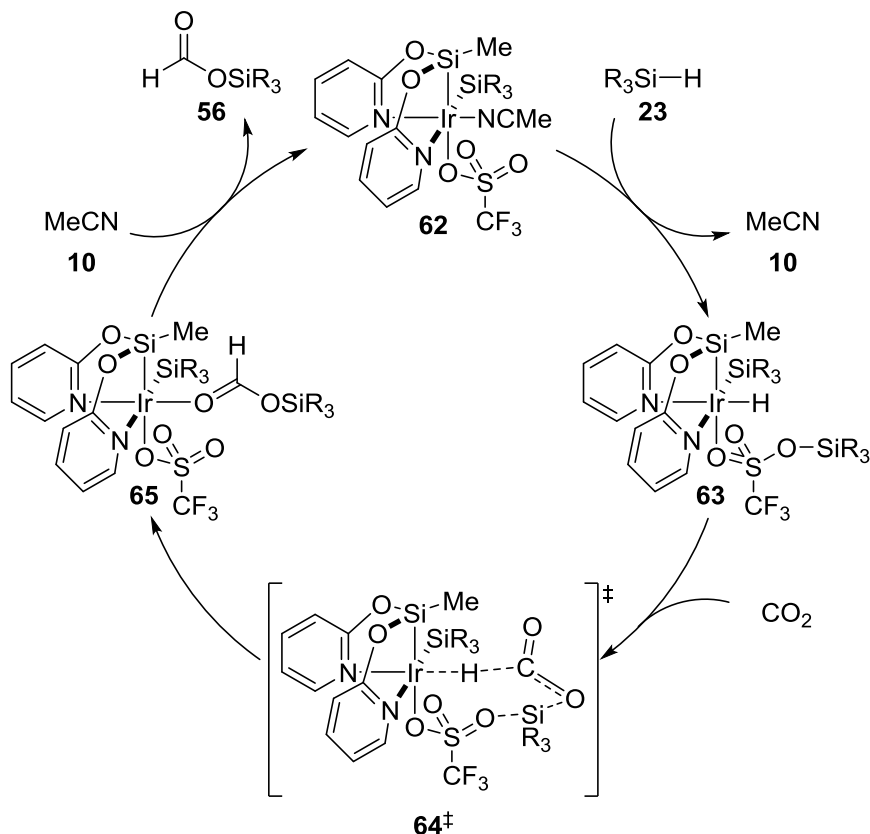
Scheme 1.30: Dehydrogenative silylation (LB = methyl ketone) and reductive hydrosilylation (LB = pyridine) catalyzed by the ruthenium thiolate **25**⁺ (counteranion $\text{BAR}_4^{\text{F}-}$ omitted for clarity).

The iridium NSiN pincer complex **62** was used by FERNÁNDEZ-ALVAREZ and ORO to hydrosilylate carbon dioxide into silyl formate **56** (Scheme 1.31).^[74] The mechanistic proposal based on DFT calculations suggested that the hydrosilane **23** would be cooperatively

2015, 127, 10414–10418; *Angew. Chem. Int. Ed.* **2015**, 54, 10276–10279; f) S. Wübbolt, M. Oestreich, *Angew. Chem.* **2015**, 127, 16103–16106; *Angew. Chem. Int. Ed.* **2015**, 54, 15876–15879.

^[74] R. Lalrempuia, M. Iglesias, V. Polo, P. J. Sanz Miguel, F. J. Fernández-Alvarez, J. J. Pérez-Torrente, L. A. Oro, *Angew. Chem.* **2012**, 124, 12996–12999; *Angew. Chem. Int. Ed.* **2012**, 51, 12824–12827.

activated by the iridium center and the oxygen atom of the triflate ligand (**63**). Concerted transfer of the hydride and the silyl group to the carbon dioxide (**64**[‡]) gives the complex **65**. Finally acetonitrile (**10**) replaces the silyl formate **56** reforming the active catalyst **62**.

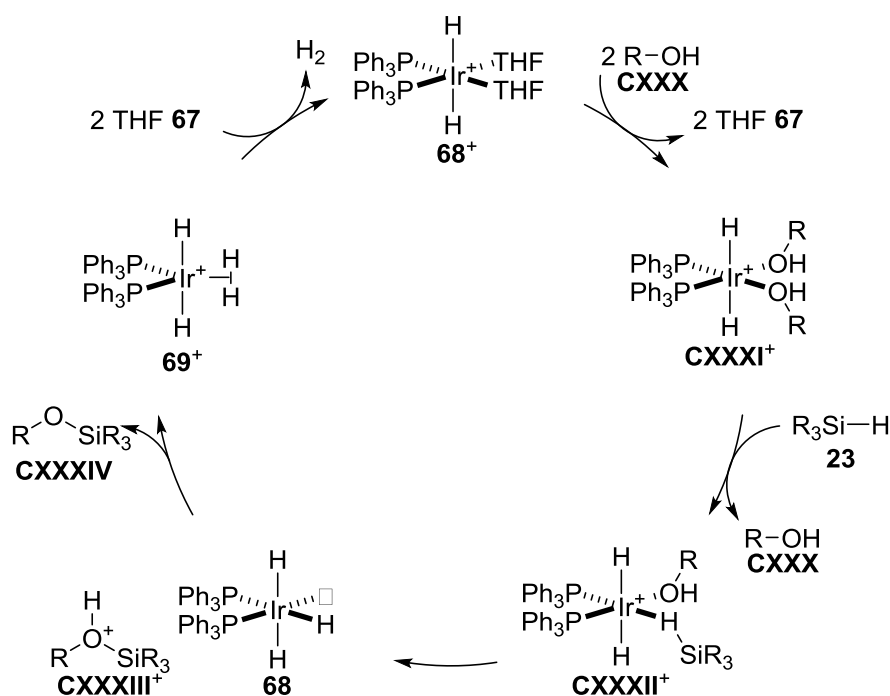


Scheme 1.31: Iridium-catalyzed cooperative hydrosilylation of carbon dioxide.

1.2.2.2 LEWIS-Acid Activation Mechanisms

The first report of an outer-sphere hydrosilylation mechanism is from 1989 by CRABTREE (Scheme 1.32).^[75] The iridium-catalyzed alcoholysis of hydrosilanes is proposed to operate by LEWIS-acid activation of the hydrosilanes. The hydrosilane **23** coordinates to the iridium center **CXXXII**⁺ in a η^2 -fashion increasing the polarization of the Si-H bond. Following nucleophilic attack by the alcohol (**CXXXIII**⁺) and deprotonation furnishes the silyl ether **CXXXIV**.

^[75] X.-L. Luo, R. H. Crabtree, *J. Am. Chem. Soc.* **1989**, *111*, 2527–2535.

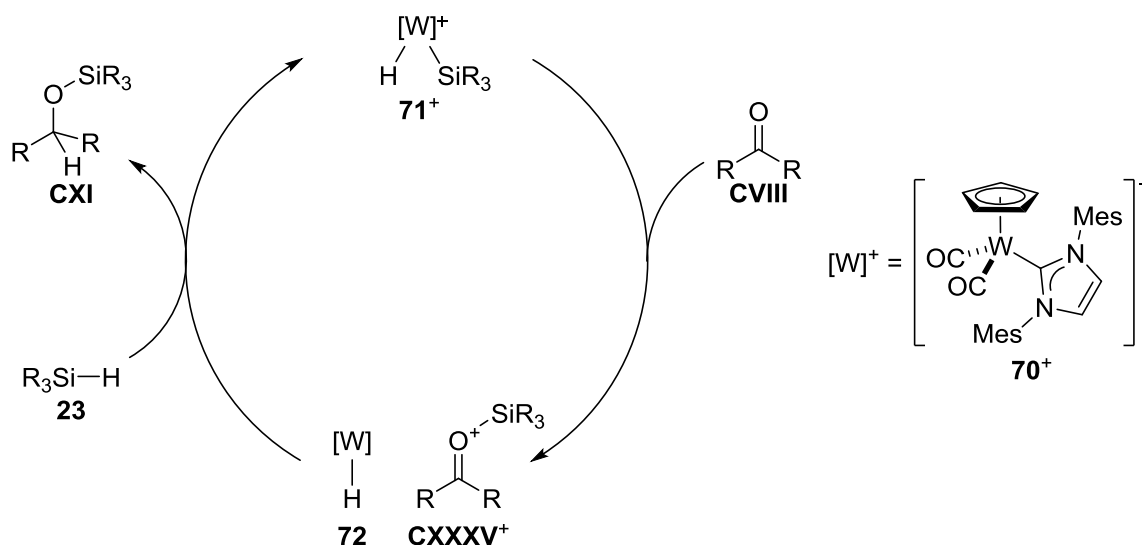


Scheme 1.32. Outer-sphere dehydrogenative coupling of hydrosilanes and alcohols (counteranion SbF_6^- omitted for clarity).

The second seminal report came in 2000 by BULLOCK (Scheme 1.33).^[76] The homogeneous tungsten-catalyzed hydrosilylation of ketones was proposed to proceed *via* a similar ionic mechanism as the related hydrogenation.^[77] The electrophilic tungsten center $\mathbf{70}^+$ was shown to coordinate the hydrosilane **23** to give complex $\mathbf{71}^+$. Nucleophilic attack by the carbonyl oxygen gave the silylcarboxonium ion \mathbf{CXXXV}^+ and the neutral tungsten hydride **72**. Hydride transfer to the carbon atom of the silylcarboxonium ion \mathbf{CXXXV}^+ and coordination of hydrosilane **23** gave the desired silyl ether **CXI** and the catalyst $\mathbf{71}^+$.

^[76] V. K. Dioumaev, R. M. Bullock, *Nature* **2003**, 424, 530–532.

^[77] a) R. M. Bullock, M. H. Voges, *J. Am. Chem. Soc.* **2000**, 122, 12594–12595; b) M. H. Voges, R. M. Bullock, *J. Chem. Soc., Dalton Trans.* **2002**, 757–770.



Scheme 1.33: Tungsten-catalyzed outer-sphere hydrosilylation of carbonyl compounds (counteranion $\text{B}(\text{C}_6\text{F}_5)_4^-$ omitted for clarity).

In 2007, BROOKHART presented the iridium(III) POCOP pincer complex $\mathbf{73}^+$ -catalyzed dehalogenation of alkyl halides $\mathbf{CXXXVII}$ (Scheme 1.34).^[78] The catalytic system was later used in the hydrosilylation of carbonyls including ketones, esters,^[79] and amides,^[80] cleavage of alkyl ethers,^[81] and in the hydrosilylation of carbon dioxide into methane.^[82] In all the reactions, the cationic iridium center was proposed to activate the hydrosilane by η^1 -coordination ($\mathbf{74}^+$). The proposed activation mode was supported by the molecular structure obtained by X-ray crystallography, DFT calculations, and NMR spectroscopy. After the transfer of the silyl group to the LEWIS-basic substrate, the neutral iridium dihydride $\mathbf{75}$ was proposed to act as the active hydride donor transferring a hydride to the silylhalonium ion $\mathbf{CXXXVIII}^+$ to give the product \mathbf{CXL} . Reoordination of hydrosilane $\mathbf{23}$ regenerates the active catalyst $\mathbf{74}^+$.

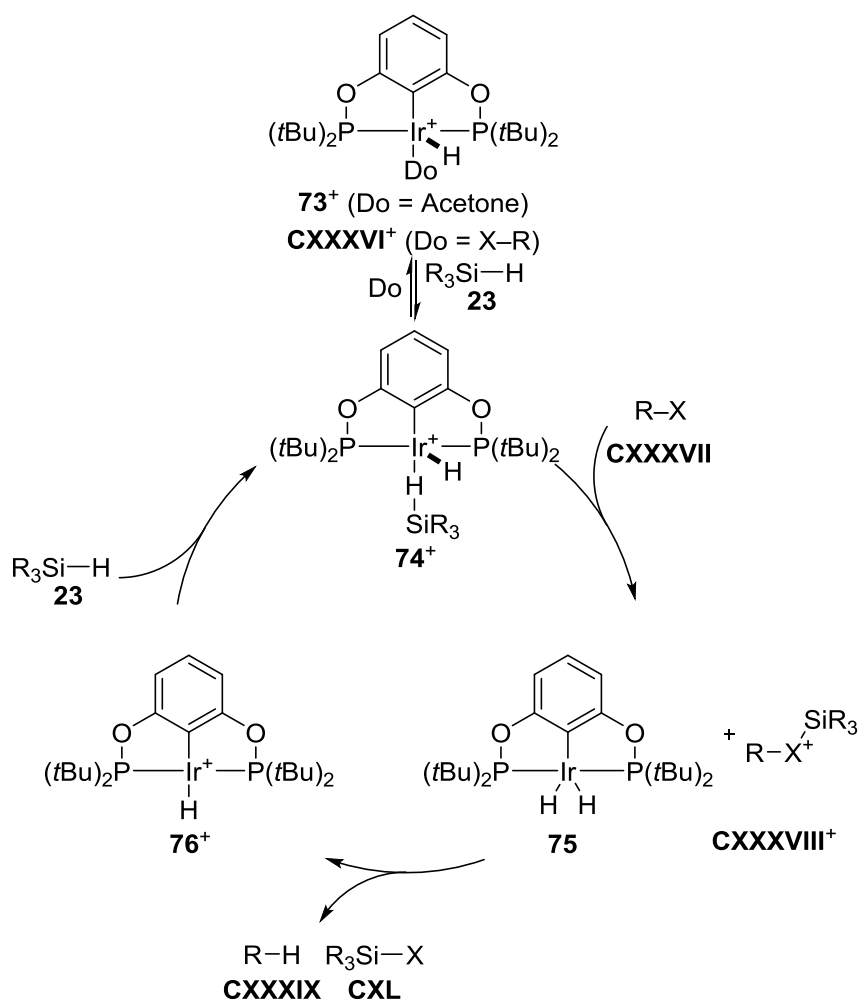
^[78] a) J. Yang, M. Brookhart, *J. Am. Chem. Soc.* **2007**, *129*, 12656–12657; b) J. Yang, M. Brookhart, *Adv. Synth. Catal.* **2009**, *351*, 175–187.

^[79] a) S. Park, M. Brookhart, *Organometallics* **2010**, *29*, 6057–6064; for a DFT investigation, see : W. Wang, P. Gu, Y. Wang, H. Wei, *Organometallics* **2014**, *33*, 847–857.

^[80] S. Park, M. Brookhart, *J. Am. Chem. Soc.* **2012**, *134*, 640–653.

^[81] a) J. Yang, P. S. White, M. Brookhart, *J. Am. Chem. Soc.* **2008**, *130*, 17509–17518; b) S. Park, M. Brookhart, *Chem. Commun.* **2011**, *47*, 3643–3645.

^[82] S. Park, D. Bézier, M. Brookhart, *J. Am. Chem. Soc.* **2012**, *134*, 11404–11407.



Scheme 1.34: Dehalogenation catalyzed by BROOKHART's POCOP pincer complex (X = F, Cl, Br, I; counteranion $\text{B}(\text{C}_6\text{F}_5)_4^-$ omitted for clarity).

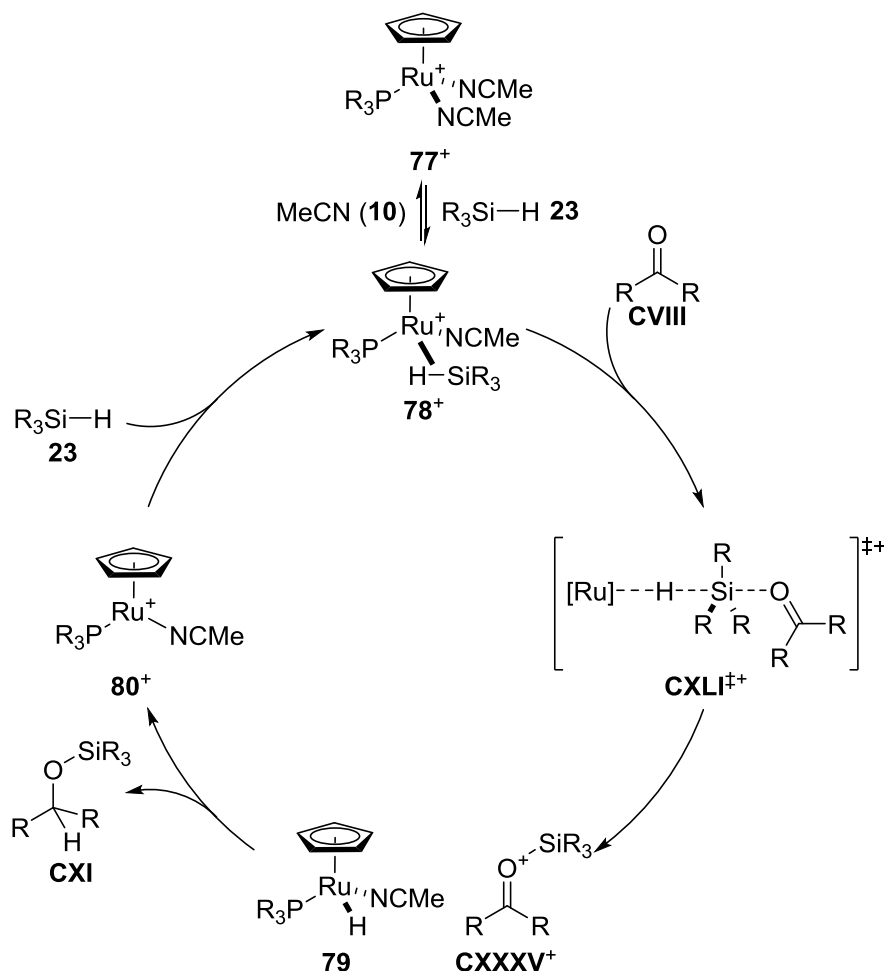
The ruthenium complex **77**⁺ was used by NIKONOV to catalyze the hydrosilylation of carbonyls,^[83] and nitriles,^[84] 1,4-hydrosilylation of pyridines^[85] as well as the dehydrogenative silylation of alcohols, carboxylic acids, and water (Scheme 1.35).^[83] Based on NMR spectroscopic evidence and DFT calculations, NIKONOV proposed that the hydrosilane **23** coordinates to the ruthenium center in an η^2 -fashion (**78**⁺). The electrophilic silicon atom is attacked by the LEWIS-basic substrate *via* a $\text{S}_{\text{N}}2$ -Si mechanism (**CXLI**⁺). The hydride transfer from the neutral ruthenium hydride **79** to the cationic intermediate **CXXXV**⁺ and following recoordination of the hydrosilane **23** give the desired product **CXI** and the active

[83] D. V. Gutsulyak, S. F. Vyboishchikov, G. I. Nikonov, *J. Am. Chem. Soc.* **2010**, 132, 5950–5951.

[84] D. V. Gutsulyak, G. I. Nikonov, *Angew. Chem.* **2010**, 122, 7715–7718; *Angew. Chem. Int. Ed.* **2010**, 49, 7553–7556.

[85] a) D. V. Gutsulyak, A. van der Est, G. I. Nikonov, *Angew. Chem.* **2011**, 123, 1420–1423; *Angew. Chem. Int. Ed.* **2011**, 50, 1384–1387; b) S.-H. Lee, D. V. Gutsulyak, G. I. Nikonov, *Organometallics* **2013**, 32, 4457–4464.

catalyst **78**⁺. The proposed mechanism was later supported by DFT calculations from HOUK and WU.^[86] However, the additional calculations indicated that the energy differences between the outer-sphere mechanism and traditional inner-sphere mechanisms are small.



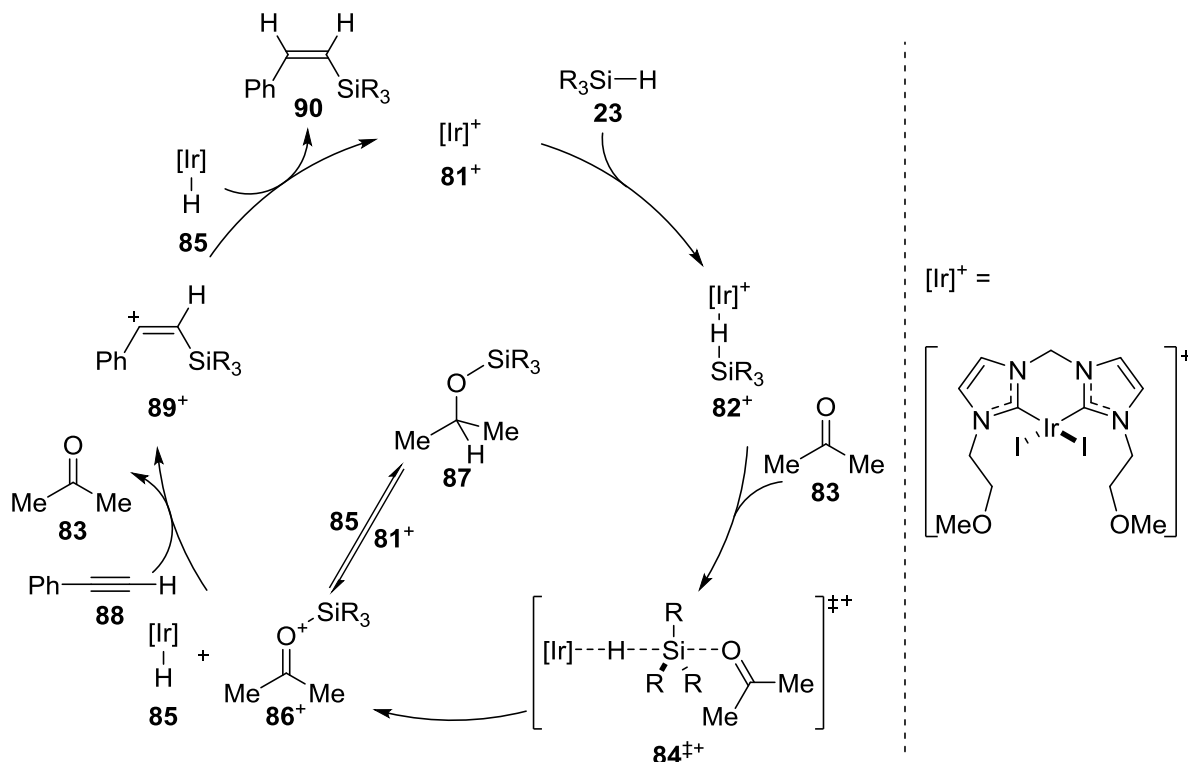
Scheme 1.35: Mechanism of ketone hydrosilylation by NIKONOV (counteranion B(C₆F₅)₄[−] omitted for clarity).

Iridium-catalyzed *trans*-hydrosilylation of alkynes was achieved by ORO through an unconventional mechanism (Scheme 1.36). The iridium complex **81**⁺ was shown to hydrosilylate alkynes in a *trans*-fashion, but only when acetone (**83**) was used as a solvent.^[87] The striking solvent-dependency was investigated computationally. The authors proposed that the iridium center activates hydrosilanes by η¹-coordination to give **82**⁺. The

^[86] Y.-F. Yang, L. W. Chung, X. Zhang, K. N. Houk, Y.-D. Wu, *J. Org. Chem.* **2014**, 79, 8856–8864.

^[87] a) M. Iglesias, P. J. Sanz Miguel, V. Polo, F. J. Fernández-Alvarez, J. J. Pérez-Torrente, L. A. Oro, *Chem. Eur. J.* **2013**, 19, 17559–17599; b) M. Iglesias, M. Aliaga-Lavrijsen, P. J. Sanz-Miguel, F. J. Fernández-Alvarez, J. J. Pérez-Torrente, L. A. Oro, *Adv. Synth. Catal.* **2015**, 357, 350–354.

silyl group is then transferred to acetone (**83**) to form silylcarboxonium ion **86⁺**. The following reduction of the intermediate **86⁺** into silyl ether **87** was calculated to be viable, but reversible. Under equilibrium, the carboxonium ion **86⁺** is proposed to transfer the silyl group to the alkyne **88** giving the carbocation **89⁺**. Following irreversible *anti*-hydride transfer from the iridium hydride **85** to **89⁺** furnishes the *trans*-silylated alkene **90** and the iridium complex **81**.

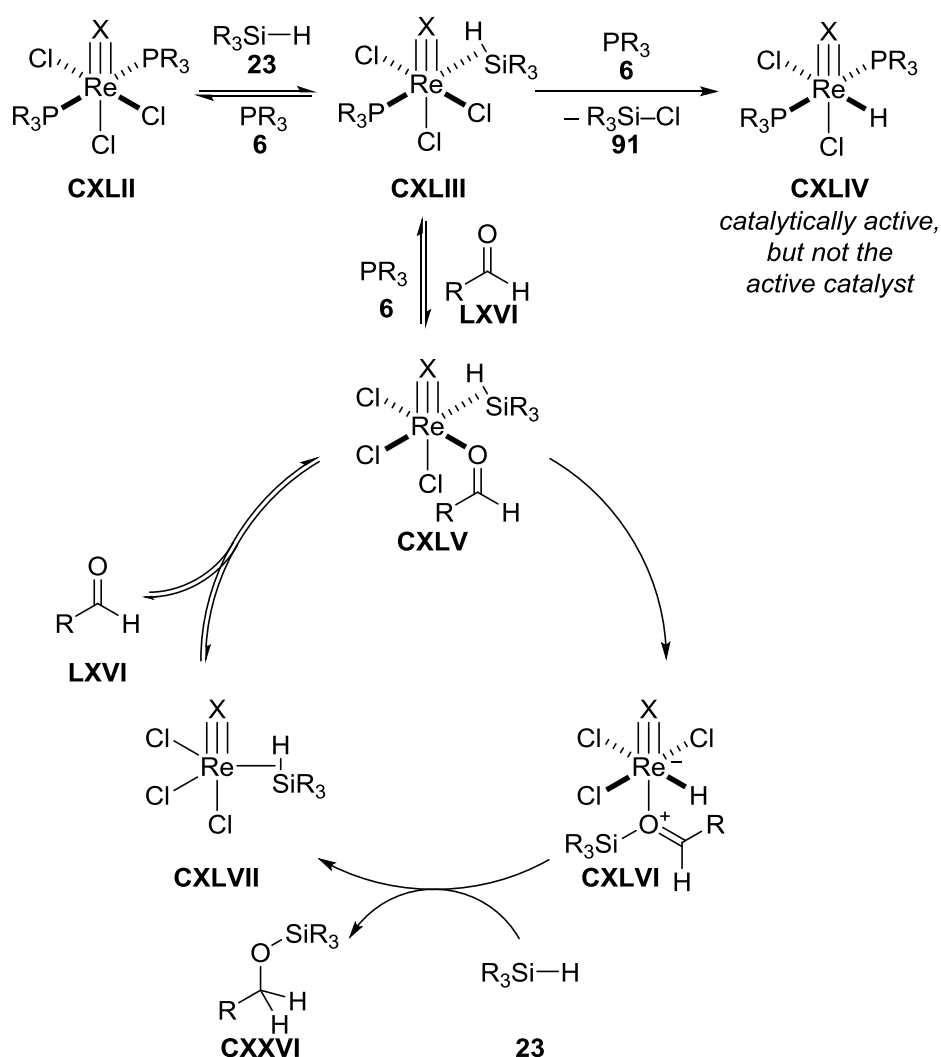


Scheme 1.36 β -(Z)-Selective hydrosilylation of alkynes by FERNÁNDEZ-ALVAREZ and ORO (counteranion BF_4^- omitted for clarity).

Various high-valent oxo-complexes have recently been shown to be active catalysts in hydrosilylation reactions. Due to controversy on their mode of action, their mechanisms have been extensively studied by stoichiometric control experiments, kinetic studies as well as DFT calculations.^[25c,88] In case of rhenium complexes **CXLII** ABU-OMAR was able to produce convincing amount of evidence that the catalyst probably operates *via* a LEWIS-acid activation mechanism (Scheme 1.37).^[88] The dissociation of a phosphine ligand **6** liberates a free coordination site at the metal center, and hydrosilane **23** coordinates to the rhenium in an η^2 -fashion to give **CXLIII**. Elimination of silyl chloride **91** and recoordination of the phosphine **6** gives rhenium hydride **CXLIV**. Although the complex **CXLIV** was shown by stoichiometric experiments to be able to facilitate the hydrosilylation, the catalytic efficiency

^[88] G. Du, P. E. Fanwick, M. M. Abu-Omar, *J. Am. Chem. Soc.* **2007**, *129*, 5180–5187.

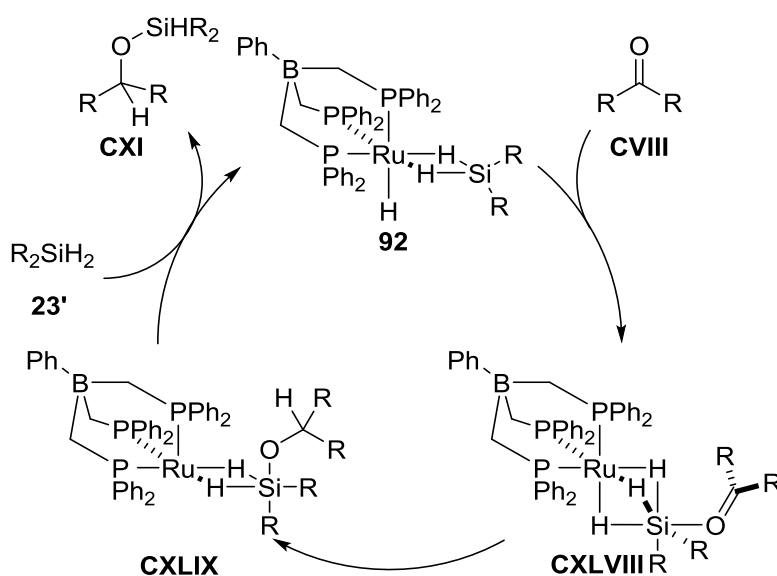
and the rate laws obtained from these experiments did not agree with the observed results from the catalytic system. Dissociation of a second phosphine **6** from **CXLIII** followed by coordination of the carbonyl group **LXVI** gives the complex **CXLV**. Silyl transfer to the oxygen gives the silylcarboxonium adduct **CXLVI**^[89] and following hydride transfer and coordination of hydrosilane **23** to the metal center yield the silyl ether **CXXVI** and the complex **CXLVII**. Interestingly, ABU-OMAR was not able to detect any catalytically viable adducts to the $\text{Re}\equiv\text{X}$ bonds (see Schemes 1.12 and 1.27).



Scheme 1.37: Mechanism of high valent rhenium complex-catalyzed hydrosilylation ($\text{X} = \text{O}, \text{N}, \text{NAr}$).

^[89] Alternative ionic mechanisms where the rhenium hydride and the silylcarboxonium ion dissociate were excluded.

TILLEY proposed activation of di- and trihydrosilanes by LEWIS-acid activation through η^3 -coordination (**92**, Scheme 1.38).^[90] Although these complexes were shown to exist in an equilibrium with the corresponding silyne form (not shown), the η^3 -coordinated complex was proposed to be the active catalyst. Coordination of the carbonyl **CVIII** to the silicon atom forms a six-coordinated silicon center **CXLVIII**. Hydride transfer from ruthenium to the carbon atom is conceivably assisted by the neighboring silicon center to give **CXLIX**. Finally, coordination of a second hydrosilane **23'** followed by dissociation of the product closes the catalytic cycle. The complex **92** is able to catalyze the hydrosilylation of benzophenone also with monohydrosilane **23**. For this reaction, a σ -bond metathesis mechanism is proposed (see Scheme 1.12).



Scheme 1.38: Mechanism of carbonyl hydrosilylation by TILLEY.

^[90] a) M. C. Lipke, T. D. Tilley, *J. Am. Chem. Soc.* **2011**, 133, 16374–16377; b) M. C. Lipke, F. Neumeyer, T. D. Tilley, *J. Am. Chem. Soc.* **2014**, 136, 6092–6102; c) M. C. Lipke, T. D. Tilley, *J. Am. Chem. Soc.* **2014**, 136, 16387–16398.

1.3 Objective

The overview across the mechanisms of metal-catalyzed main-group electrophile generation shows that the different mechanisms can be divided into two major subgroups: the inner-sphere and the outer-sphere mechanisms. Notwithstanding this simple classification, the mechanisms exhibit broad variety in their individual steps. The mechanistic studies have revealed how the intrinsic LEWIS acidity of group 13 electrophiles can be harnessed as part of the catalytic cycle. Typically, the main-group atom binds the substrate to the vicinity of the metal center. The ability of silicon to undergo rehybridization has been used by several catalyst. The electrophilicity of silicon atom has been increased both by hydride abstraction to form tricoordinate silicon intermediates as well as by the counterintuitive LEWIS-base activation to form pentacoordinate silicon intermediates.

LEWIS-acid activation of hydrosilanes has emerged as an important mode of action. In addition to electron-deficient boranes,^[91] electrophilic metal complexes such as the POCOP pincer complex **73**⁺ introduced by BROOKHART were also proposed to activate hydrosilanes by a LEWIS-acid mechanism (see Scheme 1.34). In Chapter 2, the precise mechanism of carbonyl hydrosilylation by the iridium POCOP pincer complex **73**⁺ is investigated.

Replacing expensive late-transition metals with cheap abundant metals, especially with iron, has been widely studied in several types of reactions,^[92] including hydroboration^[93] and hydrosilylation.^[94] Unlike the E–H bond activation mechanisms with late-transition metals, the corresponding mechanisms with abundant early transition metals are often not known in detail. In Chapter 3, the mechanism of iron-catalyzed carbonyl hydrosilylation using an iron(0) complex as a precatalyst is studied both experimentally and theoretically.

^[91] M. Oestreich, J. Hermeke, J. Mohr, *Chem. Soc. Rev.* **2015**, *44*, 2202–2220.

^[92] a) J. I. v. d. Vlugt, *Eur. J. Inorg. Chem.* **2011**, 363–375; b) S. Chakraborty, H. Guan, *Dalton Trans.* **2010**, 39, 7427–7436.

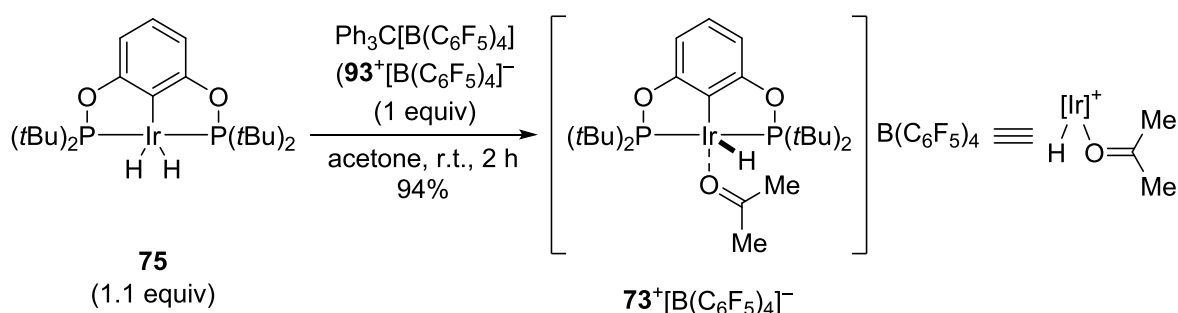
^[93] For selected examples, see: J. Y. Wu, B. Moreau, T. Ritter, *J. Am. Chem. Soc.* **2009**, *131*, 12915–12917; b) L. Zhang, D. Peng, X. Leng, Z. Huang, *Angew. Chem.* **2013**, *125*, 3764–3768; *Angew. Chem. Int. Ed.* **2013**, *52*, 3676–3680; c) J. V. Obligacion, P. J. Chirik, *Org. Lett.* **2013**, *15*, 2680–2683.

^[94] a) K. Junge, K. Schröder, M. Beller, *Chem. Commun.* **2011**, 47, 4849–4859; b) M. Zhang, A. Zhang, *Appl. Organomet. Chem.* **2010**, *24*, 751–757; c) R. H. Morris, *Chem. Soc. Rev.* **2009**, *38*, 2282–2291.

2 MECHANISTIC INVESTIGATION INTO BROOKHART'S IRIIDIUM(III) POCOP Pincer COMPLEX-CATALYZED CARBONYL HYDROSILYLATION^[95]

2.1 Introduction

The iridium POCOP pincer complex **75** was initially developed by BROOKHART for transfer dehydrogenation of alkanes.^[96] In 2007, BROOKHART presented the synthesis of the cationic pincer complex **73**⁺ by hydride abstraction from the iridium dihydride **75** (Scheme 2.1).^[78]



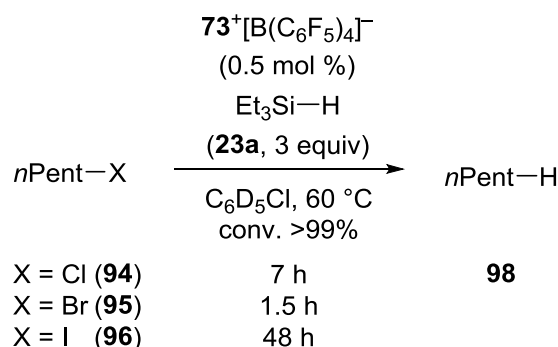
Scheme 2.1: Synthesis of the cationic pincer complex **73**⁺.

The synthetic value of the complex was shown by the reduction of primary halides **94–96** with triethylsilane (**23a**) under relatively mild conditions (Scheme 2.2). Alkyl bromides were found to be the most reactive and iodides the least reactive under the normal reaction conditions.^[78,97]

^[95] The DFT calculations included into the mechanistic investigation of the BROOKHART's POCOP pincer complex described in this chapter were done in collaboration with Dr. PETER HROBÁRIK and Prof. Dr. MARTIN KAUPP.

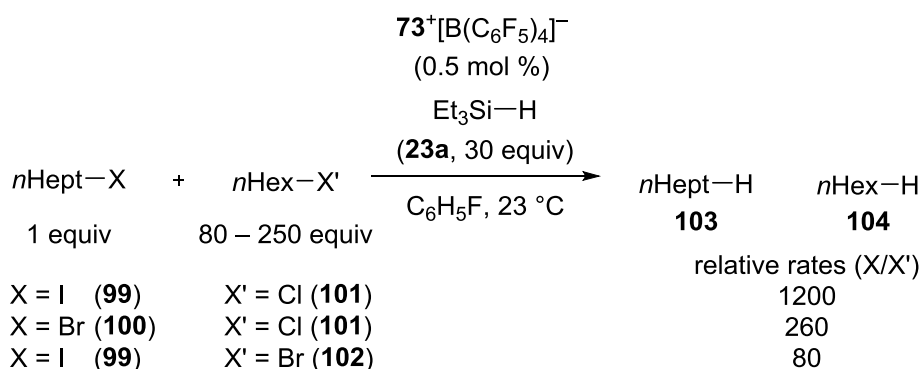
^[96] I. Göttker-Schnetmann, P. S. White, M. Brookhart, *Organometallics* **2004**, 23, 1766–1776.

^[97] The catalyst was shown to also reduce 1-fluoropentane (**97**) with 92% conversion in 50 h using 2 mol % catalyst loading. Other unidentified products in addition to *n*-pentane were observed.



Scheme 2.2: Reduction of alkyl halides **94–96** with triethylsilane (**23a**) catalyzed by complex **73**⁺.

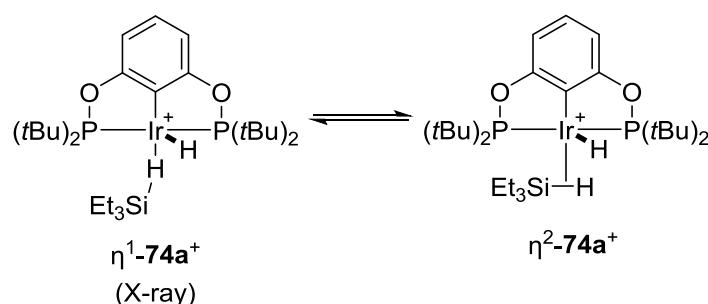
In competition experiments BROOKHART could selectively reduce the alkyl iodide **99** in the presence of excess alkyl chloride **101** (Scheme 2.3)! Similarly, the alkyl bromide **100** was reduced in the presence of the chloride **101**, and the iodide **99** in the presence of bromide **102**.



Scheme 2.3: Competition experiment between different alkyl halides.

The surprising reactivity was explained by coordination of the alkyl halides to the LEWIS-acidic iridium center (Scheme 1.34). The equilibrium between **CXXXVI**⁺ and **73**⁺ was shown to depend on the halide, with iodide being the most coordinating and bromide the least. Thus, when an alkyl iodide is being reduced, almost all the iridium is trapped as the unreactive resting state **CXXXVI**⁺, explaining the low reactivity. Introduction of a second halide releases a small amount of the highly reactive complex **73**⁺ that quickly reduces the more reactive alkyl halide (I>Br>Cl).

The proposed activation of the silane by the LEWIS-acidic iridium center was further supported by an X-ray crystal structure of the triethylsilane adduct **74a**⁺ (Scheme 2.4).^[98] The structure distinctly showed the rare η^1 -coordination of the hydrosilane (η^1 -**74a**⁺).^[99] Also in the ¹H NMR spectrum a large ¹H,²⁹Si coupling (¹J_{Si-H} = 79 Hz), typical for η^1 -coordination, was measured. The DFT calculations showed however that the η^2 -isomer η^2 -**74a**⁺ was energetically nearly identical, thus both isomers would be expected to be present in the solution during catalysis.^[100] For clarity, the assumed equilibrium (η^1 -**74a**⁺ \rightleftharpoons η^2 -**74a**⁺) is referred to as **74a**⁺ throughout this chapter.



Scheme 2.4: Structure of the hydrosilane adduct **74a**⁺ (counteranion B(C₆F₅)₄[−] omitted for clarity).

For the carbonyl hydrosilylation, BROOKHART was able to propose a more detailed mechanism based on kinetic data as well as in-situ NMR spectroscopy. The initial coordination of the hydrosilane **23** was found to be under equilibrium strongly favoring the substrate **CVIII** or the solvent **105** as a donor, **CL**⁺ and **106**⁺ respectively (Scheme 2.5). The silyl transfer to the oxygen atom of the carbonyl group **CVIII** was suggested to proceed via an S_N2-Si mechanism analogous to the mechanism proposed for the borane-catalyzed hydrosilylation.^[101] The iridium dihydride **75** was shown to enter an equilibrium with the

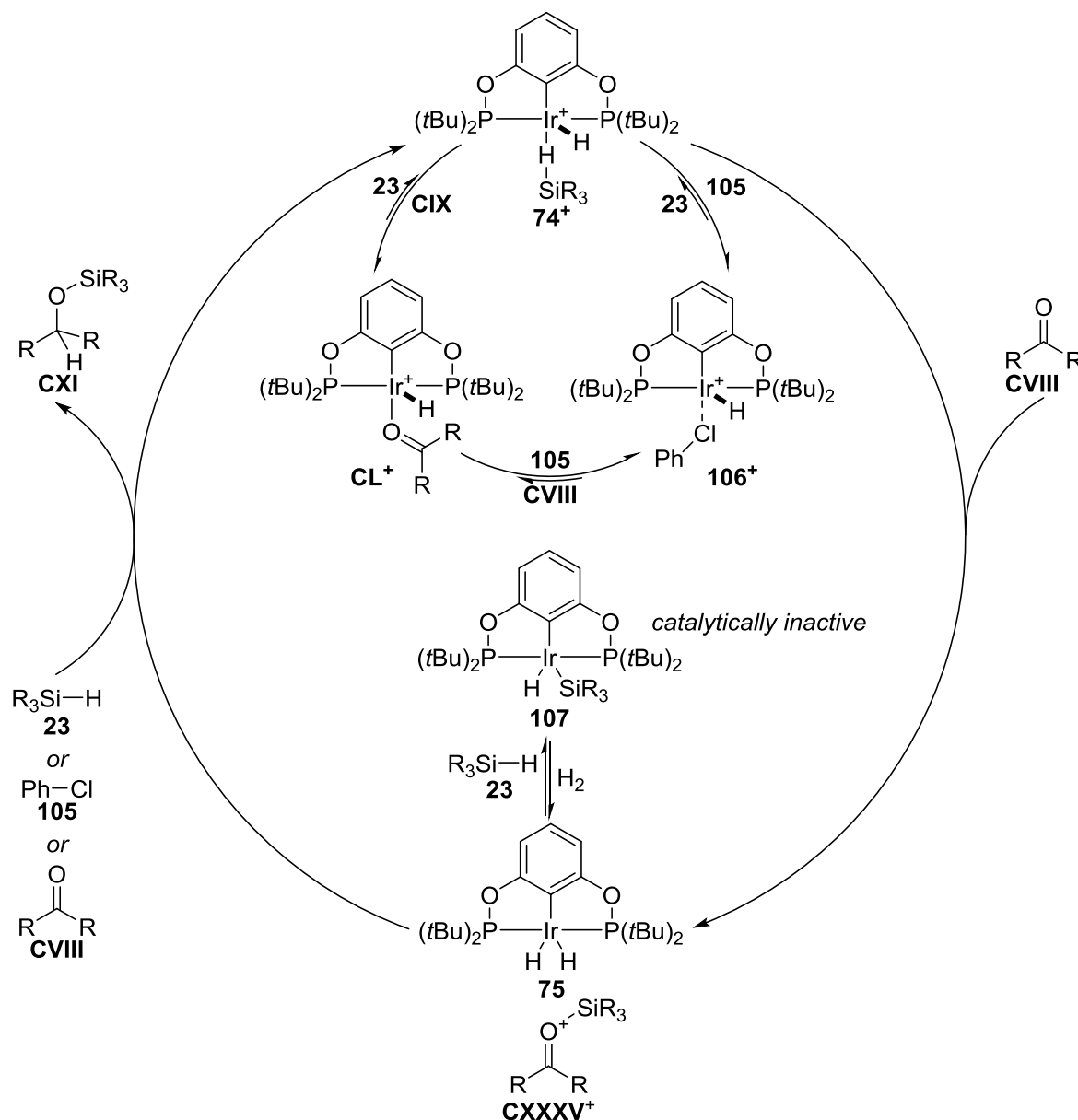
^[98] J. Yang, P. S. White, C. K. Schauer, M. Brookhart, *Angew. Chem.* **2008**, *120*, 4209–4211; *Angew. Chem. Int. Ed.* **2008**, *47*, 4141–4143.

^[99] For a related R₃B– η^1 -H–SiR₃ X-ray structure, see: A. Y. Houghton, J. Hurmalainen, A. Mansikkamäki, W. E. Piers, H. M. Tuononen, *Nat. Chem.* **2014**, *6*, 983–988.

^[100] η^2 -**74**⁺ was calculated to be favored over η^1 -**74**⁺ by 1.9 kcal mol^{−1}. The calculations were performed on a truncated complex using PMe₂ instead of P(*t*Bu)₂.

^[101] a) D. J. Parks, W. E. Piers, *J. Am. Chem. Soc.* **1996**, *118*, 9440–9441; b) D. J. Parks, J. M. Blackwell, W. E. Piers, *J. Org. Chem.* **2000**, *65*, 3090–3098; c) S. Rendler, M. Oestreich, *Angew. Chem.* **2008**, *120*, 6086–6089; *Angew. Chem. Int. Ed.* **2008**, *47*, 5997–6000; d) K. Sakata, H. Fujimoto, *J. Org. Chem.* **2013**, *78*, 12505–12512; for a recent review on borane-catalyzed reactions, see: M. Oestreich, J. Hermeke, J. Mohr, *Chem. Soc. Rev.* **2015**, *44*, 2202–2220.

catalytically inactive iridium silyl hydride **107**.^[102] The hydride transfer from the iridium dihydride **75** to the carbon atom of the silylcarboxonium ion **CXXXV**⁺ furnishes the silyl ether **CXI**. The resulting cationic iridium center was proposed to be stabilized by the coordination of chlorobenzene (**105**) to give **106**⁺. Based on the kinetic measurements the turnover frequency of the reaction was determined to be first order in hydrosilane and zero order in ketone concentration. The rate-determining step was proposed to be either the silyl transfer (**74**⁺→**75**) or the hydride transfer (**75**→**74**⁺).



Scheme 2.5: Proposed catalytic cycle of carbonyl hydrosilylation (counteranion $B(C_6F_5)_4^-$ omitted for clarity).

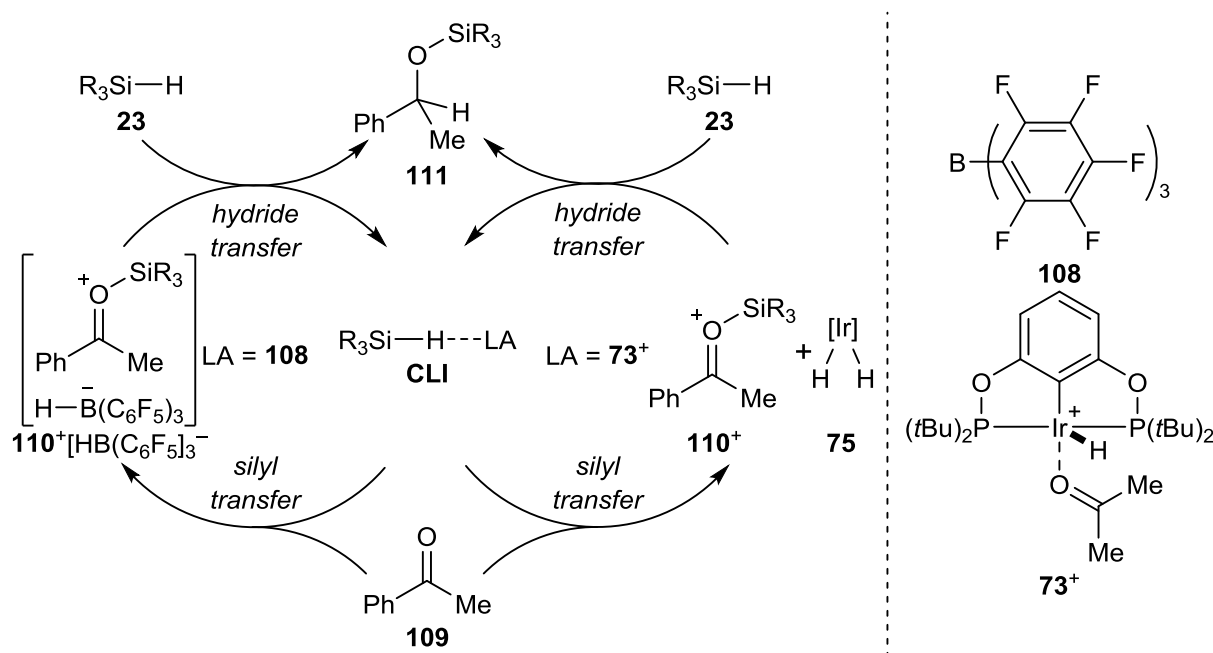
^[102] Based on kinetic measurements during the mechanistic investigation of the ether cleavage catalyzed by **73**⁺ ref. [81], the iridium silyl hydride **107** was found to be a weaker hydride donor than the dihydride **75**.

The extensive mechanistic investigations on the iridium POCOP pincer complex **73**⁺-catalyzed hydrosilylation reactions by BROOKHART established a rather clear understanding of the fundamental steps of the mechanisms involved in these reactions. First, the cationic hydrosilane complex **74**⁺ exists under equilibrium, strongly favoring complexes **CL**⁺ and **106**⁺. Once complex **74**⁺ enters the catalytic cycle, the silyl transfer to the LEWIS-basic substrate takes place presumably *via* an S_N2-Si mechanism. The formed iridium dihydride **75** is proposed to act as the active hydride donor. However, the detailed mechanisms of the silyl and the hydride transfer steps were not verified.

2.2 Mechanistic Investigation into Iridium POCOP Pincer Complex-Catalyzed Carbonyl Hydrosilylation

2.2.1 Hydrosilylation Using Silicon-Stereogenic Hydrosilanes

The carbonyl hydrosilylation mechanism by BROOKHART's pincer complex had been proposed to go through a LEWIS-acid activation of the hydrosilane **CLI**,^[79] similarly to the mechanism of the B(C₆F₅)₃ (**108**)-catalyzed hydrosilylation proposed by PIERS and co-workers (Scheme 2.6).^[101a,b] The proposed mechanism was later verified by OESTREICH using silicon-stereogenic hydrosilanes.^[101c] The observed inversion at the silicon atom proved the S_N2-Si mechanism.



Scheme 2.6: $\text{B}(\text{C}_6\text{F}_5)_3$ (**108**) and iridium complex **73⁺**-catalyzed hydrosilylation of ketone **109** (counteranion $\text{B}(\text{C}_6\text{F}_5)_4^-$ omitted for clarity).

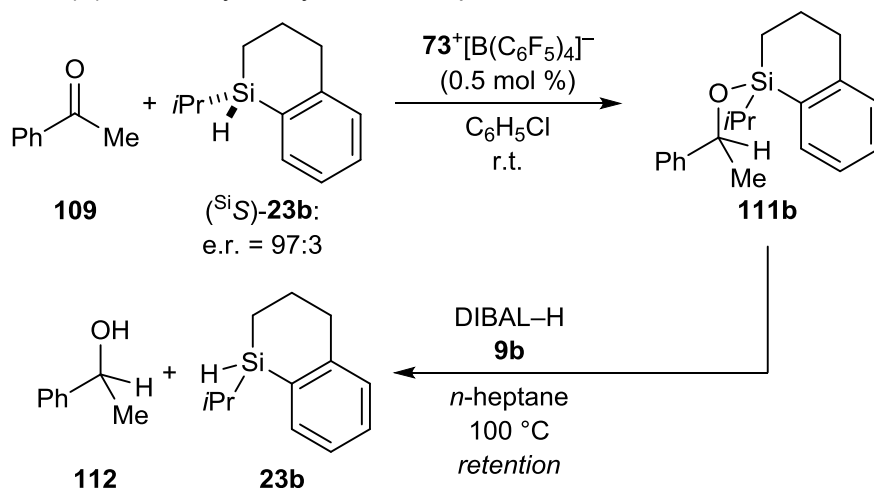
To investigate the stereochemical course at the silicon atom, the hydrosilylation of acetophenone catalyzed by iridium complex **73⁺** was performed under the standard conditions reported by BROOKHART using silicon-stereogenic silanes **23b** and **23c**. We began our study with the cyclic silicon-stereogenic hydrosilane (S)-**23b** used earlier in the investigation of the $\text{B}(\text{C}_6\text{F}_5)_3$ (**108**)-catalyzed hydrosilylation mechanism.^[101c] The reaction between acetophenone (**109**) and the rigid hydrosilane (S)-**23b** (d.r. = 97:3) was readily catalyzed by the pincer complex **73⁺**. The silyl ether **111b** was isolated in good yield as a mixture of diastereomers (Table 2.1, entry 1). The ratio of diastereomers (d.r. = 55:45) however proved to be significantly lower than in the case of $\text{B}(\text{C}_6\text{F}_5)_3$ (**108**) (d.r. = 74:26). When the silyl ether **111b** was cleaved with DIBAL-H (**9b**) under the standard conditions^[103] the hydrosilane **23b** was recovered with a negligible excess of the opposite enantiomer (e.r. = 49:51). Also, no chiral induction was obtained at the carbon stereocenter of the alcohol **112** (e.r. = 49:51). The reaction with one-to-one ratio of ketone and hydrosilane was found to be rather sluggish and required prolonged reaction times (20 h).^[104] To see whether the observed loss of enantiomeric purity occurs due to the extended reaction time, hydrosilane loading was increased from one to four equivalents (entry 2). The additional hydrosilane (S)-**23b** significantly decreased the required reaction time, and the reaction was

^[103] Known to proceed with retention at silicon atom: M. Oestreich, G. Auer, M. Keller, *Eur. J. Org. Chem.* **2005**, 184–195.

^[104] Hydrosilylation of acetophenone **109** with triethylsilane (**23a**, 3 equiv) reaches full conversion in 20 min.

completed in 30 min. The unreacted excess hydrosilane (*S*)-**23b** was recovered in a good yield without racemization (e.r. = 94:6). The silyl ether **111b** was obtained without change in diastereomeric ratio (d.r. = 55:45). After reductive cleavage with DIBAL-H (**9b**), the hydrosilane **23b** was recovered with the inverted absolute configuration in 48:52 ratio of enantiomers.

Table 2.1: Hydrosilylation of acetophenone (**109**) with cyclic silicon-stereogenic hydrosilane (*S*)-**23b** catalyzed by iridium complex **73**⁺.



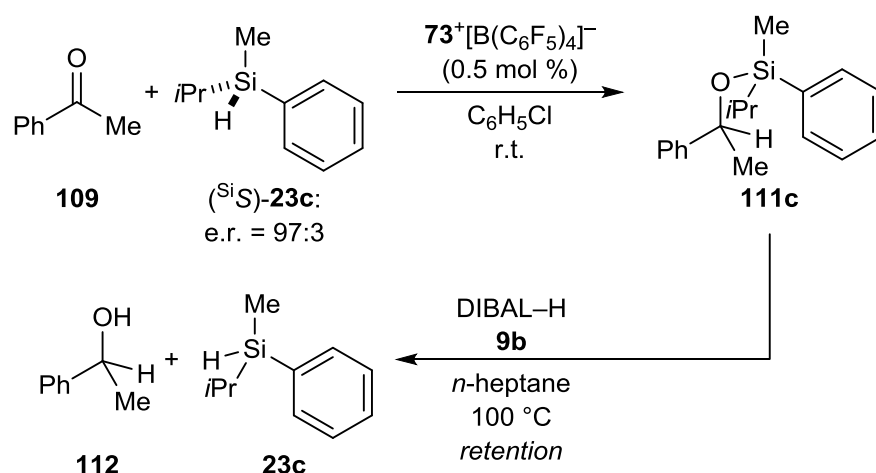
	hydrosilane	silyl ether	recovered hydrosilane	reformed hydrosilane	alcohol
entry	23b	111b	23b	23b	112
	equiv	yield (%)	yield (%)	yield (%)	yield (%)
	e.r. ^[a]	d.r. ^[b]	e.r. ^[a]	e.r. ^[a]	e.r. ^[a]
1 ^[c]	1.0	86	-	79	69
	97:3	55:45	-	49:51	51:49
2 ^[d]	4.0	86	95	99	86
	97:3	55:45	94:6	48:52	51:49

^[a] Enantiomeric ratios determined by HPLC analysis using chiral stationary phases; e.r. = *S*/*R*. ^[b] Diastereomeric ratio determined by GLC analysis. ^[c] Reaction time 20 h. ^[d] Reaction time 30 min.

The slight excess of the opposite enantiomer of the hydrosilane indicated towards the proposed S_N2 -Si mechanism. Meanwhile, the extensive loss of enantiomeric purity suggested an additional reaction pathway leading to racemization. Further information was obtained when the experiment was repeated with the acyclic enantioenriched silicon-stereogenic hydrosilane **23c**. The iridium complex **73**⁺ catalyzed reaction between **109** and one equivalent of (*S*)-**23c** (e.r. = 97:3) gave the corresponding silyl ether **111c** in a 59:41 ratio of diastereomers (Table 2.2, entry 1). Again the reductive cleavage gave the

hydrosilane **23c** in slight excess of the opposite enantiomer (e.r. = 48:52) without stereinduction on the alcohol **112** (e.r. = 49:51). When the hydrosilane loading was increased to four equivalents (entry 2), the silyl ether **111c** was obtained with a slightly increased diastereomeric ratio (d.r. = 62:38), however the recovered hydrosilane **23c** had partially racemized (e.r. = 74:26). The reductive cleavage with DIBAL-H (**9b**) furnished the reformed hydrosilane (*R*)-**23c** with significant enantiomeric ratio in the opposite configuration (e.r. = 36:64). The alcohol **112** was obtained with low enantiomeric ratio (e.r. = 46:54).

Table 2.2: Hydrosilylation of acetophenone (**109**) with acyclic silicon-stereogenic hydrosilane (*S*)-**23c** catalyzed by iridium complex **73**⁺.



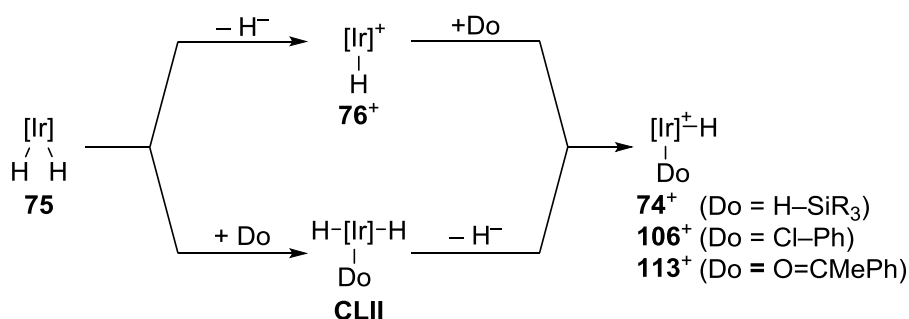
entry	hydrosilane	silyl ether	recovered hydrosilane	reformed hydrosilane	alcohol
	23c	111c	23c	23c	112
	equiv e.r. ^[a]	yield (%) d.r. ^[b]	yield (%) e.r. ^[a]	yield (%) e.r. ^[a]	yield (%) e.r. ^[a]
1 ^[c]	1.0	90	-	85	99
	97:3	59:41	-	48:52	49:51
2 ^[d]	4.0	89	85	86	93
	97:3	62:38	74:26	36:64	46:54

^[a] Enantiomeric ratios determined by HPLC analysis using chiral stationary phases; e.r. = *S*/*R*. ^[b] Diastereomeric ratio determined by GLC analysis. ^[c] Reaction time 20 h. ^[d] Reaction time 30 min.

2.2.2 Identification of the Hydride Source

The mechanism of the initial silyl transfer step seemed to proceed in accordance with the related B(C₆F₅)₃-catalyzed reaction. There is however a significant difference in the hydride transfer step: in the case of B(C₆F₅)₃ (**108**), the formed silylcarboxonium ion **110**⁺ and the

borohydride $[\text{HB}(\text{C}_6\text{F}_4)_3]^-$ intermediates are unlikely to dissociate^[105] but will rapidly react to release the desired product and regenerate $\text{B}(\text{C}_6\text{F}_5)_3$ (**108**). On the other hand, in the iridium pincer complex **73**⁺-catalyzed reaction, the silylcarboxonium ion **110**⁺ is formed together with a *neutral* iridium dihydride **75**. According to the proposed mechanism, this neutral and stable dihydride **75** would transfer a hydride to the carbon atom of the silylcarboxonium ion **110**⁺ forming a cationic monohydride intermediate **76**⁺ (Scheme 2.7, top). The unsaturated iridium center would then be coordinated by a donor. We hypothesized that the coordination of the donor could take place before the hydride transfer to form **CLII** (Scheme 2.7, bottom). The plausible donors during the reaction are chlorobenzene (**105**) used as the solvent, ketone **109**, and hydrosilane **23**.

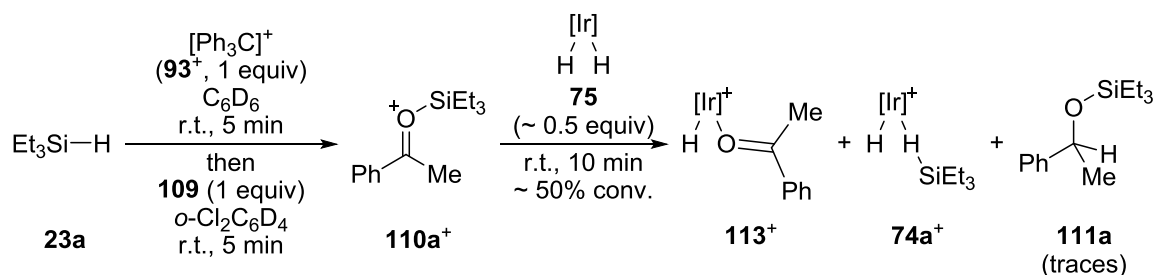


Scheme 2.7: Plausible hydride donors.

To study the hydride transfer step, we independently synthesized mixtures of plausible reactive intermediates and analyzed them using in-situ ¹H NMR spectroscopy. According to the proposed mechanism, silylcarboxonium ion **110a**⁺ would be rapidly reduced to the silyl ether **111a** by iridium dihydride **75**. When **75** (ca. 0.5 equiv) was added into a freshly prepared solution of **110a**⁺,^[106] only traces of expected silyl ether **111a** were observed (Scheme 2.8). Instead, the major products were regenerated acetophenone **113**⁺ and hydrosilane **74a**⁺ resulting from the formal backward reaction (**110a**⁺→**109**): the iridium dihydride transferred a hydride to the silicon atom, not to the carbon atom. The inability of the iridium dihydride to generate the desired product strongly suggests that **75** is not the active hydride donor.

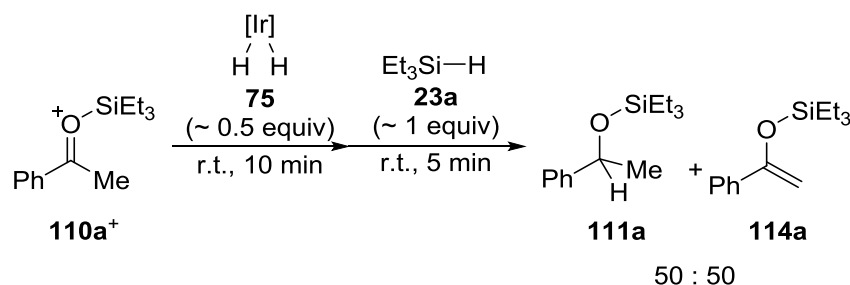
^[105] The dissociation of the ion pair is calculated to be unfavored by 15.2 kcal mol⁻¹, see ref. [101d].

^[106] Careful control of the stoichiometry during the synthesis is essential to avoid formation of bis-silylhydronium ion, see: a) M. Nava, C. A. Reed, *Organometallics* **2011**, *30*, 4798–4800; b) S. J. Connelly, W. Kaminsky, D. M. Heinekey, *Organometallics* **2013**, *32* 7478–7481.



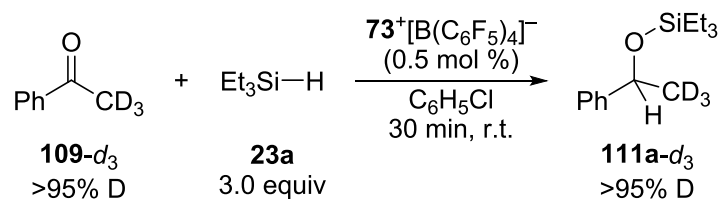
Scheme 2.8: Control experiment A (counteranion $\text{B}(\text{C}_6\text{F}_5)_4^-$ omitted for clarity).

Hydrosilane **23** was added into the previously formed mixture (Scheme 2.8) and immediate conversion of **110a**⁺ to the expected silyl ether **111a**, and silyl enol ether **114a** (ratio ca. 50:50), was observed (Scheme 2.9). The observation of the desired product **111a** gave evidence of the involvement of a second molecule of the hydrosilane in the mechanism.



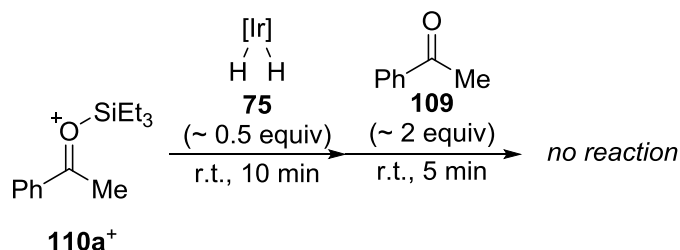
Scheme 2.9: Control experiment B (counteranion $\text{B}(\text{C}_6\text{F}_5)_4^-$ omitted for clarity).

The formation of the enol ether **114a** was unexpected and presumably only an artifact due to extremely high concentration of reactive species under the stoichiometric conditions. To exclude enol ethers from the effective catalytic cycle we performed hydrosilylation of trideuteroacetophenone (**109-d**₃). As expected, the desired silyl ether **111a-d**₃ was obtained completely deuterated at the methyl position, excluding any enol ether intermediates during the reaction (Scheme 2.10).



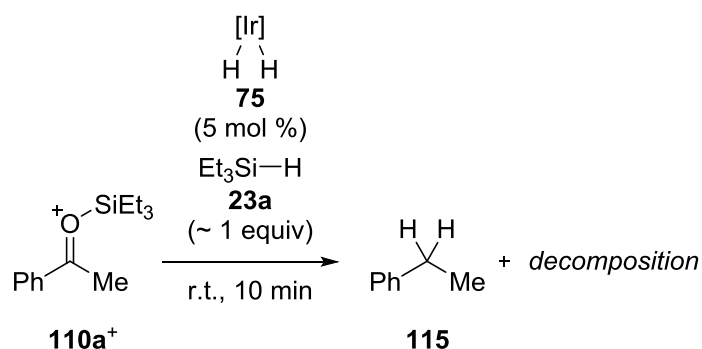
Scheme 2.10: Control experiment to exclude silyl enol ethers **114** as intermediates.

The strongest donor in the system was expected to be the substrate **109**. When iridium dihydride **75** was added together with ketone **109** into a freshly prepared solution of the silylcarboxonium ion **110a**⁺, no reaction was observed (Scheme 2.11).^[107]



Scheme 2.11: Control Experiment C (counteranion B(C₆F₅)₄[−] omitted for clarity).

The most abundant hydride source in the reaction mixture is the hydrosilane **23**.^[108] Hydrosilanes are known to rapidly deoxygenate silylcarboxonium ions^[109] but we needed to examine whether catalytic amounts of the iridium dihydride **75** would be able to inhibit the deoxygenation. When iridium dihydride **75** (5 mol %) and hydrosilane **23a** (1 equiv) were added to the freshly prepared silylcarboxonium ion **110a**⁺, we observed immediate deoxygenation to ethyl benzene (**115**) (Scheme 2.12).



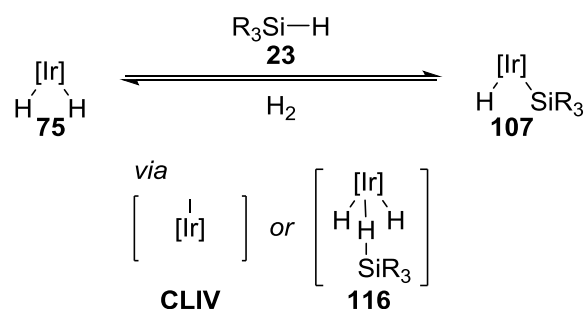
Scheme 2.12: Control experiment D (counteranion B(C₆F₅)₄[−] omitted for clarity).

^[107] Addition of hydrosilane **23a** into this mixture led to deoxygenation to give ethylbenzene **115** and decomposition.

^[108] BROOKHART proposed the hydrosilane **23** as a competing hydride source during the ether cleavage catalyzed by complex **73**⁺, ref. [81].

^[109] a) M. Kira, T. Hino, H. Sakurai, *Chem. Lett.* **1992**, 555–558; b) D. Parks, J. Blackwell, W. E. Piers, *J. Org. Chem.* **2000**, 65, 3090–3098; c) K. Mütter, M. Oestreich, *Chem. Commun.* **2011**, 47, 334–336.

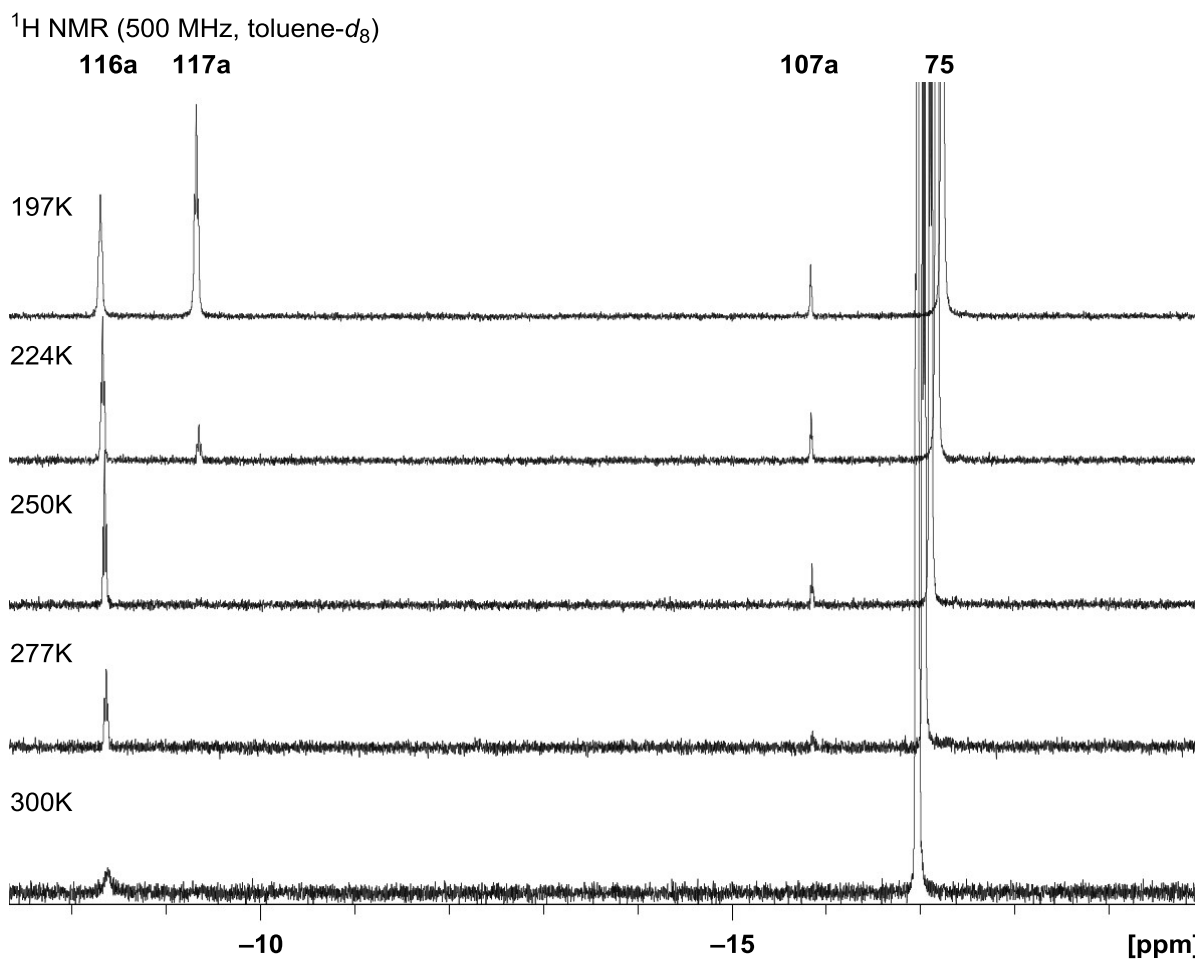
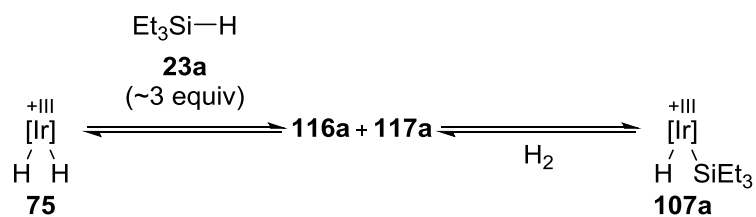
The control experiments indicated that both the iridium dihydride **75** and hydrosilane **23** were required for the efficient hydride transfer. BROOKHART had shown that iridium dihydride **75** and hydrosilane **23** are under equilibrium with iridium hydrosilane **107** and dihydrogen (Scheme 2.13). A mechanism for this formal exchange was not proposed but the reaction seemed unlikely to proceed *via* an iridium(I) intermediate **CLIV** through reductive elimination of dihydrogen and oxidative addition of hydrosilane. Instead, an elusive intermediate **116** between the two structures is proposed.^[110]



Scheme 2.13: Proposed intermediates between iridium dihydride **75** and the iridium silyl hydride **107**.

We set out to investigate the equilibrium in detail using in-situ NMR spectroscopy. A mixture of iridium hydride **75** and hydrosilane **23a** was dissolved in toluene-*d*₈ and subjected to NMR analysis (Scheme 2.14). At room temperature (300 K) the only observable signal in the hydride region was the iridium dihydride **75** at –17.0 ppm but as soon as the temperature was lowered to 277 K a new hydride signal could be observed at –8.3 ppm. As the temperature was lowered further to 197 K the expected silyl hydride **107a** became visible at –15.9 ppm together with a fourth signal at –9.3 ppm. As the temperature was increased again, identical spectra were obtained proving that the observed changes are reversible and that the spectra were recorded under equilibrium. Two previously unknown signals were observed also in the ³¹P NMR spectra with ¹H,³¹P HMQC correlations to the new ¹H NMR hydride signals. Careful integration of the ¹H and ³¹P NMR signals and comparison of the ratios of the known complexes **76**, **107a**, and the two new complexes **116a** and **117a** allowed the assignment of both of these new hydride signals to correspond to complexes with three equivalent or coalescent hydrides.

^[110] The dihydrogen/hydrosilane exchange via **116** could in fact be seen as a σ-CAM process (see Scheme 1.10).

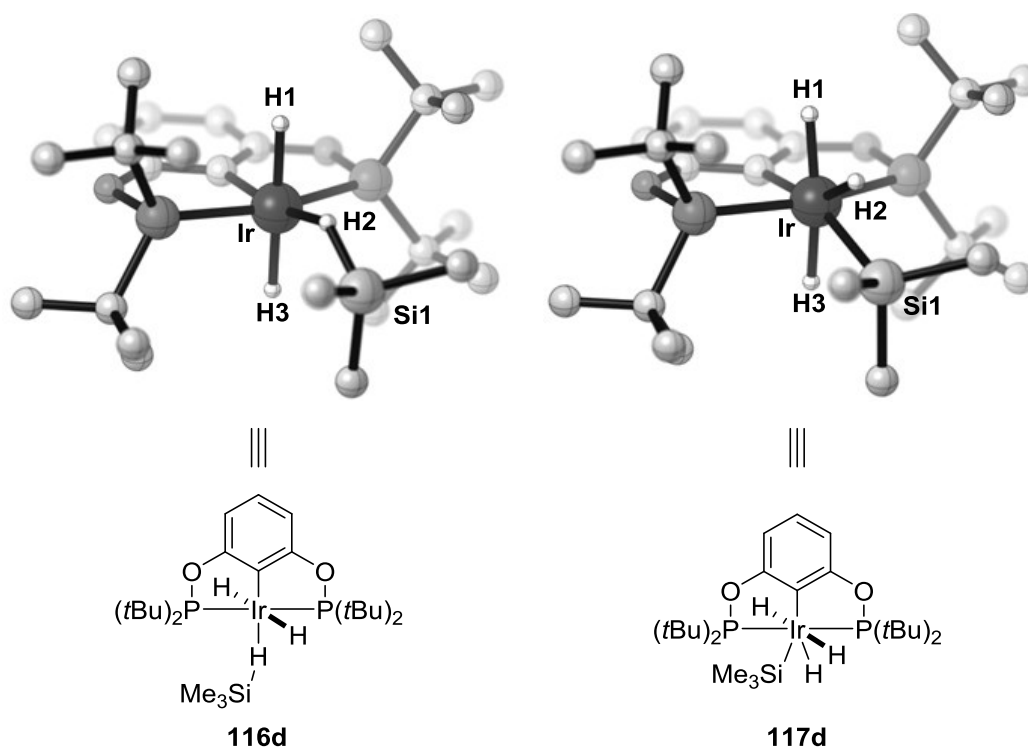


Scheme 2.14: Variable temperature ^1H NMR spectra of iridium dihydride **75** and triethylsilane (**23a**).

The assignment of the trihydrides was supported by DFT calculations (Tables 2.3 and 2.4).^[111] Complex **116d** was identified as the expected iridium(III) dihydride adduct with an η^1 -coordinated hydrosilane whereas the complex **117d** could be described as an iridium(V) complex (Scheme 2.15).

^[111] All DFT calculation performed at B3LYP-D3(BJ)/ECP/6-31++G(d,p) level using an SMD solvation model. Trimethylsilane (**23d**) was used as a model hydrosilane.

A similar iridium(V) complex had been proposed by BROOKHART earlier using dihydrosilanes in the amide reduction but as the silyl transfer intermediate not as the hydride donor.^[80] Importantly the borane complexes investigated and carefully characterized by HEINEKEY provided us a direct comparison for the hydride signals.^[112]



Scheme 2.15: Calculated structures of the iridium complexes **116d** and **117d**.

^[112] T. J. Hebden, M. C. Denney, V. Pons, P. M. B. Piccoli, T. F. Koetzle, A. J. Schultz, W. Kaminsky, K. I. Goldberg, D. M. Heinekey, *J. Am. Chem. Soc.* **2008**, *130*, 10812–10820.

Table 2.3: Selected bond parameters and NPA charges

iridium complex	bond parameters						NPA charges				
	length (Å), [Mayer bond order (in parenthesis)]					angle (°)					
	Ir–H1	Ir–H2	Ir–H3	Ir–Si	Si–H ^[a]	$\alpha(\text{Ir–H2–Si})$	Ir	H1	H2	H3	Si
[Ir]H ₂ (H–SiMe ₃) 116d	1.673 (1.003)	1.790 (0.102)	1.653 (0.837)	3.092 (0.091)	1.560 (0.769)	134.7°	–0.127	–0.255	–0.200	–0.228	1.600
[Ir]H ₃ SiMe ₃ 117d	1.653 (1.035)	1.632 (0.307)	1.640 (0.851)	2.545 (0.314)	1.852 (0.025)	93.6°	–0.263	–0.151	0.009	–0.124	1.417
[Ir]H ₂ 75	1.588 (0.748)	1.606 0.792					–0.277	0.033	–0.009		
[Ir]H ⁺ 76⁺	1.537 (0.842)						0.327	0.093			
[Ir]HSiMe ₃ 107d	1.587 (0.688)			2.448 (0.616)	2.081 (0.042)		–0.324	0.061			1.342
[Ir]H(H–SiMe ₃) 74d⁺	1.533 (0.881)	1.806 (0.018)		3.203 (0.010)	1.562 (0.929)		0.090	0.137	–0.259		1.614

^[a] The shortest Si–H(2) bond distance.

The calculated NMR shifts and comparison to the previously reported related complexes further support the assignment of the hydride signal at -8.3 ppm in the ^1H NMR to the iridium trihydride complex **116** with η^1 -coordinated hydrosilane. The hydride signal at -9.3 ppm corresponds to the proposed iridium(V) complex **117**.

Table 2.4: Selected NMR spectroscopic data of iridium pincer complexes.

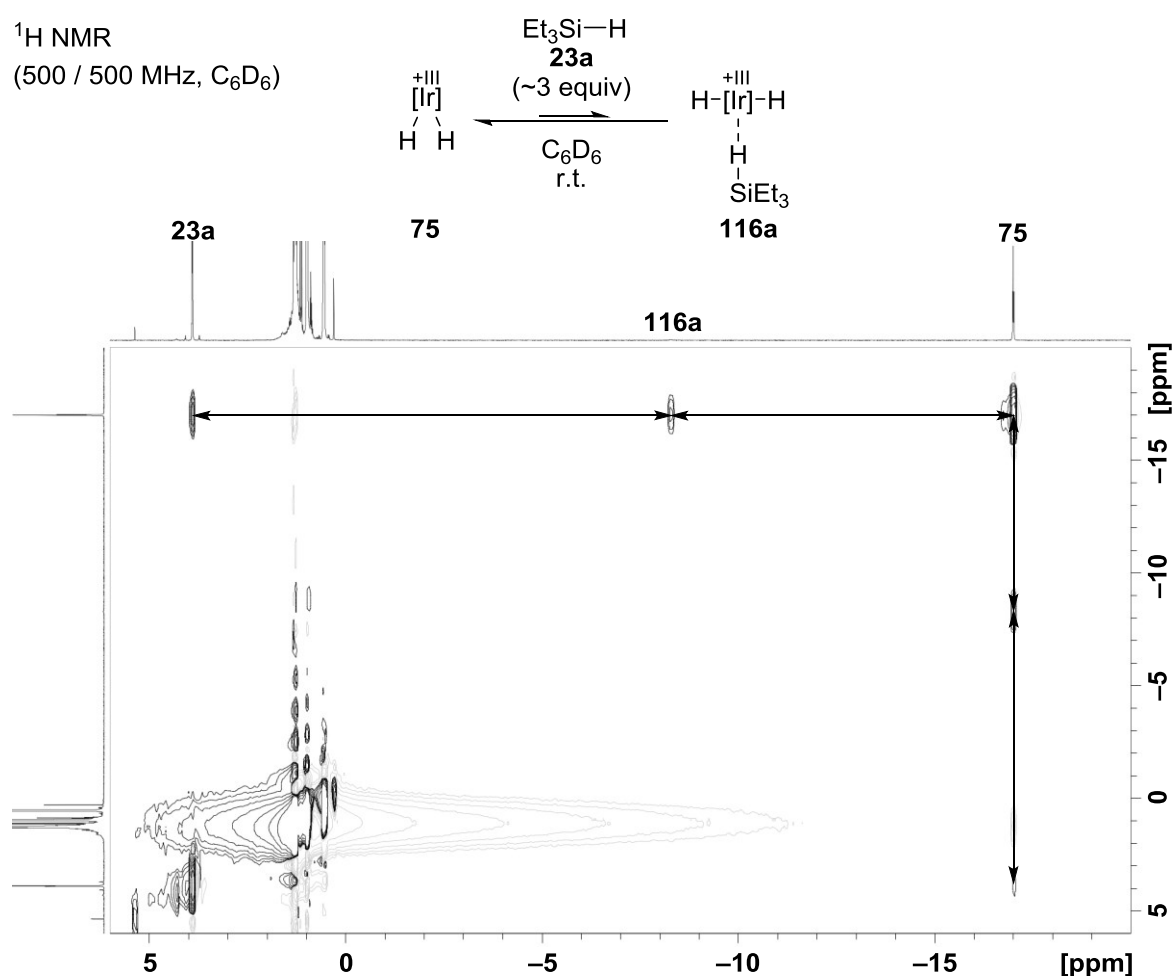
iridium complex	experimental ($\text{SiR}_3 = \text{SiEt}_3$)			calculated ^[a] ($\text{SiR}_3 = \text{SiMe}_3$)		
	δ (^1H) (ppm)	δ (^{31}P) (ppm)	δ (^{29}Si) (ppm)	δ (^1H) (ppm)	δ (^{31}P) (ppm)	
$\begin{array}{c} \text{H} \\ \\ [\text{Ir}]-\text{H}-\text{SiR}_3 \\ \\ \text{H} \end{array}$ 116	-8.3 (t, 9.0 Hz) 224 K	183.2	—	-6.8 (H1) -7.7 (H2) -6.6 (H3)	172.1	This work
$\begin{array}{c} \text{H} \\ \\ [\text{Ir}]^+-\text{H}-\text{SiR}_3 \\ \\ \text{H} \end{array}$ 117	-9.3 (t, 10.5 Hz) 197 K	171.4	-0.7	-7.2 (H1) -7.9 (H2) -6.7 (H3)	167.0	This work
$\begin{array}{c} [\text{Ir}] \\ \quad \\ \text{H} \quad \text{H} \end{array}$ 75	-17.0 (t, 8.2 Hz) 300 K	204.2	—	-16.5	204.9	ref. [96], This work
$\begin{array}{c} [\text{Ir}]-\text{H} \\ \\ \text{SiR}_3 \end{array}$ 107	-15.9 (t, 5.9 Hz) 300 K	188.8	-3.9	-14.0		ref. [78], This work
$\begin{array}{c} [\text{Ir}]^+-\text{H}-\text{SiR}_3 \\ \\ \text{H} \end{array}$ 74⁺	-4.9 (H1) -44.2 (H2) (t, 11.6 Hz) 200 K			-4.4 (H1) -40.0 (H2)		ref. [98], This work

^[a] Chemical shifts calculated at the four-component mDKS level using the PBE exchange correlation functional in conjunction with Dyal's triple- ζ basis set on iridium and fully uncontracted IGLO-III basis sets on the ligand atoms.

By plotting the ratios of the two trihydrides **116a** and **117a** at 224 and 197 K using the VAN'T HOFF equation (Equation 1) the enthalpy and entropy of the reaction is estimated to be $\Delta H = -19.27 \text{ kJ mol}^{-1}$ and $\Delta S = -84.35 \text{ J mol}^{-1} \text{ K}$, respectively. According to the thermodynamic values, the isomerization from **116a** to **117a** is thus favored by enthalpy but strongly unfavored by entropy.

$$\ln K_{eq} = -\frac{\Delta H}{RT} + \frac{\Delta S}{R} \quad (1)$$

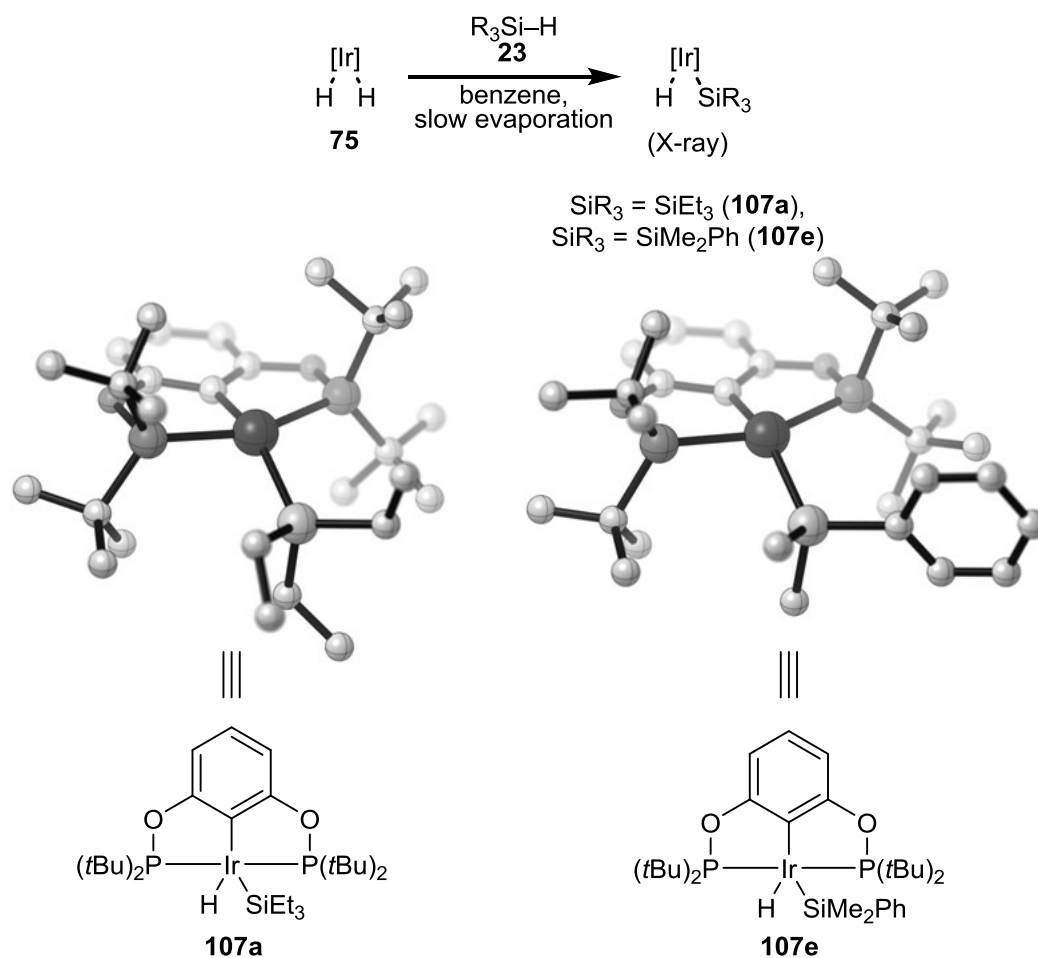
The dynamic nature of the hydrosilane **23a** coordination to the iridium dihydride **75** was further studied by an EXSY NMR experiment (Scheme 2.16). At room temperature using 300 ms mixing time, chemical exchange between the hydrides of the free hydrosilane **23a**, iridium dihydride **75**, and the iridium trihydride **116a** was observed. The measurement shows that the trihydride **116a** is kinetically accessible under the catalytic conditions.



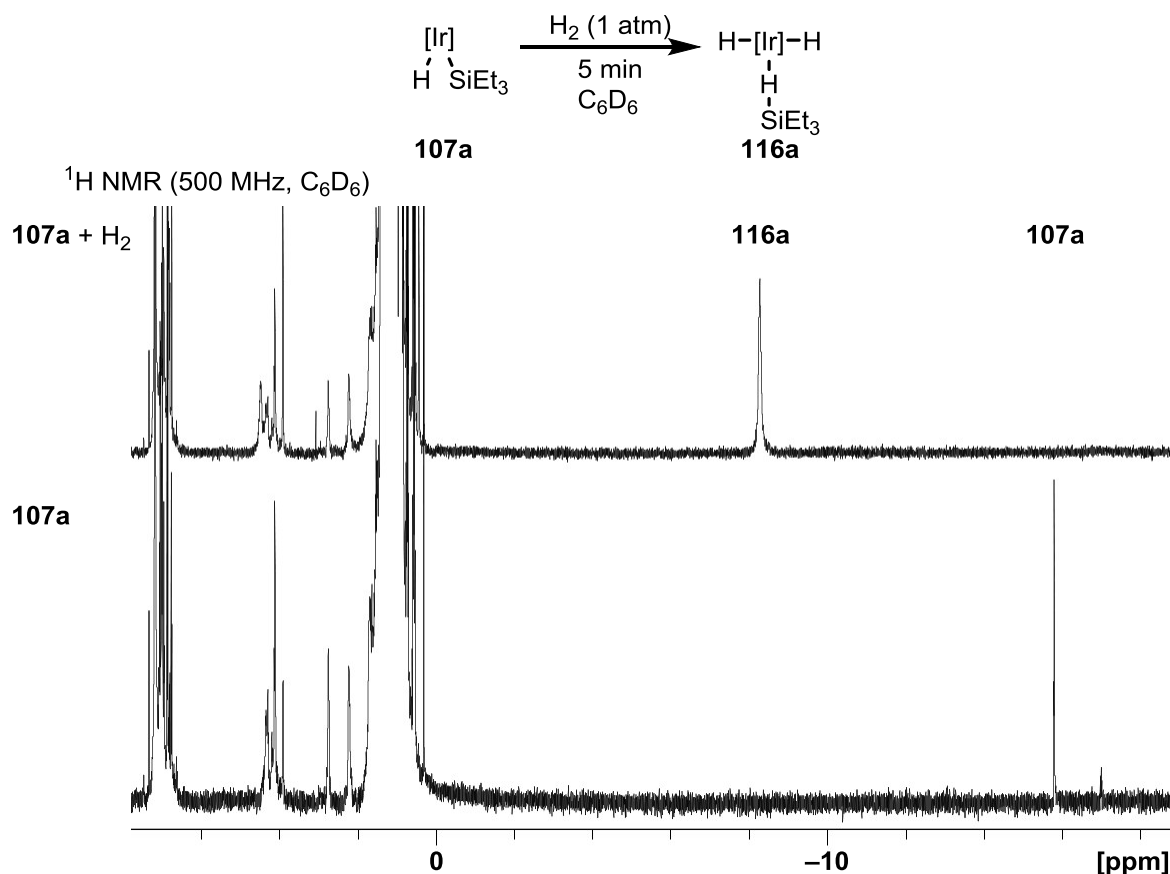
Scheme 2.16: EXSY NMR spectra of iridium dihydride **75** and triethylsilane (**23a**).

Attempts to grow crystals suitable for X-ray diffraction of the trihydrides **116** and **117** by slow evaporation of mixtures of dihydride **75** and hydrosilanes **23** led to liberation of dihydrogen and isolation of iridium silyl hydrides **107** (Scheme 2.17). Due to surrounding heavy atoms, the hydrogen atom attached to the iridium center could not be located but NMR analysis of

the crystalline material allowed the unambiguous assignment of the complex as the monohydride **107a**. Interestingly, when the NMR sample was subjected to an atmosphere of dihydrogen and immediately reanalyzed, full conversion into the trihydride **116a** was observed (Scheme 2.18). When a flask containing the red iridium silyl hydride **107** crystals was subjected to an atmosphere of dihydrogen a color change to orange was observed. Unfortunately, the crystals concomitantly collapsed into noncrystalline powder, preventing further X-ray crystallographical analysis.



Scheme 2.17: Molecular structures of the iridium silyl hydride complexes **107a** and **107e**.



Scheme 2.18: ¹H NMR analysis of iridium complex **107a** under argon (bottom) and dihydrogen (top) atmosphere.

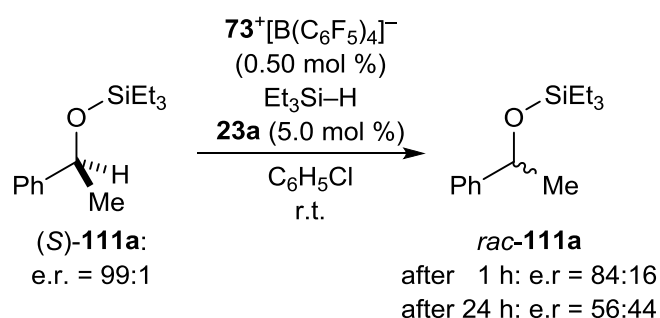
Combined experimental and theoretical experiments indicate iridium trihydride **116** or **117** as the actual active hydride donor during the catalysis. Neither the experiments nor the theoretical calculations could however distinguish between the two complexes. Calculated thermodynamic hydricities of the selected iridium hydrides show that the trihydrides **116** and **117** are the strongest hydride sources (Table 2.5). However, the difference between the two trihydrides was calculated to be only 0.8 kJ mol⁻¹ favoring **116**. Conceivably the other donors should be able to form similar adducts as **116** with the dihydride. However, unlike the other donors, only hydrosilane **23** is expected to readily undergo oxidative addition on the iridium center to form the unique iridium(V) complex **117**. Intuitively, this unusual complex **117** seems to be the most probable hydride source.

Table 2.5: Thermodynamic hydricities of relevant iridium pincer complexes and Me₃SiH (**23d**) with respect to trityl cation.^[a]

$\text{M-H} + \text{Ph}_3\text{C}^+ \rightleftharpoons \text{M}^+ + \text{Ph}_3\text{CH}$					
hydride source (M-H)	conjugate hydride acceptor (M ⁺)	ΔE_{SCF} (kJ mol ⁻¹)	ΔH^0 (kJ mol ⁻¹)	ΔS^0 (J mol ⁻¹ K ⁻¹)	ΔG^0 (kJ mol ⁻¹)
[Ir]H ₂ 75	[Ir]H ⁺ 76⁺	-141.1	-130.2	2.5	-130.7
[Ir]H ₂ (H-SiMe ₃) 116d	[Ir]H(H-SiMe ₃) ⁺ 74d⁺	-202.8	-190.2	-21.3	-183.8
[Ir]H ₃ SiMe ₃ 117d	[Ir]H(H-SiMe ₃) ⁺ 74d⁺	-198.3	-189.6	-22.0	-183.0
Me ₃ Si-H 23d	Me ₃ Si ⁺ 118d⁺	28.6	25.9	-17.5	31.1

^[a] Electronic energies including dispersion corrections ESCF, enthalpies H, entropies S and Gibbs free energies G calculated at the B3LYP-D3(BJ)/ECP/6-31++G(d,p) level using the SMD solvation model.

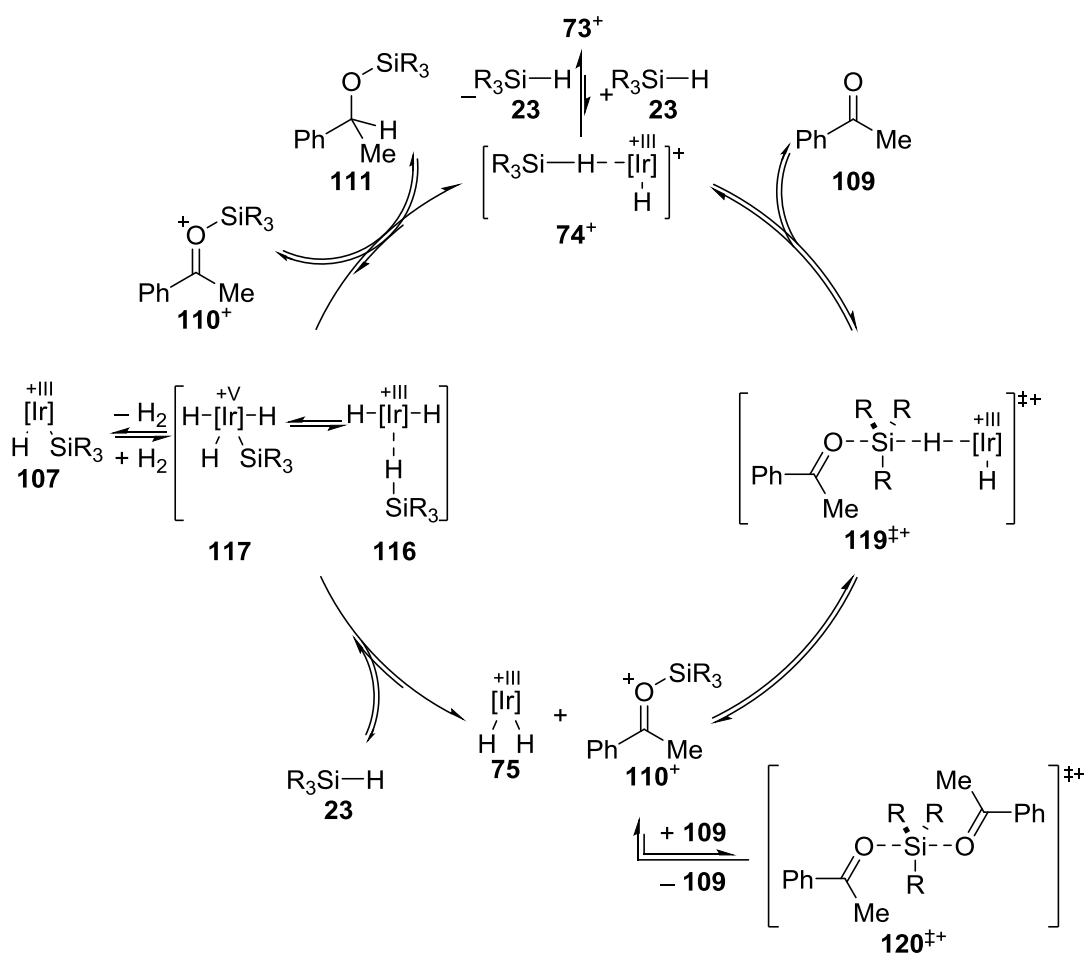
When enantioenriched silyl ether (*S*)-**111a** was subjected to catalytic conditions, slow racemization was observed (Scheme 2.19). The control experiment shows that the final hydride transfer is in fact reversible, i.e. the iridium complex **73⁺** is able to abstract a hydride from the carbon atom of silyl ether **111a**.



Scheme 2.19: Racemization of enantioenriched silyl ether (*S*)-**111a**.

Based on the mechanistic investigation, a refined and partially revised catalytic cycle is presented (2.20). The reversible hydrosilane coordination to **73⁺** gives the complex **74⁺** with activated hydrosilane. The LEWIS-basic carbonyl oxygen atom then attacks the silicon atom *via* an S_N2-Si mechanism (**119[±]**) giving silylcarboxonium ion **110⁺** with inversion of stereochemistry at the silicon atom. Subsequent attack of another ketone molecule **109**

leads to racemization at the silicon atom through intermediate **120**⁺⁺. The iridium dihydride **75** is activated by a second molecule of hydrosilane **23** to give the iridium trihydrides **116** and **117**. Reversible hydride transfer to the silylcarboxonium ion **110**⁺ releases the silyl ether **111** and regenerates the active catalyst **74**⁺.



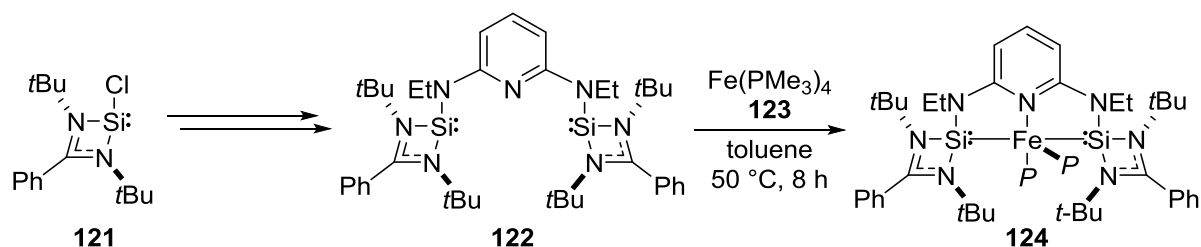
Scheme 2.20: Revised catalytic cycle of the iridium POCOP pincer complex **73**⁺-catalyzed hydrosilylation of ketones.

The detailed investigation of the mechanism of the iridium POCOP pincer complex-catalyzed hydrosilylation led to partial revision of the accepted mechanism and revealed new details about the mode of action of this important catalyst. Although the work was done using the ketone hydrosilylation as a model reaction, it is likely that the activation of the iridium dihydride by another molecule of hydrosilane **23** occurs also during the other reactions catalyzed by the complex **73**⁺.

3 MECHANISTIC INVESTIGATION INTO IRON(II) SiNSi Pincer Complex-CATALYZED CARBONYL HYDROSILYLATION^[113]

3.1 Synthesis of Iron(0) SiNSi Pincer Complex and Application in the Carbonyl Hydrosilylation

Unlike their carbon analogs, N-heterocyclic silylene (NHSi) ligands have not been extensively explored yet. A few interesting examples have shown that these strong σ -donor ligands might in some cases outperform the standard phosphine ligands as well as widely applied N-heterocyclic carbenes (NHC).^[114] DRIESS and co-workers reported recently the synthesis of an iron(0) SiNSi complex **124** (Scheme 3.1).^[115] The SiNSi ligand **122** was synthesized in two steps from the stable chlorosilylene **121**.^[116] Complexation of tetrakis(trimethylphosphine)iron(0) (**123**) gave the iron(0) SiNSi pincer complex **124**. The iron(0) complex **124** was found to be catalytically active in the hydrosilylation of ketones but the mechanism of the reaction remained unexplained. Unlike the mechanisms of late-transition metal complexes, mechanisms of iron and other abundant-metal complexes are often not well understood.^[94]



Scheme 3.1: Synthesis of the iron(0) SiNSi pincer complex **124** ($P = \text{Me}_3\text{P}$).

^[113] The mechanistic investigation of the iron SiNSi pincer complexes described in this chapter was done in collaboration with Dr. DANIEL GALLEG0 from the group of Prof. Dr. MATTHIAS DRIESS. The DFT calculations were performed by Dr. TIBOR SZILVÁSI.

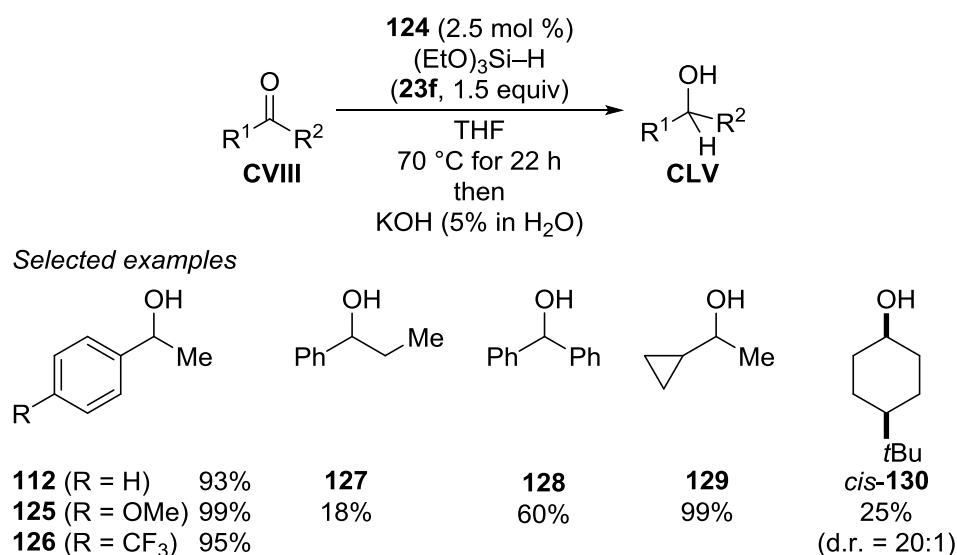
^[114] a) D. Gallego, B. Blom, G. Tan, M. Driess in *Reference Module in Chemistry, Molecular Sciences and Chemical Engineering*, Elsevier, **2015**, p. 1–15; b) B. Blom, D. Gallego, M. Driess, *Inorg. Chem. Front.* **2014**, *1*, 134–148; c) B. Blom, M. Stoelzel, M. Driess, *Chem. Eur. J.* **2013**, *19*, 40–62.

^[115] D. Gallego, S. Inoue, B. Blom, M. Driess, *Organometallics* **2014**, *33*, 6885–6897.

^[116] C.-W. So, H. W. Roesky, J. Magull, R. B. Oswald, *Angew. Chem.* **2006**, *118*, 4052–4054; *Angew. Chem. Int. Ed.* **2006**, *45*, 3948–3950.

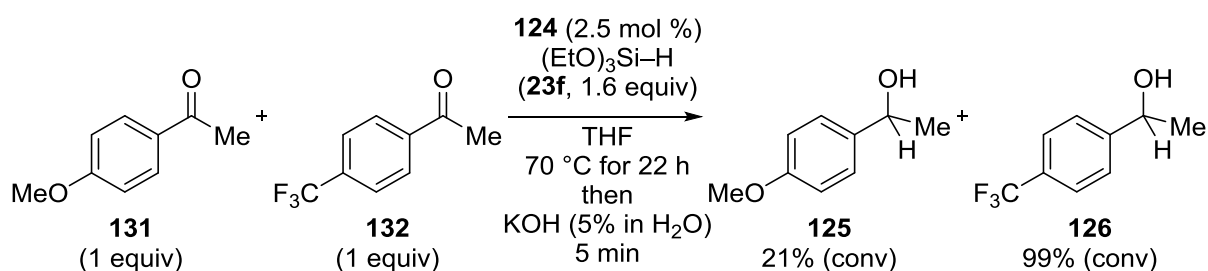
3.2 Mechanistic Investigation into Iron SiNSi Pincer Complex-Catalyzed Carbonyl Hydrosilylation

Under the optimized conditions, iron(0) SiNSi pincer complex **124** (2.5 mol %) is able to catalyze the hydrosilylation of various acetophenones (Scheme 3.2). The reaction was found to be relatively inert to electronic variation of the substrate (**125** vs. **126**), but increased sterics around the carbonyl group thwarted the reaction (**112** vs. **127** vs. **128**). Hydrosilylation of cyclopropyl substituted ketone proceeded efficiently (99% yield) without opening of the cyclopropyl ring to give **129**, contradicting single electron transfer mechanisms. The *cis*-4-*tert*-butyl cyclohexanol (*cis*-**130**) was isolated as a single diastereomer in poor yield (25%).



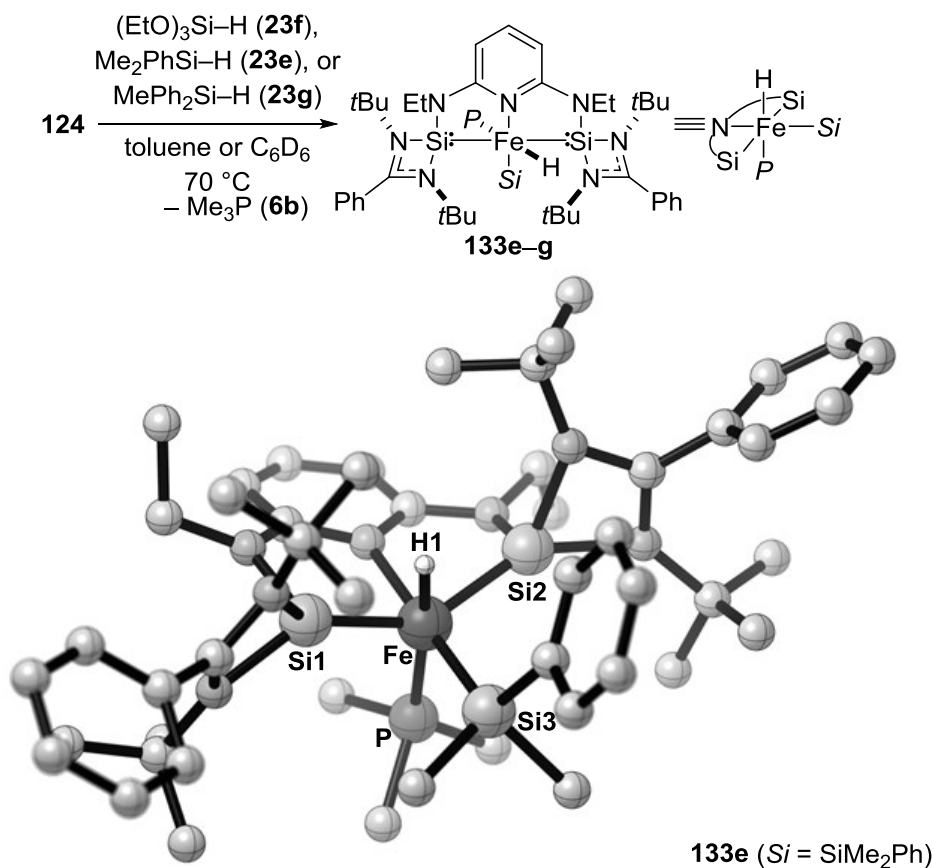
Scheme 3.2: Iron-catalyzed hydrosilylation of ketones.

Although under the optimized conditions both the electron-rich and the electron-poor substrates **131** and **132**, respectively gave full conversion, a clear difference was seen in a competition experiment between the methoxy-substituted **131** and the trifluoromethyl-substituted **132** (Scheme 3.3). Surprisingly, the electron-poor ketone **132** gave full conversion in only 5 min while the electron-rich ketone **131** had reached only 21% conversion.



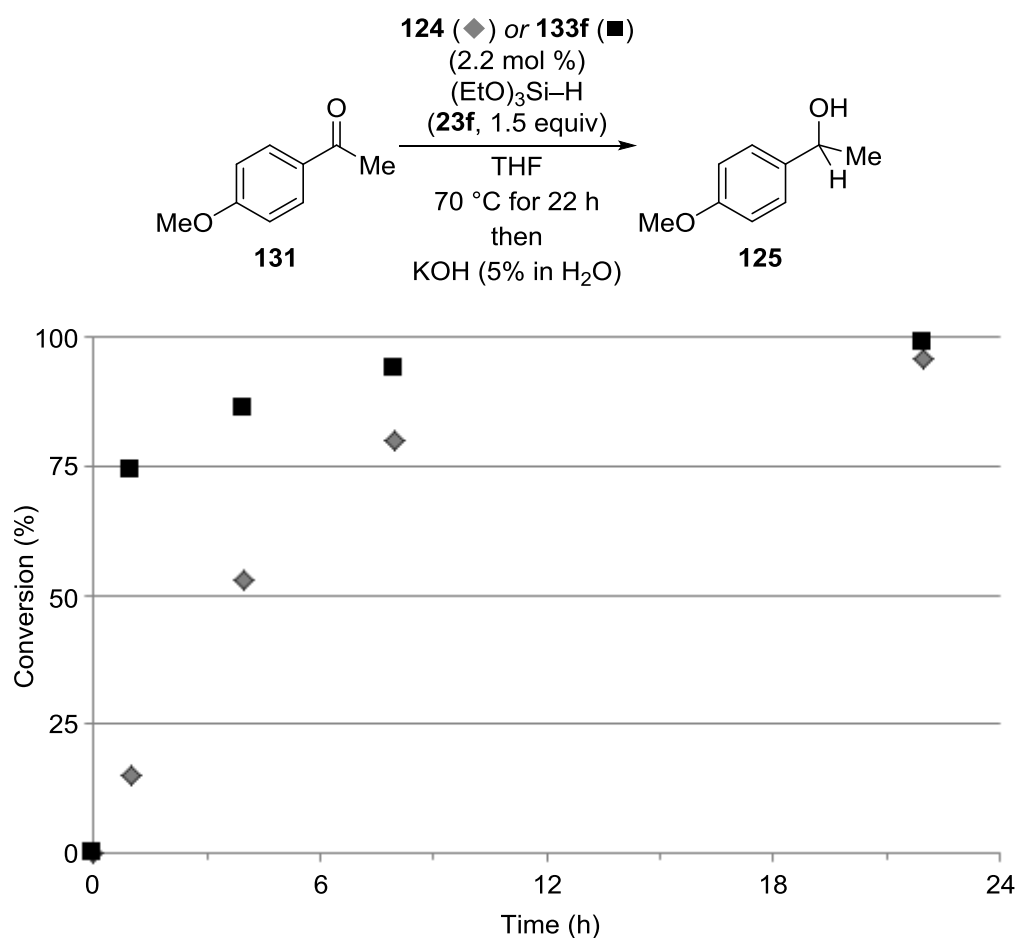
Scheme 3.3: Competition experiment between electronically different ketones **131** and **132**.

We then set out to investigate whether the iron(0) would be the real active catalyst or only a precatalyst. Heating a mixture of the complex **124** and hydrosilanes **23** led to the formation of a new iron hydride **133** which after diligent multinuclear NMR analysis was identified as an iron(II) silyl hydride complex with the hydride resting between the NHSi *tert*-butyl groups *trans* to the trimethylphosphine ligand (Scheme 3.4). The assigned molecular structure was confirmed by X-ray analysis of **133e**.



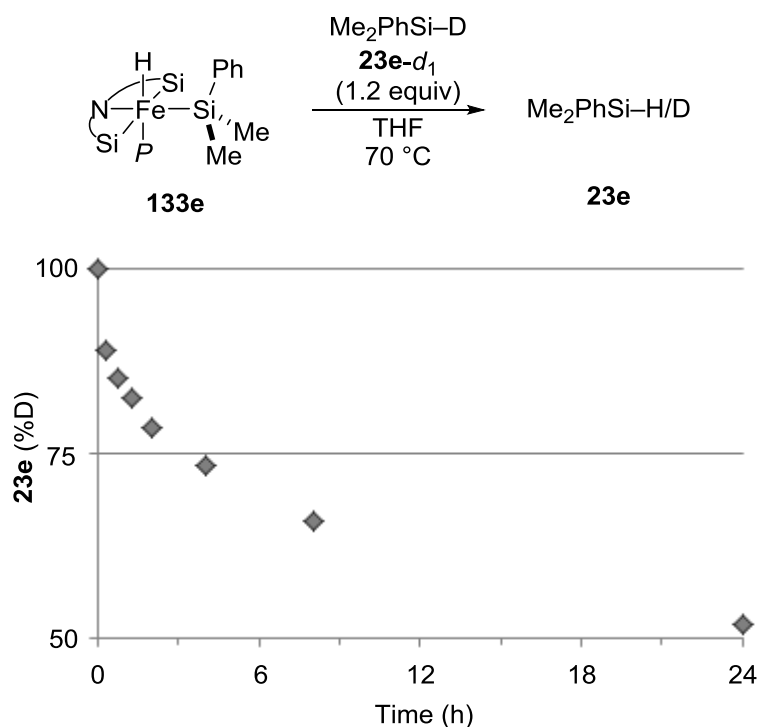
Scheme 3.4: Isolation of the iron(II) complexes **133** and the molecular structure of **133e** ($P = \text{Me}_3\text{P}$).

To verify that the iron(II) complex **133** was the active catalyst being formed *in situ* from the iron(0) complex **124**, we analyzed the kinetic profiles of each complex (Scheme 3.5). After 1 h, the reaction catalyzed by the iron(II) complex **133f** had reached 74% while the iron(0) complex **124**-catalyzed reaction had reached only 15% conversion. The experiment proves that complex **133** is not only active but also more efficient than the iron(0) complex **124** supporting the hypothesis that the complex **124** is a precatalyst that is transformed into the active catalyst **133** during the reaction.



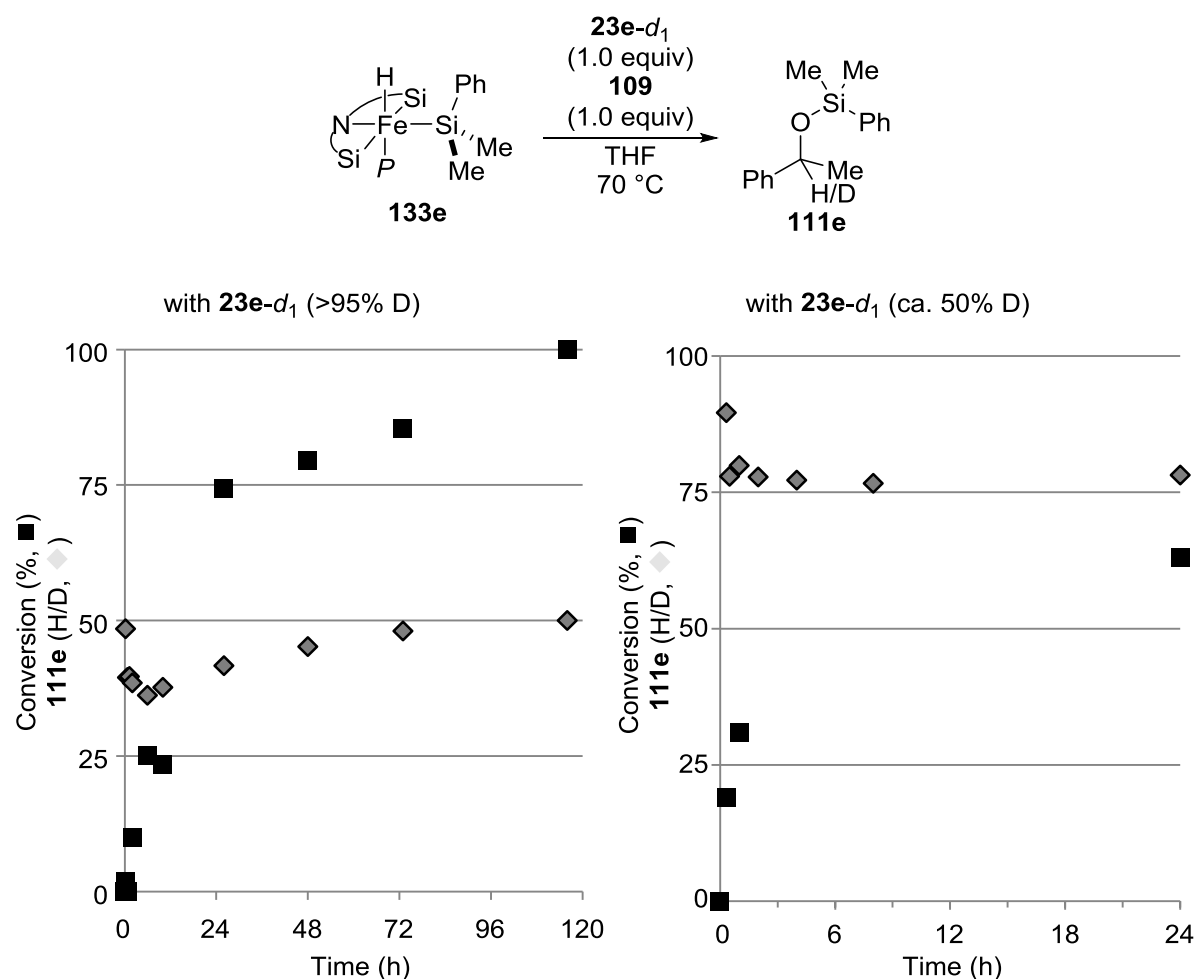
Scheme 3.5: Kinetic profiles of iron(0) complex **124** and iron(II) complex **133f**.

The structure of complex **133** was puzzling as both the metal center and the hydride were deeply embedded inside the pincer complex. To probe the reactivity of the hydride, we performed a series of reactions with deuterium-labeled hydrosilane **23e-d₁** (Scheme 3.6). Firstly, the iron(II) complex **133e** was found to slowly undergo H/D scrambling with **23e-d₁**, leading to complete scrambling in 24 h.



Scheme 3.6: H/D scrambling between iron complex **133e** and deuterium-labeled hydrosilane **23e-d₁**.

The hydrosilylation of acetophenone (**109**) with **23-d₁** however gave perplexing results (Scheme 3.7). The reaction with **23e-d₁** (>95% D) gave first low level of deuteration at the silyl ether **111e** (H/D = 48/52 at 2% conversion). Later the deuteration degree increased up to H/D = 36/64 at 25% conversion. When the reaction reached full conversion the H/D ratio had equilibrated back to H/D = 50/50. Using partially deuterated hydrosilane **23e-d₁** (ca. 50% D) led to first low-levels of deuterium incorporation (H/D = 90/10 at 19% conversion). During the reaction, the ratio again slowly rose towards the equilibrium reaching H/D = 78/22 at 63% conversion.

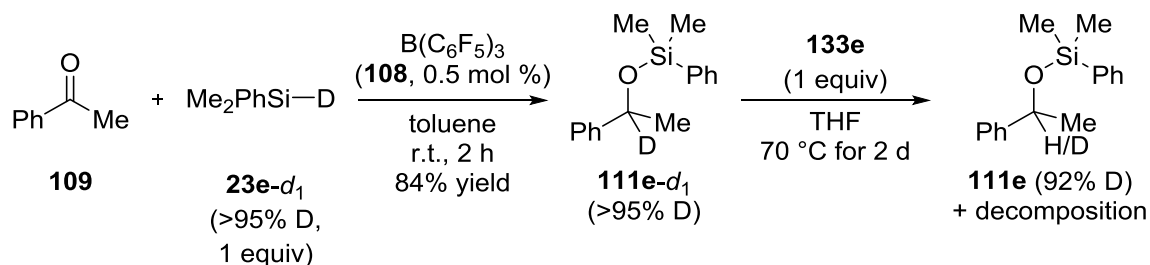


Scheme 3.7: Hydrosilylation of acetophenone **109** with deuterium-labeled hydrosilane **23e-d₁**.

To analyze the results, we must assume that the H/D scrambling between **133e** and **23e-d₁** takes place early during the reaction releasing a small concentration of undeuterated hydrosilane **23e**. A large kinetic isotope effect would lead into a significantly faster reaction with the unlabeled **23e**. Thus, the reaction would start with low level of deuterium incorporation. As the reaction proceeds the supply of **23e** is depleted and the deuterium-to-hydrogen ratio starts to increase. Toward the end of the reaction the H/D ratio decreases approaching equilibrium at 50/50. This unusual behavior would only be explained by H/D scrambling between complex **133e** and the silyl ether **111e**. Importantly, the experiment indicates that the hydride is transferred from the free hydrosilane **23e** not the iron(II) complex **133e**.

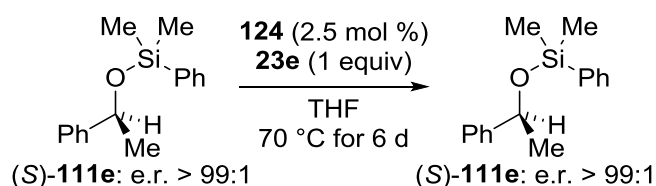
The scrambling between silyl ether **111e** and iron complex **133e** was investigated by stoichiometric control experiments (Scheme 3.8). The deuterium-labeled silyl ether **111e-d₁** was synthesized by B(C₆F₅)₃ (**108**)-catalyzed hydrosilylation of acetophenone (**109**) with **23e-d₁**. When the deuterium-labeled silyl ether **111e-d₁** was subjected to the iron(II) complex

133e, slow H/D scrambling was observed together with decomposition into unknown byproducts.



Scheme 3.8: Partial H/D scrambling at the methine position of the silyl ether **111e-d₁**.

However, the enantiomeric ratio of silyl ether (*S*)-**111e** (e.r. > 99:1) was found to remain unaffected under the catalytic conditions (Scheme 3.9).

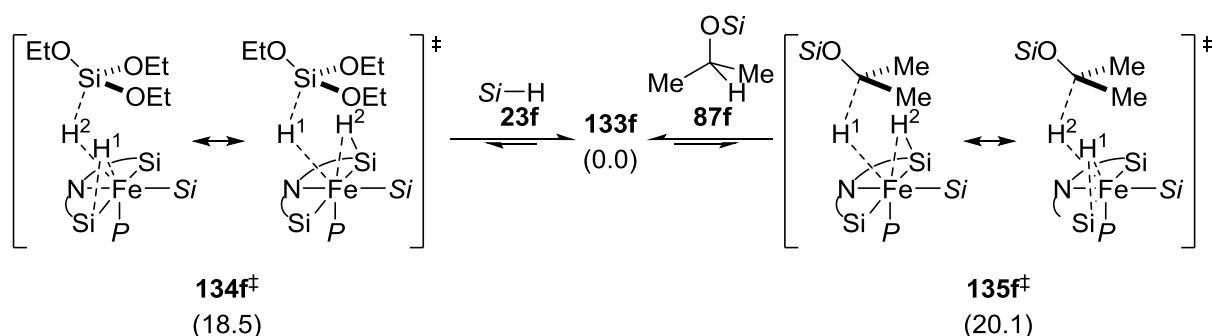


Scheme 3.9: Racemization experiment with enantiomerically enriched silyl ether (*S*)-**111e**.

The detailed mechanism of the hydride scramblings was investigated by DFT calculations (Scheme 3.10).^[117] We were able to locate structures for both hydrosilane **23f** and the silyl ether **87f** scramblings. During the exchange, the iron hydride is shifted to the neighboring silicon atom of the NHSi ligand while the hydride from the silicon or carbon atom of **23f** and **87f**, respectively, coordinates to the vacant coordination site at the iron center to give a pair of symmetrical transition states (**134f[‡]** for hydrosilane **23f** and **135f[‡]** for silyl ether **87f**). The changes in the geometry of the iron pincer complex indicate that the formal oxidative addition takes place at the silicon(II) center, not the iron(II).^[118]

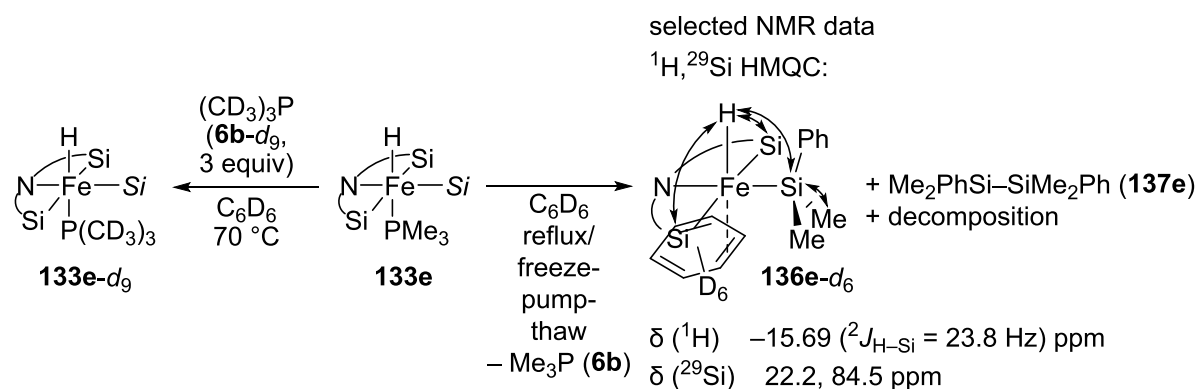
^[117] All calculations were performed at ω B97X-D/6-31G(d)[Fe:ccpVTZ] level of theory. Iron(II) complex **133f**, triethoxysilane (**23f**), and acetone (**83**) were used as model substrates.

^[118] For a review on non-innocent ligands, see: O. R. Luca, R. H. Crabtree, *Chem. Soc. Rev.* **2013**, 42, 1440–1459.



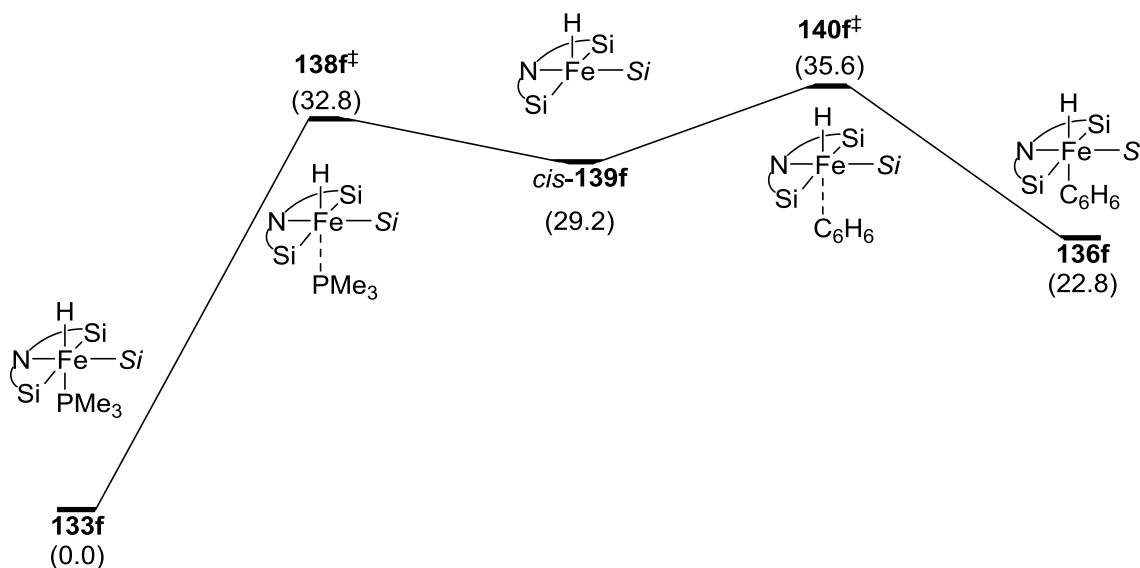
Scheme 3.10: Calculated transition states for H/D scrambling between the **133e** iron hydride and methine C–H of the silyl ether **87f** and hydrosilane **23f**.

The dissociation of the trimethylphosphine (**6b**) has been suggested to lead into the exposure of the highly reactive metal center with related iron complexes.^[119] Subjection of iron(II) pincer complex **133e** to deuterated trimethylphosphine (**6b-d₉**) did indeed give slow exchange of phosphine ligands (Scheme 3.11). Attempts to isolate the unsaturated phosphine-dissociated iron(II) complex with reflux/freezing-pump-thaw cycles led to the detection of a new iron hydride species that was, with the assistance of DFT calculations (Scheme 3.12), assigned as **136e-d₆** with C₆D₆ as a ligand. The formation of the new iron complex was accompanied by the formation of disilane **137e**. The role and mechanism of the disilane formation remains unexplained.



Scheme 3.11: Phosphine-dissociation experiments.

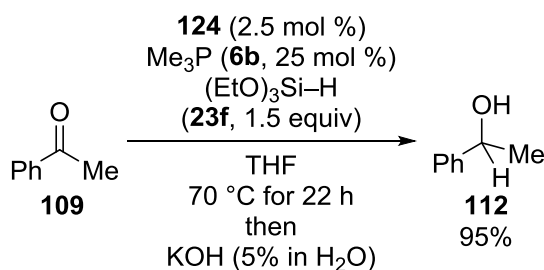
^[119] P. Bhattacharya, J. A. Krause, H. Guan, *Organometallics* **2011**, *30*, 4720–4729.



Scheme 3.12: Calculated formation of benzene adduct **136f** via unsaturated iron complex *cis*-**139f**.

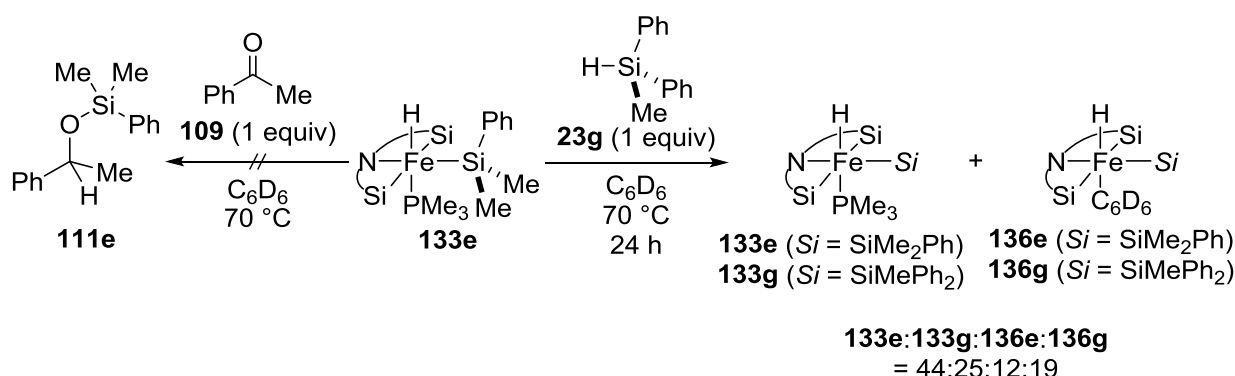
The generation of **136e-d₆** in the presence of ketone **109** did not produce any silyl ether **111e**. Instead, the dissociation of the trimethylphosphine (**6b**) from the complex **133e** was found to be significantly slower. The increased stability of **133e** in the presence of the ketone **109** suggests transient complexation of the two.

To exclude the phosphine-dissociated complex **139** as a potential intermediate during the reaction, we examined the effect of excess trimethylphosphine (**6b**) to the reaction (Scheme 3.13). The reaction proceeded smoothly with no indication of inhibition, strongly suggesting that **136-d₆** and related phosphine-dissociated complexes result from decomposition pathways, and are not part of the actual active catalytic cycle.



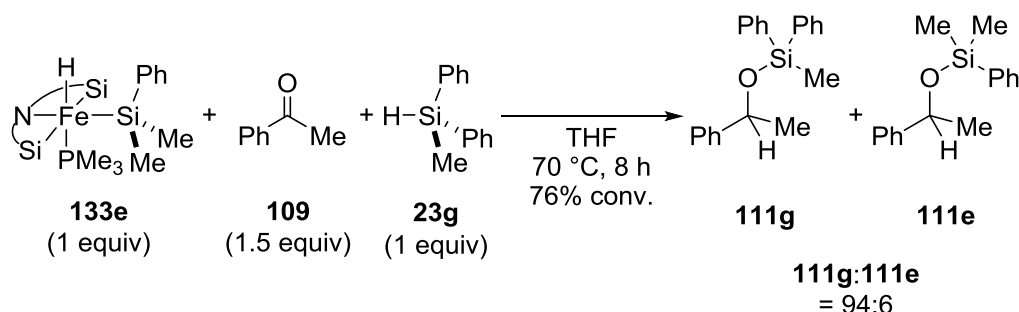
Scheme 3.13: Inhibition experiment with excess trimethylphosphine (**6b**).

The silyl transfer was investigated with stoichiometric crossover experiments (Scheme 3.14). As expected, addition of ketone **109** to iron(II) complex **133e** did not lead to product formation. The lability of the silyl group was probed by a silyl-scrambling experiment between complex **133e** and hydrosilane **23g**. After 24 h, partial exchange was observed (**133e**:**133g** = 64:25) together with the corresponding phosphine-dissociated products **136e** and **136g** as well as mixture of disilanes **137**. Importantly, only traces of liberated hydrosilane **23e** were observed, indicating that the observed silyl exchange is in fact only a side product of the decomposition.



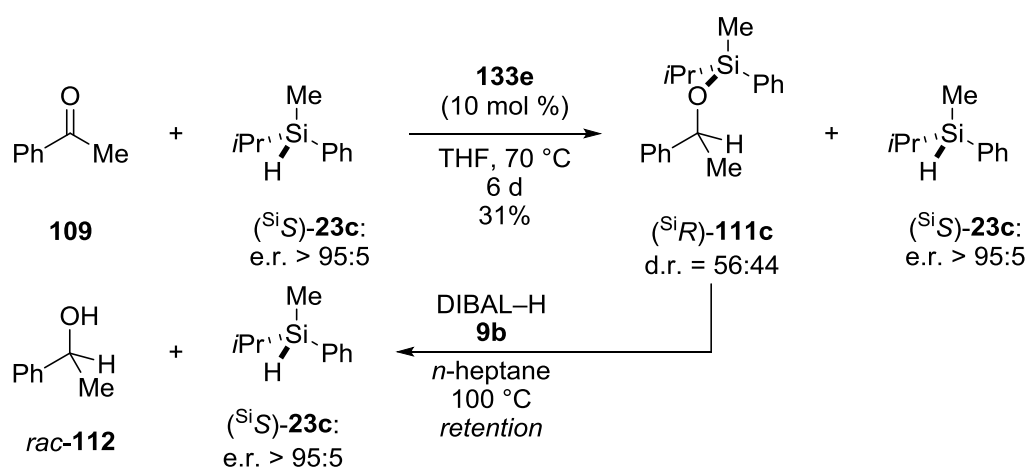
Scheme 3.14: Stoichiometric experiments with ketone **109** and hydrosilane **23g**.

Hydrosilylation of ketone **109** with hydrosilane **23g** using complex **133e** gave silyl ethers **111g** and **111e** in a ratio of 94:6 (Scheme 3.15). The experiment unequivocally shows that the silyl group is transferred from the free hydrosilane while the silyl group at the iron center remains intact.



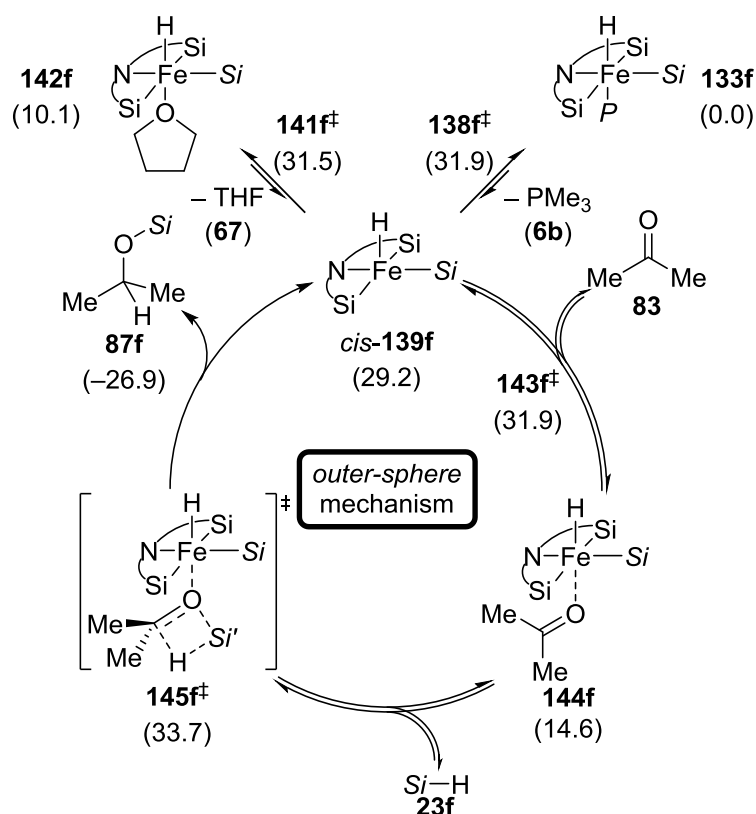
Scheme 3.15: Hydrosilane-crossover experiment.

The mechanism of the silyl group transfer was then investigated using enantioenriched silicon-stereogenic hydrosilane (*S*)-**23c** (e.r. > 95:5). The hydrosilylation of **109** with iron(II) complex **133e** proceeded sluggishly and after six days the desired silyl ether **111c** was isolated in 31% yield with low diastereomeric ratio (d.r. = 56:44) (Scheme 3.16). The unreacted hydrosilane (*S*)-**23c** was isolated with unaffected enantiomeric ratio (e.r. > 95:5). Reductive cleavage of the silyl ether **111c** released the hydrosilane (*S*)-**23c** with retention of enantiomeric ratio (e.r. > 95:5). The observed retention of configuration at the silyl ether as well as the lack of racemization of the unreacted hydrosilane (*S*)-**23c** suggests a mechanism with concerted addition across the carbonyl group.



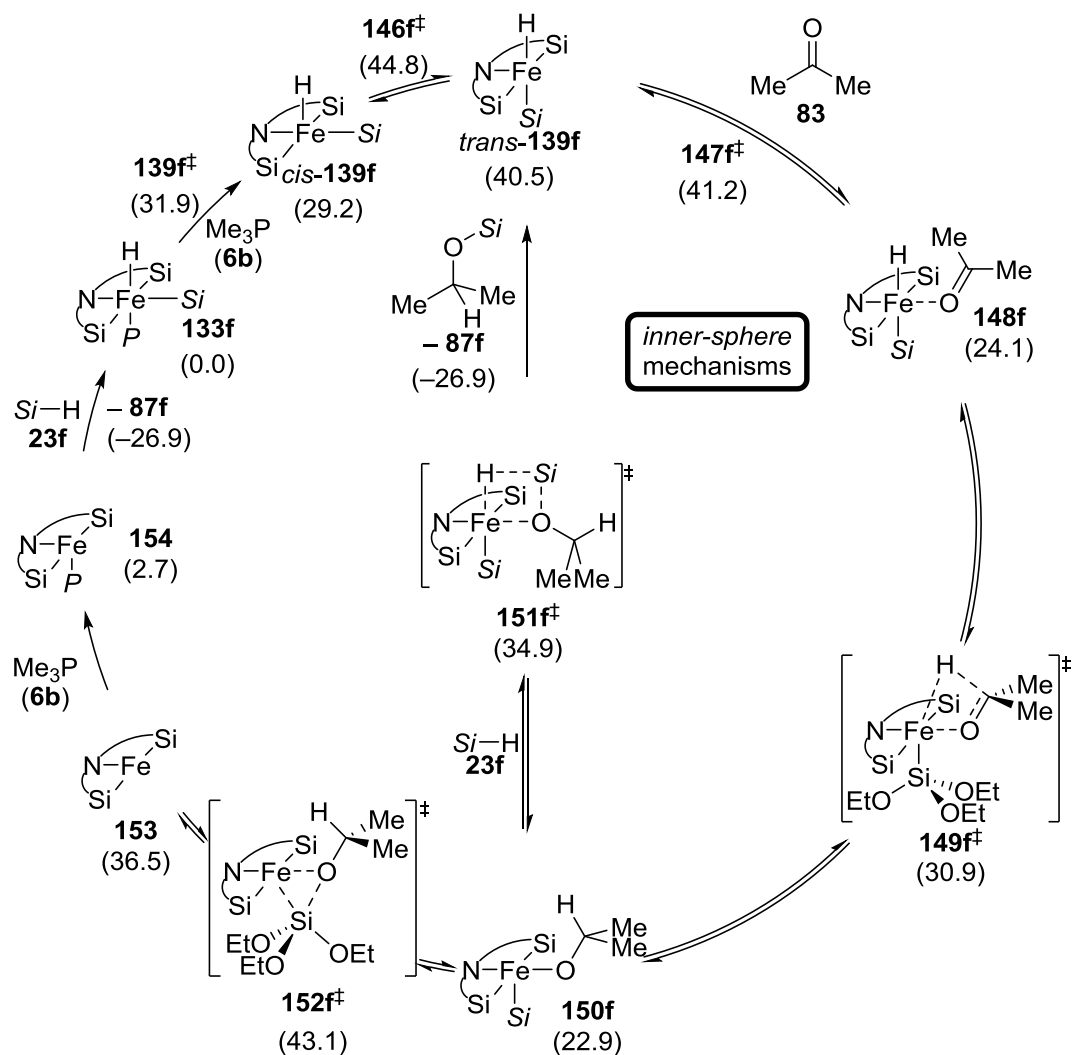
Scheme 3.16: Hydrosilylation of acetophenone **109** with acyclic silicon-stereogenic hydrosilane (*S*)-**23c** catalyzed by iron(II) complex **133e**.

The plausible reaction mechanisms were then thoroughly investigated by DFT calculations. First an outer-sphere mechanism was considered starting from the energetically unfavored phosphine-dissociated complex *cis*-**139f** (29.2 kcal mol⁻¹) (Scheme 3.17). Coordination of ketone **83** to the unsaturated iron center was found to lower the energy giving the intermediate **144f** (14.6 kcal mol⁻¹). The activated carbonyl group then undergoes concerted [2π+2σ]-hydrosilylation through the transition state **145f**[‡] (33.7 kcal mol⁻¹), releasing the silyl ether **87f**.



Scheme 3.17: Calculated outer-sphere mechanism.

Isomerization of *cis*-**139f** into *trans*-**139f** (40.5 kcal mol⁻¹) leads into alternative inner-sphere mechanisms. Again coordination of ketone **83** to the iron center significantly lowers the energy to give **148f** (24.1 kcal mol⁻¹) (Scheme 3.18). Hydride transfer from the iron to the carbon atom *via* **149f[‡]** (30.9 kcal mol⁻¹) gives the iron alkoxide complex **150f** (22.9 kcal mol⁻¹). Concerted σ -bond metathesis (**151f[‡]**, 34.9 kcal mol⁻¹) releases the silyl ether **87f** and regenerates the iron hydride *cis*-**139f**. Alternatively, the intermediate **150f** could undergo reductive elimination *via* **152f[‡]** (43.1 kcal mol⁻¹) releasing the silyl ether **87f** to give iron(0) complex **153** (36.5 kcal mol⁻¹).



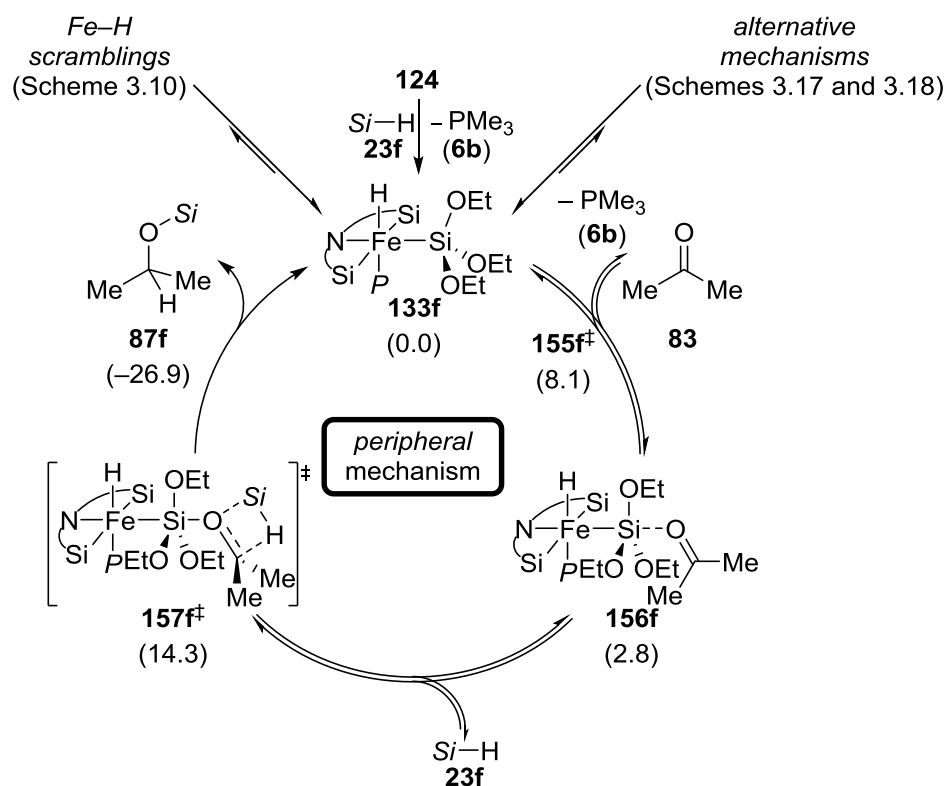
Scheme 3.18: Calculated inner-sphere mechanisms.

None of the conventional mechanisms give satisfactory fit to the experimental results. In addition, the calculated activation barriers are too high. Based on the combined results an unusual mechanism is proposed where the silicon atom of the iron-bound silyl group acts as the LEWIS acid (Scheme 3.19).^[109c,120] In this peripheral mechanism, neither the hydrosilane **23** nor the substrate **83** are in contact with the iron metal center. The adduct **156f** between iron complex **133f** and ketone **83** was located as an intermediate (2.8 kcal mol⁻¹). All attempts to experimentally observe such adducts were not successful. However, the measurement of the LEWIS acidity of the silyl group by GUTMANN–BECKETT analysis¹²¹ led to slight broadening of the ³¹P NMR signal of the Et₃PO indicating transient reversible coordination. The hydrosilylation of the activated ketone **156f** proceeds *via* a concerted

[120] A. L. Liberman-Martin, R. G. Bergman, T. D. Tilley, *J. Am. Chem. Soc.* **2015**, *137*, 5328–5331.

[121] V. Gutmann, *Coord. Chem. Rev.* **1976**, *18*, 225–255; b) M. A. Beckett, D. S. Brassington, M. E. Light, M. B. Hursthouse, *J. Chem. Soc., Dalton Trans.* **2001**, 1768–1772.

mechanism through transition state **157f[‡]** (14.3 kcal mol⁻¹), releasing the silyl ether **87f** with retention at the silicon atom.



Scheme 3.19: Carbonyl hydrosilylation by peripheral mechanism.

The calculated activation barrier for the peripheral mechanism (14.3 kcal mol⁻¹) is decidedly lower than for the outer-sphere (33.7 kcal mol⁻¹) or inner-sphere (40.5 / 43.1 kcal mol⁻¹) mechanisms. The calculated transition state **157f[‡]** is also in good agreement with the experimental evidence, including the increased rate with electron-deficient ketones (Scheme 3.3) and the apparent large kinetic isotope effect (Scheme 3.7).

The mechanistic investigation of the hydrosilylation catalyzed by the iron SiNSi complex **133** revealed several surprising details of these unusual complexes. The H/D scrambling was found to be promoted by the silylene silicon atoms showing their potential redox-activity. Similar reactivity has been observed with NHC ligands^[122] but this is the first reported

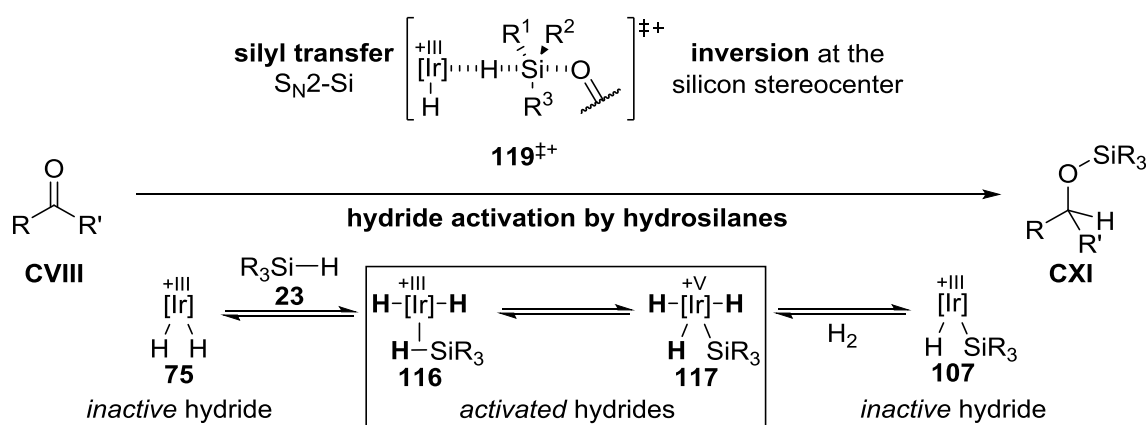
[122] For recent examples, see: a) C. Romain, K. Miqueu, J.-M. Sotiropoulos, S. Bellemin-Laponnaz, S. Dagorne, *Angew. Chem.* **2010**, 122, 2244–2247; *Angew. Chem. Int. Ed.* **2010**, 49, 2198–2201; b) L. R. Collins, G. Hierlmeier, M. F. Mahon, I. M. Riddlestone, M. K. Whittlesey, *Chem. Eur. J.* **2015**, 21, 3215–3218; c) D. Prema, Y. L. N. Mathota Arachchige, R. E. Murray, L. M. Slaughter, *Chem. Commun.* **2015**, 51, 6753–6756; d) R. M. Brown, J. B.

example of non-innocent behavior of NHSi ligands. During the hydrosilylation, the silyl group and the iron hydride remain at the metal center and the iron center does not directly participate in the reaction. The silicon atom of the silyl group acts as the LEWIS acid and catalyzes the reaction at the periphery of the metal center.

Garcia, J. Valjus, C. J. Roberts, H. M. Tuononen, M. Parvez, R. Roesler, *Angew. Chem.* **2015**, *127*, 6372–6375; *Angew. Chem. Int. Ed.* **2015**, *54*, 6274–6277; e) E. Despagne-Ayoub, M. K. Takase, J. A. Labinger, J. E. Bercaw, *J. Am. Chem. Soc.* **2015**, *137*, 10500–10503.

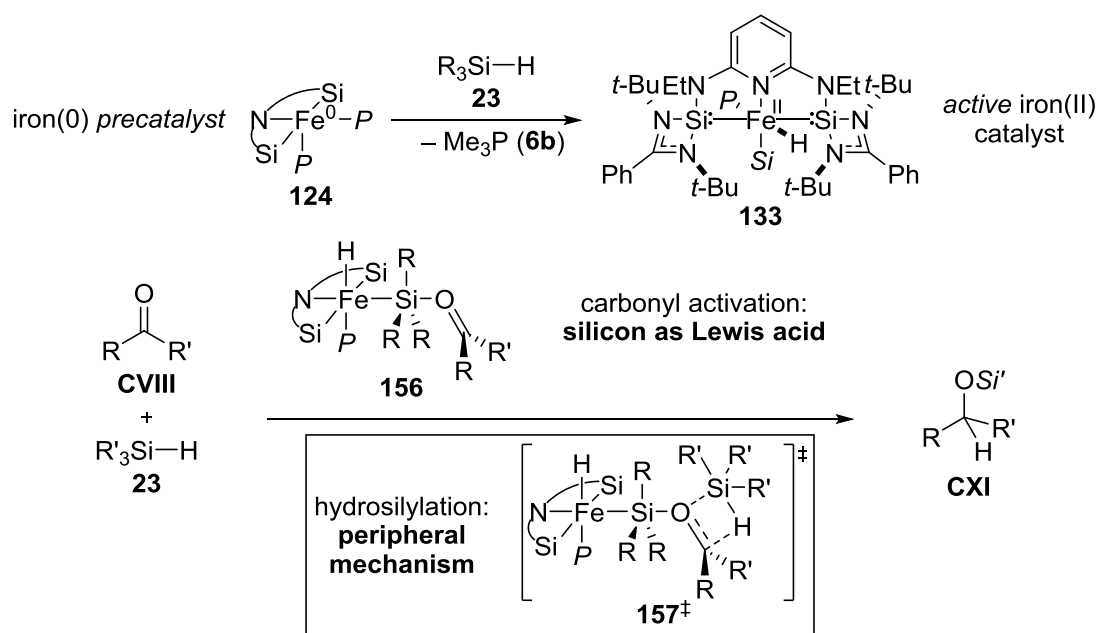
4 SUMMARY

The mechanism of carbonyl hydrosilylation catalyzed by BROOKHART's iridium(III) POCOP pincer complex **73**⁺ was investigated (Scheme 4.1). The experiments with silicon-stereogenic hydrosilanes confirmed the assumed S_N2-Si mechanism of the silyl-transfer step (**119**[‡]). The extensive loss of enantiomeric purity at the silicon stereocenter indicated that the hydride transfer would be rate determining and more complicated than expected. A series of stoichiometric experiments verified an adduct of hydrosilane **23** and the iridium dihydride **75** as the active hydride source. NMR spectroscopic, X-ray crystallographic, as well as computational analysis revealed iridium trihydrides **116** and **117** as the potential hydride donors.



Scheme 4.1: The mechanism of carbonyl hydrosilylation by iridium POCOP pincer complex **73**⁺.

Hydrosilylation of ketones with iron(0) SiNSi pincer complex **124** was found to proceed *via* unprecedented mode of action (Scheme 4.2). First, the iron(0) complex **124** undergoes oxidative addition with the hydrosilane **23** affording the active iron(II) catalyst **133**. The hydride and the silyl ligands on the iron were found to remain at the iron center through the reaction, excluding inner-sphere mechanisms. The stereochemical orientation and purity of the silicon-stereogenic hydrosilane (*S*)-**23c** was found to remain intact, supporting concerted hydrosilylation. Finally, supported by DFT calculations, a peripheral mechanism was proposed where the silicon atom of the silyl ligand acts as a LEWIS acid binding the ketone to form adduct **156**. Concerted hydrosilylation *via* transition state **157**[‡] releases the desired silyl ether **CXII**.



Scheme 4.2: The mechanism of carbonyl hydrosilylation by iron SiNSi pincer complex **133**.

The mechanistic investigations of BROOKHART's iridium(III) POCOP pincer **73⁺** and the iron SiNSi pincer complex **133** revealed new unexpected mechanistic pathways. These studies highlight the need for detailed mechanistic understanding of catalytic systems in order to understand and predict their behavior. It remains to be seen whether the hydrosilane activation of the metal hydride as found for BROOKHART's iridium(III) POCOP pincer complex is a general mode of action. Indeed, several other cationic LEWIS-acidic metal complexes have been proposed to transfer a hydride from a neutral metal hydride intermediate analogous to the dihydride **75**. The mechanisms of iron-catalyzed hydrosilylations have not been previously thoroughly investigated. The iron(II) SiNSi pincer complex **133** is admittedly an unusual iron complex restricting any general conclusions from the mechanistic study. It is however feasible to assume that the peripheral mechanism is operating in other metal-catalyzed main-group hydride activation reactions.

THEORETICAL PART II

APPLICATIONS

5 CARBON DIOXIDE REDUCTION

Efficient conversion of carbon dioxide into valuable C1 synthons is one of the greatest challenges of the chemical community.^[123] Reduction^[124] and conversion^[125] of carbon dioxide have been extensively studied in the recent years. The following chapter focuses on the use of main-group electrophiles in the reduction of carbon dioxide into formate, formaldehyde, methanol, and methane oxidation states.^[126]

5.1 Reduction of Carbon Dioxide into Formate Oxidation State

The first reports of carbon dioxide reduction into formate oxidation state using borohydrides^[127] and aluminum hydrides^[128] are already from 1950s. It was shown that LiBH_4 , NaBH_4 , and LiAlH_4 readily reduce carbon dioxide into formates. The early

^[123] a) M. Aresta, *Carbon Dioxide as Chemical Feedstock*; Wiley-VCH: Weinheim, Germany, **2010**; b) G. A. Olah, A. Goepfert, G. K. S. Prakash, *Beyond Oil and Gas: The Methanol Economy*; Wiley-VCH: Weinheim, Germany, **2006**; c) G. A. Olah, *Angew. Chem.* **2005**, *117*, 2692–2696; *Angew. Chem. Int. Ed.* **2005**, *44*, 2636–2639; d) T. J. Marks et al., *Chem. Rev.* **2001**, *101*, 953–996.

^[124] For recent reviews of carbon dioxide reduction, see: a) F. J. Fernández-Alvarez, A. M. Aitani, L. A. Oro, *Catal. Sci. Technol.* **2014**, *4*, 611–624; b) Y.-N. Li, R. Ma, L.-N. He, Z.-F. Diao, *Catal. Sci. Technol.* **2014**, *4*, 1498–1512; c) C. Costentin, M. Robert, J.-M. Savéant, *Chem. Soc. Rev.* **2013**, *42*, 2423–2436; d) G. Centi, E. A. Quadrelli, S. Perathoner, *Energy Environ. Sci.* **2013**, *6*, 1711–1731; e) Y. Oh, X. Hu, *Chem. Soc. Rev.* **2013**, *42*, 2253–2261; f) E. E. Benson, C. P. Kubiak, A. J. Sathrum, J. M. Smieja, *Chem. Soc. Rev.* **2008**, *38*, 89–99.

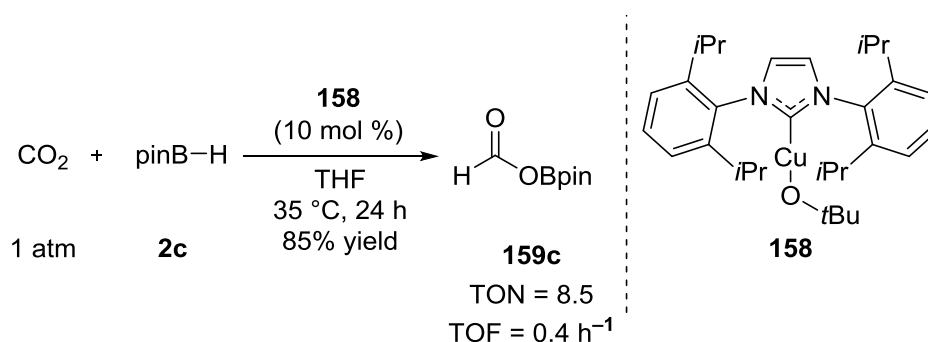
^[125] For recent reviews of carbon dioxide conversion, see: a) C. Maeda, Y. Miyazaki, T. Ema, *Catal. Sci. Technol.* **2014**, *4*, 1482–1497; b) M. Cokoja, C. Bruckmeier, B. Rieger, W. A. Herrmann, F. E. Kühn, *Angew. Chem.* **2011**, *123*, 8662–8690; *Angew. Chem. Int. Ed.* **2011**, *50*, 8510–8537; c) M. Peters, B. Köhler, W. Kuckshinrichs, W. Leitner, P. Markewitz, T. E. Müller, *ChemSusChem* **2011**, *4*, 1216–1240; d) S. N. Riduan, Y. Zhang, *Dalton Trans.* **2010**, *39*, 3347–3357.

^[126] For reduction of carbon dioxide into carbon monoxide, see: a) D. S. Laitar, P. Müller, J. P. Sadighi, *J. Am. Chem. Soc.* **2005**, *127*, 17196–17197; b) L. Gu, Y. Zhang, *J. Am. Chem. Soc.* **2010**, *132*, 914–915; c) C. Kleeberg, M. S. Cheung, Z. Lin, T. B. Marder, *J. Am. Chem. Soc.* **2011**, *133*, 19060–19063; d) R. Dobrovetsky, D. W. Stephan, *Angew. Chem.* **2013**, *125*, 2576–2579; *Angew. Chem. Int. Ed.* **2013**, *52*, 2516–2519; e) C. Lescot, D. U. Nielsen, I. S. Makarov, A. T. Lindhardt, K. Daasbjerg, T. Skrydstrup, *J. Am. Chem. Soc.* **2014**, *136*, 6142–6147; f) S. Bagherzadeh, N. P. Mankad, *J. Am. Chem. Soc.* **2015**, *137*, 10898–1090.

^[127] a) J. G. Burr, Jr., W. G. Brown, H. E. Heller, *J. Am. Chem. Soc.* **1950**, *72*, 2560–2562; b) T. Wartik, R. K. Pearson, *J. Am. Chem. Soc.* **1955**, *77*, 1075–1075; c) T. Wartik, R. K. Pearson, *J. Inorg. Nucl. Chem.* **1958**, *7*, 404–411; d) R. K. Pearson, T. Wartik, U.S. Patent 2872474, **1959**.

^[128] A. E. Finholt, E. C. Jacobson, *J. Am. Chem. Soc.* **1952**, *74*, 3943–3944.

investigations with borohydrides were recently verified, and the resulting trimetaboborohydride was characterized by X-ray diffraction as well as multinuclear NMR analysis.^[129] Unlike the highly reactive borohydrides, pinacolborane (**2c**) does not react with carbon dioxide. Copper–NHC complex **158** was needed to catalyze the hydroboration of carbon dioxide using hydroborane **2c**. Under mild conditions, 85% yield of borylformate **159c** was obtained after 24 h (Scheme 5.1).^[130]



Scheme 5.1: Copper-catalyzed hydroboration of carbon dioxide into borylformate **159c**.

Since the seminal reports by SÜSS-FINK^[131] and KOINUMA^[132] in 1981, the hydrosilylation of carbon dioxide into silylformate has been achieved with variety of catalysts.^[133] The copper-catalyzed hydrosilylation of carbon dioxide reported by BABA and co-workers was shown to be an exceptionally efficient system for this transformation.^[133c,e] Using polymethylhydrosiloxane (PMHS, **23h**), the reaction reached 70 000 turnovers at 60 °C in 24 h (Scheme 5.2).

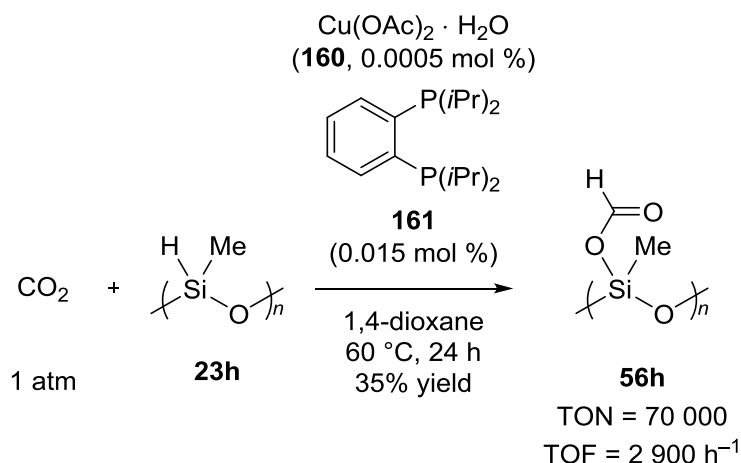
^[129] I. Knopf, C. C. Cummins, *Organometallics* **2015**, 34, 1601–1603.

^[130] R. Shintani, K. Nozaki, *Organometallics* **2013**, 32, 2459–2462.

^[131] G. Süß-Fink, J. Reiner, *J. Organomet. Chem.* **1981**, 221, C36–C38.

^[132] H. Koinuma, F. Kawakami, H. Kato, H. Hirai, *J. Chem. Soc., Chem. Commun.* **1981**, 213–214.

^[133] a) A. Jansen, H. Görls, S. Pitter, *Organometallics* **2000**, 19, 135–138; b) Ref. [69]; c) K. Motokura, D. Kashiwame, A. Miyaji, T. Baba, *Org. Lett.* **2012**, 14, 2642–2645; d) Ref [74]; e) K. Motokura, D. Kashiwame, N. Takahashi, A. Miyaji, T. Baba, *Chem. Eur. J.* **2013**, 19, 10030–10037; f) S. Itagaki, K. Yamaguchi, N. Mizuno, *J. Mol. Catal. A: Chem.* **2013**, 366, 347–352; g) L. Zhang, J. Cheng, Z. Hou, *Chem. Commun.* **2013**, 49, 4782–4784; h) L. González-Sebastián, M. Flores-Alamo, J. J. García, *Organometallics* **2013**, 32, 7186–7194; i) V. P. Taori, R. Bandari, M. R. Buchmeiser, *Chem. Eur. J.* **2014**, 20, 3292–3296; j) M. L. Scheuermann, S. P. Semproni, I. Pappas, P. J. Chirik, *Inorg. Chem.* **2014**, 53, 9463–9465.

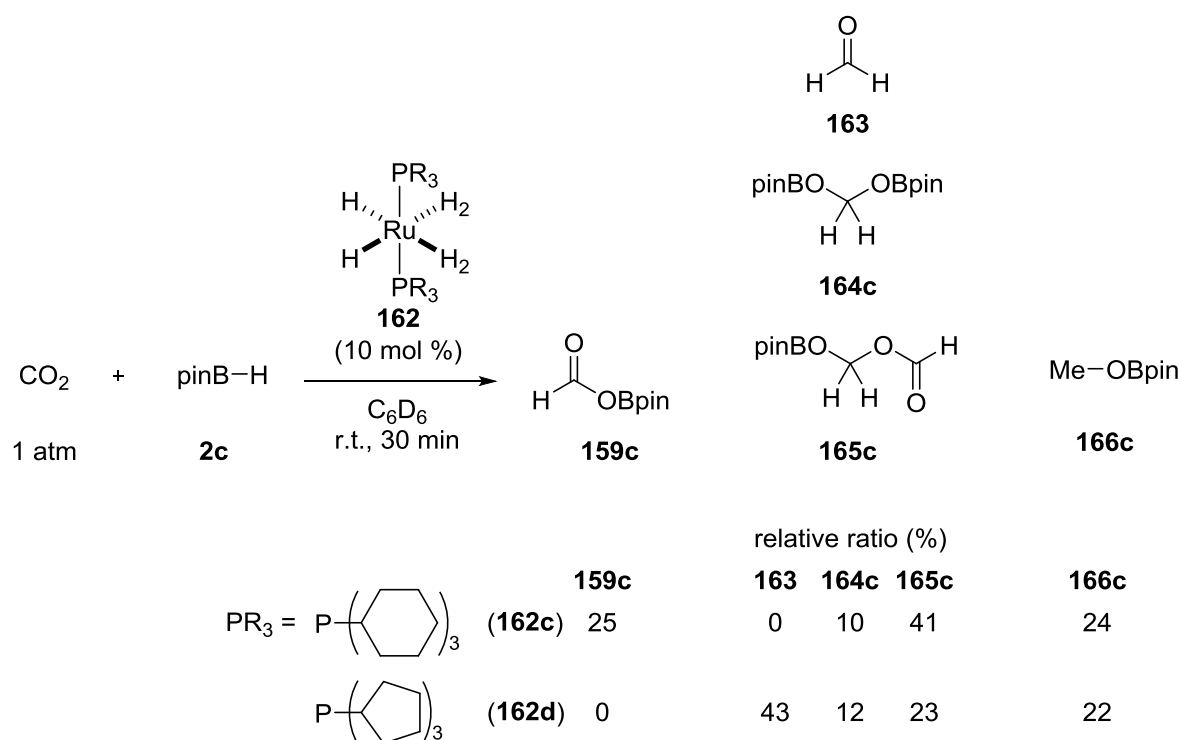


Scheme 5.2: Highly efficient copper-catalyzed hydrosilylation of carbon dioxide into polysilylformate **56h**.

5.2 Reduction of Carbon Dioxide into Formaldehyde Oxidation State

The group of SABO-ETIENNE developed a ruthenium catalyst **162** for the reduction of carbon dioxide into formaldehyde oxidation state (Scheme 5.3). The complex **162c** with tricyclohexylphosphine ligands gave products of formate, formaldehyde, and methanol oxidation states in the ratio of ca. 1:2:1 whereas with the tricyclopentylphosphine complex **162d** borylformate **159c** was not detected, and formaldehyde and methanol oxidation state products were obtained in slightly increased 3:1 ratio.^[134]

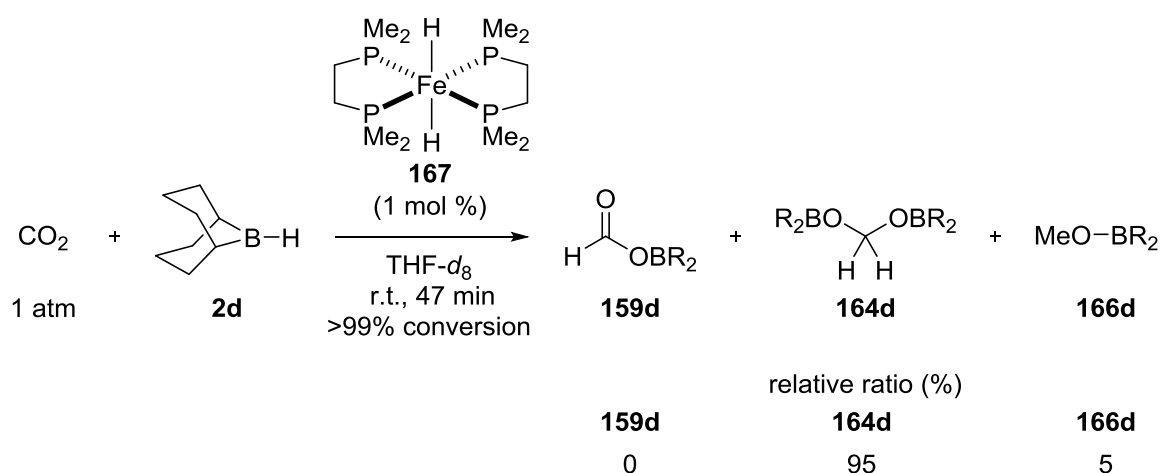
^[134] a) S. Bontemps, L. Vendier, S. Sabo-Etienne, *Angew. Chem.* **2012**, 124, 1703–1706; *Angew. Chem. Int. Ed.* **2012**, 51, 1671–1674; b) S. Bontemps, S. Sabo-Etienne, *Angew. Chem.* **2013**, 125, 10443–10445; *Angew. Chem. Int. Ed.* **2013**, 52, 10253–10255; c) S. Bontemps, L. Vendier, S. Sabo-Etienne, *J. Am. Chem. Soc.* **2014**, 136, 4419–4425.



Scheme 5.3: Hydroboration of carbon dioxide using ruthenium complex **162**.

Recently, SABO-ETIENNE and BONTEMPS reported a highly selective iron-catalyzed hydroboration of carbon dioxide in bis(boryl)acetal **164d** (Scheme 5.4).^[135] It is worth mentioning that, although (9-BBN)₂ (**2d**) does not reduce carbon dioxide, the control experiment with (9-BBN)₂ (**2d**) and 1,2-bis(dimethylphosphino)ethane ligand gave borylated products **164d** and **166d**. The conversion and the selectivity were however significantly lower: 4% conversion at 60 °C after 47 min with an **164d**:**166d** ratio 77:23.

^[135] G. Jin, G. Werncke, Y. Escudié, S. Sabo-Etienne, S. Bon Temps, *J. Am. Chem. Soc.* **2015**, *137*, 9563–9566.

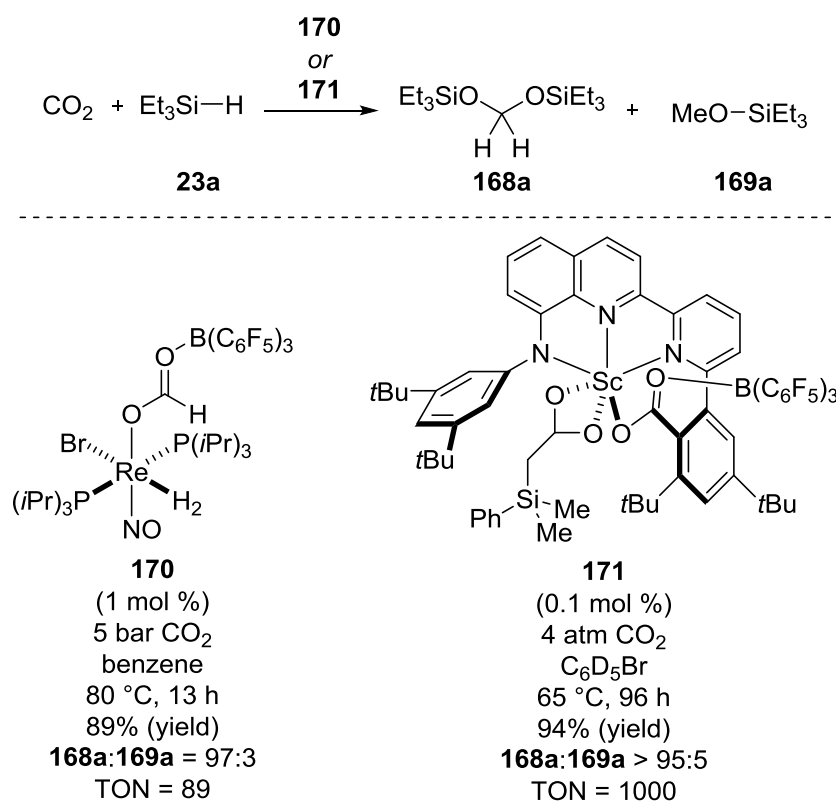


Scheme 5.4: Iron-catalyzed hydroboration of carbon dioxide into formaldehyde oxidation state.

The selective hydrosilylation of carbon dioxide into bis(silyl)acetal **168a** was first achieved by BERKE^[136] and PIERS^[137] in 2013 (Scheme 5.5). The rhenium/B(C₆F₅)₃ complex **170** used by BERKE and co-workers furnished acetal **168a** in 89% yield and with good chemoselectivity (**168a**:**169a** = 97:3). The scandium/B(C₆F₅)₃ complex **171** was found to be a highly active and selective catalyst, giving 94% yield of **168a** as the sole silicon-containing product after 96 h.

^[136] Y. Jiang, O. Blacque, T. Fox, H. Berke, *J. Am. Chem. Soc.* **2013**, 135, 7751–7760.

^[137] F. A. LeBlanc, W. E. Piers, M. Parvez, *Angew. Chem.* **2013**, 126, 808–811; *Angew. Chem. Int. Ed.* **2014**, 53, 789–792.



Scheme 5.5: Hydrosilylation of carbon dioxide into formaldehyde oxidation state.

5.3 Reduction of Carbon Dioxide into Methanol Oxidation State

Several efficient catalysts have been employed in the selective hydroboration of carbon dioxide into methanol oxidation state.^[138] One of the simplest, but also most powerful systems was reported by STEPHAN (Table 5.1, entry 1).^[138g] The bulky phosphine **6e** was able to catalyze the reaction under relatively mild conditions *via* formation of a frustrated LEWIS pair (FLP)^[139] with the bulky hydroborane **2d**. FLP activation of carbon dioxide was

^[138] a) S. Chakraborty, J. Zhang, J. A. Krause, H. Guan, *J. Am. Chem. Soc.* **2010**, *132*, 8872–8873; b) M. J. Sgro, D. W. Stephan, *Angew. Chem.* **2012**, *124*, 11505–11507; *Angew. Chem. Int. Ed.* **2012**, *51*, 11343–11345; c) M.-A. Courtemanche, M.-A. Légaré, L. Maron, F.-G. Fontaine, *J. Am. Chem. Soc.* **2013**, *135*, 9326–9329; d) C. Das Neves Gomes, E. Blondiaux, P. Thuéry, T. Cantat, *Chem. Eur. J.* **2014**, *20*, 7098–7106; e) T. Wang, D. W. Stephan, *Chem. Eur. J.* **2014**, *20*, 3036–3039; f) M. D. Anker, M. Arrowsmith, P. Bellham, M. S. Hill, G. Kociok-Köhn, D. J. Liptrot, M. F. Mahon, C. Weetman, *Chem. Sci.* **2014**, *5*, 2826–2830; g) T. Wang, D. W. Stephan, *Chem. Commun.* **2014**, *50*, 7007–7010; h) K. Fujiwara, S. Yasuda, T. Mizuta, *Organometallics* **2014**, *33*, 6692–6695; i) R. Pal, T. L. Groy, R. J. Trovitch, *Inorg. Chem.* **2015**, *54*, 7506–7515; j) Y. Yang, M. Xu, D. Song, *Chem. Commun.* **2015**, *51*, 11293–11296; k) J. A. B. Abdalla, I. M. Riddlestone, R. Tirfoin, S. Aldridge, *Angew. Chem.* **2015**, *127*, 5187–5191; *Angew. Chem. Int. Ed.* **2015**, *54*, 5098–5102.

^[139] For reviews of frustrated LEWIS pair chemistry, see: a) D. W. Stephan, *Acc. Chem. Res.* **2015**, *48*, 306–316; b) M. Alcarazo, *Synlett* **2014**, 1519–1520; c) D. W. Stephan, G. Erker, *Chem.*

later utilized by MARON and FONTAINE using phosphineborane **172** (entry 2).^[138c] Diazafluorenone **173** used initially as a bidentate ligand^[140] was shown to catalytically activate carbon dioxide.^[138j] The hydroboration was achieved with different hydroboranes, including (9-BBN)₂ (**2d**), pinB–H (**2c**), and catB–H (**2a**) (entry 3). The nickel POCOP pincer complex **174** reported by GUAN in 2010 remains one of the most efficient and selective catalysts for this transformation (entry 4).^[138a] Very recently ALDRIDGE reported that the unusual gallium hydride **175** was also catalytically active in the carbon dioxide hydroboration.^[138k] The catalytic reactivity was however low and the reaction required 10 mol % catalyst loading to reach completion (entry 5). Economically the most efficient method to transform carbon dioxide into methanol oxidation state was reported in 2014 by MIZUTA.^[138h] The commercial BH₃ · THF solution was found to react with carbon dioxide (1 atm) at room temperature to give trimethoxyboroxine. When the authors used purified^[141] borane complex, no reaction was observed. However, the addition of NaBH₄ (0.5 mol %) restored the activity, and impressive turnover numbers were achieved (entry 6).

Sci. **2014**, *5*, 2625–2641; d) *Top. Curr. Chem.* (Eds. G. Erker, D. W. Stephan), Springer, Berlin, Heidelberg, **2013**, vol. 332; e) *Top. Curr. Chem.* (Eds. G. Erker, D. W. Stephan), Springer, Berlin, Heidelberg, **2013**, vol. 334; f) D. W. Stephan, G. Erker, *Angew. Chem.* **2010**, *122*, 50–81; *Angew. Chem. Int. Ed.* **2010**, *49*, 46–76; g) D. W. Stephan, *Org. Biomol. Chem.* **2008**, *6*, 1535–1539; h) A. L. Kenward, W. E. Piers, *Angew. Chem.* **2008**, *120*, 38–42; *Angew. Chem. Int. Ed.* **2008**, *47*, 38–41.

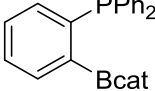
^[140] a) V. T. Annibale, D. Song, *Chem. Commun.* **2011**, *48*, 5416–5418; b) V. T. Annibale, D. A. Dalessandro, D. Song, *J. Am. Chem. Soc.* **2013**, *135*, 16175–16183.

^[141] Purified by bulb-to-bulb transfer *in vacuo*.

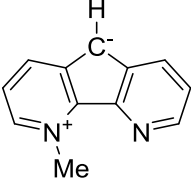
Table 5.1: Selected examples of hydroboration of carbon dioxide into borylated methanol **166**.

$$\text{CO}_2 + \text{R}_2\text{B-H} \xrightarrow{\text{cat.}} \text{MeO-BR}_2$$

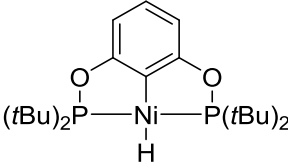
2 **166**



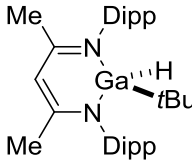
172



173



174



175

entry	catalyst (mol %)	R ₂ B-H	p[CO ₂]	T [°C]	t [h]	Yield	TON	TOF [h ⁻¹]
1 ^[138g]	<i>t</i> Bu ₃ P (6e) (0.02)	(9-BBN) ₂ 2d	5 atm	60	32	>99	5 000	156
2 ^[138c]	172 (0.1)	BH ₃ · SMe ₂ 2b · SMe ₂	2 atm	70	4	-	2 950	737
3 ^[138j]	173 (1)	catB-H 2a	1.5 atm	70	2	-	97	231
4 ^[138a]	174 (0.2)	catB-H 2a	1 atm	r.t.	1 h	61	495	495
5 ^[138k]	175 (10)	pinB-H 2c	1 atm	60	4	>95	10	2.5
6 ^[138h]	NaBH ₄ (0.5)	BH ₃ · THF 2b · THF	1 atm	r.t.	12	87	174	15

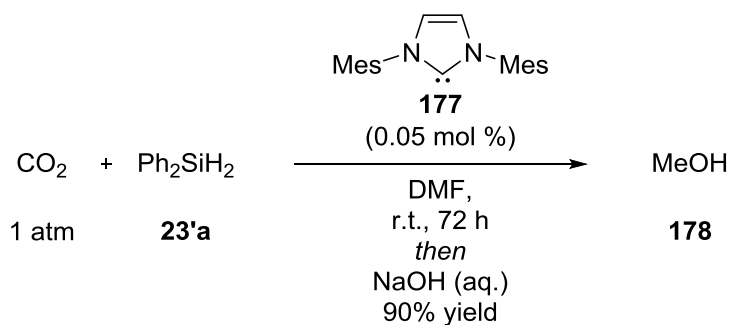
The hydroalumination of carbon dioxide into methanol was reported as early as 1948. Methanol was obtained by simply passing a stream of carbon dioxide through a LiAlH₄ solution in diethyl ether.^[142]

The corresponding hydrosilylation into silylated methanol has been reported only twice. The first report in 1989 by EISENBERG using an iridium catalyst (not shown)^[143] was followed by ZHANG and YING in 2009 by an NHC catalyst **177**.^[144] The insensitivity of the NHC-catalyzed reaction was demonstrated by using air as the CO₂ source (Scheme 5.6).^[145]

^[142] R. F. Nystrom, W. H. Yanko, W. Brown, *J. Am. Chem. Soc.* **1948**, 70, 441–441.

^[143] T. C. Eisenschmid, R. Eisenberg, *Organometallics* **1989**, 8, 1822–1824.

^[144] a) S. N. Riduan, Y. Zhang, J. Y. Ying, *Angew. Chem.* **2009**, 121, 3372–3375; *Angew. Chem. Int. Ed.* **2009**, 48, 3322–3325; for mechanistic investigations, see: b) F. Huang, L. Zhao, H. Li.



Scheme 5.6: NHC-catalyzed hydrosilylation of carbon dioxide into methanol (**178**).

5.4 Reduction of Carbon Dioxide into Methane

The full deoxygenation of carbon dioxide into methane was first accomplished by MATSUO and KAWAGUCHI in 2006, applying 0.5 mol % of a 1:1 mixture of zirconium complex **181** and $\text{B}(\text{C}_6\text{F}_5)_3$ (**108**) (Scheme 5.7).^[146] The role of the electrophilic zirconium complex was to coordinate carbon dioxide and initiate the reduction into formate and formaldehyde oxidation states. The reductions from formaldehyde oxidation state to methane were proposed to be catalyzed by $\text{B}(\text{C}_6\text{F}_5)_3$ (**108**). When the **181**:**108** ratio was decreased to 0.7, the rate of the reaction dropped (from $\text{TOF} = 7.3 \text{ h}^{-1}$ for 1:1 to $\text{TOF} = 1.1 \text{ h}^{-1}$). Excess of the zirconium (**181**:**108** = 2) decreased the reactivity and now the major silicon-containing product was bis(silyl)acetal **168**. The hydrosilylation of carbon dioxide into methane was later achieved with the combination of $\text{B}(\text{C}_6\text{F}_5)_3$ (**108**) with the co-catalysts **182** and **183** by PIERS^[147] and with the co-catalyst **184** by TURCULET.^[148] Notwithstanding the structural and mechanistical variety of the co-catalysts **181**–**184**, their function remains the same as proposed by MATSUO and KAWAGUCHI: to facilitate the fixation of carbon dioxide into formate oxidation state while the deoxygenation is catalyzed by $\text{B}(\text{C}_6\text{F}_5)_3$ (**108**).^[149]

Z.-X. Wang, *J. Am. Chem. Soc.* **2010**, *132*, 12388–12396; c) S. N. Riduan, J. Y. Ying, Y. Zhang, *ChemCatChem* **2013**, *5*, 1490–1496.

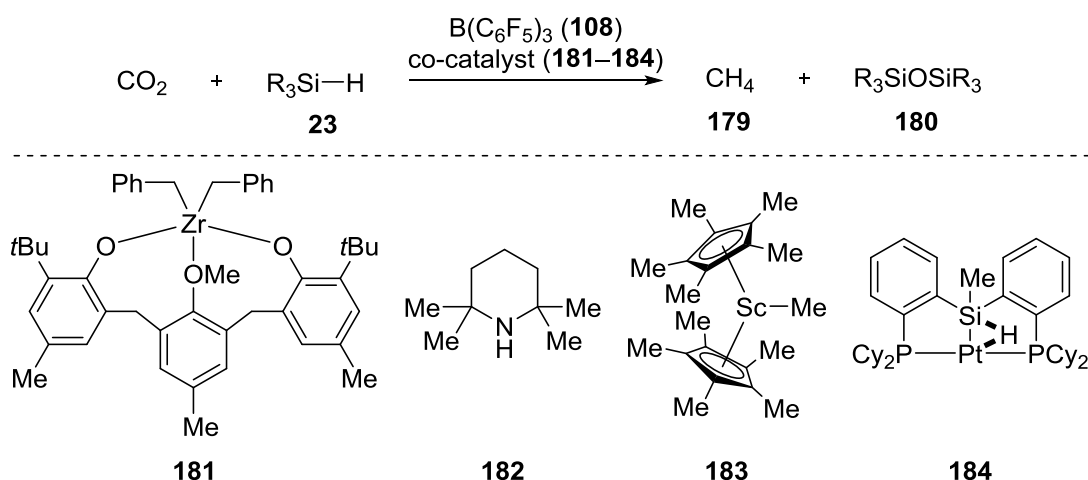
^[145] The reaction using dry air as the CO_2 source was reported to proceed slowly forming a mixture of “intermediates” and the silylated methanol **169**; however, no details on the ratio of different products or the reaction time were given.

^[146] T. Matsuo, H. Kawaguchi, *J. Am. Chem. Soc.* **2006**, *128*, 12362–12363.

^[147] a) A. Berkefeld, W. E. Piers, M. Parvez, *J. Am. Chem. Soc.* **2010**, *132*, 10660–10661; b) A. Berkefeld, W. E. Piers, M. Parvez, L. Castro, L. Maron, O. Eisenstein, *Chem. Sci.* **2013**, *4*, 2152–2162.

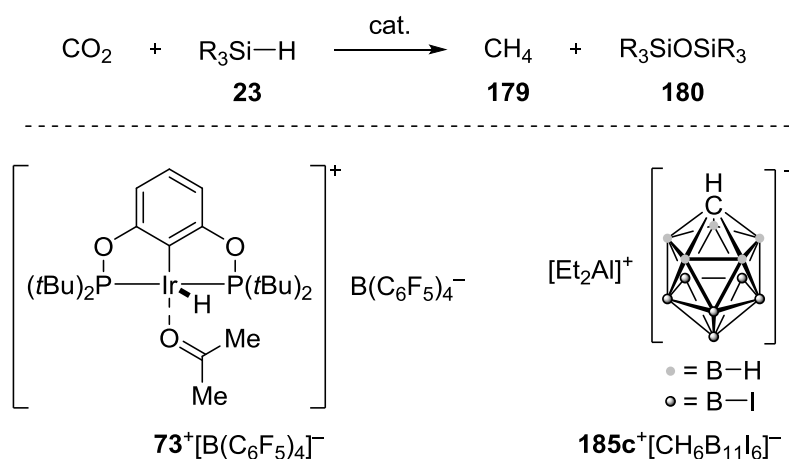
^[148] S. J. Mitton, L. Turculet, *Chem. Eur. J.* **2012**, *18*, 15258–15262.

^[149] For a recent, unselective $\text{B}(\text{C}_6\text{F}_5)_3$ (**108**)/bisborate-co-catalyzed example, see: Z. Lu, H. Hausmann, S. Becker, H. A. Wegner, *J. Am. Chem. Soc.* **2015**, *137*, 5332–5335.



Scheme 5.7: Hydrosilylation of carbon dioxide into methane using $\text{B(C}_6\text{F}_5)_3$ (**108**) and co-catalyst.

Strong LEWIS acids **73⁺** and **185c⁺** were also successfully used in the exhaustive hydrosilylation of carbon dioxide (Scheme 5.8). BROOKHART was able to use only 0.0077 mol % of iridium POCOP pincer **73⁺** to hydrosilylate carbon dioxide (1 atm) with dimethylphenylsilane (**23e**).^[82] After 72 h at room temperature, the reaction had reached ca. 8 300 turnovers. The highly reactive diethyl aluminum cation **185c⁺** by WEHMSCHULTE could be used catalytically as well but higher catalyst loading (10 mol %) and elevated temperature (80 °C) were required.^[150] An alternative aluminum cation was later utilized by the same group in CO_2 reduction but the selectivities were diminished (not shown).^[151]



Scheme 5.8: LEWIS acid-catalyzed exhaustive hydrosilylation of carbon dioxide.

^[150] M. Khandelwal, R. J. Wehmschulte, *Angew. Chem.* **2012**, 124, 7435–7439; *Angew. Chem. Int. Ed.* **2012**, 51, 7323–7326.

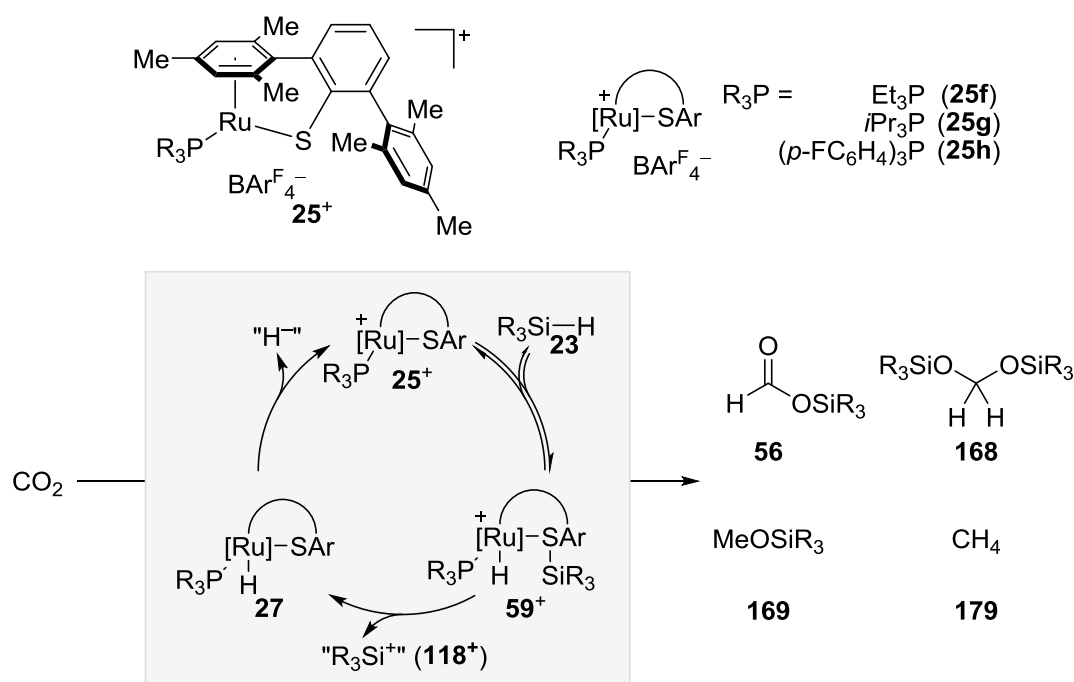
^[151] R. J. Wehmschulte, M. Saleh, D. G. Powell, *Organometallics* **2013**, 32, 6812–6819.

5.5 Summary

The reduction of carbon dioxide with main-group electrophiles has been achieved with variety of catalysts. Several efficient and selective methods to access formate and methane oxidation states have been described. However, accessing the intermediate oxidation states remains a great challenge. While a growing number of selective methods to access methanol oxidation state are being reported, only three examples^[135–137] of selective reduction of carbon dioxide into formaldehyde oxidation state using main-group electrophiles have been reported to date.

5.6 Ruthenium Thiolate-Catalyzed Hydrosilylation of Carbon Dioxide

The ruthenium thiolate complex **25**⁺ was applied to the activation of H–H,^[30] Si–H, and B–H bonds in reductions^[72] and dehydrogenative couplings.^[73] The distinct activation mode,^[71] and the unusual reactivity observed in the previously reported reactions led to expect that carbon dioxide reduction with **25**⁺ could provide unconventional results (Scheme 5.9).



Scheme 5.9: Ruthenium thiolate **25**⁺-catalyzed hydrosilylation of carbon dioxide.

To be able to detect all possible products (including methane) as well as for measurement of accurate reaction kinetics, the reactions were run in high-pressure NMR tubes. The initial

reaction conditions were identified using 4 mol % of the triethylphosphine-substituted complex **25f**⁺[BAr^F₄][−], triethylsilane (**23a**), and 5 bar CO₂ in C₆D₆. As no reaction was observed at room temperature, the temperature was gradually increased. At 80 °C, the reaction reached full conversion in 4 h, giving bis(silyl)acetal **168a** with excellent selectivity (Table 5.2, entry 1). The reaction with complex **25g**⁺[BAr^F₄][−] containing sterically demanding, electron-rich triisopropyl phosphine ligand was slower, and the selectivity was slightly diminished (entry 2). The triarylphosphine complex **25h**⁺[BAr^F₄][−] needed 72 h to reach full conversion but the selectivity was perfect (entry 3). The triethylphosphine complex **25f**⁺[BAr^F₄][−] with optimal combination of reactivity and selectivity was chosen for the hydrosilane screening.

Table 5.2: Hydrosilylation of carbon dioxide: catalyst screening.

$$\begin{array}{c}
 \text{CO}_2 + \text{Et}_3\text{Si}-\text{H} \xrightarrow[\text{C}_6\text{D}_6, 80^\circ\text{C}]{\text{25}^+[\text{BAr}^{\text{F}}_4]^- (4 \text{ mol } \%)} \\
 \text{5 bar} \qquad \text{23a} \qquad \qquad \qquad \text{56a} + \text{168a} + \text{169a}
 \end{array}$$

entry	catalyst	time (h)	conversion (%) ^[a]	ratio (56a : 168a : 169a)	TOF (h ^{−1}) ^[b]
1	25f ⁺	4	>99 (98)	1:98:1	11
2	25g ⁺	48	99 (96)	3:93:4	0.12
3	25h ⁺	72	>99 (>99)	<1:>99:<1	0.51

^[a] Conversion of hydrosilane; combined yield determined by ¹H NMR spectroscopy using toluene as internal standard in parentheses. ^[b] Initial rate based on hydrosilane conversion. TOF = turnover frequency.

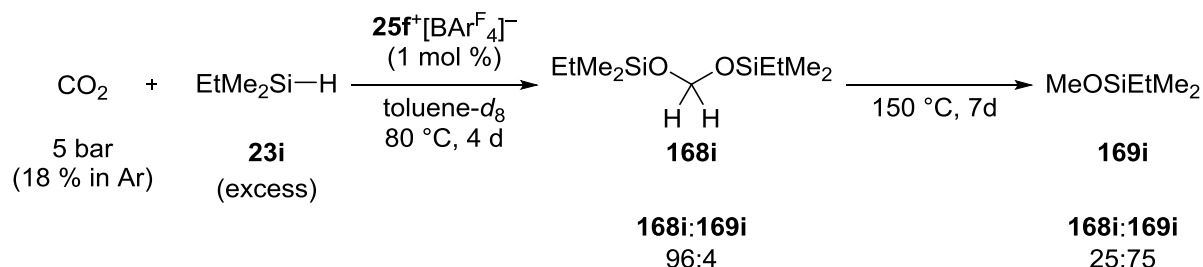
The hydrosilylation of carbon dioxide was screened with hydrosilanes with various steric and electronic properties using 2 or 4 mol % of **25f**⁺[BAr^F₄][−]. The reaction with triethylsilane (**23a**) using 2 mol % catalyst loading led to significantly decreased selectivity, namely increased amount of formate **56a** (Table 5.3, entry 1) compared to the reaction with 4 mol % catalyst loading (entry 2). The reactions with ethyldimethylsilane (**23i**) (entries 3 and 4) were comparable to the reactions with **23a** giving the corresponding acetal **168i** with slightly decreased selectivity and longer reaction times. The phenyl-substituted hydrosilanes **23g** and **23e** reacted significantly slower than the trialkylsubstituted hydrosilanes **23a** and **23i** (entries 5–8). Again, the major byproduct in these reactions was the silyl formate **56** (6–8%). Only traces of silyl methanol **169** were observed with any of the hydrosilanes **23**.

Table 5.3: Hydrosilylation of carbon dioxide: hydrosilane screening.

$ \text{CO}_2 + \text{R}_3\text{Si-H} \xrightarrow[\text{C}_6\text{D}_6, 80^\circ\text{C}]{\text{25f}^+[\text{BAR}^{\text{F}}_4]^- (2 \text{ or } 4 \text{ mol } \%)} \text{H-C(=O)-OSiR}_3 + \text{R}_3\text{SiO-CH}_2\text{-OSiR}_3 + \text{MeOSiR}_3 $ <p>5 bar 23 56 168 169</p>						
entry	7a (mol %)	hydrosilane	time (h)	conversion (%) ^[a]	ratio (56:168:169)	TOF (h ⁻¹) ^[b]
1	2	Et ₃ SiH	47	97 (97)	18:81:<1	11
2	4	(23a)	4	>99 (>99)	0:>99:0	12
3	2	EtMe ₂ SiH	73	70 (69)	6:93:<1	7.8
4	4	(23i)	11	>99 (97)	7:93:<1	12
5	2	MePh ₂ SiH	73	33 (27)	8:91:2	4.5
6	4	(23g)	36	98 (85)	6:92:1	12
7	2	Me ₂ PhSiH	73	63 (60)	8:90:1	5.2
8	4	(23e)	75	96 (86)	6:92:2	9.5

^[a] Conversion of hydrosilane; combined yield determined by ¹H NMR spectroscopy using toluene as internal standard in parentheses. ^[b] Initial rate based on hydrosilane conversion. TOF = turnover frequency.

To test the observed chemoselectivity towards bis(silyl)acetal **168**, we used a CO₂/Ar mixture to first selectively synthesize **168i** (Scheme 5.10). After 4 days at 80 °C, the reaction was found to reach a plateau,^[152] indicating full consumption of carbon dioxide into bis(silyl)acetal (**168i:169i** = 96:4). The reaction was then heated to 150 °C. Slow conversion of **168i** to **169i** was observed, and after 7 days the silylated methanol **169i** was obtained as the major product (**168i:169i** = 25:75).



Scheme 5.10: Temperature-controlled reduction of carbon dioxide into formaldehyde and methanol oxidation states.

^[152] Followed by the hydrosilane consumption.

The ruthenium thiolate **25f**⁺ was found able to catalyze the reduction of carbon dioxide using other main-group hydrides as well. The hydroboranes **2a** and **2c** used previously in the dehydrogenative borylation of indoles^[31] could be used in the carbon dioxide reduction but the reactions were slow, giving borylated methanol **166** with excellent selectivity (Table 5.4, entries 1 and 2). Tin hydrides had not been previously used with the ruthenium thiolate **25**⁺, and the reaction with tributyltin hydride **16b** did not give any conversion (entry 3).^[153] Catalytic activation of aluminum hydrides with well-defined metal complexes has not been widely applied yet. When a solution of complex **25f**⁺ and DIBAL-H (**9b**) was subjected to 5 bar of carbon dioxide, fast reaction was observed and in 30 min the solution turned green, typical for free unsaturated **25**⁺. NMR analysis of the mixture revealed full conversion into a mixture of products, containing mainly acetal-type compounds (entry 4).^[154]

Table 5.4: Hydrosilylation of carbon dioxide: application of other main-group hydrides.

$ \begin{array}{c} \text{CO}_2 \quad + \quad E-H \quad \xrightarrow[\text{C}_6\text{D}_6]{\text{25f}^+[\text{BAr}^{\text{F}}_4]^- \text{ (2 mol \%)}} \quad \text{H}-\text{C}(=\text{O})-\text{OE} \quad + \quad \text{EO}-\text{C}(\text{H})_2-\text{OE} \quad + \quad \text{MeOE} \\ \text{5 bar} \quad \quad \quad \text{I} \quad \quad \quad \text{CLVI} \quad \quad \quad \text{CLVII} \quad \quad \quad \text{CLVIII} \end{array} $						
entry	<i>E</i> -H	time	T (°C)	conversion (%) ^[a]	ratio (CLVI:CLVII:CLVIII)	TOF (h ⁻¹) ^[b]
1	catB-H (2a)	7 d	120	71 (30)	<1:<1:>98	0.21
2	pinB-H (2c)	7 d	120	45 (27)	2:<1:>97	0.13
3	Bu ₃ Sn-H (16b)	5 d	80	—	—	—
4	DIBAL-H (9b)	30 min	r.t.	>99	10:85:5 ^[c]	100

^[a] Conversion of hydride source; combined yield determined by ¹H NMR spectroscopy using toluene as internal standard in parentheses. ^[b] Initial rate based on hydride source conversion. ^[c] A mixture of several formates, acetal-like compounds as well as methoxy groups. TOF = turnover frequency.

^[153] Typically a color change from blue-green into yellow-orange occurs upon the addition of main-group hydrides into a solution of **25**⁺. In the case of the tin hydride **16b**, the solution turned quickly dark red.

^[154] The uncatalyzed reduction of carbon dioxide with DIBAL-H (**9b**) gave uncontrolled reduction leading to clogging of the NMR tube used for the reaction, separating the gas and the liquid phases. ¹H NMR analysis of the liquid phase showed no conversion.

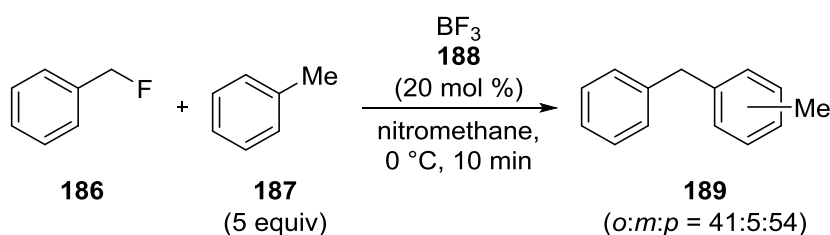
In conclusion, an efficient method for the synthesis of bis(silyl)acetals **168** using ruthenium thiolate complex **25f**⁺ was developed. At lower reaction temperature, the reaction is highly selective for the reduction to the formaldehyde oxidation state. The observed reactivity is thought to arise from the relatively low hydricity of the ruthenium hydride **27**. Only under forcing conditions, the further reduction of bis(silyl)acetals **168** into silylated methanol **169** could be accomplished. Even after prolonged reaction times (up to 30 d) at 150 °C, no exhaustive reduction into methane was observed. The reduction of carbon dioxide with other main-group electrophiles showed the versatility of the ruthenium thiolate **25**⁺. With hydroboranes **2**, borylated methanol was obtained as the major product. The reaction with DIBAL-H (**9b**) gave full conversion at room temperature in 30 min.

6 FUNCTIONALIZATION OF C–F BONDS

6.1 Introduction

The C–F bond is the strongest covalent single bond carbon forms.^[155] Development of orthogonal synthetic methodology enabling the functionalization of the C–F bonds changes this typically inert functional group into a potential reactive site.^[156] This chapter focuses on the C–F bond functionalization using main-group electrophiles.

The catalytic activation of benzylic C–F bonds for FRIEDEL–CRAFTS alkylation was investigated by OLAH in 1984.^[157] Activation of benzyl fluoride **186** was readily achieved with the strong LEWIS acid BF₃ (**188**) at 0 °C, giving diarylmethane **189** as a mixture of regioisomers (Scheme 6.1).



Scheme 6.1: FRIEDEL–CRAFTS benzylation of toluene with benzyl fluoride catalyzed by BF₃ (**188**).

Aromatic CF₃-groups can be converted into CCl₃-groups using aluminum trichloride.^[158] The fluorine/chlorine exchange followed by subsequent FRIEDEL–CRAFTS alkylation of arenes was found to give diaryldichloromethane **CLX** in good yields.^[159] In all cases, only one regioisomer (*para*) was observed (Scheme 6.2).

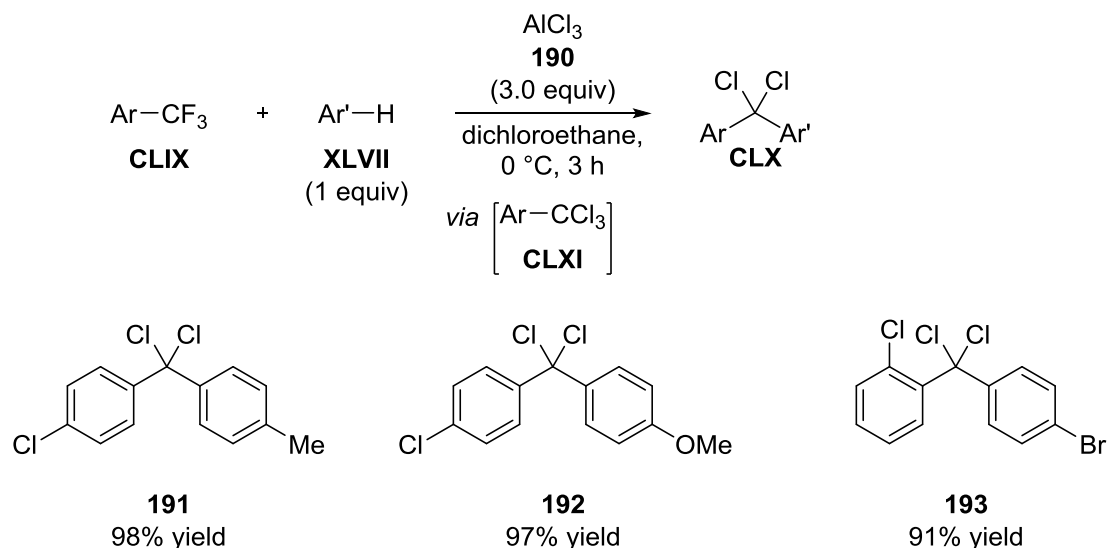
^[155] D. O'Hagan, *Chem. Soc. Rev.* **2008**, 37, 308–319.

^[156] a) T. Stahl, H. F. T. Klare, M. Oestreich, *ACS Catal.* **2013**, 3, 1578–1587; b) H. Amii, K. Uneyama, *Chem. Rev.* **2009**, 109, 2119–2183.

^[157] G. A. Olah, J. A. Olah, T. Ohyama, *J. Am. Chem. Soc.* **1984**, 106, 5284–5290.

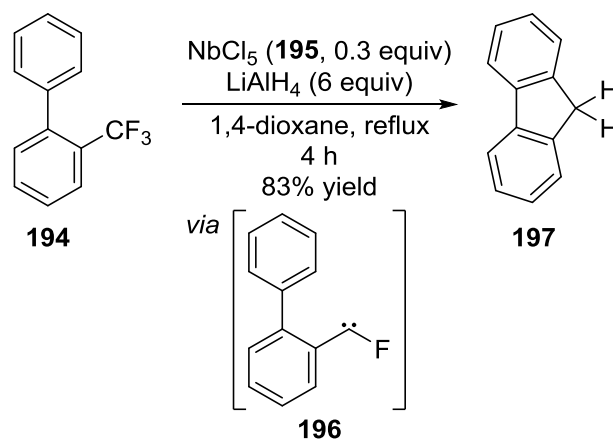
^[158] A. L. Henne, M. S. Newman, *J. Am. Chem. Soc.* **1938**, 60, 1697–1698.

^[159] a) R. K. Ramchandani, W. D. Wakharkar, A. Sudalai, *Tetrahedron Lett.* **1996**, 37, 4063–4064; For a related defluorinative arylation methodology, see: b) A. Okamoto, K. Kumeda, N. Yonezawa, *Chem. Lett.* **2010**, 39, 124–125.



Scheme 6.2: Synthesis of dichlorodiarenes through FRIEDEL-CRAFTS alkylation/halide exchange sequence.

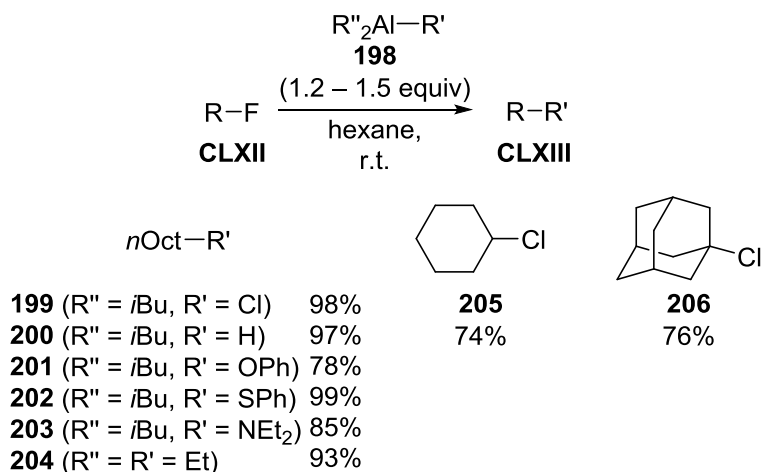
Niobium-catalyzed defluorination has been extensively studied by AKIYAMA.^[160] The intramolecular C–C bond coupling is proposed to occur *via* fluorine substituted carbene intermediate **196**. Insertion of the carbene **196** into the neighboring C–H bond followed by subsequent hydrodefluorination furnishes the fluorene **197** (Scheme 6.3).^[160e]



Scheme 6.3: Niobium-catalyzed defluorinative C–C bond coupling.

^[160] a) K. Fuchibe, T. Akiyama, *Synlett* **2004**, 1282–1284; b) K. Fuchibe, T. Akiyama, *J. Am. Chem. Soc.* **2006**, 128, 1434–1435; c) K. Fuchibe, Y. Ohshima, K. Mitomi, T. Akiyama, *Org. Lett.* **2007**, 9, 1497–1499; d) K. Fuchibe, Y. Ohshima, K. Mitomi, T. Akiyama, *J. Fluorine Chem.* **2007**, 128, 1158–1167; e) K. Fuchibe, K. Mitomi, R. Suzuki, T. Akiyama, *Chem. Asian. J.* **2008**, 3, 261–271; f) K. Fuchibe, T. Kaneko, K. Mori, T. Akiyama, *Angew. Chem.* **2009**, 121, 8214–8217; *Angew. Chem. Int. Ed.* **2009**, 48, 8070–8073; g) T. Akiyama, K. Atobe, M. Shibata, K. Mori, *J. Fluorine Chem.* **2013**, 152, 81–83; for a recent example using TiCl_4 and hydrosilanes, see: h) T. Yamada, K. Saito, T. Akiyama, *Adv. Synth. Catal.* **2016**, 358, 62–66.

TERAO and KAMBE showed in 2007 that primary, secondary as well as tertiary fluorides are readily functionalized using a variety of organoaluminum reagents, giving defluorinated products **199–206** in good yields at room temperature (Scheme 6.4).^[161]



Scheme 6.4: C–F bond functionalization using organoaluminum reagents.

Later the same year hydrodefluorination of *n*-fluorohexane was reported by ROSENTHAL and co-workers using DIBAL–H (**9b**) as the stoichiometric reductant together with catalytic amounts of trityl salt **93**⁺.^[162] However, the efficiency of the system was lower than that reported by TERAU and KAMBE, making the catalytic role of the assumed in-situ formed alumenium ions questionable.

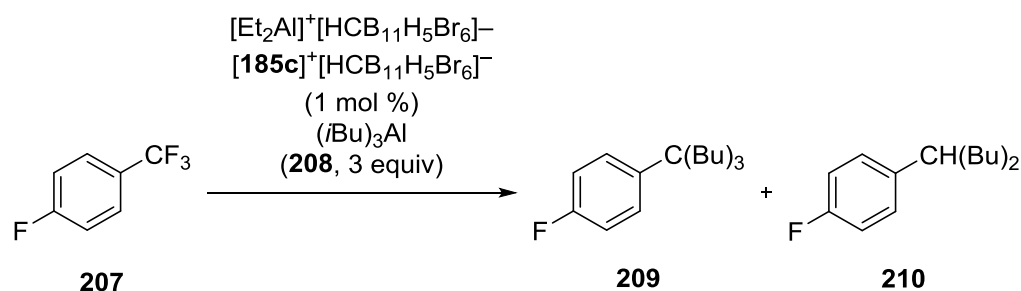
Alumenium ion-catalyzed defluorinative C–C bond formation was reported by OZEROV in 2009.^[163] Aromatic CF₃-groups were transformed into mixtures of alkylated and hydrodefluorinated products **209** and **210** (Scheme 6.5).^[164]

^[161] J. Terao, S. A. Begun, Y. Shinohara, M. Tomita, Y. Naitoh, N. Kambe, *Chem. Commun.* **2007**, 855–857.

^[162] M. Klahn, C. Fischer, A. Spannenberg, U. Rosenthal, I. Krossing, *Tetrahedron Lett.* **2007**, 48, 8900–8903.

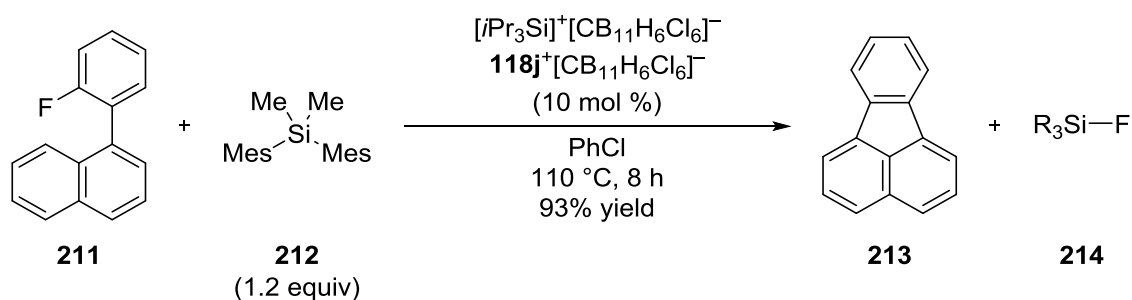
^[163] W. Gu, M. R. Haneline, C. Douvris, O. V. Ozerov, *J. Am. Chem. Soc.* **2009**, 131, 11203–11212.

^[164] The connectivity of the butyl groups (*iso* or *tert*) in the products was not disclosed.



Scheme 6.5: Trifluoromethyl functionalization using organoaluminum reagents.

In 2011, SIEGEL and co-workers reported the defluorinative FRIEDEL–CRAFTS-type aryl–aryl coupling (Scheme 6.6).^[165] The strong $\text{C}(\text{sp}^2)\text{--F}$ bond was activated with in-situ generated silylium ions $\mathbf{118}^+$. The intramolecular nucleophilic attack by the arene **211**, followed by deprotonation by **212** (leading to regeneration of silylium ion $\mathbf{118}^+$) gives cyclic **214**.

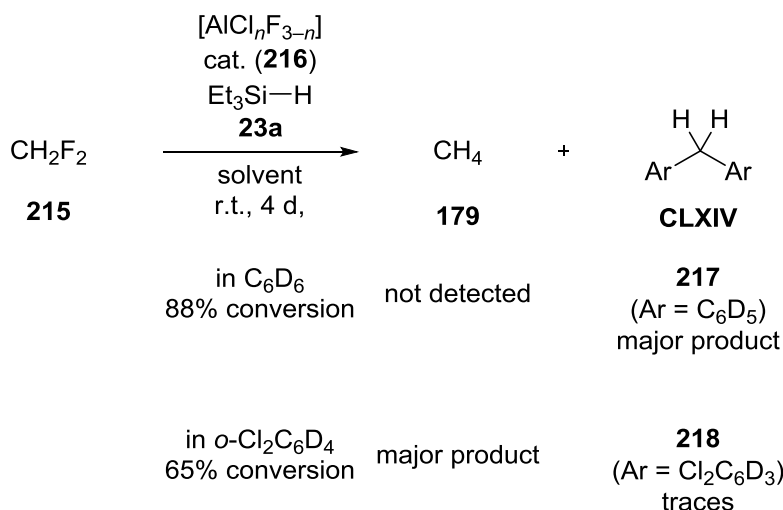


Scheme 6.6: Defluorinative FRIEDEL–CRAFTS-type aryl–aryl coupling by SIEGEL.

LEWIS-acidic aluminum chlorofluoride $[\text{AlCl}_n\text{F}_{3-n}]$ (**216**) was found to catalyze the defluorination of C--F bonds, including difluoromethane (**215**) (Scheme 6.7).^[166] When the reaction was conducted in deuterated benzene, the diarylmethane **217** was isolated as the major product. Conversely, the reaction in the electron-poor solvent $o\text{-Cl}_2\text{C}_6\text{D}_4$ led to selective hydrodefluorination into methane **179**.

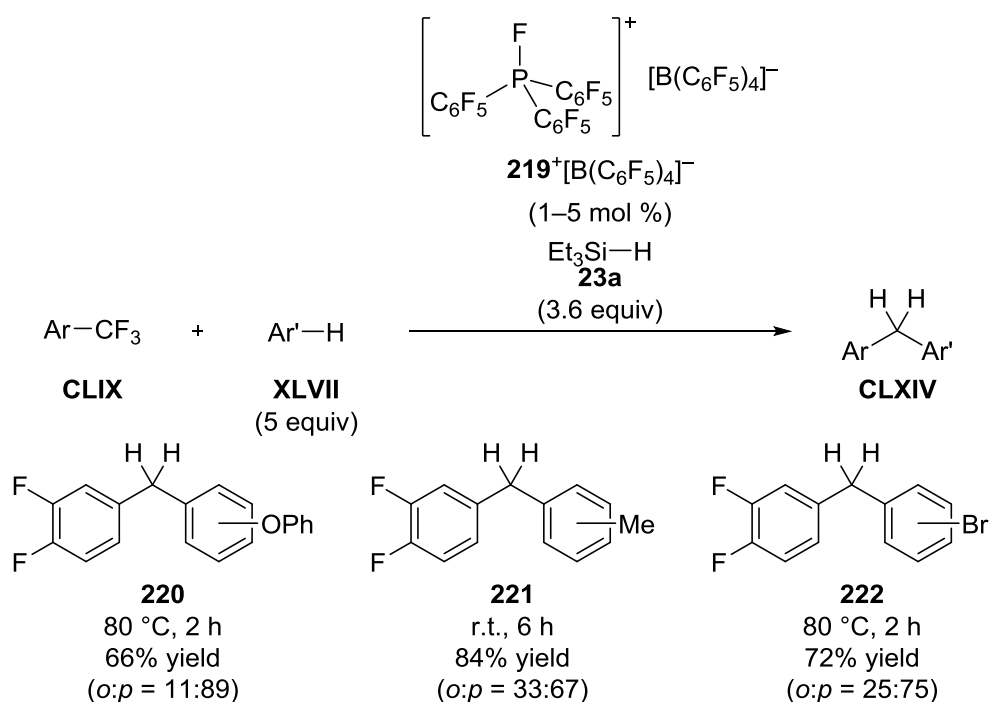
^[165] O. Alleman, S. Duttwyler, P. Romanato, K. K. Baldridge, J. S. Siegel, *Science* **2011**, 332, 574–577.

^[166] M. Ahrens, G. Scholz, T. Braun, *Angew. Chem.* **2013**, 125, 5436–5440; *Angew. Chem. Int. Ed.* **2013**, 52, 5328–5332.



Scheme 6.7: Aluminum chlorofluoride-catalyzed hydrodefluorination and FRIEDEL–CRAFTS alkylation of C₆D₆.

Recently, STEPHAN reported the defluorinative FRIEDEL–CRAFTS alkylation using phosphonium catalyst $[\mathbf{219}^+][\text{B}(\text{C}_6\text{F}_5)_4]^-$ (Scheme 6.8).^[167] The reaction tolerated both electron-rich and -poor arenes although higher catalyst loading was required for the alkylation of bromobenzene into diarylmethane **222**.

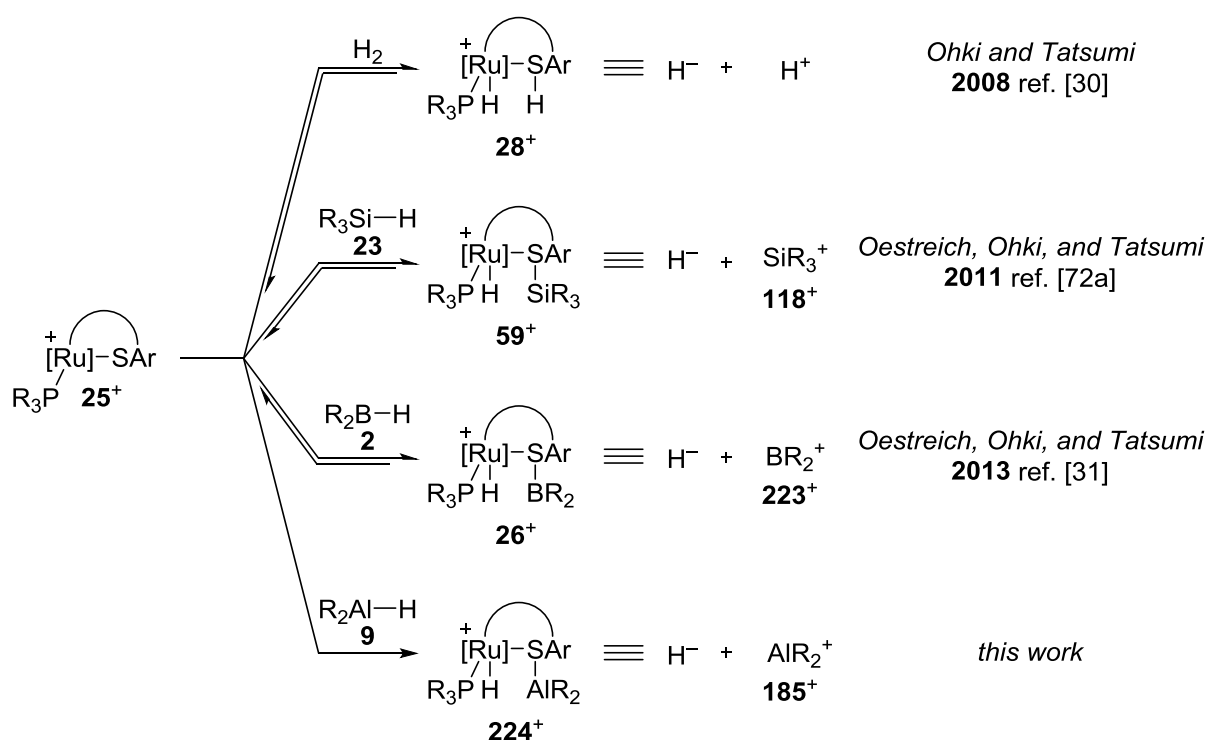


Scheme 6.8 : Defluorinative FRIEDEL–CRAFTS alkylation by STEPHAN.

^[167] a) J. Zhu, M. Pérez, C. B. Caputo, D. W. Stephan, *Angew. Chem.* **2016**, 128, 1439–1443; *Angew. Chem. Int. Ed.* **2016**, 55, 1417–1421; for hydrodefluorination with the same catalytic system, see: b) C. B. Caputo, L. J. Hounjet, R. Dobrovetsky, D. W. Stephan, *Science* **2013**, 341, 1374–1377.

6.2 Catalytic Generation of Alumenium Ions by Cooperative Al–H Bond Activation in Defluorinative FRIEDEL–CRAFTS Alkylation

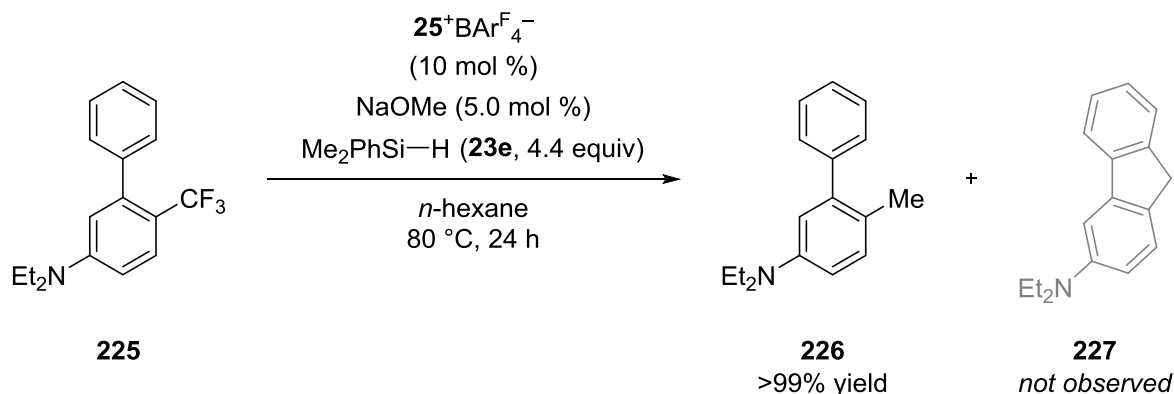
The ruthenium thiolate complex **25**⁺ was previously applied to the cooperative activation of dihydrogen, hydrosilanes **23**, and hydroboranes **2** (Scheme 6.9). During the investigation of carbon dioxide hydrosilylation, the complex **25**⁺ was found to activate Al–H bonds (see Chapter 5.6). In fact, the reaction with DIBAL–H (**9b**) was found to give full conversion at room temperature in 30 min while the corresponding hydrosilylation of carbon dioxide needed more than 2 days at 80 °C.



Scheme 6.9: Cooperative activation of dihydrogen, hydrosilanes, hydroboranes, and hydroalanes.

Encouraged by the initial results in the carbon dioxide reduction, the cooperative activation of DIBAL–H (**9b**) was further investigated. To test the potential of the proposed Al–H bond activation, defluorination was chosen as a model reaction. The corresponding hydrodefluorination of CF_3 -substituted anilines and indoles with hydrosilanes required high catalyst loading, additional base, and elevated temperatures to reach full conversion.^[72a] Interestingly, the hydrodefluorination of trifluoroarene **225** led to exclusive formation of **226**.

The lack of the corresponding FRIEDEL–CRAFTS-product **227** led to the proposal of a sulfur-stabilized carbocation intermediate (Scheme 6.10).^[168]



Scheme 6.10: Ruthenium thiolate **25**⁺-catalyzed hydrodefluorination of CF₃-substituted anilines with hydrosilanes.

During the initial investigations of the Al–H bond activation, decomposition of the BARF_4^- counteranion was observed at elevated temperatures, presumably due to defluorination of the CF₃-groups.^[169] To obtain a more robust catalyst, the BARF_4^- counteranion was replaced with $[\text{B}_{12}\text{Cl}_{12}]^{2-}$.^[170,171] The perhalogenated *closo*-dodecaboranates and the related carborates are some of the most stable anions used with strong main-group electrophiles. However, their wide use has been suppressed due to the cumbersome syntheses and low solubility in non-coordinating solvents.^[172]

^[168] T. Stahl, Dissertation, Technische Universität Berlin, **2014**.

^[169] The decomposition of the related $\text{B}(\text{C}_6\text{F}_5)_4^-$ counteranion was previously observed, see: V. J. Scott, R. Çelenligil-Çetin, O. V. Ozerov, *J. Am. Chem. Soc.* **2005**, *127*, 2852–2853.

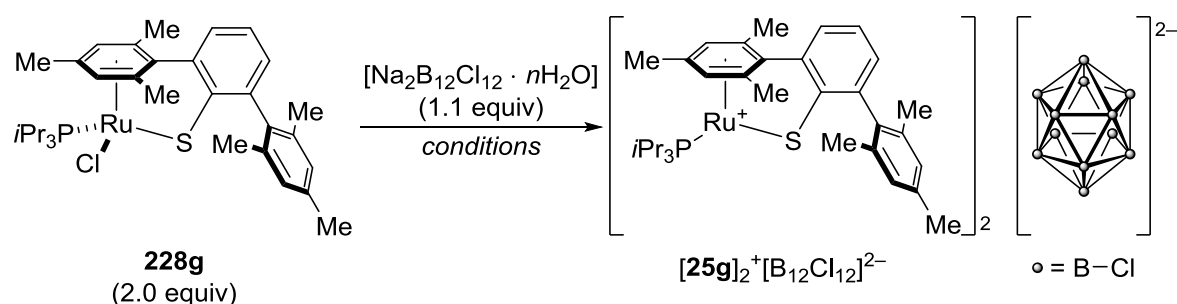
^[170] For a review of weakly coordinating anions, see: I. Krossing, I. Raabe, *Angew. Chem.* **2004**, *116*, 2116–2142; *Angew. Chem. Int. Ed.* **2004**, *43*, 2066–2090.

^[171] The $[\text{B}_{12}\text{Cl}_{12}]^{2-}$ counteranion was used earlier by our group in the synthesis and isolation of a ferrocene-stabilized silylium ion: K. Mütter, R. Fröhlich, C. Mück-Lichtenfeld, S. Grimme, M. Oestreich, *J. Am. Chem. Soc.* **2011**, *133*, 12442–12444.

^[172] The corresponding BARF_4^- and $\text{B}(\text{C}_6\text{F}_5)_4^-$ counteranions are commercially available as sodium and lithium salts, respectively. For the synthesis of perhalogenated *closo*-dodecaboranates, see: a) W. H. Knoth, H. C. Miller, J. C. Sauer, J. H. Balthis, Y. T. Chia, E. L. Muetterties, *Inorg. Chem.* **1964**, *3*, 159–167; b) V. Geis, K. Guttsche, C. Knapp, H. Scherer, R. Uzun, *Dalton Trans.* **2009**, 2687–2694; c) W. Gu, O. V. Ozerov, *Inorg. Chem.* **2011**, *50*, 2726–2728; for the synthesis and properties of the carborane counteranions, see: d) S. Körbe, P. J. Schreiber, J. Michl, *Chem. Rev.* **2006**, *106*, 5208–5249; e) C. A. Reed, *Acc. Chem. Res.* **2010**, *43*, 121–128.

The initial attempts to generate the cationic ruthenium thiolate $[25g]_2^+[B_{12}Cl_{12}]^{2-}$ via chloride abstraction using $[Na_2B_{12}Cl_{12} \cdot nH_2O]$ analogous to the synthesis of $[25g]^+BAR_4^{F-}$ either gave no product (Table 6.1, entry 1) or led to decomposition (entry 2).^[173,174] The reaction did not proceed, probably due to poor solubility of the $[Na_2B_{12}Cl_{12} \cdot nH_2O]$ in the weakly polar solvents. On the other hand, the choice of the solvent was limited by the sensitivity of the anticipated cationic ruthenium center 25^+ . During the previous investigations in our group, we had observed that the hydrosilane adducts of the ruthenium thiolate 59^+ are significantly more soluble than 25^+ . Also, the formation of the hydrosilane adduct 48^+ was expected to trap the ruthenium as a cationic complex possibly preventing the equilibration back to the ruthenium chloride **228g**. Using a mixture of chlorobenzene and dimethylethylsilane (**23i**) (ca. 9:1), the dissolution of $[Na_2B_{12}Cl_{12} \cdot nH_2O]$ was observed within minutes accompanied by gas evolution indicating dehydrogenative silylation of the trace moisture in $[Na_2B_{12}Cl_{12} \cdot nH_2O]$ into disiloxane **180i** (entry 3). Simple filtration of sodium chloride and careful evaporation of the volatiles afforded the cationic ruthenium complex $[25g]_2^+[B_{12}Cl_{12}]^{2-}$ in good yield.

Table 6.1: Synthesis of the ruthenium thiolate dodecaboranate complex $[25g]_2^+[B_{12}Cl_{12}]^{2-}$.

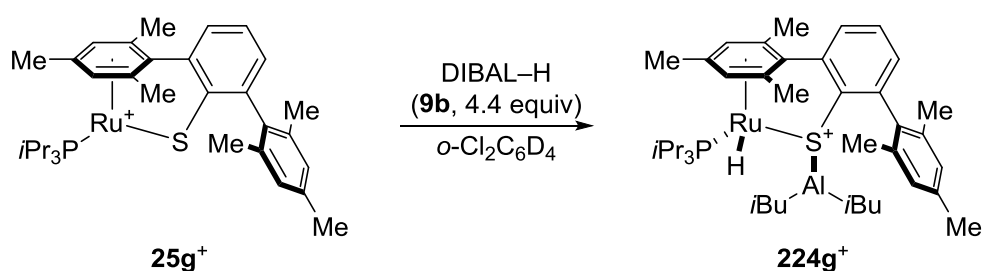


entry	solvent	temperature	yield
1	benzene, toluene, CH_2Cl_2 , PhCl, PhF, $o-Cl_2C_6H_4$, $o-F_2C_6H_4$	r.t.	no reaction
2	benzene, toluene, CH_2Cl_2 , PhCl, PhF, $o-Cl_2C_6H_4$, $o-F_2C_6H_4$	25 °C – 100 °C	low conversion, decomposition
3	PhCl : $Me_2EtSi-H$ (ratio ca. 9:1)	r.t	92%

^[173] T. Stahl, unpublished results.

^[174] The corresponding chloride abstraction with $NaBAR_4^F$ is usually completed within seconds.

Treatment of the complex $[\mathbf{25g}]_2^+[\text{B}_{12}\text{Cl}_{12}]^{2-}$ with DIBAL–H gave immediate conversion into a new ruthenium-stereogenic complex $[\mathbf{224g}]_2^+[\text{B}_{12}\text{Cl}_{12}]^{2-}$, reflected by six magnetically inequivalent methyl groups, with a ruthenium hydride signal at -13.0 (d, $J = 25.9$ Hz) ppm in the ^1H NMR spectrum (Scheme 6.11).^[175] Due to a strong, broad signal of the excess DIBAL–H in the ^{27}Al NMR spectrum, no new aluminium shift could be detected. Based on analogous hydrosilane and hydroborane complexes, the new ruthenium complex was assigned as the DIBAL–H adduct $[\mathbf{224g}]_2^+[\text{B}_{12}\text{Cl}_{12}]^{2-}$. The lack of EXSY NMR signals typically observed with the corresponding hydrosilane and hydroborane activation indicates irreversibility of the activation.

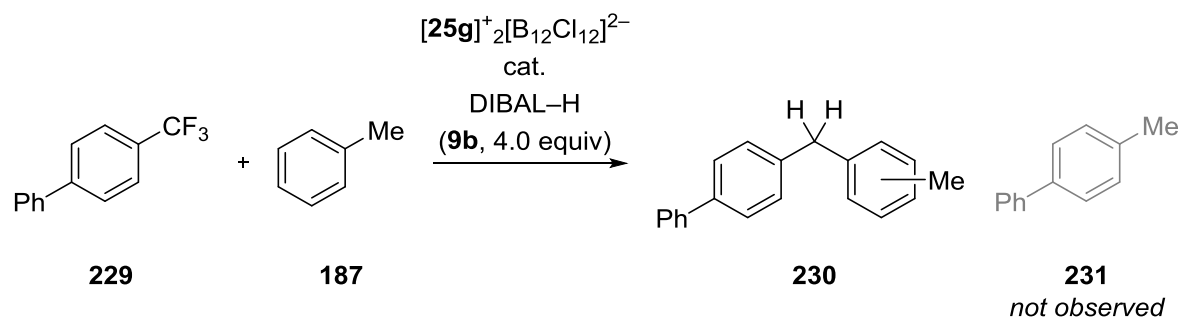


Scheme 6.11: Cooperative activation of Al–H bonds (counteranion $[\text{B}_{12}\text{Cl}_{12}]^{2-}$ omitted for clarity).

The catalytic activity of the complex $[\mathbf{25g}]_2^+[\text{B}_{12}\text{Cl}_{12}]^{2-}$ was investigated in the defluorination of aromatic CF_3 -groups. The defluorination of trifluoroarene **229** proceeded smoothly at 60°C in toluene (**187**). Instead of the expected hydrodefluorinated product **231**, defluorinated FRIEDEL–CRAFTS alkylation products **230** of toluene were observed with $p:o = 76:24$ ratio of regioisomers (Table 6.2, entry 1). Lowering the toluene (**187**) loading to 10 equiv and adding fluorobenzene as solvent dropped the reaction time to 1.5 h (entry 2). Further decreasing of the toluene (**187**) equivalence and increasing the concentration led to slightly increased regioselectivity (entries 3 and 4). The reaction temperature could be lowered to room temperature, and the catalyst loading to 1.25 mol % without affecting the regioselectivity (entries 5 and 6). Other polar, electron-poor aromatic solvents could be used as well but the regioselectivity was found to slightly decrease (entries 7–9). The reaction in hexafluorobenzene did not give any product due to low solubility (entry 10).

^[175] The corresponding ^1H NMR shift ranges for the hydrosilane and hydroborane adducts **59**⁺ and **26**⁺ are -7.5 – -8.3 and -8.1 – -11.9 ppm, respectively.

Table 6.2: Optimization of ruthenium thiolate complex $[\mathbf{25g}]_2^+[\text{B}_{12}\text{Cl}_{12}]^{2-}$ -catalyzed defluorinative FRIEDEL–CRAFTS alkylation.

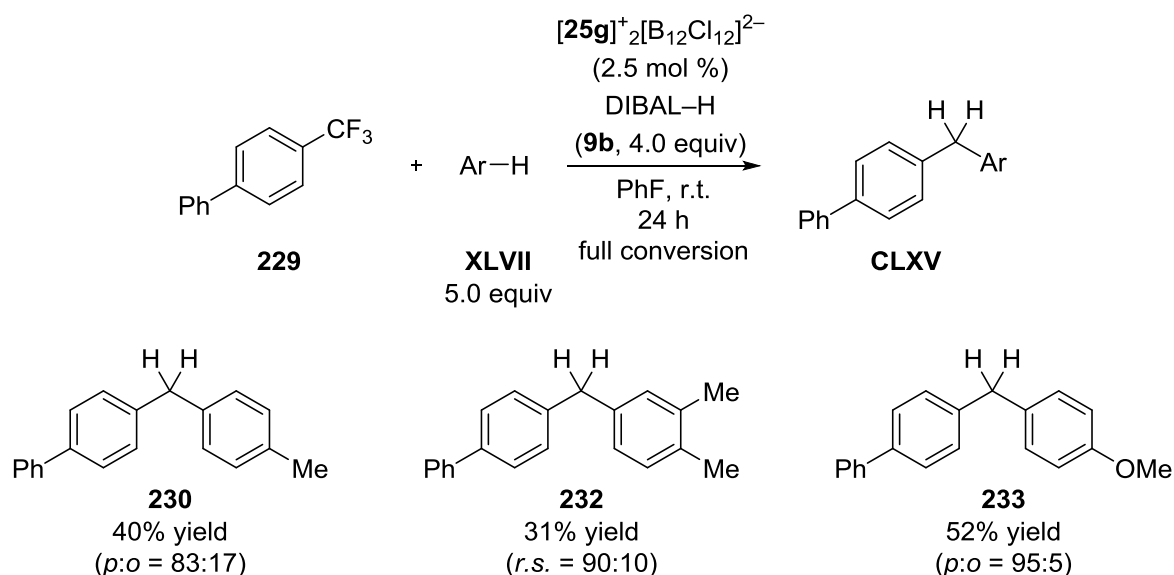


entry	catalyst loading (mol %)	toluene (equiv)	solvent	t (h)	T (°C)	conversion (%) ^[a,b]	ratio (o:p) ^[b,c]
1	2.5	50	-	24	60	99	24:76
2	2.5	10	PhF (0.08 M)	1.5	60	>99	22:78
3	2.5	5	PhF (0.08 M)	1.5	60	>99	24:76
4	2.5	5	PhF (0.4 M)	1.5	60	>99	19:81
5	2.5	5	PhF (0.4 M)	24	r.t.	>99	19:81
6	1.25	5	PhF (0.4 M)	24	r.t.	>99	19:81
7	2.5	5	1,2-F ₂ C ₆ H ₄ (0.4 M)	24	r.t.	>99	21:79
8	2.5	5	PhCl (0.4 M)	24	r.t.	>99	21:79
9	2.5	5	1,2-Cl ₂ C ₆ H ₄ (0.4 M)	24	r.t.	>99	23:77
10	2.5	5	C ₆ F ₆ (0.4 M)	24	r.t.	0	-

^[a] Based on consumption of trifluoromethylarene **229** using tetracosane as internal standard. ^[b] Average of two runs. ^[c] Determined by GLC analysis.

The optimized conditions were then employed in an initial screening of arene coupling partners (Scheme 6.12). The alkylated toluene **230** was isolated in 40% yield with good regioselectivity (*p*:*o* = 83:17). The reaction with *o*-xylene gave the product **232** in poor yield (30%) but good regioselectivity (90:10). The alkylation of anisole proceeded smoothly without ether cleavage, affording the diarylmethane **233** with 52% yield and excellent

regioselectivity ($p:o = 95:5$).^[176] Although all reactions gave full conversion in the indicated time and no significant side-products were observed by GLC analysis,^[177] the isolated yields were low. Since the formed products **CLXV** are more electron-rich and, hence, more reactive under the reaction conditions, formation of oligomers is likely.



Scheme 6.12: Ruthenium thiolate complex $[25g]^+[B_{12}Cl_{12}]^{2-}$ -catalyzed defluorinative FRIEDEL–CRAFTS alkylation of toluene, *o*-xylene, and anisole.

The reaction is proposed to begin by cooperative activation of the Al–H bond **224**⁺ (Scheme 6.13). The resulting formal alumenium ion **185**⁺^[178] abstracts a fluoride from the trifluoromethyl arene **CLIX** giving aluminum fluoride **234**^[179] and the difluorocarocation **CLXVI**⁺.^[180] The assumed reversible nucleophilic attack by the coupling arene **CLXVII** is proposed to take place *para* (**CLXVI**⁺→**CLXVIII**⁺) or *ortho* (**CLXVI**⁺→**CLXIX**⁺).^[181] The selectivity of this step is not expected to explain the observed high selectivities. Instead, the

^[176] E. Winterfeldt, *Synthesis* **1975**, 617–630.

^[177] In the case of *o*-xylene, traces (<5%) of *tert*-butylation of *o*-xylene was observed.

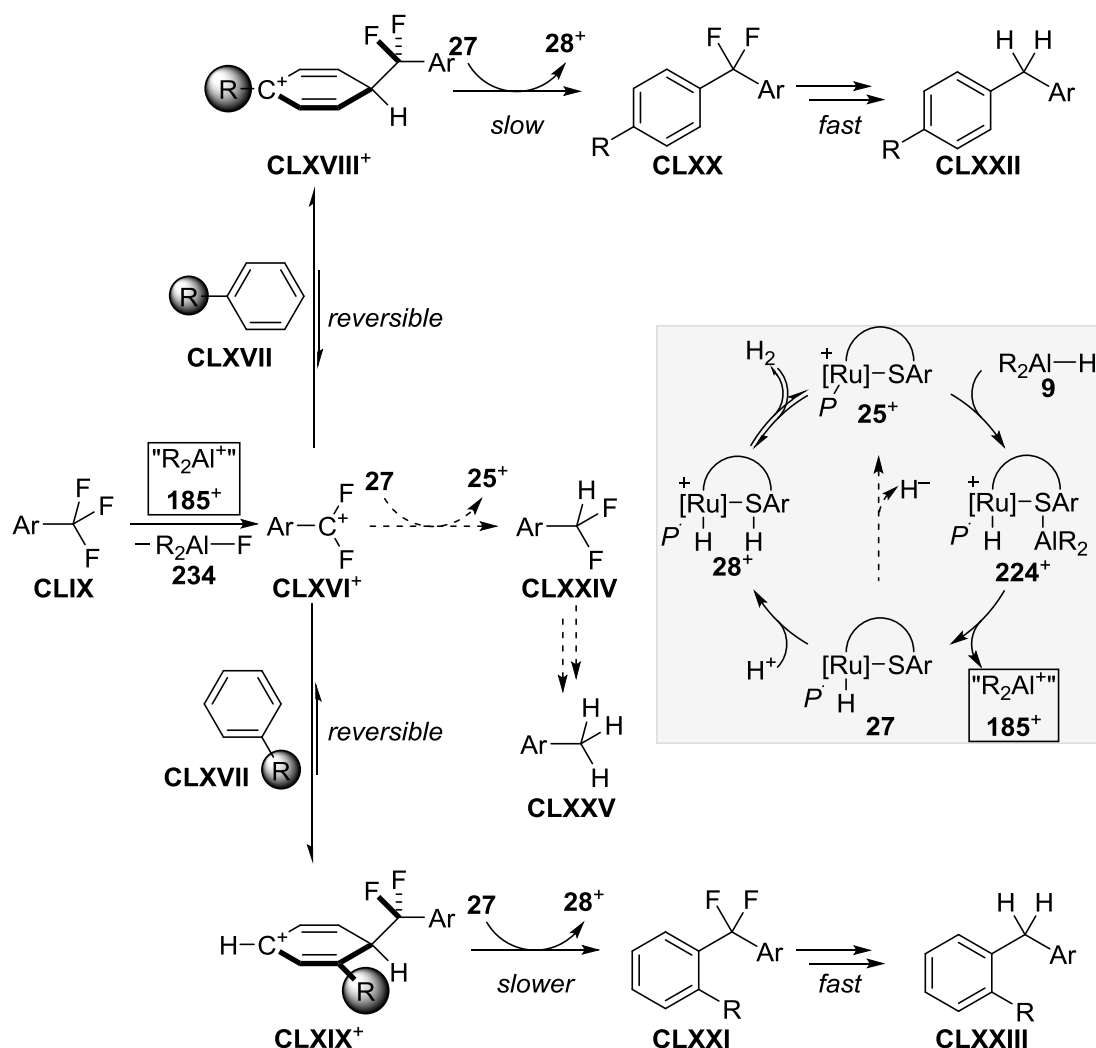
^[178] The liberation of free alumenium ion **185**⁺ seems unlikely. The cation is assumed to be stabilized by the thiolate sulfur atom or by the solvent.

^[179] The formation of Al–F has been detected by ¹⁹F NMR spectroscopy.

^[180] The R–CF₂⁺ carbocations are stabilized by backdonations from the fluorine atoms: a) G. A. Olah, M. B. Comisarow, *J. Am. Chem. Soc.* **1969**, *91*, 2955–2961; b) K. O. Christe, X. Zhang, R. Bau, J. Hegge, G. A. Olah, G. K. Surya Prakash, J. A. Sheehy, *J. Am. Chem. Soc.* **2000**, *122*, 481–487.

^[181] The FRIEDEL–CRAFTS alkylation is known to be reversible. For early examples, see: N. O. Calloway, *Chem. Rev.* **1935**, *17*, 327–392.

regioselectivity is to be determined by the deprotonation step according to the CURTIN–HAMMETT principle.^[182] The deprotonation of the *para*-isomer **CLXVIII**⁺ by the bulky ruthenium hydride **27** is expected to be sterically favored over the corresponding deprotonation of the *ortho*-isomer **CLXIX**⁺. The hydrodefluorination of the diaryl-difluoromethane intermediates **CLXX** and **CLXXI** are expected to be fast and possibly uncatalyzed. The reduction of the difluorocarbocation **CLXVI**⁺ into **CLXXIV** leading to hydrodefluorinated product **CLXXV** does not take place as both the ruthenium hydride **27** and DIBAL–H (**9b**) are poor hydride donors.



Scheme 6.13: Proposed mechanism of the defluorinative FRIEDEL–CRAFTS alkylation catalyzed by the ruthenium thiolate complex **25**⁺.

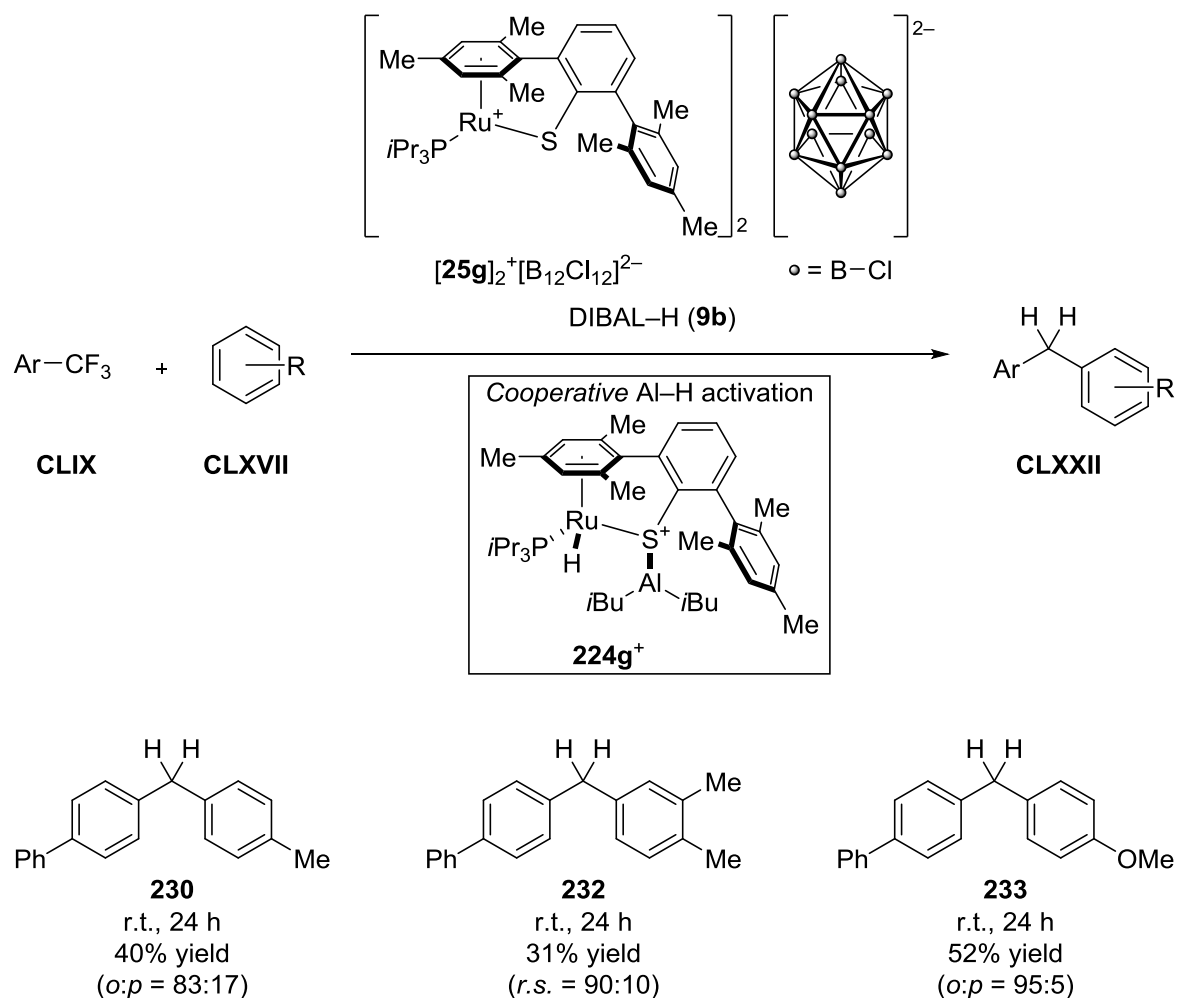
^[182] J. I. Seeman, *Chem. Rev.* **1983**, 83, 84–134.

The catalytic activation of aluminum hydrides has not been widely explored yet, and the ruthenium thiolate adduct of DIBAL–H **224g**⁺ is the first example of a well-defined NMR-spectroscopically characterized Al–H bond activation intermediate.

The cooperative Al–H bond activation by the ruthenium thiolate **25**⁺ was utilized in defluorination. The hydrodefluorination of CF₃-substituted anilines and indoles with hydrosilanes reported earlier^[72a] required high catalyst loading and additional base. Conversely the defluorination with DIBAL–H (**9b**) proceeds readily at room temperature with catalyst loading of 1.25 mol % without additional base. Instead of hydrodefluorination of CF₃-groups into methyl groups, defluorinative FRIEDEL–CRAFTS alkylation of the electron-rich solvent was obtained. The regioselectivity of the reaction is high due to the bulkiness of the ruthenium hydride acting as a base.

The ruthenium thiolate complex **25f**⁺ was applied to cooperative activation of hydrosilanes, hydroboranes, and hydroalanes in carbon dioxide reduction (Scheme 7.1). The hydrosilylation of carbon dioxide was found to be highly selective for reduction into the formaldehyde oxidation state. Under optimized conditions bis(silyl)acetal **168a** was obtained as the sole product in quantitative yield. At higher temperatures, the in-situ formed bis(silyl)acetal **168i** was hydrosilylated into silylated methanol **169i**. The corresponding hydroboration was slow, and the major product was borylated methanol **165a** while only traces of the bis(boryl)acetal **164a** was observed. DIBAL-H (**9b**) was the most reactive main-group hydride in the carbon dioxide reduction: the reaction gave full conversion at room temperature in 30 min. The selectivity was however poor and a complex mixture of various products was obtained.

temperature within 24 h. The DIBAL–H bond activation intermediate **224g**⁺ was fully characterized by NMR spectroscopy.



Scheme 7.2: Ruthenium thiolate complex **[25g]**⁺**[B₁₂Cl₁₂]**²⁻-catalyzed defluorinative FRIEDEL–CRAFTS alkylation.

EXPERIMENTAL PART

1 GENERAL INFORMATION

All reactions were performed under argon or nitrogen atmosphere in flame-dried glassware. For general cleaning, all laboratory glassware was kept overnight in an *i*-PrOH/KOH bath, rinsed with distilled water, neutralized with saturated citric acid bath, rinsed again with distilled water, and dried overnight at 120 °C. The glassware contaminated with transition metals was initially rinsed with aqua regia (conc. HCl and conc. HNO₃ in a ratio of 3:1) prior to further cleaning. For the addition of reagents and solvents through silicon/rubber septa, argon- or nitrogen-flushed disposable syringes and needles were used. All glass syringes and stainless steel needles were used several times and stored at 120 °C. Solids were added in a countercurrent of inert atmosphere or in solution. Low-temperature reactions were either cooled by an ice bath, acetone/dry ice bath, or by using cryostats EK90 from *Haake* or TC100E-F from *Huber*.

Physical Data

Melting Points (m.p.) were determined using a melting-point-determination apparatus from *Thompson Scientific* and *Stuart*. The values are not corrected.

Boiling Points (b.p.) were measured at the distillation head and are not corrected. Distillation under reduced pressure was determined directly by the connected pressure gauge (VAP 5, from Vacuumbrand).

Chromatography

Qualitative **thin-layer chromatography** (TLC) was performed on glass plates with silica gel 60 F₂₅₄ from *Merck KGaA*.

Following methods were used for indication of the analyte:

- Exposure of the TLC plate to UV light ($\lambda = 254$ nm), UV absorption by the analyte.
- Dipping the TLC plate into a solution of KMnO₄ (3.0 g), K₂CO₃ (20 g), and KOH (0.30 g) in distilled H₂O (300 mL) and then heating with a heat gun.

Flash Chromatography was performed with silica gel from *Merck* of the grain size 40-63 μ m, 230-400 mesh, ASTM.

Analytical **gas-liquid chromatography** (GLC) of the reaction mixtures and pure substances were performed using gas chromatograph of the type 7890A from *Agilent Technologies* [equipped with a fused silica capillary column of the type HP-5 capillary column (Length:

30 m; inner diameter: 0.32 mm; film thickness of the covalently bonded stationary phase: 0.25 μm]).

All GLC analyses were performed using the following program:

- Carrier gas N_2 ; injector temperature 250 $^{\circ}\text{C}$; detector temperature 300 $^{\circ}\text{C}$; flow rate 1.7 mL/min; temperature program: starting temperature 40 $^{\circ}\text{C}$, heating rate 10 $^{\circ}\text{C}/\text{min}$, final temperature 280 $^{\circ}\text{C}$ for 10 min.

Qualitative analysis by **high-performance liquid chromatography** (HPLC) were performed on an analytical HPLC system Series 1200 from *Agilent Technologies*. The following columns were used as a chiral stationary phase:

- Daicel Chiralcel OD-H, OJ-H (normal phase)
- Daicel Chiralpak IB (normal phase)
- Daicel Chiralcel OJ-RH, OD-RH (reversed-phase)

NMR Spectroscopy

^1H , ^2H , ^{11}B , ^{13}C , ^{19}F , ^{27}Al , ^{29}Si , and ^{31}P NMR spectra were recorded in CDCl_3 (Eurisotop), C_6D_6 (Eurisotop), CD_2Cl_2 (Sigma-Aldrich), *o*- $\text{Cl}_2\text{C}_6\text{D}_4$ (Eurisotop) or toluene- d_8 (Eurisotop) on AV 400, AV 500, and AV 700 instruments from Bruker at *Institut für Chemie, Technische Universität Berlin*. The ^1H and ^{13}C chemical shifts are reported in parts per million (ppm) referenced to the residual solvent resonance as the internal standard (CHCl_3 : $\delta = 7.26$ ppm for ^1H and CDCl_3 : $\delta = 77.16$ ppm for ^{13}C ; $\text{C}_6\text{D}_5\text{H}$: $\delta = 7.16$ ppm for ^1H and C_6D_6 : $\delta = 128.1$ ppm for ^{13}C ; CDHCl_2 : $\delta = 5.32$ ppm for ^1H and CD_2Cl_2 : $\delta = 53.84$ ppm for ^{13}C ; *o*- $\text{Cl}_2\text{C}_6\text{D}_3\text{H}$: $\delta = 6.94$ and 7.19 ppm for ^1H and *o*- $\text{Cl}_2\text{C}_6\text{D}_4$: $\delta = 127.2$, 130.0 , and 132.4 ppm for ^{13}C ; toluene- d_7 : $\delta = 2.08$, 6.67 , 7.01 , 7.09 ppm for ^1H and toluene- d_8 : $\delta = 20.43$, 125.13 , 127.96 , 128.87 , 137.48 ppm).^[183] For all other nuclei, the NMR resonance signals were internally calibrated using the standardized scale for chemical shifts (unified chemical shift scale).^[184] Data are reported as follows: chemical shift, multiplicity (br s = broad singlet, s = singlet, d = doublet, t = triplet, q = quartet, sept = septet, m = multiplet, and m_c = centrosymmetric multiplet), coupling constant, integration, and assignment. The assignment of signals refers to the numbering of the structures in the figures and is in accordance with careful interpretations made from 2D NMR spectroscopy. The term "Ar" refers to unspecified protons or carbon atoms of an aromatic system. Air- and moisture-

^[183] a) H. E. Gottlieb, V. Kotlyar, A. Nudelman, *J. Org. Chem.* **1997**, 62, 7512–7515; b) G. R. Fulmer, A. J. M. Miller, N. H. Sherden, H. E. Gottlieb, A. Nudelman, B. M. Stolz, J. E. Bercaw, K. I. Goldberg, *Organometallics* **2010**, 29, 2176–2179.

^[184] R. K. Harris, E. D. Becker, S. M. C. de Menezes, R. Goodfellow, P. Granger, *Pure Appl. Chem.* **2001**, 73, 1795–1818.

sensitive samples were measured in J. YOUNG NMR tubes, the carbon dioxide reductions were performed in Norell[®] Intermediate Pressure Valved NMR tubes, all other samples were measured in reusable oven-dried standard NMR tubes. For more precise integration of ¹H NMR spectra in the in-situ monitored carbon dioxide reduction, the relaxation delay was set to 15 sec.

Mass Spectrometry

High Resolution Mass Spectrometry (HRMS) measurements were performed at the analytical facilities of the *Institut für Chemie, Technische Universität Berlin* with an LTQ Orbitrap XL [atmospheric-pressure chemical ionization (APCI) or electrospray ionization (ESI)] or with a Finnigan MAT 95S (electron ionization, 70 eV) from *Thermo Scientific*. The in-detail fragmentation was omitted and only the molecular ion peak or characteristic molecular fragments are considered.

Low Resolution Mass Spectrometry (LRMS) data were measured with the GC-MS-system 5975C from *Agilent Technologies* by electron ionization (EI). The GLC is equipped with a fused silica capillary column of the type HP-5MS capillary column (Length: 30 m; inner diameter: 0.25 mm; film thickness of the covalently bonded stationary phase: 0.25 µm).

Analyses were typically performed using the following program:

- Carrier gas He; injector temperature 300 °C; detector temperature 300 °C; flow rate 0.8 mL/min; temperature program: starting temperature 40 °C, heating rate 10 °C/min, final temperature 280 °C for 10 min.

Infrared Spectroscopy

Infrared (IR) spectra were recorded on a Cary 630 FT-IR from *Agilent Technologies* equipped with an ATR unit and are reported (br = broad, w = weak, m, medium, s = strong) in wavenumbers (cm⁻¹).

Optical Rotation

The optical rotations were determined with a Polatron H532 polarimeter from *Schmidt+Haensch*. The analytes were measured as a solution in the reported solvent in 1 dm cuvettes, and the specific rotation was calculated using the following formula:

$$[\alpha]_{\lambda}^T = \frac{[\alpha] \times 100}{c \times d}$$

Where " λ " is the wavelength (nm), " T " is the measurement temperature ($^{\circ}\text{C}$), " $[\alpha]$ " is the polarimeter-determined rotation, " c " is the concentration (g/100 mL) and " d " is the length of the cuvette (dm). The sodium D-line ($\lambda = 589 \text{ nm}$) is used as the light source.

X-Ray Crystal Structural Analysis

Data sets for X-ray crystal structure analyses were collected by PAULA NIXDORF on a *Nonius KappaCCD* circle diffractometer equipped with $\text{Cu-K}\alpha$ -radiation ($\lambda = 154.178 \text{ pm}$) graphite monochromator in the analytical facility at the *Institut für Chemie, Technische Universität Berlin* and analyzed by Dr. ELISABETH IRRAN. Thermal ellipsoids are shown at the 50% probability level; R -values are given for the observed reflections, wR^2 -values are given for all reflections.

Software

GC-data were recorded and analyzed using EZChrom Elite Compact by *Agilent*. NMR data was recorded and analyzed using Topspin 3.2 by *Bruker*. The stacked NMR spectra were generated using GIMP 2.8.4 image manipulation program. GC-MS data was measured and analyzed using Enhanced ChemStation 02.02.1431 by *Agilent Technologies*. The HRMS data was analyzed using Mass++ 2.4.0 by *Shimadzu and Eisai Co., Ltd.* IR data was recorded and analyzed using Microlab and Agilent Resolutions Pro 5.2.0 by *Agilent Technologies*. X-ray structures and DFT calculated structures were analyzed using Mercury 3.1.1 by *CCDC*. 3D graphics were generated using CYLview 1.0b.^[185] All schemes in this thesis were drawn in ChemDraw Professional 15.0.0.106 by *PerkinElmer*. The references were retrieved using *Chemistry Reference Resolver*.^[186] The thesis is written using Microsoft Office 2010 by *Microsoft*.

Solvents and Reagents

Dichloromethane (CH_2Cl_2) and *n*-pentane were heated at reflux over CaH_2 and distilled under nitrogen atmosphere. Tetrahydrofuran (THF) and diethyl ether (Et_2O) were heated at reflux over potassium with benzophenone as indicator and distilled under nitrogen atmosphere. Toluene was heated at reflux over sodium with benzophenone as indicator and distilled under nitrogen atmosphere. Technical grade ethanol and acetone were used without further purification unless stated otherwise. For extraction and flash chromatography, technical grade solvents (*tert*-butyl methyl ether, cyclohexane, *n*-pentane, dichloromethane, diethyl ether, and ethyl acetate) were distilled prior to use. Solvents with high purity standard were

^[185] CYLview, 1.0b; Legault, C. Y., Université de Sherbrooke, 2009.

^[186] <http://chemsearch.kovsky.net/>

used for the high-performance liquid chromatography (HPLC): *n*-heptane (*Roth*, *Merck-Schuchardt* and *Aldrich*), *i*-PrOH (*Roth* and *Aldrich*), acetonitrile (*Roth* and *Aldrich*) and water (*Aldrich*). All solvents and liquid reagents used in a glovebox were distilled and degassed by the freeze-pump-thaw method.

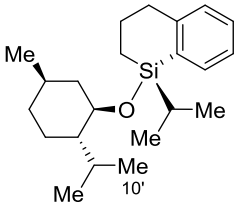
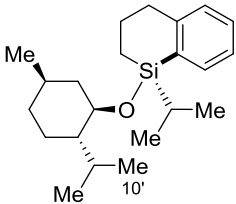
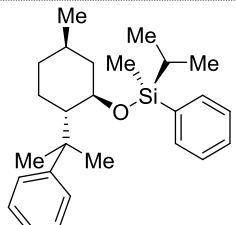
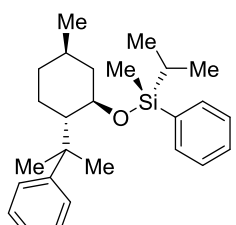
The following reagents were used in this thesis:

Reagent	Supplier
Acetophenone	<i>Fluka</i>
Acetophenone- <i>d</i> ₃	<i>Sigma-Aldrich</i>
Carbon dioxide, >99.95%	<i>Air Liquide</i>
Carbon dioxide, 18 ± 1.8% in argon	<i>Air Liquide</i>
Chlorotriethylsilane, Et ₃ SiCl	<i>Alfa Aesar</i>
Bis(1,5-cyclooctadiene)diiridium(I) dichloride	<i>Acros, STREM</i>
Diisobutylaluminium hydride, DIBAL-H	<i>Sigma-Aldrich</i>
Diisobutylaluminium hydride (in <i>n</i> -hexane)	<i>In-house stock</i>
Di- <i>tert</i> -butylchlorophosphine	<i>Alfa Aesar</i>
Di- <i>n</i> -butyl ether	<i>ABCR</i>
Dimethylaminopyridine, DMAP	<i>Sigma-Aldrich</i>
Hydrogen	<i>Air Liquide</i>
Magnesium	<i>In-house stock</i>
4-Methoxyacetophenone	<i>Sigma-Aldrich</i>
Methyl iodide- <i>d</i> ₃	<i>Sigma-Aldrich</i>
Tris(pentafluorophenyl)borane, B(C ₆ F ₅) ₃	Dr. D. HOG
(<i>S</i>)-1-Phenylethanol	<i>BASF</i>
Triphenylmethyl tetraakis(pentafluorophenyl)borate	Dr. A. SIMONNEAU, V. ROHDE
Potassium- <i>tert</i> -butoxide, KO ^{<i>t</i>} -Bu	Dr. L. DELVOS
Resorcinol	<i>Acros</i>
Sodium <i>closo</i> -dodecachlorododecaboranate, Na ₂ B ₁₂ Cl ₁₂	Dr. K. MÜTHER, J. MOHR
Sodium hydride	<i>In-house stock</i>
Triethylamine, Et ₃ N	<i>In-house stock</i>
4-(Trifluoromethyl)acetophenone	<i>Sigma-Aldrich</i>
4-(Trifluoromethyl)biphenyl	Dr. A. SIMONNEAU
Triphenylphosphite	<i>Sigma-Aldrich</i>

achieve d.r. > 20:1, at least three rounds of flash chromatography were usually required.^[190] The highly enantioenriched hydrosilanes **23b** and **23c** were released by reductive Si–O cleavage according to literature procedures.

The separation of the diastereomers could not be followed by TLC or GLC analysis as the diastereomers have identical retention times. Instead, the d.r. of each fraction was determined by ¹H NMR analysis of small aliquots by integration of the following characteristic signals.

Table 1.1: Characteristic ¹H NMR signals of silyl menthol ethers.

silyl menthol ether	R _f (cyclohexane)	¹ H NMR (400 MHz, CDCl ₃), δ(ppm)
<p>(^{Si}S)-236</p> 	0.21	0.49 (d, ³ J _{10',8'} = 6.9 Hz, 3H, H-10')
<p>(^{Si}R)-236</p> 	0.18	0.58 (d, ³ J _{10',8'} = 7.0 Hz, 3H, H-10')
<p>(^{Si}S)-237</p> 	0.24	0.38 (s, 3H, Si-CH ₃)
<p>(^{Si}R)-237</p> 	0.20	0.35 (s, 3H, Si-CH ₃)

^[190] The cyclohexane consumption required to do this can be decreased significantly by recycling the cyclohexane from the collected fractions back to the column. This way a flash column with total volume of fractions over 100 L can be operated using less than 10 L of solvent.

Nomenclature and Numbering

The numbering of compounds was done analogous to their representative structural drawing and does not correspond to the IUPAC recommendations.

2 GENERAL PROCEDURES

2.1 General Procedure for the Hydrosilylation of Ketones Catalyzed by Brookhart's Iridium(III) Pincer Complex **73**⁺ (GP1)

According to a procedure reported by Brookhart and co-workers,^[79a] iridium(III) pincer complex **73**⁺[B(C₆F₅)₄][−] (3.4 mg, 2.5 μmol, 0.50 mol %) was dissolved in chlorobenzene (0.15 mL). The hydrosilane (0.50 mmol, 1.0 equiv or 2.0 mmol, 4.0 equiv) was added dropwise, and the resulting mixture was stirred for 5 min at room temperature. The ketone (60 mg, 0.50 mmol, 1.0 equiv) was added, and the solution was stirred in a glovebox for the indicated time. After complete conversion (GLC monitoring), the reaction mixture was removed from the glovebox and quenched with one drop of Et₃N. Purification by flash column chromatography on silica gel using *n*-pentane/diethyl ether mixtures (100:0→90:10) as eluent afforded the analytically pure silylether **111** and recovered hydrosilane **23**, respectively.

2.2 General Procedure for the Reductive Si–O Bond Cleavage of Silyl Ethers (GP 2)

A SCHLENK tube equipped with a magnetic stirring bar and a reflux condenser was charged with a solution of the silyl ether (0.20 mmol, 1.0 equiv) in *n*-heptane (2.0 mL). DIBAL–H (**9b**, 0.80 mL, 0.80 mmol, 4.0 equiv, 1.0M in *n*-hexane) was added in one portion at room temperature, and the resulting reaction mixture was heated to reflux and maintained at this temperature for 20 h. The reaction mixture was allowed to cool to room temperature and quenched by careful addition of 1M aqueous HCl (20 mL). The organic layer was separated, and the aqueous phase was extracted with *tert*-butyl methyl ether (3 × 15 mL). The combined organic layers were washed with brine (10 mL), dried over Na₂SO₄, filtered, and the volatiles were evaporated under reduced pressure. The crude product was purified by flash column chromatography on silica gel using *n*-pentane/diethyl ether mixtures (100:0→90:10) as eluent, affording the analytically pure hydrosilane and alcohol.

2.3 General Procedure for the Stoichiometric Reaction of Iron(0) Complex **124** with Hydrosilanes **23** (GP 3)

Iron(0) complex **124**^[191] (44.5 mg, 50.0 μmol , 1.00 equiv) was weighed into a SCHLENK flask with a magnetic stir bar. The hydrosilane (0.15 mmol, 3.0 equiv) was weighed in a vial, dissolved in 2.0 mL of toluene (0.5 mL of C_6D_6 for NMR studies), and added into the SCHLENK flask. The reaction mixture was heated in an oil bath at 70 °C changing the color from dark purple to dark red. The time for completion (100% conversion by NMR spectroscopy) varied depending on the hydrosilane used: $(\text{EtO})_3\text{SiH}$ (**23f**) 12 h, Me_2PhSiH (**23e**) 6 days, and MePh_2SiH (**23g**) reached 90% conversion after 6 days. The reaction mixture was concentrated, and the product was obtained as a crude red oil. The crude product was dissolved in benzene, frozen, and the solvent was sublimated *in vacuo* to afford the desired product as a red powder.

2.4 Carbon Dioxide Reduction (GP 4)

In a glove box, a medium walled valved NMR tube was charged with main-group hydride reagent (0.080 mmol, 1.0 equiv), Ru–S complex **25**⁺ $[\text{B}(\text{C}_6\text{F}_5)_4]^-$ (1.6 or 3.2 μmol , 2.0 or 4.0 mol %), toluene (ca. 8 mg), and C_6D_6 (0.4 mL). The NMR tube was sealed and a ^1H NMR spectrum was measured to obtain an accurate calibration of the internal standard. The tube was pressurized at room temperature with carbon dioxide (>99.95%, 5 bar, ca. 2 mmol, ca. 25 equiv) and heated to 80 °C. The reaction was monitored with ^1H NMR using the toluene signals as internal standard.

2.5 Ruthenium Thiolate-Catalyzed Defluorinative FRIEDEL–CRAFTS Alkylation (GP 5)

In a 5-mL vial in a glovebox, the trifluoromethyl-substituted arene (**229**, 1.0 equiv), complex **[25g]**⁺ $[\text{B}_{12}\text{Cl}_{12}]^{2-}$ (2.5 mol %), and arene (5.0 equiv) were dissolved in the indicated solvent (0.4 M). The solution was mixed and DIBAL–H (**9b**, neat, 4.0 equiv) was added. The reaction was monitored by GLC analysis of aliquots (for the optimization studies, tetracosane was used as internal standard). After full conversion, the vial was removed from the glovebox, the reaction was quenched by the addition of cyclohexane:EtOH (95:5), transferred to a flask

^[191] a) ref [115]; b) D. Gallego, *PhD thesis*, Technische Universität Berlin, **2015**.

containing silica gel, and concentrated *in vacuo*. The crude product was purified by flash chromatography using cyclohexane:toluene (95:5) as eluent.

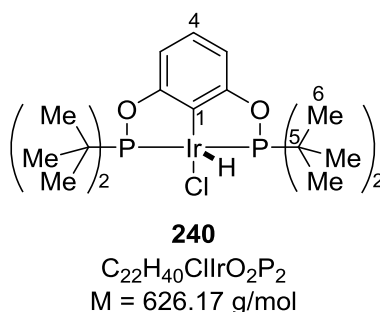
3 DESCRIPTION OF EXPERIMENTS

3.1 Mechanistic Investigations

3.1.1 Iridium(III) POCOP Pincer Complex-Catalyzed Carbonyl Hydrosilylation

3.1.1.1 Synthesis of the Cationic Pincer Complex ($73^+[\text{B}(\text{C}_6\text{F}_5)_4]^-$)

3.1.1.1.1 $[(\text{POCOP})\text{Ir}(\text{H})(\text{Cl})]$ (**240**)



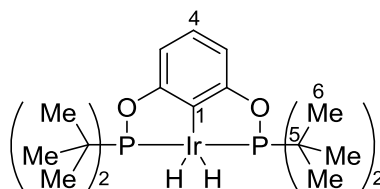
Oil-free NaH (96 mg, 4.0 mmol, 3.3 equiv) was suspended in THF (20 mL) in a 100-mL SCHLENK flask. Resorcinol (210 mg, 1.9 mmol, 1.6 equiv) as a solution in THF (20 mL) was added dropwise (H_2 evolution). After complete addition, the reaction mixture was heated at reflux for 1 h. A solution of di-*tert*-butylchlorophosphine (0.76 mL, 720 mg, 4.0 mmol, 3.3 equiv) in THF (10 mL) was added dropwise and the mixture was refluxed for 1 h. The solvent was removed *in vacuo*, the residue was extracted with *n*-pentane (80 mL), filtered through a pad of Celite[®], and concentrated *in vacuo* (50 °C, 15 h). The resulting clear viscous oil was combined with bis(1,5-cyclooctadiene)diiridium(I) dichloride (400 mg, 0.60 mmol, 0.5 equiv) and dissolved in toluene (5 mL). The mixture was heated at reflux for 3 d. The solvent was removed *in vacuo*, and the residue was extracted with *n*-pentane (*ca.* 3 mL) with sonication (2 × 15 min). The red solid was filtered, washed with *n*-pentane, and dried *in vacuo* to afford pincer complex **240** (647 mg, 1.03 mmol, 86%) as a red solid.

^1H NMR (500 MHz, CD_2Cl_2): $\delta = -41.39$ (t, $^2J_{\text{H,P}} = 13.4$ Hz, 1H, Ir–H), 1.32–1.38 (m, 36H, H-6), 6.53 (d, $^3J_{3,4} = 8.0$ Hz, 2H, H-3), 6.76 (t, $^3J_{4,3} = 8.0$ Hz, 1H, H-4) ppm.

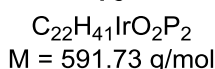
^{31}P NMR (202 MHz, CD_2Cl_2): $\delta = 175.3$ ppm.

The spectroscopic and analytical data are in accordance with those reported.^[192]

3.1.1.1.2 [(POCOP)Ir(H₂)] (75)



75



A 25-mL SCHLENK flask was charged with **240** (120 mg, 0.19 mmol, 1.0 equiv) and KO^tBu (24 mg, 0.22 mmol, 1.1 equiv). Nitrogen-free benzene^[193] (3 mL) was added under H₂ flow, and resulting solution was purged with H₂. The mixture was maintained at room temperature under a slow flow of H₂ for 3 h. The solution was cooled down to 0 °C, the frozen solvent was sublimated *in vacuo* to afford a red solid. The flask was transferred to a glovebox, *n*-pentane (5 mL) was added and the suspension was filtered through a PTFE syringe filter to a 25-mL flask. The solvent was removed *in vacuo*, the residue was dissolved in nitrogen-free benzene (3 mL), frozen, and the solvent was sublimated *in vacuo* affording pincer **75** (26.4 mg, 0.04 mmol, 20%).

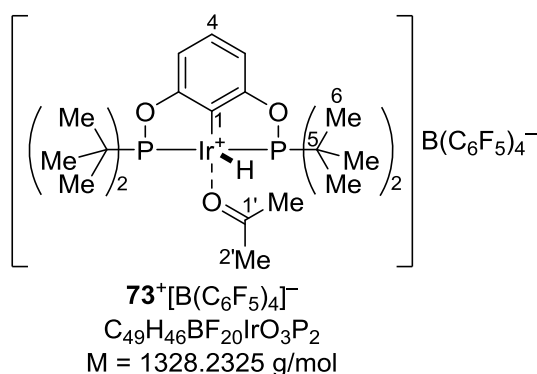
¹H NMR (500 MHz, C₆D₆): δ = −17.01 (t, ²J_{H,P} = 8.2 Hz, 2H, Ir–H), 1.21–1.35 (m, 36H, H-6), 6.90–7.01 (m, 2H, H-3), 7.03 (m, 1H, H-4) ppm.

³¹P NMR (202 MHz, C₆D₆): δ = 204.2 ppm.

The spectroscopic and analytical data are in accordance with those reported.^[96]

^[192] I. Göttker-Schnetmann, P. White, M. Brookhart, *J. Am. Chem. Soc.* **2004**, 126, 1804–1811.

^[193] Degassed by three freeze-pump-thaw cycles using argon or by bubbling H₂ through the solvent for 1 h.

3.1.1.1.3 [(POCOP)IrH(acetone)]⁺[B(C₆F₅)₄]⁻ [**73**]⁺[B(C₆F₅)₄]⁻

A 10-mL SCHLENK tube was charged with **75** (35 mg, 59 μmol, 1.0 equiv) and Ph₃C⁺[B(C₆F₅)₄]⁻ (48 mg, 85 μmol, 1.4 equiv). Freshly distilled nitrogen-free acetone (1 mL) was added, and the mixture was stirred for 2 h. The solvent was evaporated *in vacuo*, and the dark orange solid was again dissolved in acetone (0.5 mL). *n*-Pentane (2 mL) was added to precipitate a dark orange solid. The solvents were removed *via* syringe, and the recrystallization was repeated, affording pincer [**73**]⁺[B(C₆F₅)₄]⁻ as an orange solid (26 mg, 19 μmol, 33%).

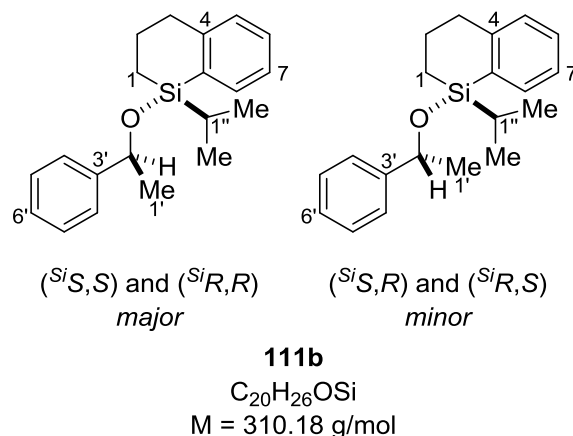
¹H NMR (500 MHz, *o*-Cl₂C₆D₄): δ = -42.25 (t, ²J_{H,P} = 11.6 Hz, 1H, Ir-H), 1.07 (s, 36H, H-6), 1.95 (s, 6H, H-2'), 6.55–6.68 (m, 2H, H-3), 6.79–6.88 (m, 1H, H-4) ppm.

³¹P-NMR (202 MHz, *o*-Cl₂C₆D₄): δ = 173.7 ppm.

The spectroscopic and analytical data are in accordance with those reported.^[78]

3.1.1.2 Stereochemical Course at the Silicon Atom of Silicon Stereogenic Hydrosilanes in Hydrosilylation of Acetophenone Catalyzed by $[73]^+[\text{B}(\text{C}_6\text{F}_5)_4]^-$

3.1.1.2.1 1-Isopropyl-1-(1-phenylethoxy)-1-silatetraline (**111b**)



Using 1.0 equiv of hydrosilane (^{Si}S)-**23b**:

Prepared from (^{Si}S)-1-isopropyl-1-silatetraline [(^{Si}S) -**23b**, 95 mg, 0.50 mmol, 1.0 equiv, $[\alpha]_{\text{D}}^{20} = -58.8$ ($c = 0.34$, CHCl_3 , e.r. = 97:3)] and acetophenone (**109**, 60 mg, 0.50 mmol, 1.0 equiv) according to **GP 1**. The reaction mixture was stirred at room temperature under argon for 20 h. Purification by flash column chromatography on silica gel afforded the analytically pure silyl ether **111b** (130 mg, 0.43 mmol, 86%, d.r. = 55:45) as a colorless oil.

Using 4.0 equiv of hydrosilane (^{Si}S)-**23b**:

Prepared from (^{Si}S)-1-isopropyl-1-silatetraline [(^{Si}S) -**23b**, 0.38 g, 2.0 mmol, 4.0 equiv, $[\alpha]_{\text{D}}^{20} = -58.8$ ($c = 0.34$, CHCl_3 , e.r. = 97:3)] and acetophenone (**109**, 60 mg, 0.50 mmol, 1.0 equiv) according to **GP 1**. The reaction mixture was stirred at room temperature under argon for 30 min. Purification by flash column chromatography on silica gel afforded the analytically pure silyl ether **111b** (130 mg, 0.43 mmol, 86%, d.r. = 55:45) and recovered hydrosilane (^{Si}S)-**23b** [270 mg, 1.4 mmol, 95%, $[\alpha]_{\text{D}}^{20} = -64.5$ ($c = 0.48$, CHCl_3 , e.r. = 94:6)] as colorless oils.

$R_f = 0.08$ (cyclohexane).

GLC: $t_R = 21.4$ min [$(^{Si}S,S)$ - and $(^{Si}R,R)$ -**111b**], $t_R = 21.3$ min [$(^{Si}S,R)$ - and $(^{Si}R,S)$ -**111b**].

IR (ATR): $\tilde{\nu}/\text{cm}^{-1} = 3268$ (w), 3054 (w), 2920 (s), 2860 (s), 1683 (m), 1589 (m), 1434 (s), 1366 (m), 1267 (m), 1086 (s), 1029 (s), 955 (s), 880 (m), 738 (s), 695 (s).

HRMS (APCI) for $\text{C}_{20}\text{H}_{27}\text{OSi}$ $[(M+H)^+]$: calculated 311.1826, found 311.1824.

NMR spectroscopic data for $(^{Si}S,S)$ - and $(^{Si}R,R)$ -**111b** (major diastereomer)

^1H NMR (500 MHz, CDCl_3): $\delta = 0.66$ (dddd, $J = 15.1$ Hz, $J = 7.9$ Hz, $J = 4.3$ Hz, $J = 0.9$ Hz, 1H, H-1A), 0.77 (ddd, $J = 15.1$ Hz, $J = 10.4$ Hz, $J = 4.8$ Hz, 1H, H-1B), 0.91–1.17 (m, 7H, H-1'', H-2''), 1.34 (d, $^3J_{1,2'} = 6.4$ Hz, 3H, H-1'), 1.63–1.71 (m, 1H, H-2A), 1.82–1.90 (m, 1H, H-2B), 2.61 (ddd, $J = 15.9$ Hz, $J = 9.7$ Hz, $J = 2.8$ Hz, 1H, H-3A), 2.70 (ddd, $J = 15.9$ Hz, $J = 7.6$ Hz, $J = 2.4$ Hz, 1H, H-3B), 4.76 (q, $^3J_{2,1'} = 6.4$ Hz, 1H, H-2'), 7.05–7.11 (m, 1H, H-Ar), 7.16–7.32 (m, 7H, H-Ar), 7.62–7.64 (m, 1H, H-Ar) ppm.

$^{13}\text{C}\{^1\text{H}\}$ NMR (126 MHz, CDCl_3): $\delta = 9.8$ (C-1), 14.2 (C-1''), 17.1 (2''A), 17.2 (2''B), 23.1 (C-2), 27.1 (C-1'), 35.5 (C-3), 71.1 (C-2'), 125.45 (C-7), 125.46 (C-4'), 126.9 (C-6'), 128.2 (C-5'), 128.6 (C-5), 129.6 (C-6), 132.2 (C-9), 134.7 (C-8), 146.8 (C-3'), 150.4 (C-4) ppm.

^{29}Si DEPT NMR (99 MHz, CDCl_3): $\delta = 0.1$ ppm.

NMR spectroscopic data for $(^{Si}S,R)$ - and $(^{Si}R,S)$ -**111b** (minor diastereomer)

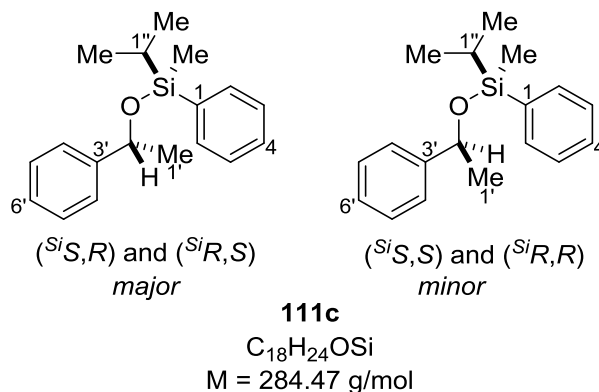
^1H NMR (500 MHz, CDCl_3): $\delta = 0.91$ –1.17 (m, 9H, H-1A, H-1B, H-1'', H-2''), 1.39 (d, $^3J_{1,2'} = 6.3$ Hz, 3H, H-1'), 1.82–1.90 (m, 1H, H-2A), 1.96–2.03 (m, 1H, H-2B), 2.66 (ddd, $J = 16.4$ Hz, $J = 6.2$ Hz, $J = 3.0$ Hz, 1H, H-3A), 2.70 (ddd, $J = 15.8$ Hz, $J = 7.5$ Hz, $J = 2.5$ Hz, 1H, H-3B), 4.83 (q, $^3J_{2,1'} = 6.4$ Hz, 1H, H-2'), 7.03–7.10 (m, 2H, H-Ar), 7.16–7.32 (m, 6H, H-Ar), 7.34–7.35 (m, 1H, H-Ar) ppm.

$^{13}\text{C}\{^1\text{H}\}$ NMR (126 MHz, CDCl_3): $\delta = 10.5$ (C-1), 14.1 (C-1''), 17.1 (2''A), 17.3 (2''B), 23.1 (C-2), 27.2 (C-1'), 35.6 (C-3), 71.2 (C-2'), 125.2 (C-7), 125.37 (C-4'), 126.8 (C-6'), 128.1 (C-5'), 128.6 (C-5), 129.5 (C-6), 131.6 (C-9), 134.8 (C-8), 146.6 (C-3'), 150.1 (C-4) ppm.

^{29}Si DEPT NMR (99 MHz, CDCl_3): $\delta = 0.0$ ppm.

The spectroscopic and analytical data are in accordance with those reported.^[101c]

3.1.1.2.2 Isopropylmethylphenyl(1-phenylethoxy)silane (**111c**)



Using 1.0 equiv of hydrosilane (^{Si}S)-**23c**:

Prepared from (^{Si}S)-isopropylmethylphenylsilane [(^{Si}S)-**23c**, 75 mg, 0.46 mmol, 1.0 equiv, $[\alpha]_{\text{D}}^{20} = -5.0$ ($c = 0.28$, CHCl_3 , e.r. = 97:3)] and acetophenone (**109**, 56 mg, 0.47 mmol, 1.0 equiv) according to **GP 1**. The reaction mixture was stirred at room temperature under argon for 20 h. Purification by flash column chromatography on silica gel afforded the analytically pure silyl ether **111c** (120 mg, 0.41 mmol, 90%, d.r. = 59:41) as a colorless oil.

Using 4.0 equiv of hydrosilane (^{Si}S)-**23c**:

Prepared from (^{Si}S)-isopropylmethylphenylsilane [(^{Si}S)-**23c**, 0.33 g, 2.0 mmol, 4.0 equiv, $[\alpha]_{\text{D}}^{20} = -5.0$ ($c = 0.28$, CHCl_3 , e.r. = 97:3)] and acetophenone (**109**, 60 mg, 0.50 mmol, 1.0 equiv) according to **GP 1**. The reaction mixture was stirred at room temperature under argon for 30 min. Purification by flash column chromatography on silica gel afforded the analytically pure silylether **111c** (130 mg, 0.45 mmol, 89%, d.r. = 62:38) and recovered hydrosilane (^{Si}S)-**23c** [210 mg, 1.3 mmol, 85%, $[\alpha]_{\text{D}}^{20} = -4.1$ ($c = 0.80$, CHCl_3 , e.r. = 74:26)] as colorless oils.

$R_f = 0.09$ (cyclohexane).

IR (ATR): $\tilde{\nu} / \text{cm}^{-1} = 3066$ (w), 3025 (w), 2954 (m), 2863 (m), 1450 (m), 1427 (m), 1367 (m), 1252 (m), 1112 (s), 1089 (s), 1031 (m), 996 (m), 957 (s), 882 (m), 735 (s), 698 (s).

GLC: $t_R = 18.7$ min [(^{Si}S,S)- and (^{Si}R,R)-**111c**], $t_R = 18.6$ min [(^{Si}S,R)- and (^{Si}R,S)-**111c**].

HRMS (APCI) for C₁₈H₂₅OSi [(M+H)⁺]: calculated 285.1669, found 285.1666.

NMR spectroscopic data for (^{Si}S,R)- and (^{Si}R,S)-**111c** (major diastereomer)

¹H NMR (500 MHz, CDCl₃): $\delta = 0.20$ (s, 3H, Si-CH₃), 0.90 (d, $^3J_{2'',H-1''} = 7.1$ Hz, 3H, H-2''A), 1.01 (d, $^3J_{2'',H-1''} = 7.0$ Hz, 3H, H-2''B), 1.03–1.13 (m, 1H, H-1''), 1.42 (d, $^3J_{2',1'} = 6.4$ Hz, 3H, H-1'), 4.85 (q, $^3J_{2',1'} = 6.3$ Hz, 1H, H-2'), 7.20–7.24 (m, 1H, H-6'), 7.28–7.34 (m, 4H, H-4', H-5'), 7.36–7.41 (m, 3H, H-3, H-4), 7.58–7.60 (m, 2H, H-2) ppm.

¹³C{¹H} NMR (126 MHz, CDCl₃): $\delta = -6.0$ (Si-CH₃), 14.5 (C-2''A), 17.0 (C-2''B, C-1'), 27.3 (C-1''), 71.3 (C-2'), 125.5 (C-4'), 127.0 (C-6'), 127.8 (C-3), 128.3 (C-5'), 129.6 (C-4), 134.3 (C-2), 136.9 (C-1), 146.8 (C-3') ppm.

²⁹Si DEPT NMR (99 MHz, CDCl₃): $\delta = 7.3$ ppm.

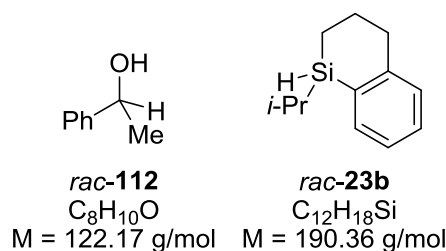
NMR spectroscopic data for (^{Si}S,S)- and (^{Si}R,R)-**111c** (minor diastereomer)

¹H NMR (500 MHz, CDCl₃): $\delta = 0.35$ (s, 3H, Si-CH₃), 0.97 (d, $^3J_{2'',1''} = 7.2$ Hz, 3H, H-2''A), 1.00 (d, $^3J_{2'',1''} = 7.1$ Hz, 3H, H-2''B), 1.03–1.13 (m, 1H, H-1''), 1.43 (d, $^3J_{1',2'} = 6.3$ Hz, 3H, H-1'), 4.89 (q, $^3J_{2',1'} = 6.4$ Hz, 1H, H-2'), 7.20–7.24 (m, 1H, H-6'), 7.28–7.34 (m, 4H, H-4', H-5'), 7.36–7.41 (m, 3H, H-3, H-4), 7.46–7.48 (m, 2H, H-2) ppm.

¹³C{¹H} NMR (125 MHz, CDCl₃): $\delta = -5.2$ (Si-CH₃), 14.4 (C-2''A), 17.2 (C-2''B, C-1'), 27.2 (C-1''), 71.3 (C-2'), 125.5 (C-4'), 126.9 (C-6'), 127.7 (C-3), 128.2 (C-5'), 129.5 (C-4), 134.3 (C-2), 136.5 (C-1), 146.6 (C-3') ppm.

²⁹Si DEPT NMR (100 MHz, CDCl₃): $\delta = 7.0$ ppm.

3.1.1.2.3 Reductive Si–O Bond Cleavage of Silyl Ether 111b



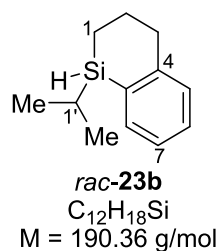
For 111b prepared by using 1.0 equiv of hydrosilane (^{Si}S)-23b:

Silyl ether **111b** (59 mg, 0.19 mmol, 1.0 equiv, d.r. = 55:45) was cleaved according to **GP 2**. Purification by flash column chromatography on silica gel afforded the analytically pure hydrosilane *rac*-**23b** (29 mg, 0.15 mmol, 79%, e.r. = 49:51) and alcohol *rac*-**112** (16 mg, 0.13 mmol, 69%, e.r. = 51:49) as colorless oils.

For 111b prepared by using 4.0 equiv of hydrosilane (^{Si}S)-23b:

Silyl ether **111b** (62 mg, 0.20 mmol, 1.0 equiv, d.r. = 55:45) was cleaved according to **GP 2**. Purification by flash column chromatography on silica gel afforded the analytically pure hydrosilane *rac*-**23b** (39 mg, 0.20 mmol, 99%, e.r. = 48:52) and alcohol *rac*-**112** (21 mg, 0.17 mmol, 86%, e.r. = 51:49) as colorless oils.

Analytical data for hydrosilane *rac*-**23b**:



^1H NMR (500 MHz, CDCl_3): δ = 0.89–0.96 (m, 1H, H-1A), 0.97–1.18 (m, 8H, H-1B, H-1', H-2'), 1.85–2.02 (m_c , 2H, H-2), 2.68–2.90 (m_c , 2H, H-3), 4.21 (m, $^1J_{\text{H,Si}}$ = 187 Hz, 1H, Si-H), 7.11 (d, $^3J_{5,6}$ = 7.6 Hz, 1H, H-5), 7.19 (dd, $^3J_{7,6}$ = $^3J_{7,8}$ = 7.1 Hz, 1H, H-7), 7.27 (m, 1H, H-6), 7.49 (d, $^3J_{8,7}$ = 7.1 Hz, 1H, H-8) ppm.

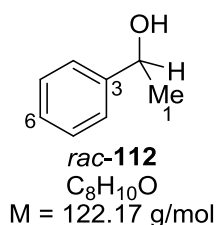
$^{13}\text{C}\{^1\text{H}\}$ (126 MHz, CDCl_3): δ = 6.3 (C-1), 12.5 (C-1'), 18.2 (C-2'A), 18.4 (C-2'B), 22.9 (C-2), 35.4 (C-3), 125.4 (C-7), 128.9 (C-5), 129.2 (C-6), 130.7 (C-9), 135.7 (C-8), 149.7 (C-4) ppm.

^{29}Si DEPT NMR (99 MHz, CDCl_3): δ = -17.4 ppm.

HRMS (APCI) for $\text{C}_{12}\text{H}_{18}\text{Si}$ [M^+]: calculated 190.1172, found 190.1164.

HPLC (Daicel Chiralcel OJ-RH, 20 °C, $\text{MeCN}:\text{H}_2\text{O}$ 50:50, flow rate 0.5 mL min^{-1} , λ = 210 nm): t_{R} = 50.7 min [$(^{\text{Si}}R)$ -**23b**], 52.5 min [$(^{\text{Si}}S)$ -**23b**].

Analytical data for alcohol *rac*-**112**:



^1H NMR (500 MHz, CDCl_3): δ = 1.39 (d, $^3J_{1,2} = 6.5 \text{ Hz}$, 3H, H-1), 1.69 (br s, 1H, O-H), 4.79 (q, $^3J_{2,1} = 6.5 \text{ Hz}$, 1H, H-2), 7.14–7.19 (m, 1H, H-6), 7.21–7.29 (m, 4H, H-4, H-5) ppm.

$^{13}\text{C}\{^1\text{H}\}$ NMR (126 MHz, CDCl_3): δ = 25.3 (C-1), 70.6 (C-2), 125.5 (C-4), 127.6 (C-6), 128.7 (C-5), 146.0 (C-3) ppm.

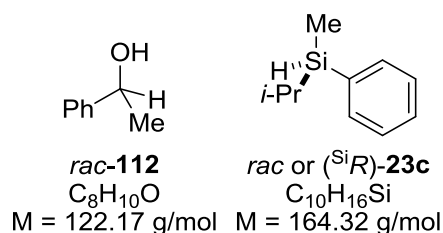
HRMS (APCI) for $\text{C}_8\text{H}_{10}\text{ONa}$ [$(\text{M}+\text{Na})^+$]: calculated 145.0624, found 145.0654.

HPLC (Daicel Chiralpak IB, 20 °C, *n*-heptane:*i*PrOH 95:5, flow rate 0.8 mL min^{-1} , λ = 210 nm): t_{R} = 8.8 min [(R) -**112**], 9.6 min [(S) -**112**].

The spectroscopic and analytical data are in accordance with those reported.^[194]

^[194] S. Rendler, M. Oestreich, C. P. Butts, G. C. Lloyd-Jones, *J. Am. Chem. Soc.* **2007**, *129*, 502–503.

3.1.1.2.4 Reductive Si–O Bond Cleavage of Silyl Ether **111c**



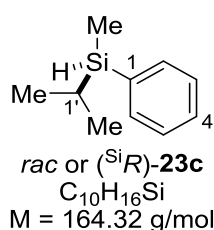
For **111c** prepared by using 1.0 equiv of hydrosilane ($^{\text{Si}}S$)-**23c**:

Silyl ether **111c** (62 mg, 0.22 mmol, 1.0 equiv, d.r. = 56:44) was cleaved according to **GP 2**. Purification by flash column chromatography on silica gel afforded the analytically pure hydrosilane rac-23c (31 mg, 0.19 mmol, 85%, e.r. = 48:52) and alcohol rac-112 (28 mg, 0.22 mmol, 99%, e.r. = 49:51) as colorless oils.

For **111c** prepared by using 4.0 equiv of hydrosilane ($^{\text{Si}}S$)-**23c**:

Silyl ether **111c** (54 mg, 0.19 mmol, 1.0 equiv, d.r. = 56:44) was cleaved according to **GP 2**. Purification by flash column chromatography on silica gel afforded the analytically pure enantioenriched hydrosilane ($^{\text{Si}}R$)-**23c** [27 mg, 0.17 mmol, 86%, e.r. = 36:64, $[\alpha]_{\text{D}}^{20} = 6.7$ ($c = 0.23$, CHCl_3)] and alcohol rac-112 (22 mg, 0.18 mmol, 93%, e.r. = 46:54) as colorless oils.

Analytical data for hydrosilane **23c**:



^1H NMR (500 MHz, CDCl_3): $\delta = 0.33$ (d, $^3J_{\text{Si-CH}_3, \text{Si-H}} = 3.8 \text{ Hz}$, 3H, Si- CH_3), 1.00–1.04 (m, 6H, H-2'), 1.05–1.13 (m, 1H, H-1'), 4.27 (qd, $^3J_{\text{Si-H, Si-CH}_3} = 3.7 \text{ Hz}$, $^3J_{\text{Si-H, 1'}} = 2.5 \text{ Hz}$, $^1J_{\text{H, Si}} = 186 \text{ Hz}$, 1H, Si-H), 7.33–7.39 (m, 3H, H-3, H-4), 7.51–7.56 (m, 2H, H-2) ppm.

$^{13}\text{C}\{^1\text{H}\}$ NMR (126 MHz, CDCl_3): $\delta = -7.7$ (Si- CH_3), 12.6 (C-1'), 18.0 (C-2'A), 18.3 (C-2'B), 127.9 (C-3), 129.3 (C-4), 134.8 (C-2), 136.0 (C-1) ppm.

^{29}Si DEPT NMR (99 MHz, CDCl_3): $\delta = -6.4$ ppm.

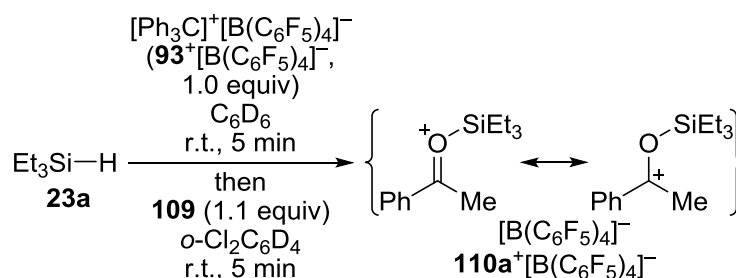
HRMS (APCI) for $\text{C}_{10}\text{H}_{16}\text{Si}$ [M^+]: calculated 164.1016, found 164.1069.

HPLC (Daicel Chiralcel OJ-H, 12 °C, *n*-heptane:*i*PrOH 99:1, flow rate 0.7 mL min $^{-1}$, $\lambda = 210$ nm): $t_{\text{R}} = 6.2$ min [($^{\text{Si}}\text{S}$)-**3b**], 6.4 min [($^{\text{Si}}\text{R}$)-**3b**].

The spectroscopic and analytical data are in accordance with those reported.^[188]

3.1.1.3 Mechanistic Control Experiments with Silylcarboxonium Ion **110a**⁺

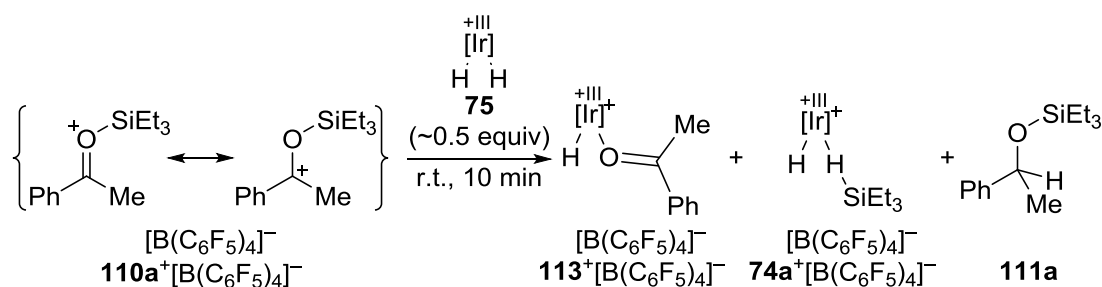
3.1.1.3.1 Generation of $[\text{Et}_3\text{Si}(\text{acetophenone})]^+[\text{B}(\text{C}_6\text{F}_5)_4]^-$ (**110a**⁺ $[\text{B}(\text{C}_6\text{F}_5)_4]^-$)



In a glovebox, $[\text{Ph}_3\text{C}]^+[\text{B}(\text{C}_6\text{F}_5)_4]^-$ (**93**⁺ $[\text{B}(\text{C}_6\text{F}_5)_4]^-$, 46 mg, 0.050 mmol, 1.0 equiv) was dissolved in a minimum amount of C_6D_6 (~0.1 mL). A solution of triethylsilane (**23a**, 8.0 mg, 0.070 mmol, 1.4 equiv) in C_6D_6 (~0.1 mL) was added, and the mixture was vigorously stirred for 5 min at room temperature. The resulting two phases were allowed to separate, and the supernatant was removed *via* cannula. The lower phase was layered with C_6D_6 (~0.1 mL), stirred for 2 min, and the supernatant was removed as previously. A solution of acetophenone (**109**, 6.6 mg, 0.060 mmol, 1.1 equiv) in C_6D_6 (~0.1 mL) was added to the freshly prepared silylium ion $[\text{Et}_3\text{Si}(\text{C}_6\text{D}_6)]^+[\text{B}(\text{C}_6\text{F}_5)_4]^-$, and the reaction mixture was vigorously stirred for 5 min at room temperature. The supernatant was removed *via* cannula, and the residue was washed with C_6D_6 (~0.1 mL). The resulting pale yellow mixture was dissolved in *o*- $\text{Cl}_2\text{C}_6\text{D}_4$ (0.6 mL), transferred into a J. YOUNG NMR tube, and subjected to ^1H NMR analysis.

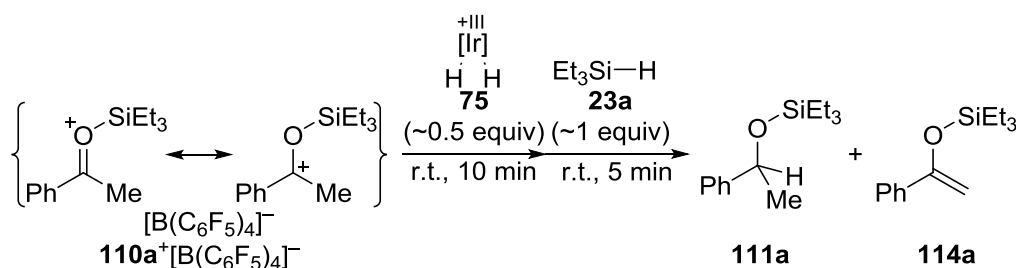
The spectroscopic data are in accordance with those reported.^[188b]

3.1.1.3.2 Control Experiment A: Addition of Iridium Dihydride **75** to Silylcarboxonium Ion **110a**⁺



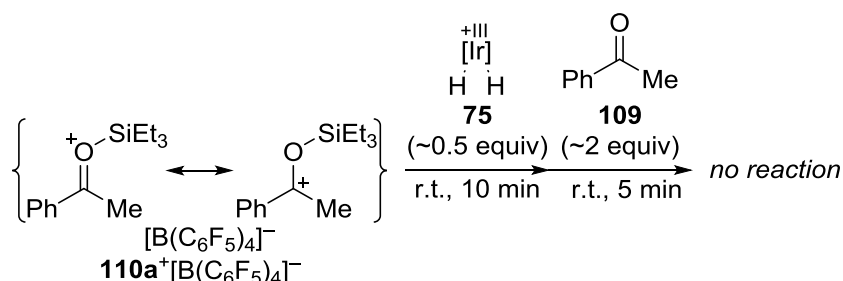
Iridium dihydride **75** (15 mg, 0.025 mmol, 0.50 equiv) was added to a freshly prepared solution of $[\text{Et}_3\text{Si}(\text{acetophenone})]^+[\text{B}(\text{C}_6\text{F}_5)_4]^-$ (**110a**⁺, 0.050 mmol, 1.0 equiv) in *o*-Cl₂C₆D₄ (0.6 mL) at room temperature. The resulting mixture was immediately subjected to ¹H NMR analysis. A mixture of **110a**⁺:**113**⁺:**111a** (53:44:3) along with **74a**⁺ was detected.

3.1.1.3.3 Control Experiment B: Addition of Triethylsilane (**23a**) to Silylcarboxonium Ion **110a**⁺ and Iridium Dihydride **75**

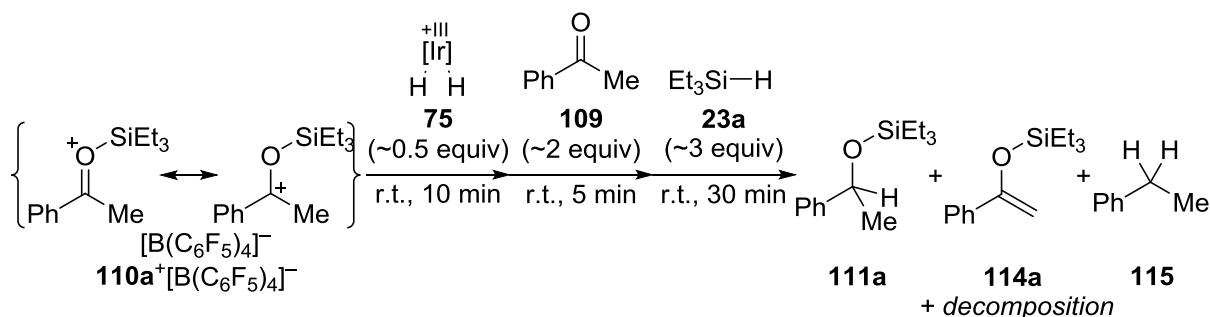


Triethylsilane (**23a**, 8 mg, 0.07 mmol, 1 equiv) was added to the solution obtained in **3.1.1.3.2**, and the resulting mixture was immediately subjected to ¹H NMR analysis. A mixture of **111a** and **114a** (50:50) was detected.

3.1.1.3.4 Control Experiments C

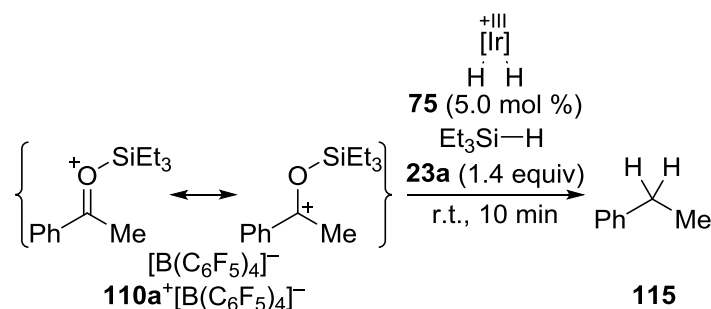
3.1.1.3.4.1 Addition of Acetophenone (**109**) to Silylcarboxonium Ion **110a**⁺ and Iridium Dihydride **75**

Acetophenone (**109**, 12 mg, 0.10 mmol, 2.0 equiv) was added to the solution obtained in **3.1.1.3.2**, and the resulting mixture was immediately subjected to ¹H NMR analysis. No reaction was detected.

3.1.1.3.4.2 Addition of Triethylsilane (**23a**) to Silylcarboxonium Ion **110a**⁺, Iridium Dihydride **75**, and Acetophenone (**109**)

Triethylsilane (**23a**, 20 mg, 0.17 mmol, 3.4 equiv) was added to the solution obtained in **3.1.1.3.4.1**, and the resulting mixture was immediately subjected to ¹H NMR analysis. Initially, a mixture of **110a**⁺:**111a**:**114a**:**115** (16:42:5:37) was obtained. After 10 min, only the formation of ethyl benzene (**115**) along with decomposition was observed.

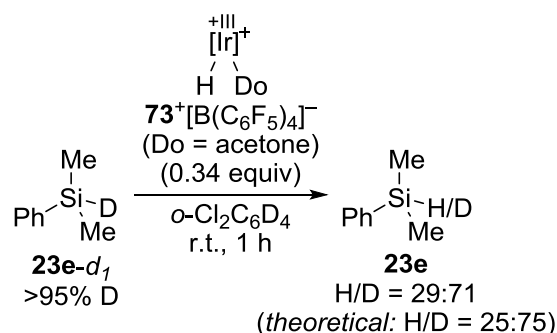
3.1.1.3.5 Control Experiment D: Addition of Triethylsilane (**23a**) and Catalytic Amounts of Iridium Dihydride **75** to the Silylcarboxonium Ion **110a**⁺



Iridium dihydride **75** (1.5 mg, 2.5 μmol , 5.0 mol %) and triethylsilane (**23a**, 8.0 mg, 0.069 mmol, 1.4 equiv) were added to a freshly prepared solution of $[\text{Et}_3\text{Si}(\text{acetophenone})]^+ [\text{B}(\text{C}_6\text{F}_5)_4]^-$ (**110a**⁺, 0.050 mmol, 1.0 equiv) in *o*-Cl₂C₆D₄ (0.6 mL) at room temperature. The resulting mixture was immediately subjected to ¹H NMR analysis. Initially, a mixture of **110a**⁺ and **117** (64:36) was detected. After 10 min, a mixture of **110a**⁺ and **115** (67:33) was observed.

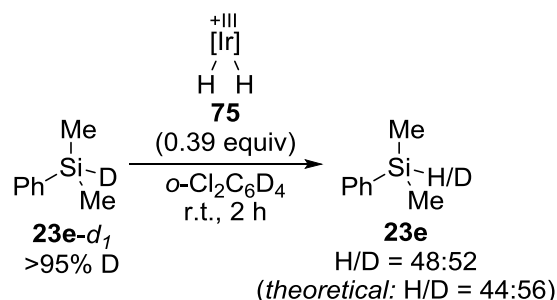
3.1.1.4 ²H-Scrambling Experiments

3.1.1.4.1 ²H-Scrambling Experiment of Deuterium-Labeled Dimethylphenylsilane (**23e-d**₁) with Brookhart's Iridium(III) Pincer Complex **73**⁺



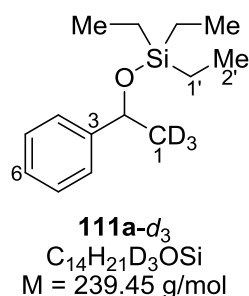
Iridium(III) pincer complex **73**⁺ $[\text{B}(\text{C}_6\text{F}_5)_4]^-$ (3.4 mg, 2.6 μmol , 0.34 equiv) and deuterium-labeled dimethylphenylsilane (**23e-d**₁, 1.5 mg, 7.5 μmol , 1.0 equiv, >95% D) were dissolved in C₆D₆ (0.6 mL), and the resulting reaction mixture was monitored by ¹H NMR spectroscopy. Complete scrambling between the silyl and iridium hydrides was detected after 5 min.

3.1.1.4.2 ^2H -Scrambling Experiment of Deuterium-Labeled Dimethylphenylsilane (**23e-d₁**) with Iridium Dihydride **75**



Iridium dihydride **75** (1.7 mg, 2.9 μmol , 0.39 equiv) and deuterium-labeled dimethylphenylsilane (**23e-d₁**, 1.5 mg, 7.5 μmol , 1.0 equiv, >95% D) were dissolved in C_6D_6 (0.6 mL), and the resulting reaction mixture was monitored by ^1H NMR spectroscopy. Complete scrambling between the silyl and iridium hydrides was detected after 2 h.

3.1.1.4.3 ^2H -Scrambling Experiment of Deuterium-Labeled Acetophenone (**109-d₃**) with Brookhart's Iridium(III) Pincer Complex **73⁺**: Synthesis of Triethyl(phenyl-trideuteromethyl-methoxy)silane (**109-d₃**)



Prepared from acetophenone- d_3 [**109-d₃**, 61 mg, 0.50 mmol, 1.0 equiv, >95% D] and triethylsilane (**23a**, 170 mg, 1.5 mmol, 3.0 equiv) according to **GP 1**. The reaction mixture was stirred at room temperature under argon for 30 min. Purification by flash column chromatography on silica gel afforded the analytically pure silylether **111a-d₃** (120 mg, 0.49 mmol, 99%, >95% D) as a colorless oil.

$R_f = 0.10$ (cyclohexane).

GLC (SE-54): $t_R = 14.0$ min.

IR (ATR): $\tilde{\nu}/\text{cm}^{-1}$ = 3063 (w), 3027 (w), 2953 (s), 2876 (s), 2121 (m), 2001 (w), 1454 (m), 1413 (m), 1359 (m), 1237 (m), 1201 (m), 1127 (s), 1065 (s), 1005 (s), 921 (m), 884 (s), 726 (s).

^1H NMR (500 MHz, CDCl_3): δ = 0.53–0.62 (m, 6H, H-1'), 0.91 (t, $^3J_{2',1'} = 7.9$ Hz, 9H, H-2'), 4.86 (s, 1H, H-2), 7.21–7.26 (m, 1H, H-6), 7.30–7.35 (m, 4H, H-4, H-5) ppm.

^2H NMR (77 MHz, CDCl_3): δ = 1.42 ppm.

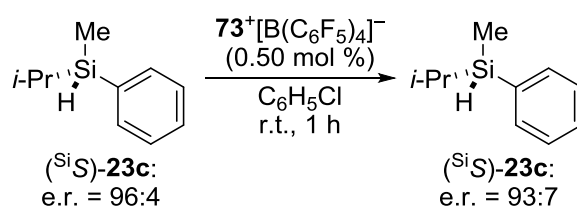
$^{13}\text{C}\{^1\text{H}\}$ NMR (175 MHz, CDCl_3): δ = 5.0 (C-1'), 6.9 (C-2'), 26.5 (sept, $^1J_{\text{C,D}} = 19.4$ Hz, C-1), 70.6 (C-2), 125.4 (C-4), 126.9 (C-6), 128.2 (C-5), 147.0 (C-3) ppm.

^{29}Si DEPT NMR (99 MHz, CDCl_3): δ = 18.5 ppm.

HRMS (APCI) for $\text{C}_{14}\text{H}_{21}\text{D}_3\text{OSiNa}$ $[(\text{M}+\text{Na})^+]$: calculated 262.1677, found 262.1649.

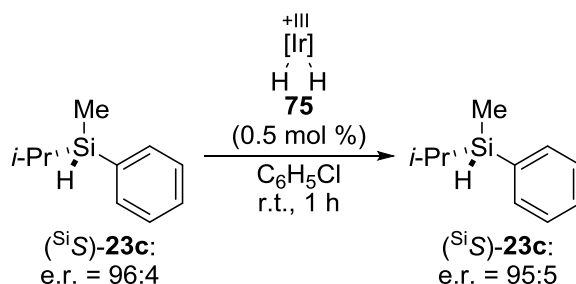
3.1.1.5 Racemization Experiments

3.1.1.5.1 Racemization Experiment of Enantioenriched Acyclic Hydrosilane ($^{\text{Si}}\text{S}$)-**23c** with Brookhart's Iridium(III) Pincer Complex **73**⁺



Iridium(III) pincer complex **73**⁺ $[\text{B}(\text{C}_6\text{F}_5)_4]^-$ (1.7 mg, 1.3 μmol , 0.50 mol %) and enantioenriched hydrosilane ($^{\text{Si}}\text{S}$)-**23c** [41 mg, 0.25 mmol, 1.0 equiv, $[\alpha]_{\text{D}}^{20} = -5.7$ ($c = 0.18$, CHCl_3 , e.r. = 96:4)] were dissolved in chlorobenzene (0.075 mL), and the resulting mixture was stirred at room temperature for 1 h. The reaction mixture was quenched with one drop of Et_3N and directly subjected to flash column chromatography on silica gel using *n*-pentane as eluent. The hydrosilane ($^{\text{Si}}\text{S}$)-**23c** (e.r. = 93:7) was reisolated as a colorless oil with 97% retention of configuration at the silicon atom.

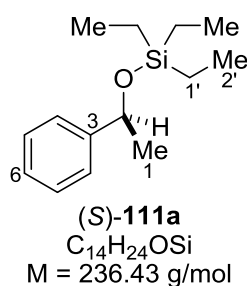
3.1.1.5.2 Racemization Experiment of Enantioenriched Acyclic Hydrosilane (^{Si}S)-**23c** with Iridium Dihydride **75**



Iridium dihydride **75** (0.8 mg, 1 μ mol, 0.5 mol %) and enantioenriched hydrosilane (^{Si}S)-**23c** [41 mg, 0.25 mmol, 1.0 equiv, $[\alpha]_D^{20} = -5.7$ ($c = 0.18$, CHCl_3 , e.r. = 96:4)] were dissolved in chlorobenzene (0.075 mL), and the resulting mixture was stirred at room temperature for 1 h. The reaction mixture was quenched with one drop of Et_3N and directly subjected to flash column chromatography on silica gel using *n*-pentane as eluent. The hydrosilane (^{Si}S)-**23c** (e.r. = 95:5) was reisolated as a colorless oil with 99% retention of configuration at the silicon atom.

3.1.1.5.3 Racemization Experiment of Enantioenriched Silyl Ether (S)-**111a** with Brookhart's Iridium(III) Pincer Complex **73**⁺

3.1.1.5.3.1 Preparation of Enantioenriched (S)-Triethyl(1-phenylethoxy)silane [(S)-**111a**]



(S)-1-Phenylethanol [(S)-**112**, 120 mg, 1.0 mmol, 1.0 equiv, e.r. > 99:1], Et_3N (110 mg, 1.1 mmol, 1.1 equiv), and DMAP (6 mg, 0.05 mmol, 0.05 equiv) were dissolved in CH_2Cl_2 (5 mL). Et_3SiCl (160 mg, 1.05 mmol, 1.05 equiv) was added dropwise, and the resulting mixture was stirred at room temperature for 16 h. The crude mixture was concentrated under reduced pressure, extracted with *n*-pentane ($3 \times 10 \text{ mL}$), and filtered through a plug of Celite[®]. Purification by flash column chromatography on silica gel using cyclohexane:ethyl

acetate (95:5) as eluent afforded the analytically pure silyl ether (S)-**111a** (220 mg, 0.94 mmol, 94%, e.r. > 99:1) as a colorless oil.

$R_f = 0.10$ (cyclohexane).

$[\alpha]_D^{20} = -74.5$ ($c = 0.11$, CHCl_3 , e.r. > 99:1)

GLC (SE-54): $t_R = 14.0$ min.

IR (ATR): $\tilde{\nu} / \text{cm}^{-1} = 2925$ (s), 2875 (m), 1690 (w), 1449 (m), 1237 (m), 1367 (m), 1413 (m), 1092 (s), 1003 (m), 954 (m), 792 (m), 724 (s).

^1H NMR (500 MHz, CDCl_3): $\delta = 0.49\text{--}0.62$ (m, 6H, H-1'), 0.91 (t, $^3J_{2,1'} = 7.9$ Hz, 9H, H-2'), 1.43 (d, $^3J_{1,2} = 6.4$ Hz, 3H, H-1), 4.86 (q, $^3J_{2,1} = 6.4$ Hz, 1H, H-2), 7.20–7.24 (m, 1H, H-6), 7.28–7.35 (m, 4H, H-4, H-5) ppm.

$^{13}\text{C}\{^1\text{H}\}$ NMR (126 MHz, CDCl_3): $\delta = 5.0$ (C-1'), 6.9 (C-2'), 27.4 (C-1), 70.7 (C-2), 125.4 (C-4), 126.9 (C-6), 128.2 (C-5), 147.1 (C-3) ppm.

^{29}Si DEPT NMR (99 MHz, CDCl_3): $\delta = 18.5$ ppm.

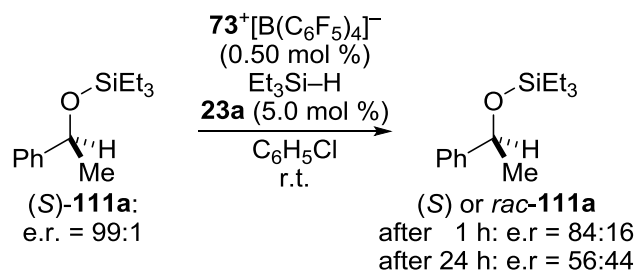
HRMS (APCI) for $\text{C}_{14}\text{H}_{24}\text{OSiNa}$ $[(\text{M}+\text{Na})^+]$: calculated 259.1489, found 259.1436.

HPLC (Daicel Chiracel OJ-RH, 20 °C, $\text{MeCN}:\text{H}_2\text{O}$ 70:30, flow rate 0.4 mL min^{-1} , $\lambda = 210 \text{ nm}$): $t_R = 17.5$ min [(S)-**111a**], 19.5 min [(R)-**111a**].

The spectroscopic and analytical data are in accordance with those reported.^[195]

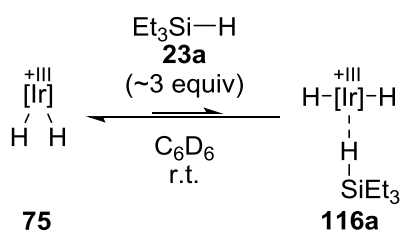
^[195] a) L. D. Field, B. A. Messerle, M. Rehr, L. P. Soler, T. W. Hambley, *Organometallics* **2003**, *22*, 2387–2395; b) M. Mewald, *Ph.D. Thesis*, Westfälische Wilhelms-Universität Münster, **2012**.

3.1.1.5.3.2 Racemization Experiment



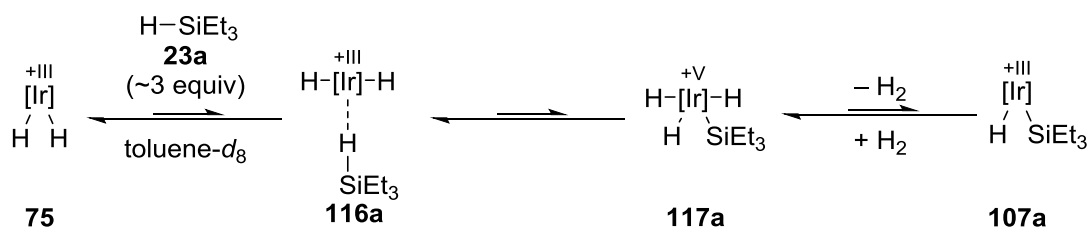
Iridium(III) pincer complex $\mathbf{73}^+[\text{B}(\text{C}_6\text{F}_5)_4]^-$ (1.7 mg, 1.3 μmol , 0.50 mol %) and triethylsilane (**23a**, 1.5 mg, 13 μmol , 5.0 mol %) were dissolved in chlorobenzene (0.075 mL). After 5 min, silyl ether (S)-**111a** [59 mg, 0.25 mmol, 1.0 equiv, $[\alpha]_{\text{D}}^{20} = -74.5$ ($c = 0.11$, CHCl_3 , e.r. = 99:1)] was added, and the resulting mixture was stirred for 1 h at room temperature. The reaction mixture was quenched with one drop of Et_3N and directly subjected to flash column chromatography on silica gel using cyclohexane:ethyl acetate (95:5) as eluent. Silyl ether ($^{\text{Si}}$ S)-**111a** (e.r. = 84:16) was reisolated as a colorless oil.

When the reaction was repeated with 24 h reaction time, silyl ether **111a** was reisolated in nearly racemic form (e.r. = 56:44).

3.1.1.6 Identification of the Adducts between Iridium(III) Dihydride **75** and Hydrosilanes **23**3.1.1.6.1 $^1\text{H}/^1\text{H}$ EXSY NMR

Iridium dihydride **75** (1.7 mg, 2.9 μmol , 1.0 equiv) and triethylsilane (**23a**, 1.1 mg, 9.4 μmol , 3.2 equiv) were dissolved in C_6D_6 (0.6 mL) and subjected to $^1\text{H}/^1\text{H}$ EXSY NMR analysis. Exchange between the hydrides of **23a**, **75**, and **116a** was observed under 300 ms mixing time.

3.1.1.6.2 Variable-Temperature NMR



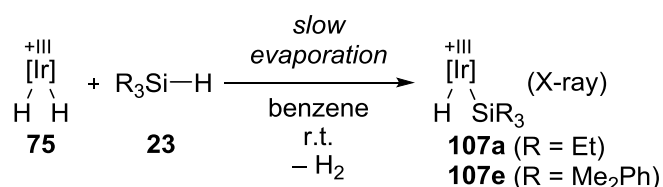
Iridium dihydride **75** (1.7 mg, 2.9 μmol, 1.0 equiv) and triethylsilane (**23a**, 1.0 mg, 8.4 μmol, 2.9 equiv) were dissolved in toluene-*d*₈ (0.6 mL) and subjected to ¹H NMR analysis. The sample was then cooled stepwise to 197 K. Mixtures of **75**, **116a**, **117a**, and **107a** were obtained (Table 3.1). NMR spectra at room temperature were identical before and after the cooling.

Table 3.1: Ratios of **75**, **116a**, **117a**, and **107a** at varied temperatures in toluene-*d*₈^[a]

T (K)	75 (%)	116a (%)	117a (%)	107a (%)
300	98.8	1.2	<0.5	<0.5
277	97.3	2.0	<0.5	0.6
250	94.6	3.5	<0.5	1.9
224	91.8	4.4	0.9	2.9
197	80.1	6.1	9.9	3.9

[a] Ratios determined by integration of the hydride signals in the ¹H NMR spectrum.

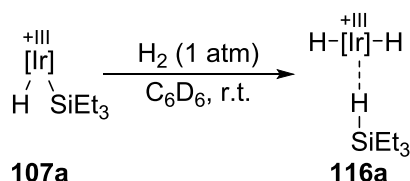
3.1.1.6.3 Crystallization Experiments



Iridium dihydride **75** (~ 2 mg) and the corresponding hydrosilane (**23a** or **23e**, ~ 20 mg, excess) were dissolved in benzene (0.5 mL). Slow evaporation (~1 week) under argon atmosphere at room temperature led to release of dihydrogen and crystallization of single crystals of **107a** and **107e** suitable for X-ray crystallography.

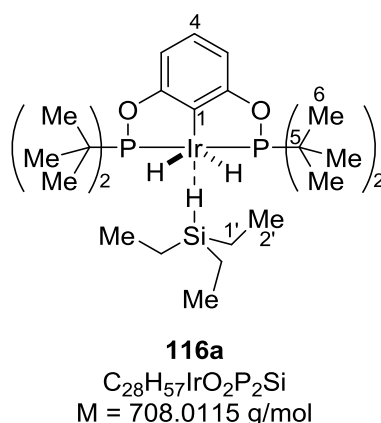
All attempts to obtain single crystals of **116** or **117** with various hydrosilanes were unsuccessful. Subjection of crystals of **107** to an atmosphere of hydrogen led to deterioration of the crystals.

3.1.1.6.4 Hydrogenation of Iridium Silyl Monohydride **107a**



Iridium silyl hydride **107a** (~5 mg) was dissolved in C₆D₆ (0.6 mL) and subjected to ¹H NMR analysis. The NMR tube was then flushed with H₂ (5 s) and sealed. Immediate ¹H NMR analysis showed quantitative conversion of **107a** into **116a**.

Selected NMR data for **116a**:



¹H NMR (500 MHz, C₆D₆, 300 K): δ = −8.29 (br s, 3H, Ir–H) ppm.^[196]

¹H NMR (500 MHz, toluene-*d*₈, 224 K): δ = −8.33 (t, ²J_{H,P} = 9.0 Hz, 3H, Ir–H) ppm.

¹H, ¹³C HMBC (500 / 126 MHz, C₆D₆, 300 K): δ = 2.8 (C-1'), 8.4 (C-2'), 28.5 (C-6), 38.4 (C-5), 105.5 (C-3), 119.0 (C-4), 167.9 (C-2) ppm.

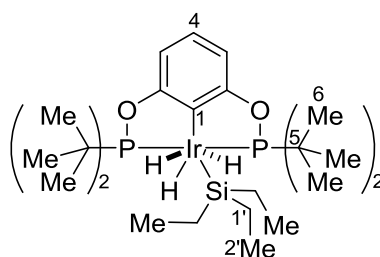
No signals were detected in ²⁹Si NMR.

^[196] All three iridium hydrides coalesce into one signal.

$^{31}\text{P}\{^1\text{H}\}$ NMR (203 MHz, C_6D_6): $\delta = 183.2$ (br s) ppm.

^1H , ^{31}P HMQC NMR (500 / 203 MHz, toluene- d_8 , 300 K): $\delta(^1\text{H}) = -8.35$ ppm / $\delta(^{31}\text{P}) = 182.7$ ppm.

Selected NMR data for **117a**:



117a

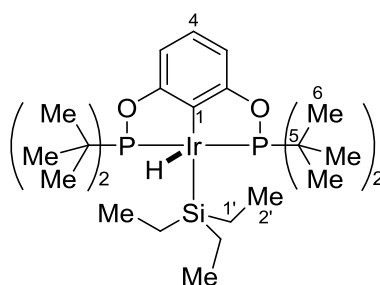
$\text{C}_{28}\text{H}_{57}\text{IrO}_2\text{P}_2\text{Si}$
M = 708.0115 g/mol

^1H NMR (500 MHz, toluene- d_8 , 197 K): $\delta = -9.31$ (t, $^2J_{\text{H,P}} = 10.5$ Hz, 3H, Ir-H) ppm.^[196]

^1H , ^{29}Si HMBC NMR (500 / 99 MHz, toluene- d_8 , 220 K): $\delta(^1\text{H}) = -9.34$ ppm / $\delta(^{29}\text{Si}) = -0.7$ ppm.

^{31}P NMR (203 MHz, toluene- d_8 , 220 K): $\delta = 171.4$ (m) ppm.

Selected NMR data for **107a**:



107a

$\text{C}_{28}\text{H}_{55}\text{IrO}_2\text{P}_2\text{Si}$
M = 705.9955 g/mol

^1H NMR (500 MHz, C_6D_6 , 300 K): $\delta = -15.81$ (t, $^2J_{\text{H,P}} = 5.9$ Hz, 1H, Ir-H) ppm.

^1H , ^{29}Si HMBC NMR (500 / 99 MHz, toluene- d_8 , 220 K): $\delta(^1\text{H}) = -15.83$ ppm / $\delta(^{29}\text{Si}) = -3.9$ ppm.

$^{31}\text{P}\{^1\text{H}\}$ NMR (203 MHz, C_6D_6): $\delta = 188.8$ ppm.

The spectroscopic data for **107a** are in accordance with those reported.^[78a]

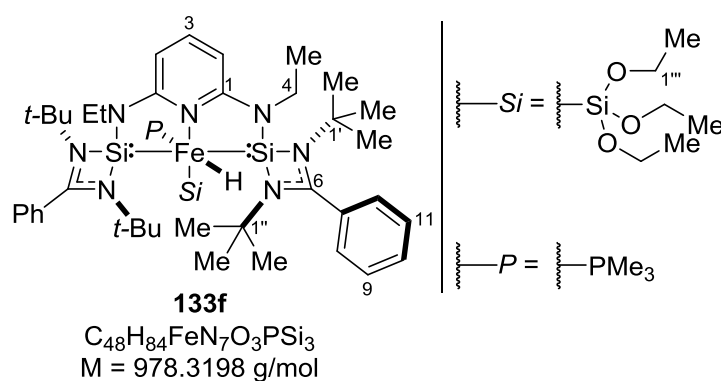
3.1.2 Iron SiNSi Pincer Complex-Catalyzed Carbonyl Hydrosilylation

The mechanistic investigation involving the iron SiNSi pincer complexes described in chapter 3.1.2 was done in collaboration with Dr. DANIEL GALLEG0 from the group of Prof. Dr. MATTHIAS DRIESS.

3.1.2.1 Identification of the Catalytically Active Iron(II) Complex 133

3.1.2.1.1 Iron(II) SiNSi Pincer Complex 133f

Prepared according to **GP3** from iron(0) complex **124** and triethoxysilane **23f**.



^1H NMR (500 MHz, C_6D_6): $\delta = -14.83$ (d, $^2J_{H,P} = 3.2 \text{ Hz}$, $^2J_{H,Si} = 19.3 \text{ Hz}$, 1H, Fe–H), 1.19 (s, 18H, H-2''), 1.41 (t, $^3J_{4,5} = 7.0 \text{ Hz}$, 6H, H-5), 1.47 (s, 18H, H-2'), 1.48 [d, $^2J_{H,P} = 6.2 \text{ Hz}$, 9H, $P(CH_3)_3$], 1.58 (t, $^3J_{2'',1'''} = 7.1 \text{ Hz}$, 9H, H-2'''), 3.38 (dq, $^2J_{4A,4B} = 14.0 \text{ Hz}$, $^3J_{4A,5} = 7.0 \text{ Hz}$, 2H, H-4A), 3.57 (dq, $^2J_{4B,4A} = 14.0 \text{ Hz}$, $^3J_{4B,5} = 7.0 \text{ Hz}$, 2H, H-4B), 4.33 (q, $^3J_{1''',2'''} = 6.9 \text{ Hz}$, 6H, H-1'''), 5.91 (d, $^3J_{2,3} = 8.1 \text{ Hz}$, 2H, H-2), 6.97–7.02 (m, 2H, H-11), 7.02–7.05 (m, 2H, H-10), 7.05–7.08 (m, 2H, H-9), 7.24 (t, $^3J_{3,2} = 8.0 \text{ Hz}$, 1H, H-3), 7.23 (d, $^3J_{12,11} = 7.2 \text{ Hz}$, 2H, H-12), 7.72 (d, $^3J_{8,9} = 7.6 \text{ Hz}$, 2H, H-8) ppm.

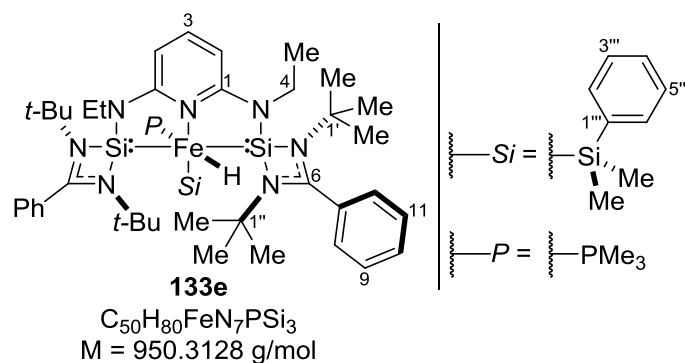
$^{13}\text{C}\{^1\text{H}\}$ NMR (126 MHz, C_6D_6): $\delta = 15.3$ (C-5), 19.8 (C-2'''), 25.9 [d, $^1J_{C-P} = 18.2 \text{ Hz}$, $P(CH_3)_3$], 31.9 (C-2''), 32.6 (C-2'), 38.9 (C-4), 53.7 (C-1'), 54.1 (C-1''), 56.9 (C-1'''), 94.2 (C-2), 127.1 (C-8), 127.2 (C-11), 127.7 (C-12), 128.5 (C-3), 129.7 (C-7), 131.0 (C-9), 133.9 (C-10), 168.1 (C-1), 171.7 (C-6) ppm.

$^{29}\text{Si}\{^1\text{H}\}$ NMR (80 MHz, C_6D_6): $\delta = 33.7$ (d, $^2J_{Si,P} = 58.8 \text{ Hz}$, $Si(OEt)_3$), 79.2 [d, $^2J_{Si,P} = 24.3 \text{ Hz}$, Si(II)] ppm.

$^{31}\text{P}\{^1\text{H}\}$ NMR (202 MHz, C_6D_6): $\delta = 16.8$ ppm.

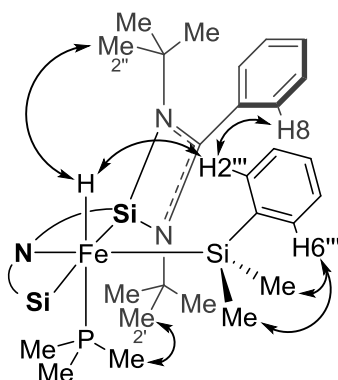
3.1.2.1.2 Iron(II) SiNSi Pincer Complex 133e

Prepared according to **GP3** from iron(0) complex **124** and dimethylphenylsilane **23e**.



^1H NMR (500 MHz, C_6D_6): $\delta = -13.95$ (d, $^2J_{\text{H,P}} = 1.4$ Hz, $^2J_{\text{H,Si}} = 19.7$ Hz, 1H, Fe–H), 1.06 (s, 18H, H-2''), 1.08 [s, 6H, Si(CH_3)], 1.28 (s, 18H, H-2'), 1.38 (t, $^3J_{5,4} = 7.0$ Hz, 6H, H-5), 1.44 [d, $^2J_{\text{H,P}} = 6.3$ Hz, 9H, P(CH_3)₃], 3.33 (dq, $^2J_{4\text{A},4\text{B}} = 13.2$ Hz, $^3J_{4\text{A},5} = 6.6$ Hz, 2H, H-4A), 3.57 (dq, $^2J_{4\text{B},4\text{A}} = 13.2$ Hz, $^3J_{4\text{B},5} = 6.6$ Hz, 2H, H-4B), 5.90 (d, $^3J_{2,3} = 7.6$ Hz, 2H, H-2), 6.93–7.02 (m, 6H, H-9, H-10, H-11), 7.15–7.19 (m, 1H, H-12), 7.24 (t, $^3J_{3,2} = 7.6$ Hz, 1H, H-3), 7.33 (t, $J = 7.1$ Hz, 1H, H-4'''), 7.45–7.50 (m, 3H, H-3''', H-5''', H-6'''), 7.76 (m, 2H, H-8). 8.57 (d, $J = 7.1$ Hz, 1H, H-2''') ppm.

$^1\text{H}/^1\text{H}$ NOESY (500 / 500 MHz, C_6D_6 , 600 ms), selected correlations:



$^{13}\text{C}\{^1\text{H}\}$ NMR (126 MHz, C_6D_6): $\delta = 15.1$ (C-5), 16.3 [Si(CH_3)₂], 25.7 [d, $^1J_{\text{C,P}} = 16.5$ Hz, P(CH_3)₃], 31.7 (C-2''), 32.5 (C-2'), 38.8 (C-4), 53.6 (C-1'), 54.0 (C-1''), 94.3 (C-2), 125.0 (C-4'''), 126.1 (C-6'''), 128.4 (C-11), 128.4 (C-8), 128.6 (C-9), 129.6 (C-7), 130.9 (C-12), 132.8

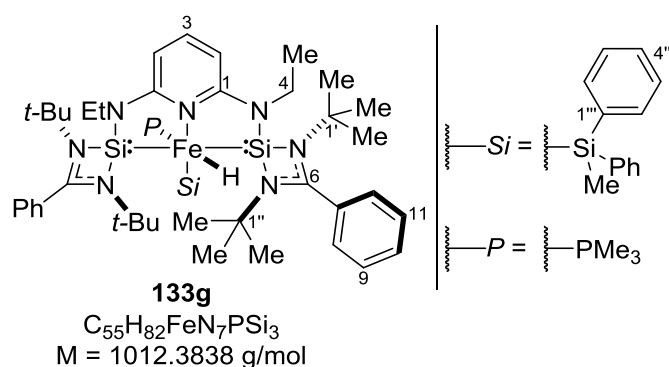
(C-3), 133.3 (C-10), 134.3 (C-3'''), 135.6 (C-5'''), 136.4 (C-2'''), 160.5 (C-1''') 168.3 (C-1), 171.8 (C-6) ppm.

^{29}Si NMR, ^1H - ^{29}Si HMQC NMR (500 MHz / 99 MHz, C_6D_6): δ = 31.1 (SiMe_2Ph), 77.2 [Si(II)] ppm.

$^{31}\text{P}\{^1\text{H}\}$ NMR (202 MHz, C_6D_6): δ = 14.7 ppm.

3.1.2.1.3 Iron(II) SiNSi pincer complex 133g

Prepared according to **GP3** from iron(0) complex **124** and methyldiphenylsilane **23g**.



^1H NMR (500 MHz, C_6D_6): δ = -13.69 (br s, 1H, Fe-H), 1.06 (s, 18H, H-2''), 1.24 (s, 18H, H-2'), 1.34 (m, 6H, H-5), 1.36 [m, 9H, $\text{P}(\text{CH}_3)_3$], 1.37 (m, 3H, SiCH_3), 3.33 (dq, $^2J_{4A,4B} = 13.0 \text{ Hz}$, $^3J_{4A,5} = 6.0 \text{ Hz}$, 2H, H-4A), 3.56 (dq, $^2J_{4B,4A} = 13.0 \text{ Hz}$, $^3J_{4B,5} = 6.5 \text{ Hz}$, 2H, H-4B), 5.86 (d, $^3J_{2,3} = 7.8 \text{ Hz}$, 2H, H-2), 6.90–6.98 (m, 2H, H-11), 6.98–7.05 (m, 4H, H-9, H-10), 7.20–7.27 (m, 3H, H-3, H-12), 7.31–7.40 (m, 6H, H-3''', H-4''', H-5'''), 7.71 (d, $^3J_{8,9} = 6.7 \text{ Hz}$, 2H, H-8), 8.22 (d, $^3J_{2''',3'''} = 6.7 \text{ Hz}$, 4H, H-2''', H-6''') ppm.

$^{13}\text{C}\{^1\text{H}\}$ NMR (126 MHz, C_6D_6): δ = 15.0 (C-5), 25.8 [d, $^1J_{C,P} = 16.7 \text{ Hz}$, $\text{P}(\text{CH}_3)_3$], 29.2 (SiCH_3), 31.7 (C-2''), 32.4 (C-2'), 38.7 (C-4), 53.7 (C-1'), 54.1 (C-1''), 94.3 (C-2), 125.0 (C-4'''), 126.2 (C-6'''), 126.8 (C-11), 128.3 (C-8), 129.1 (C-9), 129.8 (C-7), 130.7 (C-12), 133.2 (C-10), 135.6 (C-5'''), 136.4 (C-2'''), 137.2 (C-3'''), 159.8 (C-1'''), 168.5 (C-1), 172.3 (C-6) ppm.

^{29}Si NMR, ^1H - ^{29}Si HMQC (500 MHz / 99 MHz, C_6D_6): δ = 34.4 (SiMePh_2), 76.3 [Si(II)] ppm.

$^{31}\text{P}\{^1\text{H}\}$ NMR (202 MHz, C_6D_6): δ = 16.8 ppm.

3.1.2.2 Mechanistic Experiments

3.1.2.2.1 Competition Experiment

In a nitrogen-filled glovebox, iron(0) complex **124** (4.4 mg, 2.5 mol %, 5.0 μmol), 4-methoxyacetophenone (**131**, 30 mg, 0.20 mmol, 1.0 equiv, square), 4-trifluoromethylacetophenone (**132**, 38 mg, 0.20 mmol, 1.0 equiv, diamond), and triethoxysilane (**23f**, 53 mg, 0.32 mmol, 1.6 equiv) were weighed into a SCHLENK flask containing a magnetic stir bar and dissolved THF (4 mL). A sample (ca. 0.3 mL) was taken after mixing the reaction mixture (2 min) and quenched with a KOH solution (5% in H_2O). The flask was removed of the glovebox, stirred, and heated to 70 $^{\circ}\text{C}$ with an oil bath. Samples of ca. 0.3 mL were taken every 5 minutes, quenched, and hydrolyzed with KOH solution (1 mL, 5% in H_2O) for 1 h. The mixture was extracted with diethyl ether (2×1 mL). The combined organic layers were dried with anhydrous Na_2SO_4 and filtered. The sample was analyzed by GC-MS. Integration of the peaks for the ketones and the respective alcohols permitted the evaluation of the conversion for each ketone.

Table 3.2: Competition experiment.

	conversion (%)	
time (min)	131	132
2	4	84
5	21	99
15	32	99

3.1.2.2.2 Kinetics: Iron(0) complex 125 vs. Iron(II) complex 133f

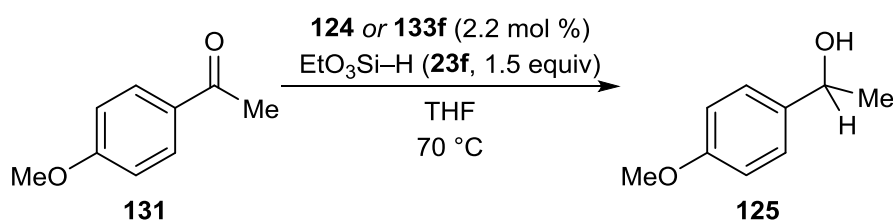
3.1.2.2.1 Iron(0) complex **124**

Iron(0) complex **124** (5 mg, 5 μ mol, 2 mol%) was weighed into a SCHLENK flask together with hydrosilane **23f** (55 mg, 0.33 mmol, 1.5 equiv) and ketone **131** (34 mg, 0.22 mmol, 1.0 equiv). 2.0 mL of THF were added through a syringe, and the mixture was heated to 70 °C. Aliquots were taken during the course of the reaction, hydrolyzed, and analyzed by GC-MS.

3.1.2.2.2 Iron(II) complex **133f**

Iron(0) complex **124** (5 mg, 5 μ mol, 2 mol%) was weighed into a SCHLENK flask together with hydrosilane **23f** (55 mg, 0.33 mmol, 1.5 equiv). 2.0 mL of THF was added through a syringe, and the mixture was heated to 70 °C for 30 min while the color changed from dark purple to clear orange. Ketone **131** (34 mg, 0.22 mmol, 1.0 equiv) was added into the reaction mixture and heating was continued at 70 °C. Aliquots were taken during the course of the reaction, hydrolyzed, and analyzed by GC-MS.

Table 3.3: Kinetic experiment with iron(0) and iron(II) complexes.



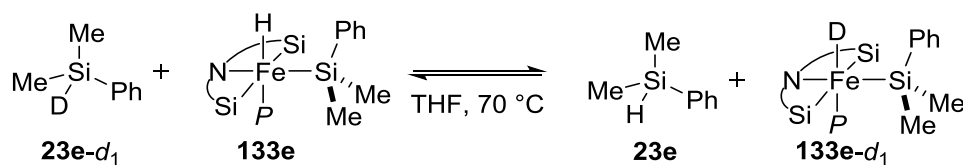
time (h)	conversion (%)	
	iron(0)	iron(II)
	complex 124	complex 133f
0.08		32
0.25		50
0.5		62
1	15	74
2	35	
4	53	86
6	72	
8	80	94
22	96	99

3.1.2.2.3 Scrambling at the Si–H Bond

3.1.2.2.3.1 Hydrosilane Si–D/Fe–H Scrambling Using Me₂PhSi–D (23e-d₁)

Complex **133e** (54 mg, 0.057 mmol, 1.0 equiv) was mixed in a SCHLENK flask with deuterium-labeled dimethylphenylsilane (**23e-d₁**, 9.5 mg, 0.069 mmol, 1.2 equiv) in 2.0 mL of THF. The reaction mixture was heated at 70 °C in an oil bath. The course of the reaction was followed by analysis of an aliquot (0.1 mL) by GC-MS. The deuterated dimethylphenylsilane/dimethylphenylsilane ratio (Si–D/Si–H) was calculated according to the intensity of molecular ion peaks at 122/121 [M–CH₃]⁺ in the mass spectrum for the GC peak corresponding to dimethylphenylsilane **23e**.

Table 3.4: Hydrosilane Si–D/Fe–H scrambling experiment.

	
time (h)	23e D/H (%)
0	>95
15	89
45	85
75	83
120	78
240	73
480	66
1440	52

3.1.2.2.3.2 Deuteration Studies with Me₂PhSi–D (23e-d₁)

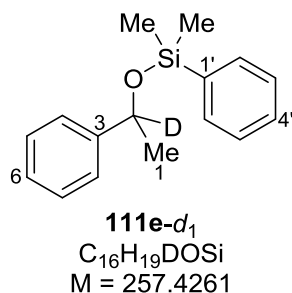
Complex **133e** (49 mg, 0.051 mmol, 0.88 equiv) was mixed in a SCHLENK flask with acetophenone (**109**, 9.2 mg, 0.077 mmol, 1.3 equiv) and deuterium-labeled dimethylphenylsilane (**23e-d₁**, 8.0 mg, 0.058 mmol, 1.0 equiv) in 2.0 mL of THF. The reaction mixture was heated at 70 °C in an oil bath. The course of the reaction was followed by analysis of aliquots (0.1 mL) by GC-MS. The D/H ratio on the product was calculated according to the intensity of molecular ion peaks at 242/241 [M–CH₃]⁺ in the mass spectrum for the GC peak corresponding to the silyl ether product **111e**.

Table 3.5: Hydrosilylation of acetophenone **109** with deuterium-labeled hydrosilane **23e-d₁**.

109	23e-d₁	133e		
<hr/>				
time	23e-d₁ >95% D		23e-d₁ ca. 50% D	
(min)	conversion	111e D/H (%)	conversion	111e D/H (%)
15	2	48		
20			19	90
30				78
45		39		
60			31	80
75		40		
120	10	38		78
240				77
360	25	36		
480				77
600	23	38		
1440			63	78
1560	74	42		
2880	80	45		
4380	85	48		
6960	>99	50		

3.1.2.2.4 Scrambling at the C–H Bond

3.1.2.2.4.1 Scrambling Experiment with Deuterated Silyl Ether (**8eb-d₁**)

3.1.2.2.4.1.1 Dimethyl(phenyl)(1-phenylethoxy-1-*d*)silane **111e-d₁**

According to a literature procedure,^[197] a 2-mL vial was charged with acetophenone (**109**, 100 mg, 0.84 mmol, 1.0 equiv), deuterium-labeled dimethylphenylsilane (**23e-d₁**, 120 mg, 0.87 mmol, 1.0 equiv), and B(C₆F₅)₃ (**108**, 2 mg, 3 μmol, 0.5 mol %) in toluene (0.5 mL). The reaction mixture was stirred at room temperature for 2 h and then subjected directly to flash column chromatography on silica gel using cyclohexane:ethyl acetate (97:3) as eluent, yielding the silyl ether **111e-d₁** (180 mg, 0.71 mmol, 84%, >95% D) as a colorless oil.

R_f = 0.5 (cyclohexane:ethyl acetate = 97:3).

¹H NMR (500 MHz, CDCl₃): δ = 0.24 (s, 3H, Si-C^AH₃), 0.29 (s, 3H, Si-C^BH₃), 1.37 (s, 3H, H-1), 7.18–7.20 (m, 1H, H-Ar), 7.25 (m, 2H, H-Ar), 7.31–7.34 (m, 3H, H-Ar), 7.50–7.52 (m, 2H, H-Ar), 7.55–7.57 (m, 2H, H-Ar) ppm.

¹³C{¹H} NMR (126 MHz, CDCl₃): δ = 0.0 (Si-C^AH₃), 0.5 (Si-C^BH₃), 28.1 (C-1), 72.1 (t, ¹J_{C,D} = 21.7 Hz, C-2), 126.8 (C-4), 128.3 (C-6), 129.1 (C-3'), 129.5 (C-5), 130.9 (C-4'), 134.9 (C-2'), 139.5 (C-1'), 147.6 (C-3) ppm.

²⁹Si DEPT NMR (99 MHz, CDCl₃): δ = 6.6 ppm.

IR (ATR): $\tilde{\nu}$ /cm⁻¹ = 3066 (w), 3023 (w), 2970 (m), 2924 (w), 2130 (w), 1427 (m), 1368 (m), 1251 (s), 1137 (s), 1115 (s), 1095 (m), 1010 (s), 861 (m), 820 (s), 783 (s), 695 (s).

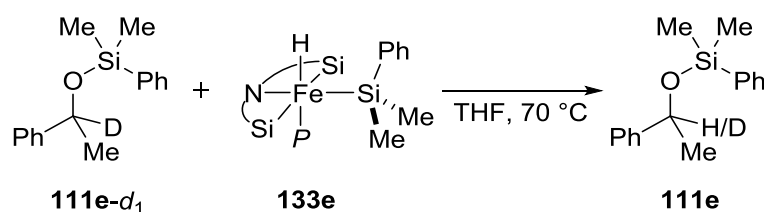
HRMS (APCI) for C₁₆H₂₀DOSi [(M+H)⁺]: calculated 258.1419, found 258.1462.

^[197] J. Mohr, M. Durmaz, E. Irran, M. Oestreich, *Organometallics* **2014**, 33, 1108–1111.

3.1.2.2.4.1.2 Scrambling Experiment

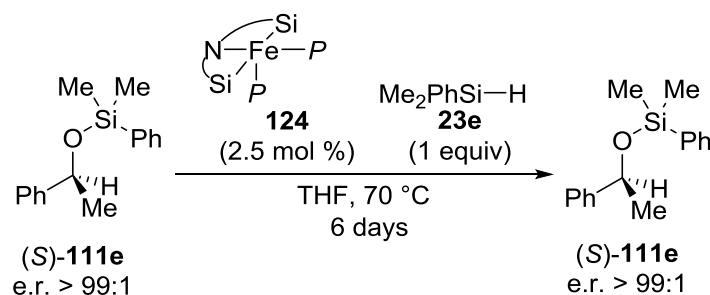
Deuterium-labeled silyl ether **111e-d₁** (13 mg, 0.049 mmol, 1.1 equiv) and iron hydride complex **133e** (43 mg, 0.045 mmol, 1.0 equiv) were dissolved in THF (2.0 mL), stirred at 70 °C, and the reaction was followed by analysis of an aliquot (0.1 mL) by GC-MS. The H/D ratio of the product was calculated according to the intensity of peaks at 242/241 [M-CH₃]⁺ in the mass spectrum for the GC peak corresponding to the silyl ether product **111e**.

Table 3.6: Scrambling at the C-H Bond



time (h)	111e D/H (%)
0	99
5	98
10	99
20	99
32	99
60	98
120	99
240	98
480	98
1440	98
2880	92
4320	93

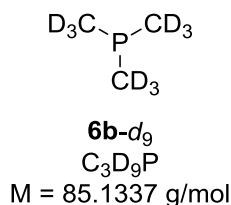
3.1.2.2.5 Racemization Experiment with Enantiopure Silyl Ether (S)-111e



The enantiomerically enriched silyl ether (S)-111e (49 mg, 0.19 mmol, 1.0 equiv, e.r. > 99:1) was subjected to the catalytic conditions in the presence of dimethylphenylsilane (**23e**, 13 mg, 90 μ mol, 0.47 equiv) and the iron complex **124** (4.8 mg, 5.0 μ mol, 2.5 mol %). The reaction mixture was maintained at 70 °C for 6 days, and aliquots passed through a short plug of silica gel and analyzed by chiral HPLC analysis showed no racemization during the course of the reaction.

3.1.2.2.6 Phosphine Scrambling

3.1.2.2.6.1 Trimethylphosphine- d_9 (6b- d_9)



In a 100-mL SCHLENK flask magnesium turnings (2.3 g, 90 mmol, 3.8 equiv) were thermally and mechanically activated *in vacuo*. Freshly degassed di-*n*-butyl ether (15 mL) was added followed by rapid addition of methyl iodide- d_3 (0.36 mL, 5.6 mmol, 0.30 equiv) under nitrogen atmosphere at room temperature. After the initiation of the reaction (color change to dark brown and heat formation), the solution was cooled to 0 °C, and the rest of methyl iodide- d_3 (3.3 mL, 50 mmol, 3.0 equiv) was added dropwise. The solution was allowed to warm to room temperature and stirred for additional 3 h. The solution was cooled to 0 °C, and a solution of triphenylphosphite (5.0 g, 15 mmol, 1.0 equiv) in di-*n*-butyl ether (40 mL) was added slowly over 2 h. The solution was warmed to room temperature and stirred for 30 min. The dropping funnel was replaced by a distillation apparatus equipped with a Vigreux

column (10 cm), and the desired deuterated phosphine **6b-d₉** (560 mg, 6.6 mmol, 44%) was distilled at 160 °C (oil bath).

b.p.: 38 °C.

²H NMR (77 MHz, C₆D₆/C₆H₆): δ = 0.72 ppm.

¹³C{¹H} NMR (176 MHz, C₆D₆/C₆H₆): δ = 15.4 (dsept, *J*_{C-P} = 6.7, *J*_{C,D} = 16.4 Hz) ppm.

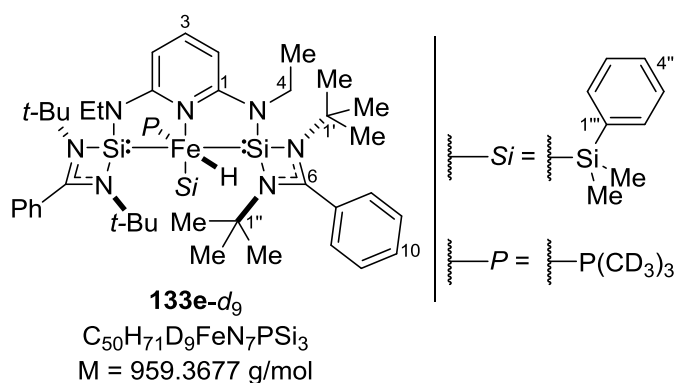
³¹P NMR (202 MHz, C₆D₆/C₆H₆): δ = −65.5 ppm.

The spectroscopic data for **6b-d₉** are in accordance with those reported.^[198]

3.1.2.2.6.2 Scrambling between Complex **133e** and Trimethylphosphine-d₉ (**6b-d₉**)

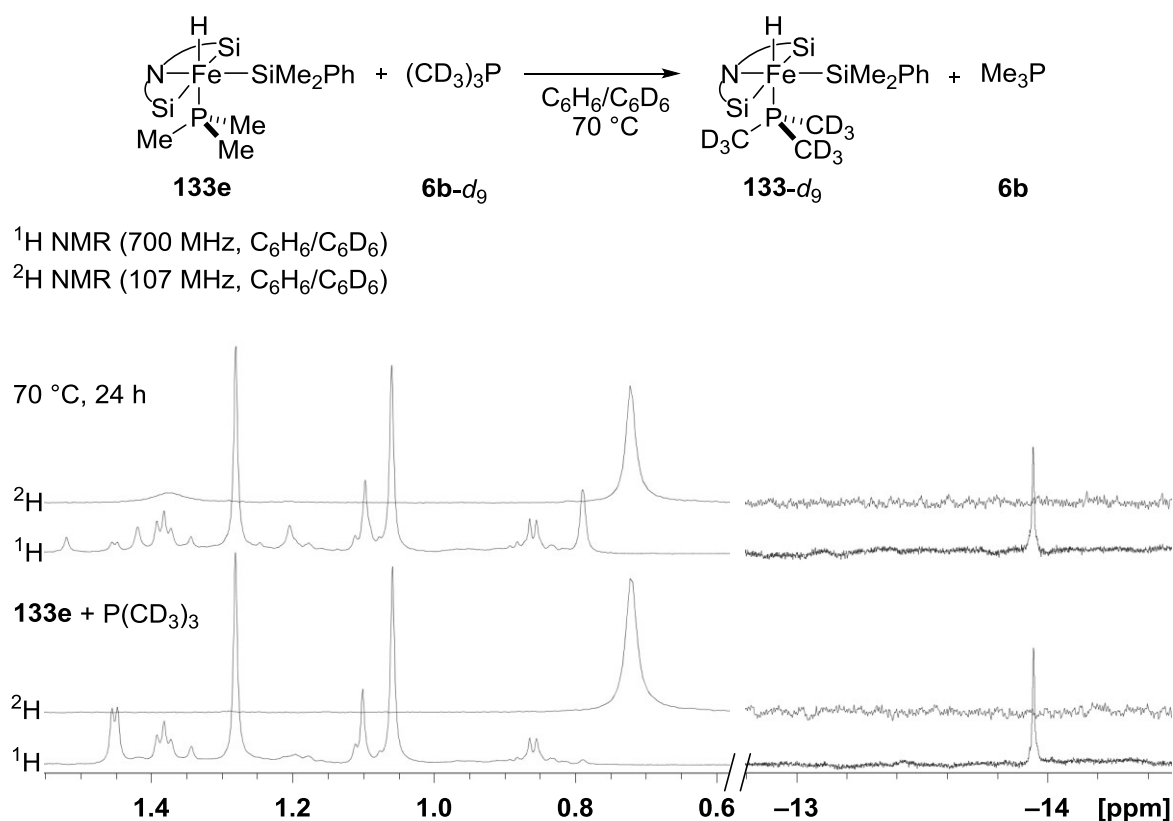
Complex **133e** (10 mg, 0.011 mmol 1.0 equiv) was mixed with trimethylphosphine-d₉ (**6b-d₉**, 2.5 mg, 0.029 mmol, 2.7 equiv), dissolved in C₆D₆ (0.5 mL) in a J. YOUNG NMR tube, heated to 70 °C, and monitored by ¹H and ²H NMR spectroscopy. Slow formation of **133e-d₉** was observed.

Selected NMR data for **133e-d₉**



¹H, ³¹P HMQC NMR (500 MHz / 203 MHz, C₆H₆/C₆D₆, 298 K): δ(¹H) = −13.9 / δ(³¹P) = 12.4 ppm.

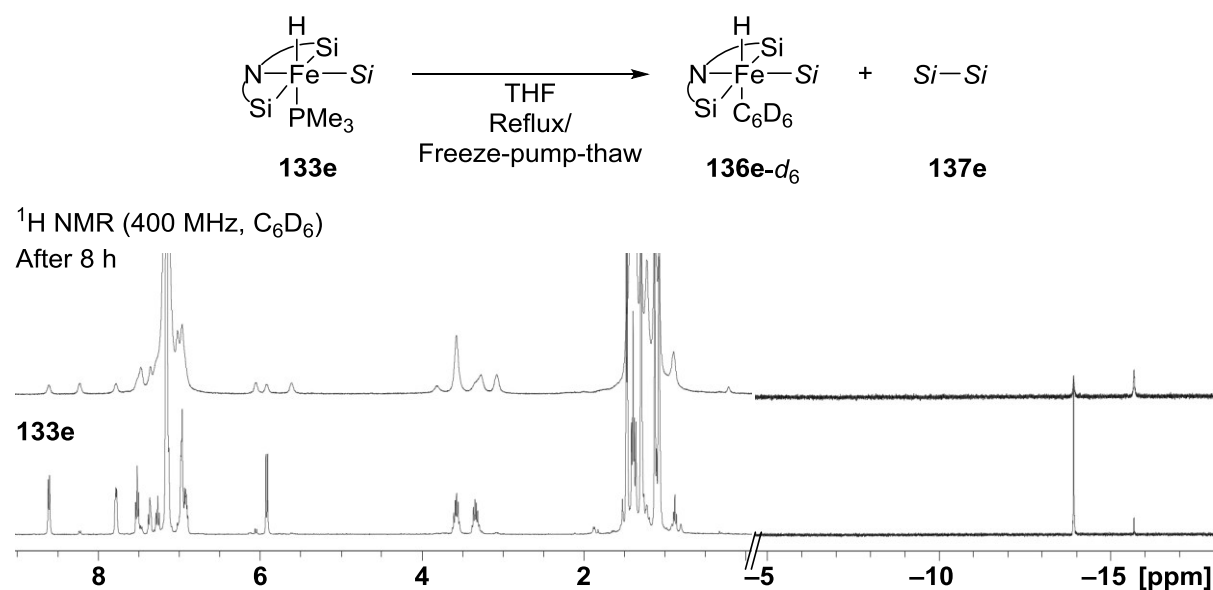
^[198] a) T. T. Wenzel, R. G. Bergman, *J. Am. Chem. Soc.* **1986**, *108*, 4856–4867; b) A. Kornath, F. Neumann, H. Oberhammer, *Inorg. Chem.* **2003**, *42*, 2894–2901.



Scheme 3.1: Phosphine-scrambling experiment.

3.1.2.2.7 Phosphine Dissociation

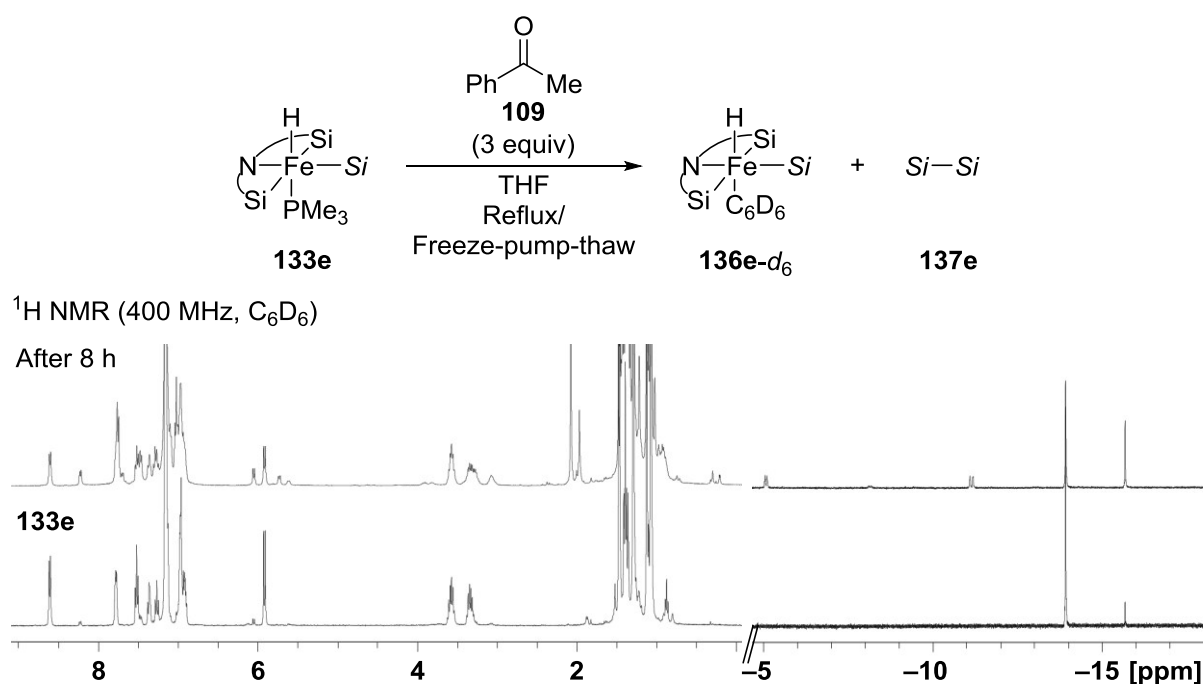
Complex **133e** (5 mg, 5 μmol) was dissolved in THF (2.0 mL). The closed system was maintained at 70 $^\circ\text{C}$ for 2 h. The sample was frozen, and the gas phase was purged with N_2 while thawing the sample. This procedure was repeated three times with the same period of time between each other. After 8 h, all volatiles were removed *in vacuo* and the sample was dissolved in 0.5 mL of C_6D_6 for ^1H and $^{31}\text{P}\{^1\text{H}\}$ NMR analyses.



Scheme 3.2: Phosphine-dissociation experiment.

3.1.2.2.7.1 Phosphine Dissociation in the Presence of Acetophenone (109)

Complex **133e** (5 mg, 5 μ mol, 1 equiv) was dissolved in THF (2.0 mL). Acetophenone (**109**, 2 mg, 0.02 mmol, 4 equiv) was added and the closed system was heated up to 70 $^{\circ}$ C for a period of 2 h. The sample was frozen, and the gas phase was changed by three purge-cycles with N₂ while thawing the sample. This procedure was repeated three times with the same period of time between each other. After 8 h, all volatiles were removed *in vacuo* and the sample was dissolved in C₆D₆ (0.5 mL) for ¹H and ³¹P{¹H} NMR analyses.

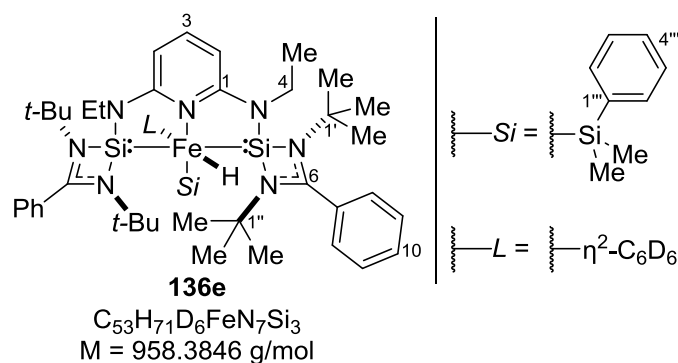


Scheme 3.3: Phosphine-dissociation experiment in the presence of acetophenone **109**.

3.1.2.2.8 Silyl Scrambling

Complex **133e** (10 mg, 0.011 mmol 1.0 equiv) was mixed with methyldiphenylsilane **23g** (4.0 mg, 0.020 mmol, 1.8 equiv) in C₆D₆. The sample was closed under nitrogen in a J. YOUNG NMR tube, heated to 70 °C, and monitored by ¹H NMR spectroscopy.

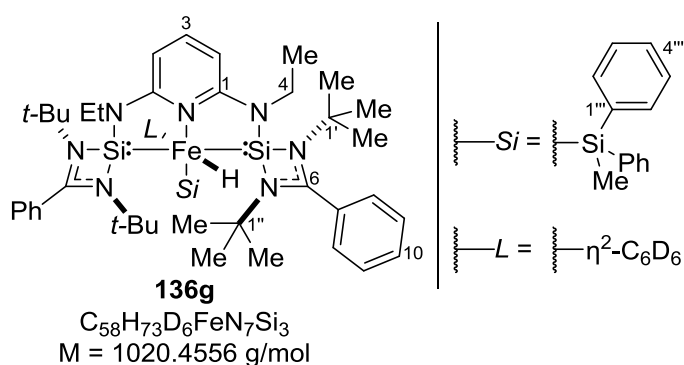
Selected NMR data for **136e-d₆**:



^1H NMR (500 MHz, C_6D_6): $\delta = -15.69$ (s, $^2J_{\text{H-Si}} = 23.8 \text{ Hz}$, 1H, Fe–H) ppm.

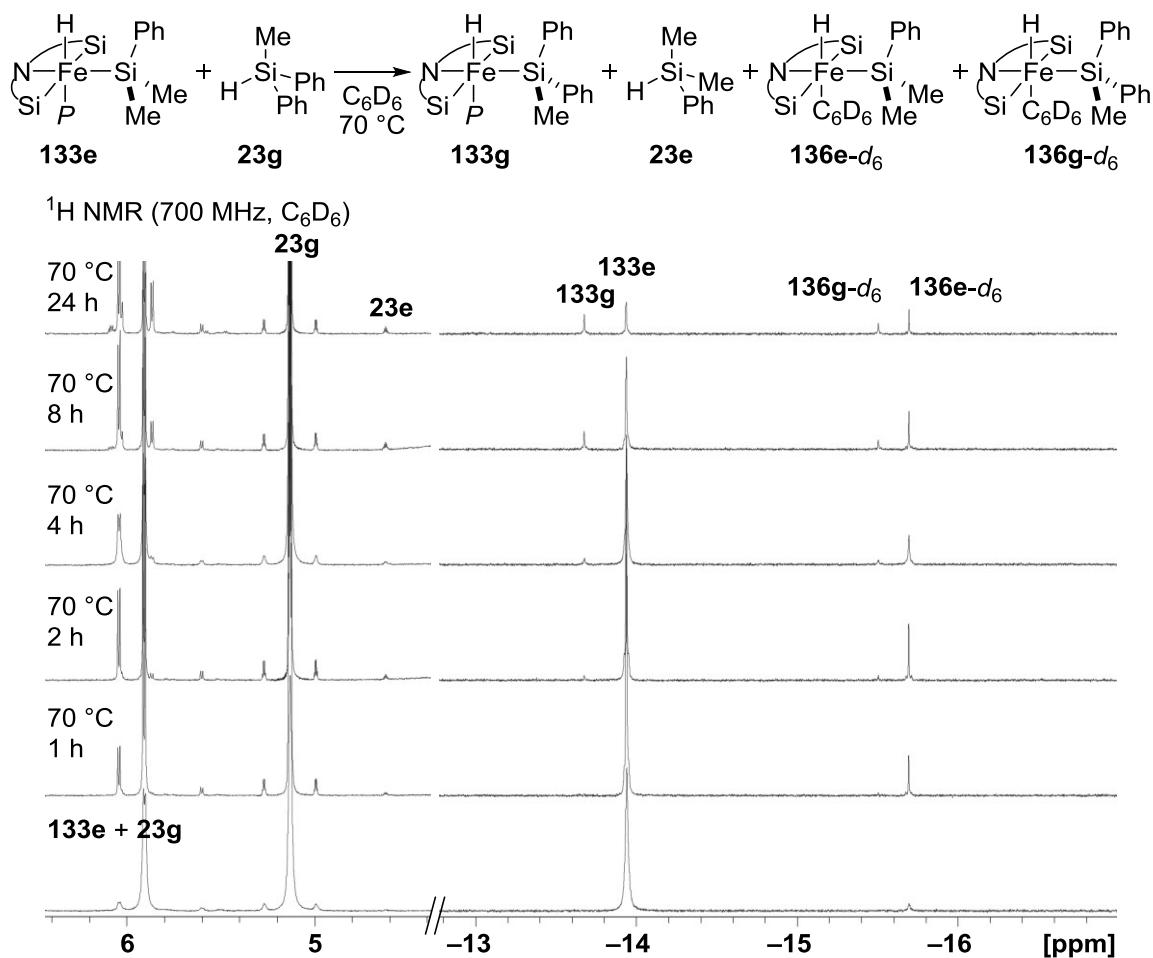
^1H , ^{29}Si HMQC NMR (500 MHz / 99 MHz, C_6D_6): $\delta(^1\text{H}) = -15.7$ / $\delta(^{29}\text{Si}) = 22.2$ (SiMe_2Ph),
 $\delta(^1\text{H}) = -15.7$ / $\delta(^{29}\text{Si}) = 84.5$ [Si(II)] ppm.

Selected NMR data for **136g-d₆**:



^1H NMR (500 MHz, C_6D_6): $\delta = -15.50$ (s, $^2J_{\text{H-Si}} = 23.7 \text{ Hz}$, 1H, Fe–H) ppm.

^1H , ^{29}Si HMQC NMR (500 MHz / 99 MHz, C_6D_6): $\delta(^1\text{H}) = -15.5$ / $\delta(^{29}\text{Si}) = 27.7$ (SiMe_2Ph),
 $\delta(^1\text{H}) = -15.5$ / $\delta(^{29}\text{Si}) = 83.0$ [Si(II)] ppm.



Scheme 3.4: Silyl-scrambling experiment.

Table 3.7: Silyl-scrambling experiment.

time (h)	iron hydride product distribution			
	133e	133g	136g-d ₆	136e-d ₆
0	96	-	-	4
1	91	-	-	9
2	85	1	<1	13
4	79	3	2	16
8	68	10	5	17
24	44	25	12	19

3.1.2.2.9 Hydrosilane-Crossover Experiment

Complex **133e** (48 mg, 0.050 mmol, 1.00 equiv) was mixed in a SCHLENK flask with acetophenone (**109**, 8.8 mg, 0.073 mmol, 1.5 equiv), and methyldiphenylsilane (**23g**, 11 mg,

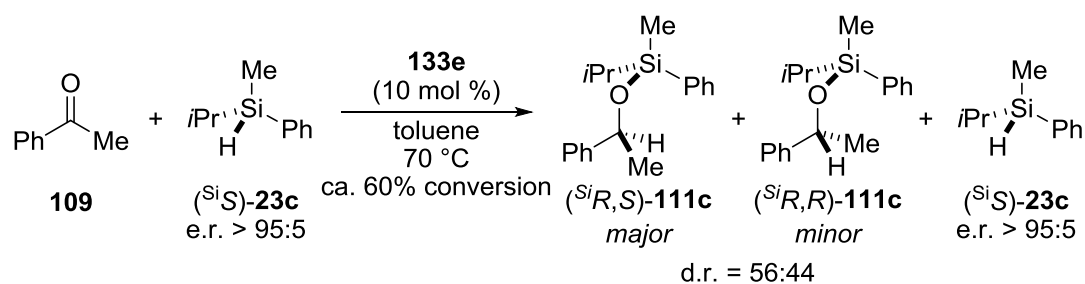
0.053 mmol, 1.1 equiv) in 2.0 mL of THF. The reaction mixture was heated at 70 °C with an oil bath. The course of the reaction was followed by analysis of aliquots (0.1 mL) by GC-MS.

Table 3.8: Hydrosilane-crossover experiment.

109	23g	133e	111g	111e
	time (min)	conversion (%)	ratio 111g/111e (%)	
	15	23	100	
	45	27	100	
	75	42	97	
	120	51	96	
	240	59	95	
	480	71	95	
	720	69	94	
	960	76	94	

3.1.2.2.10 Hydrosilylation with Silicon-Stereogenic Hydrosilane

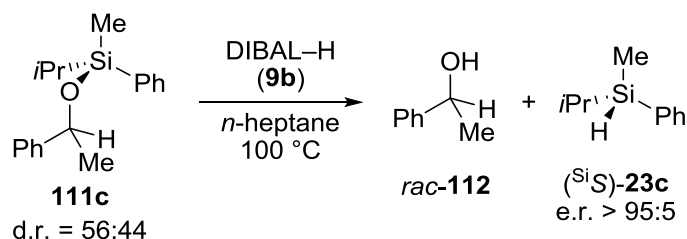
3.1.2.2.10.1 Catalytic Reaction between Acetophenone (**109**) with Enantioenriched Acyclic Hydrosilane (^{Si}S)-**23c**



Acetophenone (**109**, 60 mg, 0.50 mmol, 1.0 equiv), (^{Si}S)-isopropylmethylphenylsilane [(^{Si}S)-**23c**, 82 mg, 0.50 mmol, 1.0 equiv, e.r. > 95:5], and the iron hydride complex **133e** (49 mg, 0.052 mmol, 10 mol %) were dissolved in toluene (3 mL). The reaction mixture was maintained at 70 °C in an oil bath for 6 days reaching ca. 60% conversion. Purification by flash column chromatography using *n*-pentane:diethyl ether (99:1) as eluting solvent mixture gave silyl

ether **111c** (44 mg, 0.15 mmol, 31% yield, d.r. = 56:44) and unreacted hydrosilane (^{Si}S)-**23c** (10 mg, 0.07 mmol, 15%, e.r. > 95:5).

3.1.2.2.10.2 Reductive Si–O Bond Cleavage of Silyl Ether **111c**



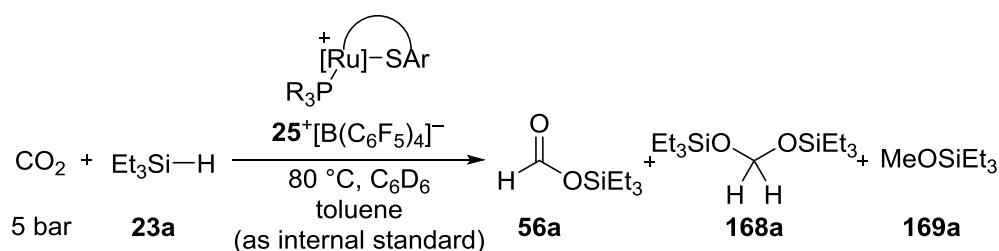
According to **GP2**, a SCHLENK tube equipped with a magnetic stir bar and a reflux condenser was charged with a solution of the silyl ether **111c** (25 mg, 0.089 mmol, 1.0 equiv) in *n*-heptane (1.0 mL). DIBAL-H (**9b**, 0.5 mL, 0.5 mmol, 6 equiv, 1.0M in *n*-hexane) was added in one portion at room temperature, and the resulting reaction mixture was heated to reflux and maintained at this temperature for 20 h. The reaction mixture was allowed to cool to room temperature and quenched by careful addition of aqueous HCl (1M, 5 mL). The organic layer was separated, and the aqueous phase was extracted with *tert*-butyl methyl ether (3 × 5 mL). The combined organic layers were washed with brine (5 mL), dried over Na₂SO₄, filtered, and the volatiles were evaporated under reduced pressure. The crude product was purified by flash column chromatography on silica gel using *n*-pentane/diethyl ether mixtures (100:0→90:10) as eluent, affording the analytically pure hydrosilane (^{Si}S)-**23c** (9.3 mg, 0.057 mmol, 64%, e.r. > 95:5) as a colorless oil.

3.2 Applications of Catalytically Generated Main-Group Electrophiles

3.2.1 Hydrosilylation of Carbon Dioxide Catalyzed by Ruthenium Thiolate Complex

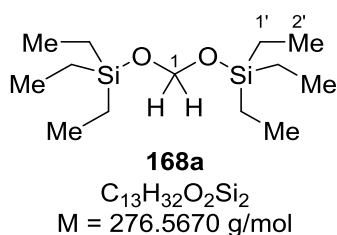
3.2.1.1 Optimization Studies

3.2.1.1.1 Catalyst Screening



In a glovebox, a medium-walled valved NMR tube was charged with triethylsilane (**23a**, 9.3 mg, 0.080 mmol, 1.0 equiv), the indicated Ru–S complex (**25**⁺[BAr^F₄][−], 3.2 μmol, 0.040 equiv), toluene (ca. 8 mg), and C₆D₆ (0.4 mL). The NMR tube was sealed, and a ¹H NMR spectrum was measured to obtain an accurate calibration of the internal standard. The tube was pressurized at room temperature with carbon dioxide (>99.95%, 5 bar, ca. 2 mmol, ca. 25 equiv) and heated to 80 °C. The reaction was monitored with ¹H NMR spectroscopy.

NMR spectroscopic data for bis(triethylsilyl)acetal (**168a**):



¹H NMR (500 MHz, C₆D₆): δ = 0.64 (q, ³J_{1',2'} = 8.3 Hz, 12H, H-1'), 1.02 (t, ³J_{2',1'} = 8.0 Hz, 18H, H-2'), 5.05 (s, 2H, H-1) ppm.

¹³C{¹H} NMR (126 MHz, C₆D₆): δ = 5.3 (C-1'), 7.0 (C-2'), 84.5 (C-1) ppm.

²⁹Si DEPT NMR (99 MHz, C₆D₆): δ = 18.32 ppm.

The spectroscopic data are in accordance with those reported.^[136,137]

3.2.1.1.1 Hydrosilylation of Carbon Dioxide Catalyzed by Ru–S Complex $25f^+[\text{BAr}^F_4]^-$

Table 3.9: Conversion and yields of **56a**, **168a**, and **169a** over time with 4 mol % of $25f^+[\text{BAr}^F_4]^-$

time (h)	conversion (%) ^[a]	yield (%)			combined yield (%)	TOF (h ⁻¹) ^[b]
		56a	168a	169a		
1	43	<1	45	<1	45	11
4	99	<1	99	1	>99	6.2

^[a] Based on hydrosilane consumption using toluene signals as internal standard. ^[b] (conversion/catalyst loading)/time.

3.2.1.1.2 Hydrosilylation of Carbon Dioxide Catalyzed by Ru–S Complex $25g^+[\text{BAr}^F_4]^-$

Table 3.10: Conversion and yields of **56a**, **168a**, and **169a** over time with 4 mol % of $25g^+[\text{BAr}^F_4]^-$

time (h)	conversion (%) ^[a]	yield (%)			combined yield (%)	TOF (h ⁻¹) ^[b]
		56a	168a	169a		
1	<1	<1	<1	<1	4	<0.01
4	2	<1	2	<1	13	0.12
20	55	3	41	4	45	0.69
48	98	4	89	5	93	0.51

^[a] Based on hydrosilane consumption using toluene signals as internal standard. ^[b] (conversion/catalyst loading)/time.

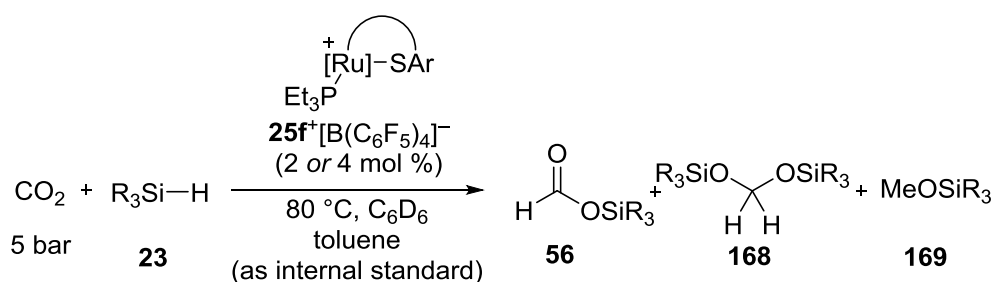
3.2.1.1.1.3 Hydrosilylation of Carbon Dioxide Catalyzed by Ru-S Complex $25\text{h}^+[\text{BAr}^{\text{F}}_4]^-$

Table 3.11: Conversion and yields of **56a**, **168a**, and **169a** over time with 4 mol % of $25\text{h}^+[\text{BAr}^{\text{F}}_4]^-$

time (h)	conversion (%) ^[a]	yield (%)			combined yield (%)	TOF (h ⁻¹) ^[b]
		56a	168a	169a		
1	<1	<1	2	<1	2	0.00
4	6	<1	2	1	3	0.39
20	41	<1	32	2	34	0.51
48	89	<1	92	1	93	0.47
72	99	1	>99	1	>99	0.34

^[a] Based on hydrosilane consumption using toluene signals as internal standard. ^[b] (conversion/catalyst loading)/time.

3.2.1.1.2 Hydrosilane Screening



In a glove box, a medium-walled valved NMR tube was charged with hydrosilane (0.080 mmol, 1.0 equiv), Ru-S complex $25\text{f}^+[\text{BAr}^{\text{F}}_4]^-$ (2.3 mg, 1.6 μmol , 0.020 equiv *or* 4.5 mg, 3.2 μmol , 0.040 equiv), toluene (ca. 8 mg), and C_6D_6 (0.4 mL). The NMR tube was sealed, and a ^1H NMR spectrum was measured to obtain an accurate calibration of the internal standard. The tube was pressurized at room temperature with carbon dioxide (>99.95%, 5 bar, ca. 2 mmol, ca. 25 equiv) and heated to 80 $^\circ\text{C}$. The reaction was monitored with ^1H NMR spectroscopy.

3.2.1.1.2.1 Hydrosilylation of Carbon Dioxide with Triethylsilane (23a)

Table 3.12: Conversion and yields of **56a**, **168a**, and **169a** over time with 2 mol % of $25f^+ [BAr^F_4]^-$

time (h)	conversion (%) ^[a]	yield (%)			combined yield (%)	TOF (h ⁻¹) ^[b]
		56a	168a	169a		
1	17	<1	15	<1	15	8.6
2	46	<1	44	1	44	11
9	73	9	67	1	76	4.0
24	89	15	73	1	89	1.9
32	95	18	80	1	98	1.5
47	97	18	79	1	97	1.0

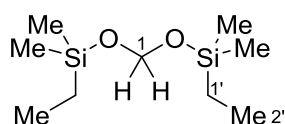
^[a] Based on hydrosilane consumption using toluene signals as internal standard. ^[b] (conversion/catalyst loading)/time.

Table 3.13: Conversion and yields of **56a**, **168a**, and **169a** over time with 4 mol % of $25f^+ [BAr^F_4]^-$

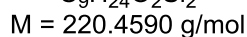
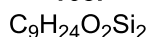
time (h)	conversion (%) ^[a]	yield (%)			combined yield (%)	TOF (h ⁻¹) ^[b]
		56a	168a	169a		
1	42	<1	42	<1	42	11
2	95	<1	97	<1	97	12
4	100	<1	>99	<1	>99	6.3

^[a] Based on hydrosilane consumption using toluene signals as internal standard. ^[b] (conversion/catalyst loading)/time.

3.2.1.1.2.2 Hydrosilylation of Carbon Dioxide with Ethyldimethylsilane (23i)



168i



NMR spectroscopic data for bis(ethyldimethylsilyl)acetal (**168i**):

^1H NMR (500 MHz, C_6D_6): δ = 0.13 [s, 12H, $\text{Si}-(\text{CH}_3)_2$], 0.59 (q, $^3J_{1',2'} = 7.9$ Hz, 4H, H-1'), 0.98 (t, $^3J_{2',1'} = 8.0$ Hz, 6H, H-2'), 5.02 (s, 2H, H-1) ppm.

$^{13}\text{C}\{^1\text{H}\}$ NMR (126 MHz, C_6D_6): δ = -2.5 [$\text{Si}-(\text{CH}_3)_2$], 6.5 (C-1'), 8.4 (C-2'), 84.0 (C-1) ppm.

^{29}Si DEPT NMR (99 MHz, C_6D_6): δ = 17.72 ppm.

Table 3.14: Conversion and yields of **56i**, **168i**, and **169i** over time with 2 mol % of **25f**⁺[BAr^F₄][−]

time (h)	conversion (%) ^[a]	yield			combined yield (%)	TOF (h ^{−1}) ^[b]
		56i	168i	169i		
1	16	<1	8	<1	8	7.8
2	20	1	13	1	14	5.1
9	31	3	25	1	28	1.7
24	45	4	41	1	45	0.93
32	50	4	46	1	51	0.78
47	58	4	58	1	62	0.62
55	62	5	64	1	69	0.57
73	70	4	64	1	69	0.48

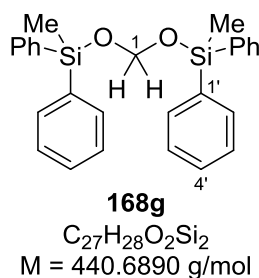
^[a] Based on hydrosilane consumption using toluene signals as internal standard. ^[b] (conversion/catalyst loading)/time.

Table 3.15: Conversion and yields of **56i**, **168i**, and **169i** over time with 4 mol % of **25f**⁺[BAr^F₄][−]

time (h)	conversion (%) ^[a]	yield (%)			combined yield (%)	TOF (h ^{−1}) ^[b]
		57i	168i	169i		
1	49	0	38	1	39	12
2	65	2	55	2	58	8.2
6	88	4	80	2	85	3.7
11	>99	6	90	3	97	2.3

^[a] Based on hydrosilane consumption using toluene signals as internal standard. ^[b] (conversion/catalyst loading)/time.

3.2.1.1.2.3 Hydrosilylation of Carbon Dioxide with Methyldiphenylsilane (23g)



NMR spectroscopic data for bis(methyldiphenylsilyl)acetal (**168g**):

1H NMR (500 MHz, C_6D_6): $\delta = 0.13$ (s, 6H, Si- CH_3), 5.21 (s, 2H, H-1), 7.16–7.18 (m, 12H, H-3', H-4'), 7.59–7.61 (m, 8H, H-2')

$^{13}C\{^1H\}$ NMR (126 MHz, C_6D_6): $\delta = -2.6$ (Si-(CH_3), 84.9 (C-1), 128.2 (C-3'), 129.7 (C-4'), 134.5 (C-2'), 135.9 (C-1')

^{29}Si DEPT NMR (99 MHz, C_6D_6): $\delta = -2.74$ ppm.

Table 3.16: Conversion and yields of **56g**, **168g**, and **169g** over time with 2 mol % of **25f**⁺[BAr^F₄][−]

time (h)	conversion (%) ^[a]	yield (%)			combined yield (%)	TOF (h ^{−1}) ^[b]
		56g	168g	169g		
1	8	<1	7	<1	7	3.9
2	18	<1	13	1	13	4.5
9	22	1	20	1	22	1.2
24	28	2	22	1	24	0.58
32	30	2	22	1	25	0.47
47	31	2	23	1	26	0.33
55	31	2	23	1	25	0.28
73	33	2	24	1	27	0.23

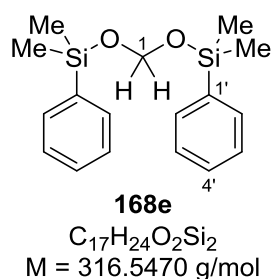
^[a] Based on hydrosilane consumption using toluene signals as internal standard. ^[b] (conversion/catalyst loading)/time.

Table 3.17: Conversion and yields of **56g**, **168g**, and **169g** over time with 4 mol % of **25f**⁺[BAr^F₄][−]

time (h)	conversion (%) ^[a]	yield (%)			combined yield (%)	TOF (h ^{−1}) ^[b]
		56g	168g	169g		
1	48	1	36	2	37	12
2	64	2	50	3	53	8.0
6	81	1	67	3	70	3.4
11	88	3	72	3	76	2.0
24	96	4	80	3	85	1.0
36	98	5	79	3	85	0.68

^[a] Based on hydrosilane consumption using toluene signals as internal standard. ^[b] (conversion/catalyst loading)/time.

3.2.1.1.2.4 Hydrosilylation of Carbon Dioxide with Dimethylphenylsilane (**23e**)



NMR spectroscopic data for bis(dimethylphenylsilyl)acetal (**168e**):

¹H NMR (500 MHz, C₆D₆): δ = 0.34 [s, 12H, Si-(CH₃)₂], 5.06 (s, 2H, C-1), 7.19–7.21 (m, 6H, H-3', H-4'), 7.55–7.57 (m, 4H, H-2') ppm.

¹³C{¹H} NMR (126 MHz, C₆D₆): δ = −1.5 [Si-(CH₃)₂], 84.5 (C-1), 128.2 (C-3'), 129.5 (C-4'), 133.5 (C-2'), 137.6 (C-1') ppm.

²⁹Si DEPT NMR (99 MHz, C₆D₆): δ = 6.99 ppm.

Table 3.18: Conversion and yields of **56e**, **168e**, and **169e** over time with 2 mol % of **25f**⁺[BAr^F₄][−]

time (h)	conversion (%) ^[a]	yield (%)			combined yield (%)	TOF (h ^{−1}) ^[b]
		56e	168e	169e		
1	12	<1	7	1	7	6.2
2	21	1	13	1	14	5.2
9	29	3	24	2	27	1.6
24	40	4	36	2	40	0.84
32	48	4	39	2	44	0.74
47	54	5	45	2	50	0.58
55	56	6	50	2	56	0.51
73	63	5	55	2	60	0.43

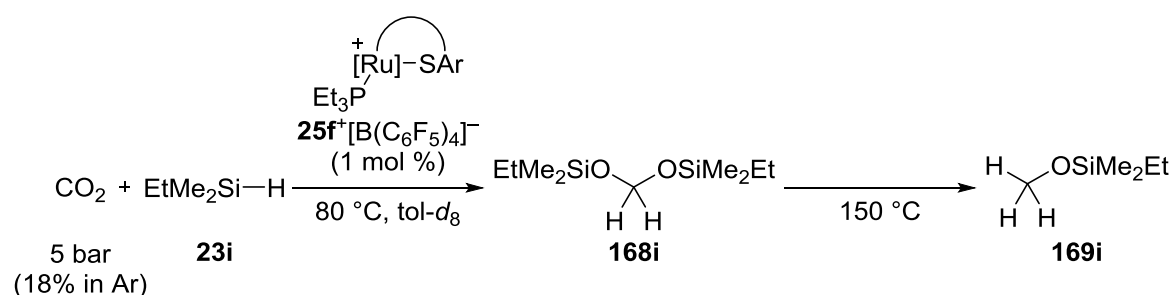
^[a] Based on hydrosilane consumption using toluene signals as internal standard. ^[b] (conversion/catalyst loading)/time.

Table 3.19: Conversion and Yields of **56e**, **168e**, and **169e** over Time with 4 mol % of **25f**⁺[BAr^F₄][−]

time (h)	conversion (%) ^[a]	yield (%)			combined yield (%)	TOF (h ^{−1}) ^[b]
		56e	168e	169e		
1	38	<1	26	3	27	9.5
2	47	<1	37	4	38	5.9
6	64	<1	48	4	49	2.7
11	71	1	56	4	59	1.6
24	81	2	68	5	72	0.85
36	85	3	72	5	77	0.59
75	96	5	79	5	86	0.32

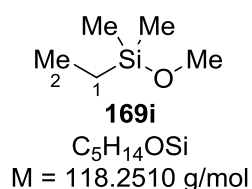
^[a] Based on hydrosilane consumption using toluene signals as internal standard. ^[b] (conversion/catalyst loading)/time.

3.2.1.2 Carbon dioxide Hydrosilylation to Silylated Methanol (169)



In a glovebox a medium walled valved NMR tube was charged with ethyldimethylsilane (**23i**, 32 mg, 0.32 mmol, 1.0 equiv), Ru-S complex (**25f**⁺[BAR^F₄][−], 4.6 mg, 3.2 μmol, 0.01 equiv) and toluene-*d*₈ (0.4 mL). The NMR tube was sealed, and an ¹H NMR spectrum was measured. The tube was pressurized with carbon dioxide in argon mixture (18 ± 1.8 % CO₂ in Ar, 5 bar, ca. 0.1 mmol, ca. 0.3 equiv) at room temperature and heated to 80 °C. The reaction was monitored with ¹H NMR spectroscopy. After no further hydrosilane consumption was observed (between 3 and 4 days), the reaction was heated to 150 °C and further monitored with ¹H NMR spectroscopy.

NMR spectroscopic data for ethyl(methoxy)dimethylsilane (**169i**):

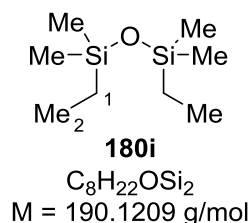


¹H NMR (500 MHz, toluene-*d*₈): δ = 0.12 [s, 6H, Si-(CH₃)₂], 0.52–0.58 (m, 2H, H-1), 0.97–1.03 (m, 3H, H-2), 3.31 (s, 3H, O-CH₃) ppm.

¹³C{¹H} NMR (126 MHz, toluene-*d*₈): δ = −2.7 [Si-(CH₃)₂], 4.6 (C-1), 8.2 (C-2), 49.9 (O-CH₃) ppm.

¹H, ²⁹Si HMBC NMR (500 / 99 MHz, toluene-*d*₈): δ(¹H) = −0.1, 0.6, 1.0, 3.3 ppm / δ(²⁹Si) = −18.5 ppm.

NMR spectroscopic data for 1,3-diethyltetramethyldisiloxane (**180i**)



¹H NMR (500 MHz, toluene-*d*₈): δ = 0.12 [s, 12H, Si-(CH₃)₂], 0.52–0.58 (m, 4H, H-1), 0.97–1.03 (m, 6H, H-2) ppm.

$^{13}\text{C}\{^1\text{H}\}$ NMR (126 MHz, toluene- d_8): $\delta = -0.1$ [Si-(CH₃)₂], 7.0 (C-1), 10.4 (C-2) ppm.

^{29}Si DEPT NMR (99 MHz, toluene- d_8): $\delta = 8.19$ ppm.

The spectroscopic data are in accordance with those reported.^[82]

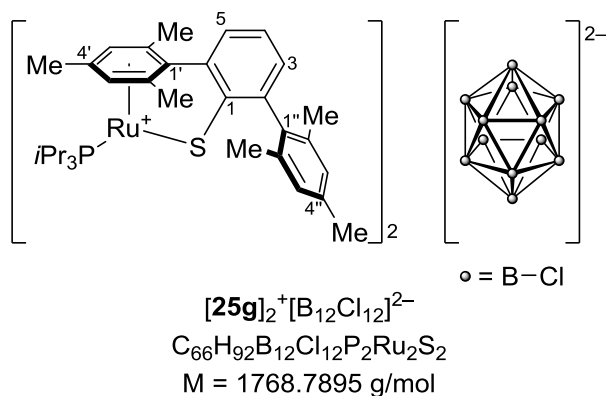
Table 3.20: Yield of **168i** and **169i** over time with 1 mol % of **25f**⁺[BAr^F₄][−]

time (d)	T (°C)	yield (%) ^[a]		ratio (168i : 169i)
		168i	169i	
0.17	80	17	<1	98:2
1		60	2	96:4
2		73	4	95:5
3		79	4	95:5
4		81	4	95:5
5	150	79	21	79:21
6		59	28	68:32
7		48	37	57:43
8		38	44	46:54
9		31	50	38:62
10		24	56	30:70
11		19	56	25:75
13		13	54	19:81
15		8	47	14:86
16		6	45	11:89
17		5	43	10:90
18		4	40	9:91
19		3	38	8:92
20		3	41	7:93
22		3	40	6:94
24		1	39	3:97

^[a] Residual signals for the hydrosilane used as internal standard. The maximum combined yield at 5 days was calibrated as 100% yield.

3.2.2 Catalytic Generation of Alumenium Ions by Cooperative Al–H Bond Activation in Defluorinative FRIEDEL–CRAFTS Alkylation

3.2.2.1 Synthesis of $[(i\text{Pr}_3\text{P})\text{Ru}(\text{SDmp})]^+{}_2[\text{B}_{12}\text{Cl}_{12}]^{2-} [\text{25g}]_2^+[\text{B}_{12}\text{Cl}_{12}]^{2-}$



In a glovebox a 10-mL SCHLENK tube was charged with $[(i\text{Pr}_3\text{P})\text{Ru}(\text{SDmp})\text{Cl}]$ (**228g**, 100 mg, 160 μmol , 2.0 equiv) and $[\text{Na}_2\text{B}_{12}\text{Cl}_{12} \cdot n\text{H}_2\text{O}]$ (50 mg, 83 μmol , 1.1 equiv). Chlorobenzene (4 mL) is added to afford a red solution. Ethyldimethylsilane (**23i**, 0.5 mL, excess) was added, and the solution was stirred over night at room temperature (*gas evolution*). The solution was removed from the glovebox, cooled to 0 °C, and concentrated *in vacuo*. The residue was dissolved in chlorobenzene (1 mL), filtered through a PTFE syringe filter, and benzene (3 mL) was added. The resulting solution was frozen and the solvent is sublimated *in vacuo*. The resulting green solid was further dried *in vacuo* using a turbomolecular pump (1×10^{-5} mbar, 40 °C, 6 h) affording the desired complex as a green air-sensitive solid (130 mg, 71 μmol , 92%).

^1H NMR (500 MHz, $o\text{-Cl}_2\text{C}_6\text{D}_4$): δ = 0.76 [dd, $^3J_{\text{CH}_3,\text{P}}$ = 14.6 Hz, $^3J_{\text{CH}_3,\text{CH}}$ = 7.2 Hz, 18H, $\text{PCH}(\text{CH}_3)_2$], 1.69 (s, 6H, 2'- CH_3), 1.89–1.95 [m, 3H, $\text{PCH}(\text{CH}_3)_2$], 1.95 (s, 6H, 2''- CH_3), 2.00 (s, 3H, 4''- CH_3), 2.09 (s, 3H, 4'- CH_3), 4.67 (s, 2H, H-3'), 6.75 (s, 2H, H-3''), 6.94 (m, 1H, H-3), 7.24–7.25 (m, 1H, H-5), 7.55–7.56 (m, 1H, H-4) ppm.

^{11}B NMR (161 MHz, $o\text{-Cl}_2\text{C}_6\text{D}_4$): δ = –11.7 ppm.

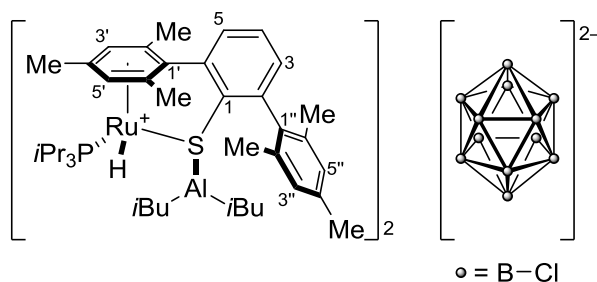
$^{13}\text{C}\{^1\text{H}\}$ NMR (126 MHz, $o\text{-Cl}_2\text{C}_6\text{D}_4$): δ = 18.3 (2'- CH_3), 19.6 [$\text{P}(\text{CH}(\text{CH}_3))_2$], 19.8 (4'- CH_3), 20.4 (2''- CH_3), 21.0 (4''- CH_3), 24.9 [d, $^1J_{\text{C},\text{P}}$ = 20.9 Hz, $\text{P}(\text{CH}(\text{CH}_3))_2$], 71.4 (C-3'), 102.6 (C-2'), 107.1 (C-4'), 109.2 (d, $J_{1',\text{P}}$ = 8.5 Hz, C-1'), 128.1 (C-5), 128.4 (C-4), 128.6 (C-3''), 132.1 (C-

6), 132.4 (C-3), 134.2 (C-1''), 135.3 (C-2''), 137.7 (C-4''), 142.2 (C-2), 162.6 (d, $J_{1,P} = 7.5$ Hz, C-1) ppm.

$^{31}\text{P}\{^1\text{H}\}$ NMR (202 MHz, $o\text{-Cl}_2\text{C}_6\text{D}_4$): $\delta = 53.9$ ppm.

HRMS (ESI) $\text{C}_{33}\text{H}_{46}\text{PRuS}$ [**25g** $^+$]: calculated 607.2096, found 607.2094.
 $\text{B}_{12}\text{Cl}_{12}$ [**M-2(25g)**] $^{2-}$: calculated 277.8687, found 277.8685.

3.2.2.1.1 $[(i\text{Pr}_3\text{P})\text{Ru}(\text{SDmp})\text{DIBAL-H}]_2\text{B}_{12}\text{Cl}_{12}$ [**224g**] $_2^+[\text{B}_{12}\text{Cl}_{12}]^{2-}$



[**224g**] $_2^+[\text{B}_{12}\text{Cl}_{12}]^{2-}$

$\text{C}_{82}\text{H}_{130}\text{Al}_2\text{B}_{12}\text{Cl}_{12}\text{P}_2\text{Ru}_2\text{S}_2$

$M = 2053.2326$ g/mol

In a glovebox $[(i\text{Pr}_3\text{P})\text{Ru}(\text{SDmp})]_2\text{B}_{12}\text{Cl}_{12}$ [**25g**] $_2^+[\text{B}_{12}\text{Cl}_{12}]^{2-}$, 10 mg, 5.7 μmol , 1.0 equiv) was dissolved in $o\text{-Cl}_2\text{C}_6\text{D}_4$ (0.4 mL). DIBAL-H (**9b**, 3.6 mg, 25 μmol , 4.4 equiv) was added, the mixture was transferred into a J. YOUNG NMR tube, and subjected to NMR analysis at room temperature.

^1H NMR (500 MHz, $o\text{-Cl}_2\text{C}_6\text{D}_4$): $\delta = -13.00$ (d, $^2J_{\text{H,P}} = 25.9$ Hz, 1H, RuH), 0.92–1.06 [m, $\text{PCH}(\text{CH}_3)_2$, $\text{PCH}(\text{CH}_3)_2$, 21H], 1.88 (s, 3H, 2'- CH_3), 1.92 (s, 3H, 6''- CH_3), 2.06 (s, 3H, 2''- CH_3), 2.10 (s, 3H, 4'- CH_3), 2.20 (d, $J_{\text{CH}_3,\text{P}} = 1.9$ Hz, 3H, 6'- CH_3), 2.23 (s, 3H, 4''- CH_3), 5.56 (s, 1H, H-3'), 5.68 (s, 1H, H-5'), 6.81 (m, 2H, H-3'', H-5''), 7.00–7.11 (m, 2H, H-3, H-5), 7.24–7.25 (m, 1H, H-4) ppm. Signals of the isobutyl groups could not be resolved from the excess DIBAL-H.

^{11}B NMR (161 MHz, $o\text{-Cl}_2\text{C}_6\text{D}_4$): $\delta = -11.8$ ppm.

$^{13}\text{C}\{^1\text{H}\}$ NMR (126 MHz, $o\text{-Cl}_2\text{C}_6\text{D}_4$): $\delta = 18.5$ (2'- CH_3), 19.6 [$\text{PCH}(\text{CH}_3)_2$], 20.3 (6'- CH_3), 20.8 (2''- CH_3), 21.08 (4'- CH_3), 21.10 (6''- CH_3), 21.5 (4''- CH_3), 29.0 [d, $^1J_{\text{C,P}} = 20.8$ Hz, $\text{PCH}(\text{CH}_3)_2$], 83.6 (C-5'), 99.0 (C-2'), 100.3 (C-3'), 101.8 (C-4'), 103.6 (d, $J_{\text{C,P}} = 7.7$ Hz, C-6'),

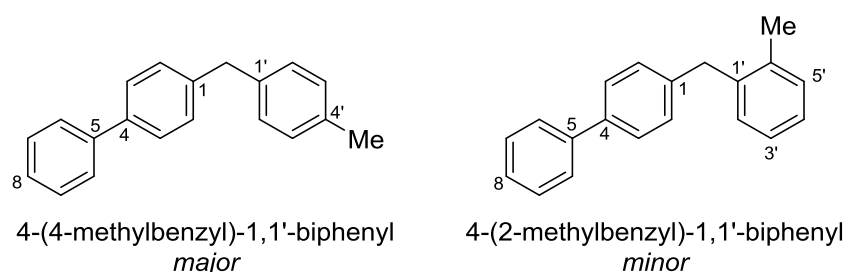
112.6 (d, $J_{1,P} = 4.4$ Hz, C-1'), 128.4 (C-5), 128.5 (C-4), 128.7 (C-3''), 129.7 (C-5''), 134.2 (C-3), 134.4 (C-1''), 135.2 (C-2''), 135.9 (C-6''), 137.2 (C-4''), 137.9 (C-6), 142.6 (d, $J_{1,P} = 3.0$ Hz, C-1), 145.7 (C-2) ppm.

^{27}Al NMR (130 HMz, $o\text{-Cl}_2\text{C}_6\text{D}_4$): $\delta = 77$ (br s) ppm. The signal overlaps with DIBAL-H.

$^{31}\text{P}\{^1\text{H}\}$ NMR (202 MHz, $o\text{-Cl}_2\text{C}_6\text{D}_4$): $\delta = 62.3$ ppm.

3.2.2.2 Defluorinative FRIEDEL–CRAFTS Alkylation

3.2.2.2.1 4-(4-Methylbenzyl)-1,1'-biphenyl (230)



230
 $\text{C}_{20}\text{H}_{18}$
 $M = 258.3640$ g/mol

In a 5-mL vial in a glovebox, 4-trifluoromethyl biphenyl (**229**, 8.9 mg, 40 μmol , 1.0 equiv), ruthenium thiolate complex $[\mathbf{25g}]_2^+[\text{B}_{12}\text{Cl}_{12}]^{2-}$ (1.7 mg, 1 μmol , 2.5 mol %), and toluene (18 mg, 200 μmol , 5.0 equiv) were dissolved in fluorobenzene (100 μL). The solution was mixed, and DIBAL-H (**9b**, 23 mg, 160 μmol , 4 equiv) was added. The solution was maintained at room temperature for 24 h. The reaction was removed from the glovebox, quenched by the addition of cyclohexane:EtOH (95:5, 2 mL), transferred to a 10-mL flask containing ca. 3 g silica gel, and concentrated *in vacuo*. The crude product was purified by flash chromatography using cyclohexane:toluene (95:5) as eluent, giving the desired product **230** as a 83:17 mixture of regioisomers (4.1 mg, 16 μmol , 40%).

m.p.: 77 °C (cyclohexane).

R_f : 0.25 (cyclohexane:toluene = 95:5).

GLC: $t_R = 23.8$ min (major), $t_R = 23.8$ min (minor).

HRMS (EI) $C_{20}H_{18}$ [**230**⁺]: calculated 258.14030, found 258.14016.

IR (ATR): $\tilde{\nu}/\text{cm}^{-1}$ = 3088 (w), 3026 (w), 1602 (w), 1514 (m), 1487 (s), 1372 (m), 1046 (m), 747 (s).

NMR spectroscopic data for *para*-**230** (*major* isomer):

^1H NMR (500 MHz, CDCl_3): δ = 2.32 (s, 3H, 4'- CH_3), 3.99 (s, 2H, 1- CH_2 -1'), 7.12 (s, 2H, H-3'), 7.16–7.19 (m, H-2'), 7.26 (d, $^3J_{2,3}$ = 7.8 Hz, 2H, H-2), 7.30–7.34 (m, 1H, H-8), 7.42 (t, $^3J_{7,8}$ = $^3J_{7,6}$ = 7.7 Hz, 2H, H-7), 7.51 (d, $^3J_{3,2}$ = 7.8 Hz, 2H, H-3), 7.56–7.58 (m, 2H, H-6) ppm.

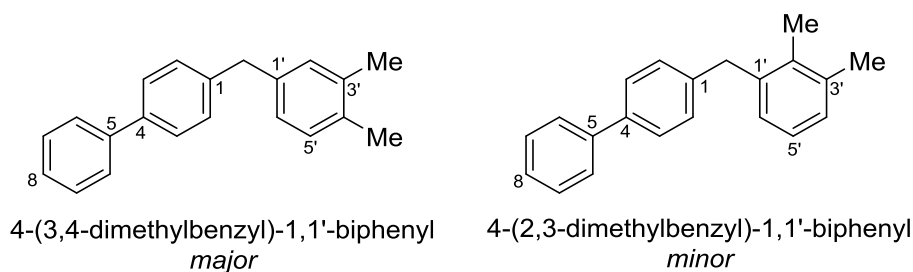
$^{13}\text{C}\{^1\text{H}\}$ NMR (126 MHz, CDCl_3): δ = 21.2 (4'- CH_3), 41.3 (1- CH_2 -1'), 127.2 (C-6), 127.27 (C-8), 127.34 (C-3), 128.4 (C-7), 129.0 (C-2'), 129.36 (C-3'), 129.40 (C-2), 135.8 (C-4') 138.1 (C-1'), 139.1 (C-4), 140.7 (C-1), 141.2 (C-5) ppm.

NMR spectroscopic data for *ortho*-**230** (*minor* isomer):

^1H NMR (500 MHz, CDCl_3): δ = 2.28 (s, 3H, 6'- CH_3), 4.03 (s, 2H, 1- CH_2 -1') ppm. The aromatic signals overlap with the major isomer.

$^{13}\text{C}\{^1\text{H}\}$ NMR (126 MHz, CDCl_3): δ = 27.1 (6'- CH_3), 53.8 (1- CH_2 -1') ppm. The aromatic signals overlap with the major isomer.

3.2.2.2.2 4-(3,4-Dimethylbenzyl)-1,1'-biphenyl (**232**)



232
 $C_{21}H_{20}$
M = 272.3910 g/mol

In a 5-mL vial in a glovebox 4-trifluoromethyl biphenyl (**229**, 8.9 mg, 40 μmol , 1.0 equiv), ruthenium thiolate complex $[\mathbf{25g}]_2^+[\text{B}_{12}\text{Cl}_{12}]^{2-}$ (1.7 mg, 1 μmol , 2.5 mol%), and *o*-xylene (21 mg, 200 μmol , 5.0 equiv) were dissolved in fluorobenzene (100 μL). The solution was mixed, and DIBAL-H (**9b**, 23 mg, 160 μmol , 4 equiv) was added. The solution was maintained at room temperature for 24 h. The reaction was removed from the glovebox, quenched by the addition of cyclohexane:EtOH (95:5, 2 mL), transferred to a 10-mL flask containing ca. 3 g silica gel, and concentrated *in vacuo*. The crude product was purified by flash chromatography using cyclohexane:toluene (95:5) as eluent, giving the desired product **232** as a 90:10 mixture of regioisomers (3.4 mg, 12 μmol , 31%).

m.p.: 75 °C (cyclohexane).

R_f : 0.24 (cyclohexane:toluene = 95:5).

GLC: t_R = 25.0 min (major), t_R = 25.1 min (minor).

HRMS (EI) $\text{C}_{21}\text{H}_{20}$ [**232** $^+$]: calculated 272.15595, found 272.15632.

IR (ATR): $\tilde{\nu}/\text{cm}^{-1}$ = 3024 (w), 2916 (w), 1600 (m), 1502 (m), 1485 (s), 1441 (m), 1019 (m), 741 (s).

NMR spectroscopic data for 1,3,4-**232** (*major* isomer):

^1H NMR (500 MHz, CDCl_3): δ = 2.24 (s, 3H, 4'- CH_3), 2.36 (s, 3H, 3'- CH_3), 3.96 (s, 2H, 1- CH_2 -1'), 6.97 (dd, $^3J_{6',5'} = 7.5$ Hz, $^4J_{6',2'} = 1.7$ Hz, 1H, H-6'), 7.01 (d, $^4J_{2',6'} = 1.3$ Hz, 1H, H-2'), 7.07 (d, $^3J_{5',6'} = 7.7$ Hz, 1H, H-5'), 7.25–7.28 (m, 2H, H-2), 7.32 (tt, d, $^3J_{8,7} = 7.3$ Hz, $^4J_{8,6} = 1.4$ Hz, 1H, H-8), 7.41–7.43 (m, 2H, H-7), 7.51 (d, $^3J_{3,4} = 8.3$ Hz, 2H, H-3), 7.56–7.58 (m, 2H, H-6) ppm.

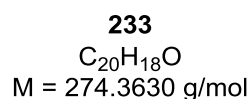
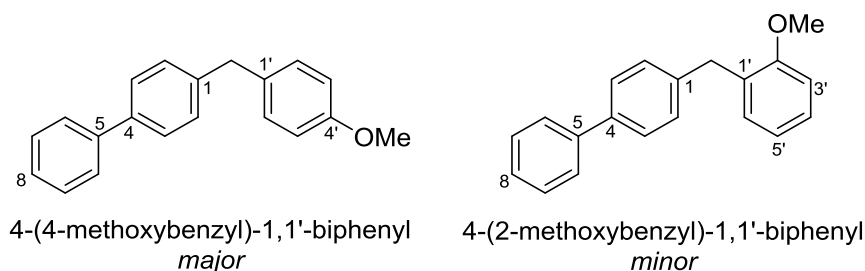
$^{13}\text{C}\{^1\text{H}\}$ NMR (126 MHz, CDCl_3): δ = 19.5 (4'- CH_3), 19.9 (3'- CH_3), 41.3 (1- CH_2 -1'), 126.5 (C-6'), 127.1 (C-8), 127.2 (C-6), 127.3 (C-3), 128.8 (C-7), 129.2 (C-5'), 129.4 (C-2), 130.4 (C-2'), 134.4 (C-3'), 136.8 (C-4'), 138.6 (C-1'), 139.1 (C-4), 140.8 (C-1), 141.2 (C-5) ppm.

NMR spectroscopic data for 1,2,3-**232** (*minor* isomer):

^1H NMR (500 MHz, CDCl_3): δ = 2.18 (s, 3H, Ar- CH_3), 2.36 (s, 3H, Ar- CH_3), 4.06 (s, 2H, 1- CH_2 -1') ppm. The aromatic signals overlap with the major isomer.

$^{13}\text{C}\{^1\text{H}\}$ NMR (126 MHz, CDCl_3): δ = 21.6 (2'/3'- CH_3), 39.8 (1- CH_2 -1') ppm. The aromatic signals overlap with the major isomer.

3.2.2.2.3 4-(4-Methoxybenzyl)-1,1'-biphenyl (233)



In a 5-mL vial in a glovebox 4-trifluoromethyl biphenyl (**229**, 8.9 mg, 40 μmol , 1.0 equiv), ruthenium thiolate complex $[\mathbf{25g}]_2^+[\text{B}_{12}\text{Cl}_{12}]^{2-}$ (1.7 mg, 1 μmol , 2.5 mol%), and anisole (22 mg, 200 μmol , 5.0 equiv) were dissolved in fluorobenzene (100 μL). The solution was mixed and DIBAL-H (**9b**, 23 mg, 160 μmol , 4 equiv) was added. The solution was maintained at room temperature for 24 h. The reaction was removed from the glovebox, quenched by the addition of cyclohexane/EtOH (95:5, 2 mL), transferred to a 10-mL flask containing ca. 3 g silica gel, and concentrated *in vacuo*. The crude product was purified by flash chromatography using cyclohexane:toluene (95:5) as eluent, giving the desired product **233** as a 85:15 mixture of regioisomers (5.7 mg, 21 μmol , 52%).

m.p.: 83 $^\circ\text{C}$ (cyclohexane).

R_f : 0.15 (cyclohexane:toluene = 95:5).

GLC: t_R = 25.7 min (major), t_R = 24.7 min (minor).

HRMS (EI) $\text{C}_{20}\text{H}_{18}\text{O}$ [**233** $^+$]: calculated 274.13522, found 274.13476.

IR (ATR): $\tilde{\nu}/\text{cm}^{-1}$ = 2360 (m), 2339 (m), 1509 (s), 1488 (m), 1246 (s), 1035 (m), 802 (m).

NMR spectroscopic data for *para*-**233** (*major* isomer):

^1H NMR (500 MHz, CDCl_3): δ = 3.79 (s, 3H, O- CH_3), 3.97 (s, 2H, 1- CH_2 -1'), 6.85 (d, $^3J_{3',2'} = 8.8$ Hz, 2H, H-3'), 7.15 (d, $^3J_{2',3'} = 8.8$ Hz, 2H, H-2'), 7.25 (d, $^3J_{2,3} = 8.4$ Hz, 2H, H-2), 7.30–7.34 (m, 1H, H-8), 7.40–7.43 (m, 1H, H-7), 7.50–7.52 (m, 2H, H-3), 7.56–7.58 (m, 2H, H-6) ppm.

$^{13}\text{C}\{^1\text{H}\}$ NMR (126 MHz, CDCl_3): δ = 40.8 (1- CH_2 -1'), 55.4 (O- CH_3), 114.1 (C-3'), 127.17 (C-6), 127.20 (C-8), 127.3 (C-3), 128.9 (C-7), 129.3 (C-2'), 133.2 (C-2), 139.0 (C-1'), 140.7 (C-1), 141.2 (C-5), 146.6 (C-4), 158.1 (C-4') ppm.

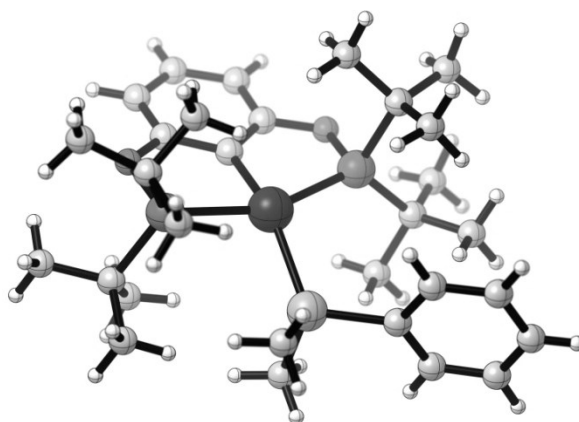
NMR spectroscopic data for *ortho*-**233** (*minor* isomer):

^1H NMR (500 MHz, CDCl_3): δ = 3.84 (s, 3H, O- CH_3), 4.01 (s, 2H, 1- CH_2 -1') ppm. The aromatic signals overlap with the major isomer.

APPENDIX

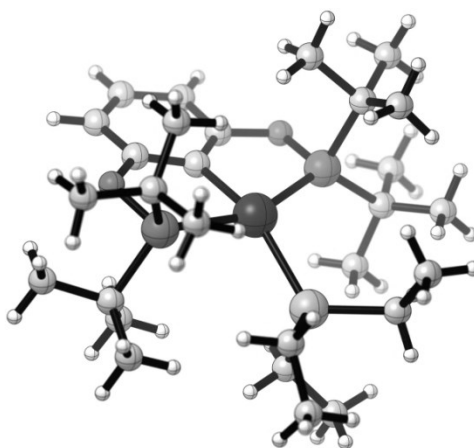
A1 X-RAY CRYSTAL STRUCTURE DATA

A1.1 Molecular Structure of 107e



Cambridge Structural Database	CCDC-1000410
Empirical formula	$\text{C}_{30}\text{H}_{51}\text{IrO}_2\text{P}_2\text{Si}$
M (g/mol)	725.94
Space group	P-1
Crystal system	Triclinic
a [Å]	8.2456(6)
b [Å]	10.6240(7)
c [Å]	19.2156(10)
α [°]	82.080(5)
β [°]	86.182(5)
γ [°]	79.073(6)
V [Å ³]	1635.61(18)
Z	2
ρ_{calcd} [mg m ⁻³]	1.474
Wavelength [Å]	1.54184
μ [mm ⁻¹]	9.350
crystal size [mm ³]	0.10 × 0.11 × 0.18
reflections collected	10662
independent reflections	5885 [$R_{\text{int}} = 0.0488$]
refined parameters	372
R	0.0469
wR	0.1177
GOF	1.054
max., min. peaks [eÅ ⁻³]	2.519 and -2.867

A1.2 Molecular Structure of 107a



Cambridge Structural Database	CCDC-1000409
Empirical formula	C ₂₈ H ₅₅ IrO ₂ P ₂ Si
M (g/mol)	705.95
Space group	P-1
Crystal system	Triclinic
<i>a</i> [Å]	8.2047(4)
<i>b</i> [Å]	11.0592(5)
<i>c</i> [Å]	18.8425(9)
α [°]	88.450(4)
β [°]	78.995(4)
γ [°]	68.363(4)
<i>V</i> [Å ³]	1558.27(13)
<i>Z</i>	2
ρ_{calcd} [mg m ⁻³]	1.505
Wavelength [Å]	1.54184
μ [mm ⁻¹]	9.792
crystal size [mm ³]	0.05 × 0.12 × 0.16
reflections collected	9605
independent reflections	5602 [<i>R</i> _{int} = 0.0958]
refined parameters	389
<i>R</i>	0.0838
<i>wR</i>	0.2148
GOF	1.193
max., min. peaks [eÅ ⁻³]	5.737 and -6.326

A2 ABBREVIATIONS

$[\alpha]$	specific rotation
δ	chemical shift
λ	wavelength
$\tilde{\nu}$	wavenumber
σ -CAM	σ -complex-assisted metathesis
Å	Ångström
Ac	acetyl
APCI	atmospheric pressure chemical ionization
Ar	aryl
ATR	attenuated total reflection
BAr^F₄	tetrakis[3,5-bis(trifluoromethyl)phenyl]borate
b.p.	boiling point
br	broad
<i>n</i> Bu	<i>n</i> -butyl
<i>i</i> Bu	<i>iso</i> -butyl
<i>t</i> Bu	<i>tert</i> -butyl
°C	degree Celsius
<i>c</i>	concentration
calc.	calculated
cat.	catalytic
cat	catechol
cm	centimeter
COD	1,5-cyclooctadiene
COE	cyclooctene
COSY	correlation spectroscopy
Cy	cyclohexyl
d	doublet
DEPT	distortionless enhancement by polarization transfer
DFT	density functional theory
DIBAL	diisobutylaluminum

dm	decimeter
DMAP	4-dimethylaminopyridine
Do	donor
d.r.	diastereomeric ratio
E	main-group element
ee	enantiomeric excess
EI	electronic ionization
<i>ent</i>	enantiomer
e.r.	enantiomeric ratio
ESI	electron spray ionization
Et	ethyl
equiv	equivalent
EXSY	exchange spectroscopy
g	gram
GLC	gas-liquid chromatography
GP	General Procedure
h	hour
<i>n</i> Hept	<i>n</i> -heptyl
<i>n</i> Hex	<i>n</i> -hexyl
HMBC	heteronuclear multiple bond coherence
HMQC	heteronuclear multiple quantum coherence
HPLC	high-performance liquid chromatography
HSQC	heteronuclear single quantum coherence
IR	infrared spectroscopy
J	coupling constant
k	rate constant
L	ligand <i>or</i> liter
LA	LEWIS acid
LB	LEWIS base

M	molecular mass <i>or</i> metal <i>or</i> mega
M	molar
m	multiplet <i>or</i> medium <i>or</i> milli <i>or</i> meter
<i>m</i>	<i>meta</i>
m _c	centrosymmetric multiplet
Me	methyl
Mes	mesityl
min	minute
mol %	mole percent
m.p.	melting point
MS	mass spectrometry
<i>n</i>	number of units
NHC	N-heterocyclic carbene
NHSi	N-heterocyclic silylene
NMR	nuclear magnetic resonance
NOESY	nuclear OVERHAUSER effect spectroscopy
NPA	Natural Population Analysis
<i>o</i>	<i>ortho</i>
<i>n</i> Oct	<i>n</i> -octyl
OTf	triflate
<i>p</i>	<i>para</i>
<i>n</i> Pent	<i>n</i> -pentyl
Ph	phenyl
pin	pinacolato
PMHS	polymethylhydrosiloxane
ppm	parts per million
<i>i</i> Pr	isopropyl
q	quartet
R	organic rest <i>or</i> as defined in the text
R _f	retention factor
<i>rac</i>	racemic
r.s.	regio selectivity

r.t.	room temperature
s	singlet <i>or</i> strong
S _N 2	second-order nucleophilic substitution
t	triplet
t _R	retention time
THF	tetrahydrofuran
TLC	thin-layer chromatography
TOF	turnover frequency
Tol	tolyl
TON	turnover number
UV	ultraviolet
w	weak
X	heteroatom
(9-BBN) ₂	9-borabicyclo(3.3.1)nonane dimer

A3 BIBLIOGRAPHY

- [1] For the synthesis and reactivity of boron cations, see: a) K. Kölle, H. Nöth, *Chem. Rev.* **1985**, 85, 399–418; b) W. E. Piers, S. C. Bourke, K. D. Conroy, *Angew. Chem.* **2005**, 117, 5142–5163; *Angew. Chem. Int. Ed.* **2005**, 44, 5016–5036; for aluminum, gallium, and indium cations, see: c) D. A. Atwood, *Coord. Chem Rev.* **1998**, 176, 407–430.
- [2] For the synthesis and reactivity of silylium ions, see: a) A. Schulz, A. Villinger, *Angew. Chem.* **2012**, 124, 4602–4604; *Angew. Chem. Int. Ed.* **2012**, 51, 4526–4528; b) H. F. T. Klare, M. Oestreich, *Dalton Trans.* **2010**, 39, 9176–9184; for germylium ions, see: c) A. Schäfer, M. Reißmann, S. Jung, A. Schäfer, W. Saak, E. Bredler, T. Müller, *Organometallics* **2013**, 32, 4713–4722; for stannylum ions, see: d) A. Schäfer, W. Saak, D. Haase, T. Müller, *J. Am. Chem. Soc.* **2011**, 133, 14562–14565; for selected reviews, see: e) V. Y. Lee, A. Sekiguchi, *Organometallic Compounds of Low-Coordinate Si, Ge, Sn and Pb*; Wiley, Chichester, **2010**; f) V. Y. Lee, A. Sekiguchi, *Acc. Chem. Res.* **2007**, 40, 410–419; g) T. Müller, *Adv. Organomet. Chem.* **2005**, 53, 155–215.
- [3] a) O. Eisenstein, R. H. Crabtree, *New J. Chem.* **2013**, 37, 21–27; b) A. Comas-Vives, G. Ujaque, A. Lledós, *Adv. Inorg. Chem.* **2010**, 62, 231–260; c) R. M. Bullock, *Chem. Eur. J.* **2004**, 10, 2366–2374; d) R. Noyori, M. Yamakawa, S. Hashiguchi, *J. Org. Chem.* **2001**, 66, 7931–7944.
- [4] M. Iglesias, F. J. Fernández-Alvarez, L. A. Oro, *ChemCatChem* **2014**, 6, 2486–2489.
- [5] a) N. Miyaura, *Top. Curr. Chem.* **2002**, 219, 11–59; b) N. Miyaura, A. Suzuki, *Chem. Rev.* **1995**, 95, 2457–2483; c) A. Suzuki, *Acc. Chem. Rev.* **1982**, 15, 178–184; d) A. Pelter, *Chem. Soc. Rev.* **1982**, 11, 191–225.
- [6] a) M. Dahlmann, M. Lautens in *Catalytic Heterofunctionalization* (Eds.: A. Togni, H. Grützmacher), Wiley-VCH, Chichester, **2001**; b) *Reduction by the Alumino- and Borohydrides in Organic Synthesis*, 2nd edition (Ed.: J. Seyden-Penne), Wiley-VCH, New York, **1997**.
- [7] D. Männing, H. Nöth, *Angew. Chem.* **1985**, 97, 854–855; *Angew. Chem. Int. Ed. Engl.* **1985**, 24, 878–879.
- [8] a) D. A. Evans, G. C. Fu, *J. Org. Chem.* **1990**, 55, 2280–2282; b) D. A. Evans, G. C. Fu, B. A. Anderson, *J. Am. Chem. Soc.* **1992**, 114, 6679–6685.
- [9] K. Burgess, W. A. van der Donk, S. A. Wescott, T. B. Marder, R. T. Baker, J. C. Calabrese, *J. Am. Chem. Soc.* **1992**, 114, 9350–9359.

- [10] This so-called “Trojan-horse mechanism” was proposed for other hydroboration reactions: a) K. Burgess, M. Jaspars, *Tetrahedron Lett.* **1993**, 34, 6813–6816; b) S. Harder, J. Spielmann, *J. Organomet. Chem.* **2012**, 698, 7–14.
- [11] a) D. G. Musaev, A. M. Mebel, K. Morokuma, *J. Am. Chem. Soc.* **1994**, 116, 10693–10702; b) A. E. Dorigo, P. von Ragué Schleyer, *Angew. Chem.* **1995**, 107, 108–111; *Angew. Chem. Int. Ed. Engl.* **1995**, 34, 115–118; c) C. Widauer, H. Grützmacher, T. Ziegler, *Organometallics* **2000**, 19, 2097–2107.
- [12] a) J. J. Eisch, K. C. Fichter, *J. Am. Chem. Soc.* **1974**, 96, 6815–6817; b) J. J. Eisch, S. R. Sexsmith, K. C. Fichter, *J. Organomet. Chem.* **1990**, 382, 273–293; c) J. J. Eisch, X. Ma, M. Singh, G. Wilke, *J. Organomet. Chem.* **1997**, 527, 301–304.
- [13] I. Beletskaya, A. Pelter, *Tetrahedron* **1997**, 53, 4957–5026.
- [14] T. Ohmura, Y. Yamamoto, N. Miyaura, *J. Am. Chem. Soc.* **2000**, 122, 4990–4991.
- [15] C. Gunanathan, M. Hölscher, F. Pan, W. Leitner, *J. Am. Chem. Soc.* **2012**, 134, 14349–14352.
- [16] B. Sundararaju, A. Fürstner, *Angew. Chem.* **2013**, 125, 14300–14304; *Angew. Chem. Int. Ed.* **2013**, 52, 14050–14054.
- [17] The proposed mechanism is similar to the TROST–WU mechanism of *trans*-hydrosilylation of alkynes (Scheme 1.19).
- [18] a) T. Ishiyama, J. Takagi, K. Ishida, Miyaura, N. R. Anastasi, J. F. Hartwig, *J. Am. Chem. Soc.* **2002**, 124, 390–391; b) T. M. Boller, J. M. Murphy, M. Hapke, T. Ishiyama, N. Miyaura, J. F. Hartwig, *J. Am. Chem. Soc.* **2005**, 127, 14263–14278; for reviews of C–H bond borylation, see: c) I. A. I. Mkhalid, J. H. Barnard, T. B. Marder, J. M. Murphy, J. F. Hartwig, *Chem. Rev.* **2010**, 110, 890–931; d) J. F. Hartwig, *Chem. Soc. Rev.* **2011**, 40, 1992–2002.
- [19] a) C. N. Muhoro, X. He, J. F. Hartwig, *J. Am. Chem. Soc.* **1999**, 121, 5033–5046; b) J. F. Hartwig, C. N. Muhoro, *Organometallics* **2000**, 19, 30–38.
- [20] A. A. Oluyadu, S. Ma, C. N. Muhoro, *Organometallics* **2012**, 32, 70–78.
- [21] For La–H, see: a) K. N. Harrison, T. J. Marks, *J. Am. Chem. Soc.* **1992**, 114, 9220–9221; for Zr–H, see: b) S. Pereira, M. Srebnik, *Organometallics* **1995**, 14, 3127–3128; for Ti, see c) X. He, J. F. Hartwig, *J. Am. Chem. Soc.* **1996**, 118, 1696–1702; d) for Mg–H, see: M. Arrowsmith, T. J. Hadlington, M. S. Hill, G. Kociok-Köhn, *Chem. Commun.* **2012**, 48, 4567–4569; for Sn–H and Ge–H, see: e) T. J. Hadlington, M. Hermann, G. Frenking, C. Jones, *J. Am. Chem. Soc.* **2014**, 136, 3028–3031; for a review of σ -bond metathesis, see: f) R. Waterman, *Organometallics* **2013**, 32, 7249–7263.
- [22] R. N. Perutz, S. Sabo-Etienne, *Angew. Chem.* **2007**, 119, 2630–2645; *Angew. Chem. Int. Ed.* **2007**, 46, 2578–2592.

- [23] C. E. Webster, Y. Fan, M. B. Hall, D. Kunz, J. F. Hartwig, *J. Am. Chem. Soc.* **2003**, *125*, 858–859.
- [24] D. Mukherjee, A. Ellern, A. D. Sadow, *Chem. Sci.* **2014**, *5*, 959–964.
- [25] a) A. C. Fernandes, C. C. Romão, *Tetrahedron Lett.* **2007**, *48*, 9176–9179; b) A. C. Fernandes, J. A. Fernandes, F. A. Almeida Paz, C. C. Romão, *Dalton Trans.* **2008**, 6686–6688; c) S. C. A. Sousa, I. C. Cabrita, A. C. Fernandes, *Chem. Soc. Rev.* **2012**, *41*, 5641–5653.
- [26] For recent reviews, see: a) J. R. Knusnutdinova, D. Milstein, *Angew. Chem.* **2015**, *127*, 12406–12445; *Angew. Chem. Int. Ed.* **2015**, *54*, 12236–12273; b) M. Trincado, H. Grützmaier in *Cooperative Catalysis* (Ed.: R. Peters), Wiley-VCH, Weinheim, **2015**, p. 67–110.
- [27] B. L. Conley, M. K. Pennington-Boggio, E. Boz, T. J. Williams, *Chem. Rev.* **2010**, *110*, 2294–2312.
- [28] L. Koren-Selfridge, H. N. Londino, J. K. Vellucci, B. J. Simmons, C. P. Casey, T. B. Clark, *Organometallics* **2009**, *28*, 2085–2090.
- [29] C. P. Casey, S. W. Singer, D. R. Powell, R. K. Hayashi, M. Kavana, *J. Am. Chem. Soc.* **2001**, *123*, 1090–1100.
- [30] Y. Ohki, Y. Takikawa, H. Sadohara, C. Kesenheimer, B. Engendahl, E. Kapatina, K. Tatsumi, *Chem. Asian. J.* **2008**, *3*, 1625–1635.
- [31] T. Stahl, K. Müther, Y. Ohki, K. Tatsumi, M. Oestreich, *J. Am. Chem. Soc.* **2013**, *135*, 10978–10981.
- [32] J. B. Geri, N. K. Szymczak, *J. Am. Chem. Soc.* **2015**, *137*, 12808–12814.
- [33] The mechanism where the ruthenium center remains a bystander during the active catalytic cycle, could be defined as a peripheral mechanism (*vide infra*).
- [34] a) *The Chemistry of Organic Silicon Compounds*, Vol. 3 (Eds.: Z. Rappoport, Y. Apeloig), Wiley, Chichester, **2001**; b) *The Chemistry of Organic Silicon Compounds*, Vol. 2 (Eds.: Z. Rappoport, Y. Apeloig), Wiley, Chichester, **1998**; c) *The Chemistry of Organic Silicon Compounds* (Eds.: S. Patai, Z. Rappoport), Wiley, Chichester, **1989**.
- [35] *The chemistry of organic germanium, tin and lead compounds*, Vol. 1 (Ed.: S. Patai), Wiley, Chichester, **1995**.
- [36] C. Chatgililoglu, *Chem. Rev.* **1995**, *95*, 1229–1251.
- [37] N. D. Smith, J. Mancuso, M. Lautens, *Chem. Rev.* **2000**, *100*, 3257–3282.
- [38] A. J. Chalk, J. F. Harrod, *J. Am. Chem. Soc.* **1965**, *87*, 16–21.
- [39] H. Konoshita, T. Nakamura, H. Kakiya, H. Shinokubo, S. Matsubara, K. Oshima, *Org. Lett.* **2001**, *3*, 2521–2524.
- [40] L. T. Leung, S. K. Leung, P. Chiu, *Org. Lett.* **2005**, *7*, 5249–5252.

- [41] a) M. A. Schroeder, M. S. Wrighton, *J. Organomet. Chem.* **1977**, *128*, 345–358; b) C. L. Reichel, M. S. Wrighton, *Inorg. Chem.* **1980**, *19*, 3858–3860; c) C. L. Randolph, M. S. Wrighton, *J. Am. Chem. Soc.* **1986**, *108*, 3366–3374.
- [42] For comparative computational analysis of CHALK–HARROD and the modified CHALK–HARROD mechanisms, see: a) S. Sakaki, N. Mizoe, M. Sugimoto, *Organometallics* **1998**, *17*, 2510–2523; b) G. Giorgi, F. De Angelis, N. Re, A. Sgamellotti, *Fut. Gen. Comp. Syst.* **2004**, *20*, 781–791.
- [43] For early examples of dehydrogenative silylation of alkenes, see: a) A. Millan, E. Towns, P. M. Maitlis, *J. Chem. Soc., Chem. Commun.* **1981**, 673–674; b) F. Seitz, M. S. Wrighton, *Angew. Chem.* **1988**, *100*, 281–283; *Angew. Chem. Int. Ed. Engl.* **1988**, *27*, 289–291; c) M. R. Kesti, R. M. Waymouth, *Organometallics* **1992**, *11*, 1095–1103, for recent examples of selective synthesis of vinylic or allylic silanes, see: d) J. R. McAtee, S. E. S. Martin, D. T. Ahneman, K. A. Johnson, D. A. Watson, *Angew. Chem.* **2012**, *124*, 3723–3727; *Angew. Chem. Int. Ed.* **2012**, *51*, 3663–3667 (vinylic silanes using R_3Si-I); e) J. R. McAtee, G. P. A. Yap, D. A. Watson, *J. Am. Chem. Soc.* **2014**, *136*, 10166–10172 (allylic silanes using R_3Si-I); f) C. C. H. Atienza, T. Diao, K. J. Weller, S. A. Nye, K. M. Lewis, J. G. P. Delis, J. L. Boyer, A. K. Roy, P. J. Chirik, *J. Am. Chem. Soc.* **2014**, *136*, 12108–12118 (allylic silanes using R_3Si-H).
- [44] For dehydrogenative germylation, see: N. Furukawa, N. Kourogi, Y. Seki, *Organometallics* **1999**, *18*, 3764–3767. Although no mechanism was provided, the reaction is likely to proceed *via* a similar mechanism as shown here for the dehydrogenative silylation.
- [45] Often a sacrificial dihydrogen acceptor is required for efficient turnover.
- [46] Y. Ichinose, H. Oda, K. Oshima, K. Utimoto, *Bull. Chem. Soc. Jpn.* **1987**, *60*, 3468–3470.
- [47] A. Trofimov, M. Rubina, M. Rubin, V. Gevorgyan, *J. Org. Chem.* **2007**, *72*, 8910–8920.
- [48] B. Marciniec in *Hydrosilylation. A Comprehensive Review on Recent Advances* (Ed. B. Marciniec), Springer, Netherlands, **2009**, p. 53–86.
- [49] K. A. Brady, T. A. Nile, *J. Organomet. Chem.* **1981**, *206*, 299–304.
- [50] R. S. Tanke, R. H. Crabtree, *J. Am. Chem. Soc.* **1990**, *112*, 7984–7989.
- [51] a) B. M. Trost, Z. T. Ball, *J. Am. Chem. Soc.* **2001**, *123*, 12726–12727; b) B. M. Trost, Z. T. Ball, *J. Am. Chem. Soc.* **2002**, *125*, 30–31.
- [52] L. W. Chung, Y.-D. Wu, B. M. Trost, Z. T. Ball, *J. Am. Chem. Soc.* **2003**, *125*, 11578–11582.

- [53] S. Ding, L.-J. Song, L. W. Chung, X. Zhang, J. Sun, Y.-D. Wu, *J. Am. Chem. Soc.* **2013**, *135*, 13835–13842.
- [54] B. Marciniec, E. Walczuk-Guściora, C. Pietraszuk, *Organometallics* **2001**, *20*, 3423–3428.
- [55] a) I. Ojima, M. Nihonyanagi, T. Kogure, M. Kumagai, S. Horiuchi, K. Nakatsugawa, Y. Nagai, *J. Organomet. Chem.* **1975**, *94*, 449–461; b) I. Ojima, T. Kogure, M. Kumagai, S. Horiuchi, T. Sato, *J. Organomet. Chem.* **1976**, *122*, 83–97.
- [56] G. Z. Zheng, T. H. Chan, *Organometallics* **1995**, *14*, 70–79.
- [57] The mechanism with di- and trihydrosilanes could in fact be considered as an outer-sphere mechanism.
- [58] a) P. B. Glaser, T. D. Tilley, *J. Am. Chem. Soc.* **2003**, *125*, 13640–13641; b) M. A. Rankin, D. F. MacLean, G. Schatte, R. McDonald, M. Stradiotto, *J. Am. Chem. Soc.* **2007**, *129*, 15855–15864.
- [59] N. Schneider, M. Finger, C. Haferkemper, S. Bellemin-Laponnaz, P. Hofmann, L. H. Gade, *Angew. Chem.* **2009**, *121*, 1637–1641; *Angew. Chem. Int. Ed.* **2009**, *48*, 1609–1613.
- [60] S. Rendler, M. Oestreich in *Modern Reduction Methods* (Eds.: P. G. Andersson, I. J. Munslow), Wiley-VCH, Weinheim, **2008**, p. 183–207.
- [61] a) B. H. Lipshutz, W. Chrisman, K. Noson, *J. Organomet. Chem.* **2001**, *624*, 367–371; the related dehydrogenative silylation of alcohols has been shown to proceed via a σ -bond metathesis mechanism, see: b) H. Ito, T. Ishizuka, T. Okumura, H. Yamanaka, J.-i. Tateiwa, M. Sonoda, A. Hosomi, *J. Organomet. Chem.* **1999**, *574*, 102–106; c) S. Rendler, G. Auer, M. Oestreich, *Angew. Chem.* **2005**, *117*, 7793–7797; *Angew. Chem. Int. Ed.* **2005**, *44*, 7620–7624; d) S. Rendler, O. Plefka, B. Karatas, G. Auer, R. Fröhlich, C. Mück-Lichtenfeld, S. Grimme, M. Oestreich, *Chem. Eur. J.* **2008**, *14*, 11512–11528.
- [62] B. H. Lipshutz, K. Noson, W. Chrisman, A. Lower, *J. Am. Chem. Soc.* **2003**, *125*, 8779–8789.
- [63] O. G. Shirobokov, L. G. Kuzmina, G. I. Nikonov, *J. Am. Chem. Soc.* **2011**, *133*, 6487–6489.
- [64] LIPSHUTZ proposed a silyl cuprate as the active catalyst, whereas NIKONOV proposed that the copper center would activate the carbonyl as a LEWIS acid. For more proposed mechanisms, see: a) Ref. [61b]; b) C. R. Waidmann, L. A. Silks, R. Wu, J. C. Gordon, *Catal. Sci. Technol.* **2013**, *3*, 1240–1245.
- [65] J. Spielmann, S. Harder, *Eur. J. Inorg. Chem.* **2008**, 1480–1486.
- [66] a) S. E. Denmark, G. L. Beutner, *Angew. Chem.* **2008**, *120*, 1584–1663; *Angew. Chem. Int. Ed.* **2008**, *47*, 1560–1638; b) S. Rendler, M. Oestreich, *Synthesis* **2005**,

- 1727–1747; c) M. Kira, L. C. Zhang in *Chemistry of Hypervalent Compounds* (Ed.: K.-y. Akiba), Wiley-VCH, New York, **1999**, p. 147–169; d) C. Chuit, R. J. P. Corriu, C. Reye, J. C. Young, *Chem. Rev.* **1993**, 93, 1371–1448.
- [67] For Ge–H bond activation involving proposed σ -CAM mechanism, see: M. Murai, K. Matsumoto, R. Okada, K. Takai, *Org. Lett.* **2014**, 16, 6492–6495.
- [68] a) J. J. Kennedy-Smith, K. A. Nolin, H. P. Gunterman, F. D. Toste, *J. Am. Chem. Soc.* **2003**, 125, 4056–4057; b) K. A. Nolin, J. R. Krumper, M. D. Pluth, R. G. Bergman, F. D. Toste, *J. Am. Chem. Soc.* **2007**, 129, 14684–14696.
- [69] P. Deglmann, E. Ember, P. Hofmann, S. Pitter, O. Walter, *Chem. Eur. J.* **2007**, 13, 2864–2879.
- [70] K. D. Hesp, R. McDonald, M. J. Ferguson, M. Stradiotto, *J. Am. Chem. Soc.* **2008**, 130, 16394–16406.
- [71] T. Stahl, P. Hrobárik, C. D. F. Königs, Y. Ohki, K. Tatsumi, S. Kemper, M. Kaupp, H. F. T. Klare, M. Oestreich, *Chem. Sci.* **2015**, 6, 4324–4334.
- [72] a) T. Stahl, H. F. T. Klare, M. Oestreich, *J. Am. Chem. Soc.* **2013**, 135, 1248–1251; b) C. D. F. Königs, H. F. T. Klare, M. Oestreich, *Angew. Chem.* **2013**, 125, 10260–10263; *Angew. Chem. Int. Ed.* **2013**, 125, 10260–10263.
- [73] a) H. F. T. Klare, M. Oestreich, J.-i. Ito, H. Nishiyama, Y. Ohki, K. Tatsumi, *J. Am. Chem. Soc.* **2011**, 133, 3312–3315; b) C. D. F. Königs, H. F. T. Klare, Y. Ohki, K. Tatsumi, M. Oestreich, *Org. Lett.* **2012**, 14, 2842–2845; c) C. D. F. Königs, M. F. Müller, N. Aiguabella, H. F. T. Klare, M. Oestreich, *Chem. Commun.* **2013**, 49, 1506–1508; d) J. Hermeke, H. F. T. Klare, M. Oestreich, *Chem. Eur. J.* **2014**, 20, 9250–9254; e) L. Omann, M. Oestreich, *Angew. Chem.* **2015**, 127, 10414–10418; *Angew. Chem. Int. Ed.* **2015**, 54, 10276–10279; f) S. Wübbolt, M. Oestreich, *Angew. Chem.* **2015**, 127, 16103–16106; *Angew. Chem. Int. Ed.* **2015**, 54, 15876–15879.
- [74] R. Lalrempuia, M. Iglesias, V. Polo, P. J. Sanz Miguel, F. J. Fernández-Alvarez, J. J. Pérez-Torrente, L. A. Oro, *Angew. Chem.* **2012**, 124, 12996–12999; *Angew. Chem. Int. Ed.* **2012**, 51, 12824–12827.
- [75] X.-L. Luo, R. H. Crabtree, *J. Am. Chem. Soc.* **1989**, 111, 2527–2535.
- [76] V. K. Dioumaev, R. M. Bullock, *Nature* **2003**, 424, 530–532.
- [77] a) R. M. Bullock, M. H. Voges, *J. Am. Chem. Soc.* **2000**, 122, 12594–12595; b) M. H. Voges, R. M. Bullock, *J. Chem. Soc., Dalton Trans.* **2002**, 757–770.
- [78] a) J. Yang, M. Brookhart, *J. Am. Chem. Soc.* **2007**, 129, 12656–12657; b) J. Yang, M. Brookhart, *Adv. Synth. Catal.* **2009**, 351, 175–187.

- [79] a) S. Park, M. Brookhart, *Organometallics* **2010**, *29*, 6057–6064; for a DFT investigation, see : W. Wang, P. Gu, Y. Wang, H. Wei, *Organometallics* **2014**, *33*, 847–857.
- [80] S. Park, M. Brookhart, *J. Am. Chem. Soc.* **2012**, *134*, 640–653.
- [81] a) J. Yang, P. S. White, M. Brookhart, *J. Am. Chem. Soc.* **2008**, *130*, 17509–17518; b) S. Park, M. Brookhart, *Chem. Commun.* **2011**, *47*, 3643–3645.
- [82] S. Park, D. Bézier, M. Brookhart, *J. Am. Chem. Soc.* **2012**, *134*, 11404–11407.
- [83] D. V. Gutsulyak, S. F. Vyboishchikov, G. I. Nikonov, *J. Am. Chem. Soc.* **2010**, *132*, 5950–5951.
- [84] D. V. Gutsulyak, G. I. Nikonov, *Angew. Chem.* **2010**, *122*, 7715–7718; *Angew. Chem. Int. Ed.* **2010**, *49*, 7553–7556.
- [85] a) D. V. Gutsulyak, A. van der Est, G. I. Nikonov, *Angew. Chem.* **2011**, *123*, 1420–1423; *Angew. Chem. Int. Ed.* **2011**, *50*, 1384–1387; b) S.-H. Lee, D. V. Gutsulyak, G. I. Nikonov, *Organometallics* **2013**, *32*, 4457–4464.
- [86] Y.-F. Yang, L. W. Chung, X. Zhang, K. N. Houk, Y.-D. Wu, *J. Org. Chem.* **2014**, *79*, 8856–8864.
- [87] a) M. Iglesias, P. J. Sanz Miguel, V. Polo, F. J. Fernández-Alvarez, J. J. Pérez-Torrente, L. A. Oro, *Chem. Eur. J.* **2013**, *19*, 17559–17599; b) M. Iglesias, M. Aliaga-Lavrijsen, P. J. Sanz-Miguel, F. J. Fernández-Alvarez, J. J. Pérez-Torrente, L. A. Oro, *Adv. Synth. Catal.* **2015**, *357*, 350–354.
- [88] G. Du, P. E. Fanwick, M. M. Abu-Omar, *J. Am. Chem. Soc.* **2007**, *129*, 5180–5187.
- [89] Alternative ionic mechanisms where the rhenium hydride and the silylcarboxonium ion dissociate were excluded.
- [90] a) M. C. Lipke, T. D. Tilley, *J. Am. Chem. Soc.* **2011**, *133*, 16374–16377; b) M. C. Lipke, F. Neumeyer, T. D. Tilley, *J. Am. Chem. Soc.* **2014**, *136*, 6092–6102; c) M. C. Lipke, T. D. Tilley, *J. Am. Chem. Soc.* **2014**, *136*, 16387–16398.
- [91] M. Oestreich, J. Hermeke, J. Mohr, *Chem. Soc. Rev.* **2015**, *44*, 2202–2220.
- [92] a) J. I. v. d. Vlugt, *Eur. J. Inorg. Chem.* **2011**, 363–375; b) S. Chakraborty, H. Guan, *Dalton Trans.* **2010**, *39*, 7427–7436.
- [93] For selected examples, see: J. Y. Wu, B. Moreau, T. Ritter, *J. Am. Chem. Soc.* **2009**, *131*, 12915–12917; b) L. Zhang, D. Peng, X. Leng, Z. Huang, *Angew. Chem.* **2013**, *125*, 3764–3768; *Angew. Chem. Int. Ed.* **2013**, *52*, 3676–3680; c) J. V. Obligation, P. J. Chirik, *Org. Lett.* **2013**, *15*, 2680–2683.
- [94] a) K. Junge, K. Schröder, M. Beller, *Chem. Commun.* **2011**, *47*, 4849–4859; b) M. Zhang, A. Zhang, *Appl. Organomet. Chem.* **2010**, *24*, 751–757; c) R. H. Morris, *Chem. Soc. Rev.* **2009**, *38*, 2282–2291.

- [95] The DFT calculations included into the mechanistic investigation of the BROOKHART's POCOP pincer complex described in this chapter were done in collaboration with Dr. PETER HROBÁRIK and Prof. Dr. MARTIN KAUPP.
- [96] I. Göttker-Schnetmann, P. S. White, M. Brookhart, *Organometallics* **2004**, *23*, 1766–1776.
- [97] The catalyst was shown to also reduce 1-fluoropentane (**97**) with 92% conversion in 50 h using 2 mol % catalyst loading. Other unidentified products in addition to *n*-pentane were observed.
- [98] J. Yang, P. S. White, C. K. Schauer, M. Brookhart, *Angew. Chem.* **2008**, *120*, 4209–4211; *Angew. Chem. Int. Ed.* **2008**, *47*, 4141–4143.
- [99] For a related $R_3B-\eta^1-H-SiR_3$ X-ray structure, see: A. Y. Houghton, J. Hurmalainen, A. Mansikkamäki, W. E. Piers, H. M. Tuononen, *Nat. Chem.* **2014**, *6*, 983–988.
- [100] η^2 -**74a** was calculated to be favored over η^1 -**74a** by 1.9 kcal mol⁻¹. The calculations were performed on a truncated complex using PMe₂ instead of P(*t*Bu)₂.
- [101] a) D. J. Parks, W. E. Piers, *J. Am. Chem. Soc.* **1996**, *118*, 9440–9441; b) D. J. Parks, J. M. Blackwell, W. E. Piers, *J. Org. Chem.* **2000**, *65*, 3090–3098; c) S. Rendler, M. Oestreich, *Angew. Chem.* **2008**, *120*, 6086–6089; *Angew. Chem. Int. Ed.* **2008**, *47*, 5997–6000; d) K. Sakata, H. Fujimoto, *J. Org. Chem.* **2013**, *78*, 12505–12512; for a recent review on borane-catalyzed reactions, see: M. Oestreich, J. Hermeke, J. Mohr, *Chem. Soc. Rev.* **2015**, *44*, 2202–2220.
- [102] Based on kinetic measurements during the mechanistic investigation of the ether cleavage catalyzed by **73**⁺ ref. [81], the iridium silyl hydride **107** was found to be a much weaker hydride donor than the dihydride **76**.
- [103] Known to proceed with retention at silicon atom: M. Oestreich, G. Auer, M. Keller, *Eur. J. Org. Chem.* **2005**, 184–195.
- [104] Hydrosilylation of acetophenone **73**⁺ with triethyl silane (**23a**, 3 equiv) reaches full conversion in 20 min.
- [105] The dissociation of the ion pair is calculated to be unfavored by 15.2 kcal mol⁻¹, see ref. [101d].
- [106] Careful control of the stoichiometry during the synthesis is essential to avoid formation of bis-silylhydronium ion, see: a) M. Nava, C. A. Reed, *Organometallics* **2011**, *30*, 4798–4800; b) S. J. Connelly, W. Kaminsky, D. M. Heinekey, *Organometallics* **2013**, *32*, 7478–7481.
- [107] Addition of hydrosilane **23a** into this mixture led to deoxygenation to give ethylbenzene **119** and decomposition.
- [108] BROOKHART proposed the hydrosilane **23** as a competing hydride source during the ether cleavage catalyzed by complex **73**⁺, ref. [81].

- [109] a) M. Kira, T. Hino, H. Sakurai, *Chem. Lett.* **1992**, 555–558; b) D. Parks, J. Blackwell, W. E. Piers, *J. Org. Chem.* **2000**, 65, 3090–3098; c) K. Mütter, M. Oestreich, *Chem. Commun.* **2011**, 47, 334–336.
- [110] The dihydrogen/hydrosilane exchange via **116** could in fact be seen as a σ -CAM process (see Scheme 1.10).
- [111] All DFT calculation performed at B3LYP-D3(BJ)/ECP/6-31++G(d,p) level using an SMD solvation model. Trimethylsilane (**23d**) was used as a model hydrosilane.
- [112] T. J. Hebden, M. C. Denney, V. Pons, P. M. B. Piccoli, T. F. Koetzle, A. J. Schultz, W. Kaminsky, K. I. Goldberg, D. M. Heinekey, *J. Am. Chem. Soc.* **2008**, 130, 10812–10820.
- [113] The mechanistic investigation of the iron SiNSi pincer complexes described in this chapter was done in collaboration with Dr. DANIEL GALLEG0 from the group of Prof. Dr. MATTHIAS DRIESS. The DFT calculations were performed by Dr. TIBOR SZILVÁSI.
- [114] a) D. Gallego, B. Blom, G. Tan, M. Driess in *Reference Module in Chemistry, Molecular Sciences and Chemical Engineering*, Elsevier, **2015**, p. 1–15; b) B. Blom, D. Gallego, M. Driess, *Inorg. Chem. Front.* **2014**, 1, 134–148; c) B. Blom, M. Stoelzel, M. Driess, *Chem. Eur. J.* **2013**, 19, 40–62.
- [115] D. Gallego, S. Inoue, B. Blom, M. Driess, *Organometallics* **2014**, 33, 6885–6897.
- [116] C.-W. So, H. W. Roesky, J. Magull, R. B. Oswald, *Angew. Chem.* **2006**, 118, 4052–4054; *Angew. Chem. Int. Ed.* **2006**, 45, 3948–3950.
- [117] All calculations were performed at ω B97X-D/6-31G(d)[Fe:ccpVTZ] level of theory. Iron(II) complex **133f**, triethoxysilane (**23f**), and acetone (**84**) were used as model substrates.
- [118] For a review on non-innocent ligands, see: O. R. Luca, R. H. Crabtree, *Chem. Soc. Rev.* **2013**, 42, 1440–1459.
- [119] P. Bhattacharya, J. A. Krause, H. Guan, *Organometallics* **2011**, 30, 4720–4729.
- [120] A. L. Liberman-Martin, R. G. Bergman, T. D. Tilley, *J. Am. Chem. Soc.* **2015**, 137, 5328–5331.
- [121] V. Gutmann, *Coord. Chem. Rev.* **1976**, 18, 225–255; b) M. A. Beckett, D. S. Brassington, M. E. Light, M. B. Hursthouse, *J. Chem. Soc., Dalton Trans.* **2001**, 1768–1772.
- [122] For recent examples, see: a) C. Romain, K. Miqueu, J.-M. Sotiropoulos, S. Bellemin-Laponnaz, S. Dagorne, *Angew. Chem.* **2010**, 122, 2244–2247; *Angew. Chem. Int. Ed.* **2010**, 49, 2198–2201; b) L. R. Collins, G. Hierlmeier, M. F. Mahon, I. M. Riddlestone, M. K. Whittlesey, *Chem. Eur. J.* **2015**, 21, 3215–3218; c) D. Prema, Y. L. N. Mathota Arachchige, R. E. Murray, L. M. Slaughter, *Chem. Commun.* **2015**, 51, 6753–6756; d) R. M. Brown, J. B. Garcia, J. Valjus, C. J. Roberts, H. M.

- Tuononen, M. Parvez, R. Roesler, *Angew. Chem.* **2015**, *127*, 6372–6375; *Angew. Chem. Int. Ed.* **2015**, *54*, 6274–6277; e) E. Despagnet-Ayoub, M. K. Takase, J. A. Labinger, J. E. Bercaw, *J. Am. Chem. Soc.* **2015**, *137*, 10500–10503.
- [123] a) M. Aresta, *Carbon Dioxide as Chemical Feedstock*; Wiley-VCH: Weinheim, Germany, **2010**; b) G. A. Olah, A. Goepfert, G. K. S. Prakash, *Beyond Oil and Gas: The Methanol Economy*; Wiley-VCH: Weinheim, Germany, **2006**; c) G. A. Olah, *Angew. Chem.* **2005**, *117*, 2692–2696; *Angew. Chem. Int. Ed.* **2005**, *44*, 2636–2639; d) H. Arakawa, M. Aresta, J. N. Armor, M. A. Barteau, E. J. Beckman, A. T. Bell, J. E. Bercaw, C. Creutz, E. Dinjus, D. A. Dixon, K. Domen, D. L. DuBois, J. Eckert, E. Fujita, D. H. Gibson, W. A. Goddard, D. W. Goodman, J. Keller, G. J. Kubas, H. H. Kung, J. E. Lyons, L. E. Manzer, T. J. Marks, K. Morokuma, K. M. Nicholas, R. Periana, L. Que, J. Rostrup-Nielsen, W. M. H. Sachtler, L. D. Schmidt, A. Sen, G. A. Somorjai, P. C. Stair, B. R. Stults, W. Tumas, *Chem. Rev.* **2001**, *101*, 953–996.
- [124] For recent reviews of carbon dioxide reduction, see: a) F. J. Fernández-Alvarez, A. M. Aitani, L. A. Oro, *Catal. Sci. Technol.* **2014**, *4*, 611–624; b) Y.-N. Li, R. Ma, L.-N. He, Z.-F. Diao, *Catal. Sci. Technol.* **2014**, *4*, 1498–1512; c) C. Costentin, M. Robert, J.-M. Savéant, *Chem. Soc. Rev.* **2013**, *42*, 2423–2436; d) G. Centi, E. A. Quadrelli, S. Perathoner, *Energy Environ. Sci.* **2013**, *6*, 1711–1731; e) Y. Oh, X. Hu, *Chem. Soc. Rev.* **2013**, *42*, 2253–2261; f) E. E. Benson, C. P. Kubiak, A. J. Sathrum, J. M. Smieja, *Chem. Soc. Rev.* **2008**, *38*, 89–99.
- [125] For recent reviews of carbon dioxide conversion, see: a) C. Maeda, Y. Miyazaki, T. Ema, *Catal. Sci. Technol.* **2014**, *4*, 1482–1497; b) M. Cokoja, C. Bruckmeier, B. Rieger, W. A. Herrmann, F. E. Kühn, *Angew. Chem.* **2011**, *123*, 8662–8690; *Angew. Chem. Int. Ed.* **2011**, *50*, 8510–8537; c) M. Peters, B. Köhler, W. Kuckshinrichs, W. Leitner, P. Markewitz, T. E. Müller, *ChemSusChem* **2011**, *4*, 1216–1240; d) S. N. Riduan, Y. Zhang, *Dalton Trans.* **2010**, *39*, 3347–3357.
- [126] For reduction of carbon dioxide into carbon monoxide, see: a) D. S. Laitar, P. Müller, J. P. Sadighi, *J. Am. Chem. Soc.* **2005**, *127*, 17196–17197; b) L. Gu, Y. Zhang, *J. Am. Chem. Soc.* **2010**, *132*, 914–915; c) C. Kleeberg, M. S. Cheung, Z. Lin, T. B. Marder, *J. Am. Chem. Soc.* **2011**, *133*, 19060–19063; d) R. Dobrovetsky, D. W. Stephan, *Angew. Chem.* **2013**, *125*, 2576–2579; *Angew. Chem. Int. Ed.* **2013**, *52*, 2516–2519; e) C. Lescot, D. U. Nielsen, I. S. Makarov, A. T. Lindhardt, K. Daasbjerg, T. Skrydstrup, *J. Am. Chem. Soc.* **2014**, *136*, 6142–6147; f) S. Bagherzadeh, N. P. Mankad, *J. Am. Chem. Soc.* **2015**, *137*, 10898–1090.
- [127] a) J. G. Burr, Jr., W. G. Brown, H. E. Heller, *J. Am. Chem. Soc.* **1950**, *72*, 2560–2562; b) T. Wartik, R. K. Pearson, *J. Am. Chem. Soc.* **1955**, *77*, 1075–1075; c) T.

- Wartik, R. K. Pearson, *J. Inorg. Nucl. Chem.* **1958**, 7, 404–411; d) R. K. Pearson, T. Wartik, U.S. Patent 2872474, **1959**.
- [128] A. E. Finholt, E. C. Jacobson, *J. Am. Chem. Soc.* **1952**, 74, 3943–3944.
- [129] I. Knopf, C. C. Cummins, *Organometallics* **2015**, 34, 1601–1603.
- [130] R. Shintani, K. Nozaki, *Organometallics* **2013**, 32, 2459–2462.
- [131] G. Süss-Fink, J. Reiner, *J. Organomet. Chem.* **1981**, 221, C36–C38.
- [132] H. Koinuma, F. Kawakami, H. Kato, H. Hirai, *J. Chem. Soc., Chem. Commun.* **1981**, 213–214.
- [133] a) A. Jansen, H. Görls, S. Pitter, *Organometallics* **2000**, 19, 135–138; b) Ref. [69]; c) K. Motokura, D. Kashiwame, A. Miyaji, T. Baba, *Org. Lett.* **2012**, 14, 2642–2645; d) Ref [74]; e) K. Motokura, D. Kashiwame, N. Takahashi, A. Miyaji, T. Baba, *Chem. Eur. J.* **2013**, 19, 10030–10037; f) S. Itagaki, K. Yamaguchi, N. Mizuno, *J. Mol. Catal. A: Chem.* **2013**, 366, 347–352; g) L. Zhang, J. Cheng, Z. Hou, *Chem. Commun.* **2013**, 49, 4782–4784; h) L. González-Sebastián, M. Flores-Alamo, J. J. García, *Organometallics* **2013**, 32, 7186–7194; i) V. P. Taori, R. Bandari, M. R. Buchmeiser, *Chem. Eur. J.* **2014**, 20, 3292–3296; j) M. L. Scheuermann, S. P. Semproni, I. Pappas, P. J. Chirik, *Inorg. Chem.* **2014**, 53, 9463–9465.
- [134] a) S. Bontemps, L. Vendier, S. Sabo-Etienne, *Angew. Chem.* **2012**, 124, 1703–1706; *Angew. Chem. Int. Ed.* **2012**, 51, 1671–1674; b) S. Bontemps, S. Sabo-Etienne, *Angew. Chem.* **2013**, 125, 10443–10445; *Angew. Chem. Int. Ed.* **2013**, 52, 10253–10255; c) S. Bontemps, L. Vendier, S. Sabo-Etienne, *J. Am. Chem. Soc.* **2014**, 136, 4419–4425.
- [135] G. Jin, G. Werncke, Y. Escudié, S. Sabo-Etienne, S. Bontemps, *J. Am. Chem. Soc.* **2015**, 137, 9563–9566.
- [136] Y. Jiang, O. Blacque, T. Fox, H. Berke, *J. Am. Chem. Soc.* **2013**, 135, 7751–7760.
- [137] F. A. LeBlanc, W. E. Piers, M. Parvez, *Angew. Chem.* **2013**, 126, 808–811; *Angew. Chem. Int. Ed.* **2014**, 53, 789–792.
- [138] a) S. Chakraborty, J. Zhang, J. A. Krause, H. Guan, *J. Am. Chem. Soc.* **2010**, 132, 8872–8873; b) M. J. Sgro, D. W. Stephan, *Angew. Chem.* **2012**, 124, 11505–11507; *Angew. Chem. Int. Ed.* **2012**, 51, 11343–11345; c) M.-A. Courtemanche, M.-A. Légaré, L. Maron, F.-G. Fontaine, *J. Am. Chem. Soc.* **2013**, 135, 9326–9329; d) C. Das Neves Gomes, E. Blondiaux, P. Thuéry, T. Cantat, *Chem. Eur. J.* **2014**, 20, 7098–7106; e) T. Wang, D. W. Stephan, *Chem. Eur. J.* **2014**, 20, 3036–3039; f) M. D. Anker, M. Arrowsmith, P. Bellham, M. S. Hill, G. Kociok-Köhn, D. J. Liptrót, M. F. Mahon, C. Weetman, *Chem. Sci.* **2014**, 5, 2826–2830; g) T. Wang, D. W. Stephan, *Chem. Commun.* **2014**, 50, 7007–7010; h) K. Fujiwara, S. Yasuda, T. Mizuta, *Organometallics* **2014**, 33, 6692–6695; i) R. Pal, T. L. Groy, R. J. Trovitch,

- Inorg. Chem.* **2015**, *54*, 7506–7515; j) Y. Yang, M. Xu, D. Song, *Chem. Commun.* **2015**, *51*, 11293–11296; k) J. A. B. Abdalla, I. M. Riddlestone, R. Tirfoin, S. Aldridge, *Angew. Chem.* **2015**, *127*, 5187–5191; *Angew. Chem. Int. Ed.* **2015**, *54*, 5098–5102.
- [139] For reviews of frustrated LEWIS pair chemistry, see: a) D. W. Stephan, *Acc. Chem. Res.* **2015**, *48*, 306–316; b) M. Alcarazo, *Synlett* **2014**, 1519–1520; c) D. W. Stephan, G. Erker, *Chem. Sci.* **2014**, *5*, 2625–2641; d) *Top. Curr. Chem.* (Eds. G. Erker, D. W. Stephan), Springer, Berlin, Heidelberg, **2013**, vol. 332; e) *Top. Curr. Chem.* (Eds. G. Erker, D. W. Stephan), Springer, Berlin, Heidelberg, **2013**, vol. 334; f) D. W. Stephan, G. Erker, *Angew. Chem.* **2010**, *122*, 50–81; *Angew. Chem. Int. Ed.* **2010**, *49*, 46–76; g) D. W. Stephan, *Org. Biomol. Chem.* **2008**, *6*, 1535–1539; h) A. L. Kenward, W. E. Piers, *Angew. Chem.* **2008**, *120*, 38–42; *Angew. Chem. Int. Ed.* **2008**, *47*, 38–41.
- [140] a) V. T. Annibale, D. Song, *Chem. Commun.* **2011**, *48*, 5416–5418; b) V. T. Annibale, D. A. Dalessandro, D. Song, *J. Am. Chem. Soc.* **2013**, *135*, 16175–16183.
- [141] Purified by bulb-to-bulb transfer *in vacuo*.
- [142] R. F. Nystrom, W. H. Yanko, W. Brown, *J. Am. Chem. Soc.* **1948**, *70*, 441–441.
- [143] T. C. Eisenschmid, R. Eisenberg, *Organometallics* **1989**, *8*, 1822–1824.
- [144] a) S. N. Riduan, Y. Zhang, J. Y. Ying, *Angew. Chem.* **2009**, *121*, 3372–3375; *Angew. Chem. Int. Ed.* **2009**, *48*, 3322–3325; for mechanistic investigations, see: b) F. Huang, L. Zhao, H. Li, Z.-X. Wang, *J. Am. Chem. Soc.* **2010**, *132*, 12388–12396; c) S. N. Riduan, J. Y. Ying, Y. Zhang, *ChemCatChem* **2013**, *5*, 1490–1496.
- [145] The reaction using dry air as the CO₂ source was reported to proceed slowly forming a mixture of “intermediates” and the silylated methanol **X**; however, no details on the ratio of different products or the reaction time were given.
- [146] T. Matsuo, H. Kawaguchi, *J. Am. Chem. Soc.* **2006**, *128*, 12362–12363.
- [147] a) A. Berkefeld, W. E. Piers, M. Parvez, *J. Am. Chem. Soc.* **2010**, *132*, 10660–10661; b) A. Berkefeld, W. E. Piers, M. Parvez, L. Castro, L. Maron, O. Eisenstein, *Chem. Sci.* **2013**, *4*, 2152–2162.
- [148] S. J. Mitton, L. Turculet, *Chem. Eur. J.* **2012**, *18*, 15258–15262.
- [149] For a recent, unselective B(C₆F₅)₃ (**108**)/bisborate-co-catalyzed example, see: Z. Lu, H. Hausmann, S. Becker, H. A. Wegner, *J. Am. Chem. Soc.* **2015**, *137*, 5332–5335.
- [150] M. Khandelwal, R. J. Wehmschulte, *Angew. Chem.* **2012**, *124*, 7435–7439; *Angew. Chem. Int. Ed.* **2012**, *51*, 7323–7326.
- [151] R. J. Wehmschulte, M. Saleh, D. G. Powell, *Organometallics* **2013**, *32*, 6812–6819.

- [152] Followed by the hydrosilane consumption.
- [153] Typically a color change from blue-green into yellow-orange occurs upon the addition of main-group hydrides into a solution of **25**⁺. In the case of the tin hydride **16b**, the solution turned quickly dark red.
- [154] The uncatalyzed reduction of carbon dioxide with DIBAL-H (**9b**) gave uncontrolled reduction leading to clogging of the NMR tube used for the reaction, separating the gas and the liquid phases. ¹H NMR analysis of the liquid phase showed no conversion.
- [155] D. O'Hagan, *Chem. Soc. Rev.* **2008**, 37, 308–319.
- [156] a) T. Stahl, H. F. T. Klare, M. Oestreich, *ACS Catal.* **2013**, 3, 1578–1587; b) H. Amii, K. Uneyama, *Chem. Rev.* **2009**, 109, 2119–2183.
- [157] G. A. Olah, J. A. Olah, T. Ohyama, *J. Am. Chem. Soc.* **1984**, 106, 5284–5290.
- [158] A. L. Henne, M. S. Newman, *J. Am. Chem. Soc.* **1938**, 60, 1697–1698.
- [159] a) R. K. Ramchandani, W. D. Wakharkar, A. Sudalai, *Tetrahedron Lett.* **1996**, 37, 4063–4064; For a related defluorinative arylation methodology, see: b) A. Okamoto, K. Kumeda, N. Yonezawa, *Chem. Lett.* **2010**, 39, 124–125.
- [160] a) K. Fuchibe, T. Akiyama, *Synlett* **2004**, 1282–1284; b) K. Fuchibe, T. Akiyama, *J. Am. Chem. Soc.* **2006**, 128, 1434–1435; c) K. Fuchibe, Y. Ohshima, K. Mitomi, T. Akiyama, *Org. Lett.* **2007**, 9, 1497–1499; d) K. Fuchibe, Y. Ohshima, K. Mitomi, T. Akiyama, *J. Fluorine Chem.* **2007**, 128, 1158–1167; e) K. Fuchibe, K. Mitomi, R. Suzuki, T. Akiyama, *Chem. Asian. J.* **2008**, 3, 261–271; f) K. Fuchibe, T. Kaneko, K. Mori, T. Akiyama, *Angew. Chem.* **2009**, 121, 8214–8217; *Angew. Chem. Int. Ed.* **2009**, 48, 8070–8073; g) T. Akiyama, K. Atobe, M. Shibata, K. Mori, *J. Fluorine Chem.* **2013**, 152, 81–83; for a recent example using TiCl₄ and hydrosilanes, see: h) T. Yamada, K. Saito, T. Akiyama, *Adv. Synth. Catal.* **2016**, 358, 62–66.
- [161] J. Terao, S. A. Begun, Y. Shinohara, M. Tomita, Y. Naitoh, N. Kambe, *Chem. Commun.* **2007**, 855–857.
- [162] M. Klahn, C. Fischer, A. Spannenberg, U. Rosenthal, I. Krossing, *Tetrahedron Lett.* **2007**, 48, 8900–8903.
- [163] W. Gu, M. R. Haneline, C. Douvris, O. V. Ozerov, *J. Am. Chem. Soc.* **2009**, 131, 11203–11212.
- [164] The connectivity of the butyl groups (*iso* or *tert*) in the products was not disclosed.
- [165] O. Alleman, S. Duttwyler, P. Romanato, K. K. Baldrige, J. S. Siegel, *Science* **2011**, 332, 574–577.
- [166] M. Ahrens, G. Scholz, T. Braun, *Angew. Chem.* **2013**, 125, 5436–5440; *Angew. Chem. Int. Ed.* **2013**, 52, 5328–5332.

- [167] a) J. Zhu, M. Pérez, C. B. Caputo, D. W. Stephan, *Angew. Chem.* **2016**, *128*, 1439–1443; *Angew. Chem. Int. Ed.* **2016**, *55*, 1417–1421; for hydrodefluorination with the same catalytic system, see: b) C. B. Caputo, L. J. Hounjet, R. Dobrovetsky, D. W. Stephan, *Science* **2013**, *341*, 1374–1377.
- [168] T. Stahl, Dissertation, Technische Universität Berlin, **2014**.
- [169] The decomposition of the related $\text{B}(\text{C}_6\text{F}_5)_4^-$ counteranion was previously observed, see: V. J. Scott, R. Çelenligil-Çetin, O. V. Ozerov, *J. Am. Chem. Soc.* **2005**, *127*, 2852–2853.
- [170] For a review of weakly coordinating anions, see: I. Krossing, I. Raabe, *Angew. Chem.* **2004**, *116*, 2116–2142; *Angew. Chem. Int. Ed.* **2004**, *43*, 2066–2090.
- [171] The $[\text{B}_{12}\text{Cl}_{12}]^{2-}$ counteranion was used earlier by our group in the synthesis and isolation of a ferrocene-stabilized silylium ion: K. Müther, R. Fröhlich, C. Mück-Lichtenfeld, S. Grimme, M. Oestreich, *J. Am. Chem. Soc.* **2011**, *133*, 12442–12444.
- [172] The corresponding $\text{BAr}^{\text{F}}_4^-$ and $\text{B}(\text{C}_6\text{F}_5)_4^-$ counteranions are commercially available as sodium and lithium salts, respectively. For the synthesis of perhalogenated *closo*-dodecaboranates, see: a) W. H. Knoth, H. C. Miller, J. C. Sauer, J. H. Balthis, Y. T. Chia, E. L. Muetterties, *Inorg. Chem.* **1964**, *3*, 159–167; b) V. Geis, K. Guttsche, C. Knapp, H. Scherer, R. Uzun, *Dalton Trans.* **2009**, 2687–2694; c) W. Gu, O. V. Ozerov, *Inorg. Chem.* **2011**, *50*, 2726–2728; for the synthesis and properties of the carborane counteranions, see: d) S. Körbe, P. J. Schreiber, J. Michl, *Chem. Rev.* **2006**, *106*, 5208–5249; e) C. A. Reed, *Acc. Chem. Res.* **2010**, *43*, 121–128.
- [173] T. Stahl, unpublished results.
- [174] The corresponding chloride abstraction with $\text{NaBAr}^{\text{F}}_4$ is usually completed within seconds.
- [175] The corresponding ^1H NMR shift ranges for the hydrosilane and hydroborane adducts **61**⁺ and **26**⁺ are –7.5/–8.3 and –8.1/–11.9 ppm, respectively.
- [176] E. Winterfeldt, *Synthesis* **1975**, 617–630.
- [177] In the case of *o*-xylene, traces (<5%) of *tert*-butylation of *o*-xylene was observed.
- [178] The liberation of free alumenium ion **185**⁺ seems unlikely. The cation is assumed to be stabilized by the thiolate sulfur atom or by the solvent.
- [179] The formation of Al–F has been detected by ^{19}F NMR spectroscopy.
- [180] The R-CF_2^+ carbocations are stabilized by backdonations from the fluorine atoms: a) G. A. Olah, M. B. Comisarow, *J. Am. Chem. Soc.* **1969**, *91*, 2955–2961; b) K. O. Christe, X. Zhang, R. Bau, J. Hegge, G. A. Olah, G. K. Surya Prakash, J. A. Sheehy, *J. Am. Chem. Soc.* **2000**, *122*, 481–487.

- [181] The FRIEDEL–CRAFTS alkylation is known to be reversible. For early examples, see: N. O. Calloway, *Chem. Rev.* **1935**, 17, 327–392.
- [182] J. I. Seeman, *Chem. Rev.* **1983**, 83, 84–134.
- [183] CYLview, 1.0b; Legault, C. Y., Université de Sherbrooke, 2009.
- [184] <http://chemsearch.kovsky.net/>
- [185] S. Rendler, *PhD thesis*, Westfälische Wilhelms-Universität Münster, **2007**.
- [186] a) ref. [73a]; b) H. F. T. Klare, *PhD thesis*, Westfälische Wilhelms-Universität Münster, **2011**.
- [187] M. Yan, T. Jin, Y. Ishikawa, T. Minato, T. Fujita, L.-Y. Chen, M. Bao, N. Asao, M.-W. Chen, Y. Yamamoto, *J. Am. Chem. Soc.* **2012**, 134, 17536–17542.
- [188] The cyclohexane consumption required to do this can be decreased significantly by recycling the cyclohexane from the collected fractions back to the column. This way a flash column with total volume of fractions over 100 L can be operated using less than 10 L of solvent.
- [189] a) ref [115]; b) D. Gallego, *PhD thesis*, Technische Universität Berlin, **2015**.
- [190] I. Göttker-Schnetmann, P. White, M. Brookhart, *J. Am. Chem. Soc.* **2004**, 126, 1804–1811.
- [191] Degassed by three freeze-pump-thaw cycles using argon or by bubbling H₂ through the solvent for 1 h.
- [192] S. Rendler, M. Oestreich, C. P. Butts, G. C. Lloyd-Jones, *J. Am. Chem. Soc.* **2007**, 129, 502–503.
- [193] a) L. D. Field, B. A. Messerle, M. Rehr, L. P. Soler, T. W. Hambley, *Organometallics* **2003**, 22, 2387–2395; b) M. Mewald, *Ph.D. Thesis*, Westfälische Wilhelms-Universität Münster, **2012**.
- [194] All three iridium hydrides coalesce into one signal.
- [195] J. Mohr, M. Durmaz, E. Irran, M. Oestreich, *Organometallics* **2014**, 33, 1108–1111.
- [196] a) T. T. Wenzel, R. G. Bergman, *J. Am. Chem. Soc.* **1986**, 108, 4856–4867; b) A. Kornath, F. Neumann, H. Oberhammer, *Inorg. Chem.* **2003**, 42, 2894–2901.

CURRICULUM VITAE**Personal Details**

Name	Toni Tapio Metsänen
Date and place of birth	April 7 th 1986 in Viljakkala, Finland
Nationality	Finnish
Marital Status	Married, one child

Education

September 2012 – April 2016	Technische Universität Berlin, Berlin Dissertation under the supervision of Prof. Dr. MARTIN OESTREICH, Thesis: " <i>Metal-Catalyzed Generation of Main-Group Electrophiles: Mechanisms and Applications</i> "
March 2011 – August 2012	University of Liverpool, Liverpool, United Kingdom Postgraduate studies under the supervision of Prof. Dr. P. ANDREW EVANS,
September 2010 – February 2011	University of Jyväskylä, Finland Master thesis under the supervision of Prof. Dr. PETRI M. PIHKO, Thesis: " <i>Enantioselective synthesis of isoxazolines with bifunctional organocatalysts</i> "
January 2010 – March 2010	University of Jyväskylä, Finland Bachelor thesis under the supervision of Prof. Dr. PETRI M. PIHKO, Thesis: " <i>Synthesis of thioesters for enolization studies</i> "

Military Service

January 2006 – January 2007	Pioneerirykmentti, Keuruu, Finland Rank: Corporal
-----------------------------	--

Matriculation Examination

May 2005	Tammerkosken lukio, Tampere, Finland
----------	--------------------------------------